Developing Integrated Approaches to Mitochondrial DNA Analysis Using Microfluidic Chips

by

Victoria Northrup

A thesis submitted in partial fulfillment of the requirements for the degree of

Master of Science

Department of Cell Biology
University of Alberta

© Victoria Northrup, 2015

Abstract

Mutations in the mitochondrial genome (mtDNA) have been linked to a wide variety of disorders. mtDNA analyses require large starting samples and are complicated by the presence of nuclear mitochondrial pseudogenes (NUMTs), which can cause false positives in PCR-based approaches. Microfluidic chips (MFCs) allow assays, which are typically run at the laboratory bench, to be performed on small microchips, thus facilitating high-throughput analyses. We have used MFCs to analyze plasmid DNA (pDNA) and mtDNA, in an attempt to develop mtDNA diagnostic capabilities using small sample volumes.

We were able to successfully manipulate 1 pg of pDNA, the approximate amount of mtDNA in 1500 fibroblasts, which is the lowest concentration of DNA to be successfully manipulated on MFCs that we are aware of. Based on this plasmid isolation we were also able to develop a MFC-based plasmid miniprep using 5 orders of magnitude fewer starting cells. Modification of these approaches resulted in the isolation of mtDNA from fibroblasts and leukocytes, albeit with some nuclear DNA (nDNA) contamination.

Using the Supercoiled DNA (SC) ladder, we were able to develop a capillary electrophoresis (CE)-based plasmid separation that could resolve two plasmids with a 1.5 kb size difference. This resolution is sufficient to allow identification of the vast majority of reported mtDNA deletions. These experiments reported here therefore lay the groundwork for performing mtDNA diagnostics on MFCs.

Acknowledgements

I would like to thank my supervisors Dr. D. Moira Glerum and Dr. Chris Backhouse for their guidance and support throughout my graduate program. I am grateful to Dr. Rick Rachubinski for agreeing to be my supervisor in the middle of my graduate degree when Dr. D. Moira Glerum and Dr. Chris Backhouse moved to the University of Waterloo. I would also like to thank the members of my committee Dr. Stacey Hume and Dr. Joel Dacks for their guidance.

I would like to acknowledge Tianchi Ma for the fabrication of the PMMA MFCs, Lorraine Fung for her help during the summer of 2012, Leanne from the University of Alberta Molecular Diagnostic Lab and Marg Burnett from the University of Waterloo Kinesiology department for performing venipuncture to obtain blood, and Anjali Gopal for her help with editing.

I am grateful to Alberta Innovates Health Solutions and the Natural Sciences and Engineering Research Council for funding during my graduate program.

I would like to thank the University of Alberta Cell Biology office staff for their help as well the Biology department and Waterloo Institute for Nanotechnology for allowing me to work as a visiting scientist at the University of Waterloo for the past two years.

TABLE OF CONTENTS

List of Tables

List of Figures

Abbreviations

ACE	Agarose capillary electrophoresis
ADP	Adenosine diphosphate
AGE	Agarose gel electrophoresis
AIBN	Azobisisobutyronitrile
ANT	Adenine nucleotide translocator
ASO	Allele-specific oligonucleotide
ATP	Adenosine triphosphate
BER	Base excision repair
bp	Base pair
BR	Buffer reservoir
BSA	Bovine serum albumin
BW	Buffer waste reservoir
CE	Capillary electrophoresis
cm	Centimeter
CO	Cytochrome *c* oxidase subunit genes
COC	Cyclic olefin copolymers
COX	Cytochrome *c* oxidase
CPA	Cross-linked polyacrylamide
CPEO	Chronic progressive external ophthalmoplegia
CRS	Cambridge reference sequence
CSB	Conserved sequence block
CT	Computer tomography
Cyt*b*	Cytochrome *b*
D-loop	Displacement loop
DGGE	Denaturant gradient gel electrophoresis
dHPLC	Denaturing high performance liquid chromatography
DMSO	Dimethyl sulfoxide

DMA	N,N-dimethyl acrylamide
DNA	Deoxyribonucleic acid
dNTP	Deoxyribonucleoside triphosphate
dRP	5` deoxyribose phosphate
EDTA	Ethylenediaminetetraacetic acid
EOF	Electroosmotic flow
ETC	Electron transport chain
FACS	Fluorescence activated cell sorting
FCS	Fetal calf serum
FWHM	Full width at half max
gDNA	Genomic DNA
H-strand	Heavy strand
HA-SSCP	Heteroduplex analysis with SSCP
HEA	N-hydroxyethylacrylamide
HR	Homologous recombination
HSP	H-strand promoter
HVR	Hypervariable region
IMM	Inner mitochondrial membrane
IMS	Intermembrane space
indels	Insertion/deletions
IP	Immunopercipitation
kb	Kilobase
KSS	Kearns-Sayre syndrome
L-strand	Light strand
LB	Luria broth
LBa	Lithium boric acid
LHON	Leber’s hereditary optic neuropathy
LIF	Laser induced fluorescence

LPA	Linear polyacrylamide
LSP	L-strand promoter
Mb	Megabases
MDS	mtDNA depletion syndrome
MERRF	Myclonic epilepsy with ragged red fibers
MELAS	Mitochondrial encephalomyopathy, lactic acidosis, and stroke-like episodes
MFC	Microfluidic chip
mm	Millimeter
MMR	Mismatch repair
mRNA	Messenger RNA
mtDNA	Mitochondrial DNA
mL	Milliliter
mtSSB	Mitochondrial single-stranded binding protein
NARP	Neurogenic muscle weakness, ataxia, retinitis, pigmentosa
NCR	Non-coding region
ND	NADH Dehydrogenase subunit
NEB	New England Biolabs
nDNA	Nuclear DNA
NGS	Next-Generation Sequencing
ng	Nanogram
NHEJ	Non-homologous end joining
nm	Nanometer
NUMT	Nuclear mitochondrial pseudogenes
OD	Optical density
O_H	Origin of replication of the H-strand
O_L	Origin of replication of the L-strand

OMM	Outer mitochondrial membrane
OXPHOS	Oxidative phosphorylation
PBS	Phosphate buffered saline
PC	Polycarbonate
PCR	Polymerase chain reaction
PDMA	Poly-N,N-dimethylacrylamide
PDMS	Polydimethylsiloxane
pDNA	Plasmid DNA
PEO	Progressive external ophthalmoplegia
PET	Polyethylene terephthalate
PFGE	Pulse field gel electrophoresis
PHEA	Poly-N-hydroxyethylacrylamide
PMMA	Poly (methylmethacrylate)
P_i	Inorganic phosphate
PMT	Photomultiplier tube
POC	Point-of-care
POLγ	DNA polymerase gamma
POLRMT	Mitochondrial RNA polymerase
PS	Pearson syndrome
PVP	Polyvinylpyrrolidone
qPCR	Quantitative PCR
rCRS	Revised Cambridge sequence
Re	Reynolds number
RFLP	Restriction fragment length polymorphism
RITOLS	Ribonucleotides are Incorporated Throughout the Lagging strand
RNA	Ribonucleic acid
ROS	Reactive oxygen sequence

rpm	Rotations per minute
rRNA	Ribosomal RNA
RRF	Ragged-red fiber
RRM2B	Ribonucleotide reductase M2B subunit
SBa	Sodium Boric acid
SDH	Succinate dehydrogenase
SDS	Sodium dodecyl sulfate
SO	Sytox orange
SR	Sample reservoir
SSCP	Single-stranded conformation polymorphism
ssDNA	Single-stranded DNA
SNP	Single nucleotide polymorphism
ST	Sodium Threonine
STD	Standard deviation
STE	Sodium Threonine EDTA
SW	Sample waste reservoir
TAE	Tris-Acetate-EDTA
TAS	Termination association sequence
TBE	Tris Borate EDTA
TEMED	N,N,N,N-tetramethylethylenediamine
TFAM	Mitochondrial transcription factor A
TFB2M	Mitochondrial transcription factor B2
TOPmt1	Mitochondrial topoisomerase
TPE	Thermoset polyester
tRNA	Transfer RNA
TTE	Tris-TAPS-EDTA
TGGE	Temperature gradient gel electrophoresis
V	Volts

WT	Wild type
4-PM	‘4-port mini’ MFC
α-MEM	Eagle’s alpha minimal essential media
μm	Micrometer
μTAS	Micro total analysis system
μTK	Microfluidic tool kit

CHAPTER 1-INTRODUCTION

1. 1 The Mitochondrion

1.1.1 A Brief History of Mitochondrial Discoveries

The first documented observations of subcellular structures that we now know as mitochondria were made in the 1840's. These observations of mitochondria were made by numerous groups, but they did not recognize they were all examining the same organelle due to the difference in sizes and shapes observed. It was not until 1890 that Richard Altmann recognized that these subcellular structures were ubiquitous (Ernster and Schatz, 1981). He named them "bioblasts" because of their resemblance to free living bacteria. This resemblance to bacteria is not by coincidence, but is due to their endosymbiotic origin (which will discussed further below). The phenomenon of endosymbiosis was first proposed by Konstantin Merezkovskji to explain the origins of plastids (Chan and Bhattacharya, 2010; Martin and Kowallik, 1999) and was first proposed to explain the origin of mitochondria by Ivan Wallin in 1923 (Chan and Bhattacharya, 2010; Wallin, 1923). However, it was not until 1960s that endosymbiosis became the prevailing explanation for the origin of mitochondria (Chan and Bhattacharya, 2010; Margulis, 1970; Sagan, 1967). The term mitochondria, from the Greek word "mitos", meaning thread, and "chondros", meaning granule, was introduced by Benda in 1898, based on the appearance of the mitochondria during spermatogenesis (Ernster and Schatz, 1981; Scheffler, 2007).

The discovery that mitochondria had their own genome was made in 1963 (Nass and Nass, 1963; Schatz *et al.*, 1964). The sequence for the human mitochondrial genome was published by Anderson *et al.*(Anderson *et al*., 1981) in 1981, but it was not until 1986 that the final reading frame was identified (Chomyn *et al*., 1986; Chomyn *et al.*,

1985). Two years later, in 1988, the first disease-causing mutations in the mitochondrial genome were identified in humans (Holt *et al*., 1988; Wallace *et al.*, 1988). In the past 25 years, there have been over 250 mutations found in the mitochondrial genome that are associated with a wide variety of disorders (Ruiz-Pesini *et al.*, 2007; Tuppen *et al.*, 2010).

1.1.2 The Structure and Function of Mitochondria

The mitochondrion is a double-membrane bound, semiautonomous organelle in eukaryotic cells. Mitochondria have a wide range of morphologies that are dependent on the cell type and energy demands of the cell (Scheffler, 2007). Mitochondria are usually rod shaped and are between 0.2 – 1.0 μm in diameter and 1 – 4 μm in length. There are hundreds to thousands of mitochondria per cell, occupying 15-20 % of the cellular volume, with more energy demanding cells containing more mitochondria (Karp, 1999).

The two membranes of the mitochondrion are the outer mitochondrial membrane (OMM) and the inner mitochondrial membrane (IMM). The OMM encases the mitochondrion and is composed of a 50:50 ratio of proteins to lipids, which is typical of a eukaryotic membrane. The IMM folds to form cristae, which increase the surface area of the IMM. The arrangement of the cristae, and therefore the size of the IMM, also varies by cell type, with more surface area (i.e. more cristae) in more energy demanding cell types. The protein to lipid ratio of the IMM is 75:25, which is more typical of a prokaryotic membrane. The two membranes create two compartments within the mitochondrion, the intermembrane space (IMS) and the matrix. The IMS is located between the OMM and IMM, and the matrix is located within the IMM (Figure 1.1A) (Karp, 1999; Scheffler, 2007; Voet *et al*., 2008). This compartmentalization creates

different environments within the mitochondrion that help to facilitate the many different functions of the organelle.

The primary function of the mitochondrion is cellular respiration by oxidative phosphorylation (OXPHOS), which is the only mitochondrial function under dual genomic control (Scheffler, 2007). OXPHOS is a process by which five enzyme complexes, which have subunits encoded by both the mitochondrial and nuclear genomes, generate approximately 90% of the cellular energy in the form of adenosine triphosphate (ATP) (Hatefi, 1985; McFarland and Turnbull, 2009). The five complexes, which are embedded in the IMM, are: NADH: ubiquinone oxidoreductase (Complex I), succinate: ubiquinone oxidoreductase (Complex II), ubiquinol: cytochrome *c* oxidoreductase (Complex III), cytochrome *c* oxidase (Complex IV) and ATP synthase (Complex V) (Figure 1.1B). The first four complexes comprise the electron transport chain (ETC), which, results in the pumping of protons from the matrix to the IMS to generate a proton gradient across the IMM. The proton gradient is then used by Complex V to generate ATP (Figure 1.1B) (Karp, 1999; Voet *et al.*, 2008). The majority of the ATP produced by OXPHOS will be exported from the mitochondrial matrix by the adenine nucleotide translocator (ANT) for use in numerous cellular processes (Smeitink *et al.*, 2001).

Complex I is the largest complex of the ETC in humans. Complex I is composed of 45 subunits in humans, of which seven are encoded by the mitochondrial deoxyribonucleic acid (DNA) (mtDNA) (Brandt, 2006; Pagniez-Mammeri *et al*., 2012). Complex II is the smallest complex of the ETC and is composed of four subunits

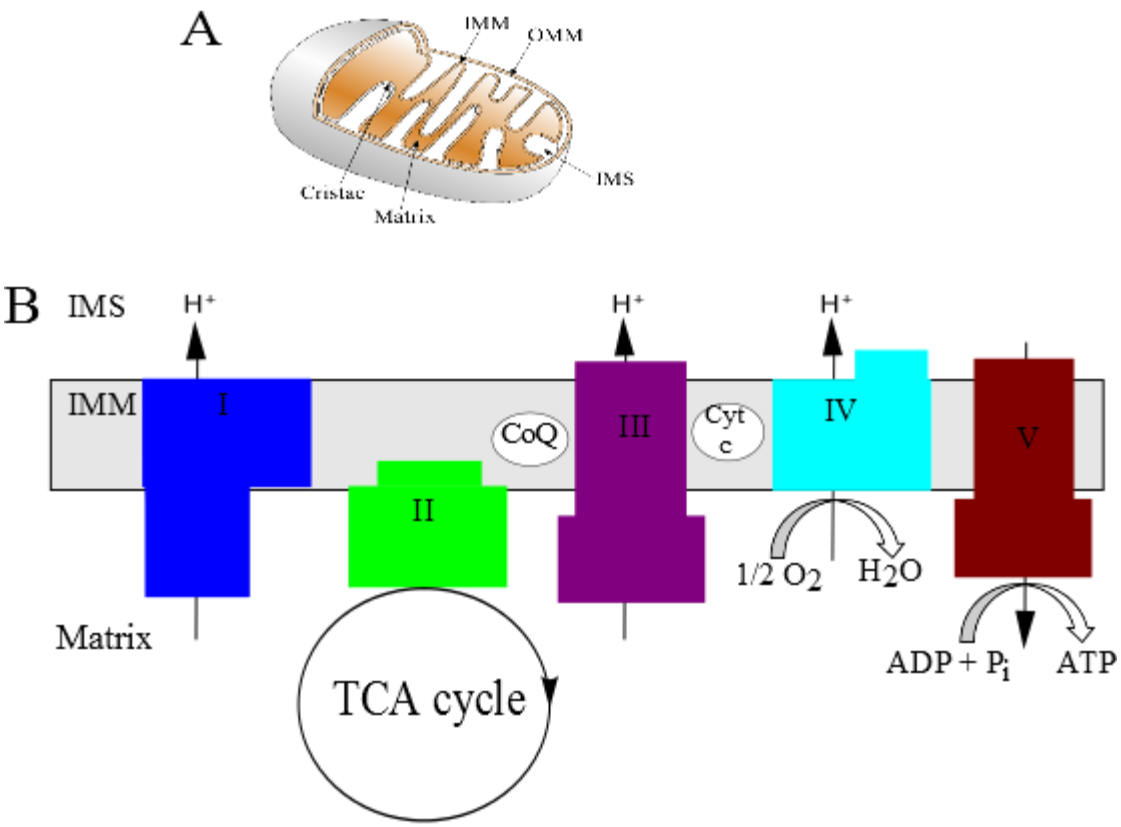

Name	**Complex I** NADH: ubiquinone oxidoreducatase	**Complex II** Succinate: ubiquinone oxidoreducatase	**Complex III** Ubiquinol: cytochrome c oxidoreductase	**Complex IV** Cytochrome oxidase	**Complex V** ATP synthase
Subunit	45	4	11	13	16
mtDNA encoded subunits	7	0	1	3	2

Figure 1.1. Structure and function of the mitochondrion. A) Structure of the mitochondrion. IMM=inner mitochondrial membrane, OMM= outer mitochondrial membrane, IMS=intermembrane space. B) Schematic of OXPHOS. IMM and IMS are the same as A. Each of the five complexes are indicated by their number and the soluble electron carriers ubiquinol (CoQ) and cytochrome *c* (Cyt *c*) are represented by white ovals. The Kreb cycle (TCA cycle) is shown under Complex II due to the dual role that Complex II plays in both OXPHOS and the Kreb cycle. Arrows through the complexes show the direction of protons and curved arrows at Complexes IV and V represents the reactions using oxygen as the terminal electron acceptor and the generation of ATP, respectively. The name of each of the complexes are shown below the schematic with the total number of subunits in the complex and the number of subunits encoded by the mtDNA. Adapted from (Punter, 2003).

(Lancaster and Kröger, 2000; Mewies *et al*., 1998). Complex II is the only complex in OXPHOS that is exclusively encoded by the nuclear genome (Cecchini, 2003). The electrons from Complex I and Complex II are shuttled to Complex III by ubiquinone. Complex III is composed of 11 subunits, of which one is encoded by the mtDNA (Yu *et al*., 1999). Complex IV is composed of 13 subunits, three of which are encoded by the mtDNA (Abramson *et al*., 2001). In the final step of the ETC, Complex IV accepts the electrons from the reduced cytochrome *c* and transfers them to oxygen, which acts as the terminal electron acceptor (Hatefi, 1985). Complex V is composed of 16 subunits, of which two are encoded by the mtDNA. Complex V uses the proton gradient generated by the ETC to convert adenosine diphosphate (ADP) and inorganic phosphate (P_i) to ATP (Hatefi, 1985; Scheffler, 2007; Smeitink *et al*., 2001; van den Heuvel and Smeitink, 2001) (Figure 1.1B).

Although OXPHOS is considered the primary role of mitochondria, as reflected in reference to the "powerhouse" of the cell, it is not the sole function. Mitochondria are involved in a diversity of processes required for normal cellular function. Along with OXPHOS, the mitochondria are also the site of the Krebs cycle and part of the urea cycle, which both occur in the mitochondrial matrix. Mitochondria are also involved in fatty acid and amino acid metabolism and the biosynthesis of heme and iron-sulfur clusters. The mitochondria have also been found to have an important role in apoptosis (Scheffler, 2007). Given the diverse roles of mitochondria, it is no wonder that mitochondrial dysfunction has been implicated in a wide range of disorders.

1.1.3 The Endosymbiotic Origins of Mitochondria

The endosymbiotic theory is widely accepted as the explanation for the origin of mitochondria. According to the endosymbiotic theory, a free living α-proteobacterium entered into an endosymbiotic relationship with an eukaryote approximately two billion years ago (Andersson *et al*., 2003; Gray *et al.*, 2001; Lang *et al.*, 1999; Scheffler, 2007). The early earth's atmosphere would have had only a small amount of oxygen and consisted mainly of carbon dioxide and reduced forms of sulfur, nitrogen and carbon. Around two billion years ago, the oxygen produced by cyanobacteria through photosynthesis caused the oxygen levels in the atmosphere to rise (Flannery and Walter, 2012). This rise in oxygen would have presented a dilemma to anaerobic organisms, for whom oxygen was toxic. One solution used by an eukaryote was the engulfing of an α-proteobacterium capable of using oxygen. In this endosymbiotic relationship, the host eukaryote would have provided carbohydrates to the prokaryote in return for ATP produced by the prokaryote through OXPHOS, in which oxygen was the terminal electron acceptor (Andersson *et al*., 2003). Over the past two billion years, there has been gene transfer from the original α-proteobacterial genome (s) to the nuclear genome (s), and protein import machinery was adapted to import and export molecules and proteins between the host cytosol and the α-proteobacterium to create the mitochondrion that is seen in almost all extant eukaryotes (Andersson *et al*., 2003; Emelyanov, 2001; Gray *et al.*, 2001; Lang *et al.*, 1999; Scheffler, 2007).

Since the establishment of the endosymbiotic relationship two billion years ago, the genome of the symbiote has decreased between 100 to 300 fold (Selosse *et al.*, 2001) to the current mitochondrial genome. To facilitate this reduction, genes that were no

longer required, either because their function was no longer necessary or their function was taken over by a nuclear gene, were lost. Other genes were transferred from the genome of the symbiote to the nuclear genome of the host (Gaziev and Shaikhaev, 2010). This gene transfer has resulted in most of the more than 1000 mitochondrial proteins being encoded by the nuclear genome. Although many genes were either lost or transferred, a small subset of genes remain in the mitochondrial genome, despite their attempts to transfer to the nuclear genome. For each of the genes found in the mitochondrial genome, there are nuclear mitochondrial pseudogenes (NUMTs) in the nuclear genome that represent failed gene transfers (Selosse *et al*., 2001).

There are 296 known NUMTs found in the human nuclear genome, making up approximately 0.016% of the nuclear genome. These NUMTs range in size from 106 bp to 14 654 bp, with 15 NUMTs larger than 5842 bp and up to 30% of these NUMTs corresponding to two or more mtDNA-based genes (Gaziev and Shaikhaev, 2010). NUMTs are evenly distributed within the nuclear DNA (nDNA) and can cause erroneous results for PCR-based mtDNA analyses if they are not properly accounted for (Bensasson *et al.*, 2001; Calvignac *et al*., 2011; Yao *et al.*, 2008; Zhang and Hewitt, 1996).

1.1.4 Dynamics of Mitochondrial Morphology

Mitochondria are dynamic organelles that are constantly undergoing fission and fusion. These two processes work together to maintain the appropriate morphology and quantity of mitochondria in a cell. Fission and fusion are also involved in the response to cellular stress, apoptosis, fluctuations in respiratory capacity and stability of the mtDNA. If fission is decreased, the mitochondria become elongated and excessively

interconnected. Mitochondrial fusion allows for functional complementation of mitochondria, as dysfunctional mitochondrion can fuse with a normal mitochondrion and the proteins from the healthy mitochondrion can compensate for the defective proteins in the dysfunctional organelle (Youle and van der Bliek, 2012). When fusion is reduced, the mitochondria become fragmented (Chan, 2012). Mitochondria do not arise *de novo,* but instead undergo fission to proliferate (Chen and Chan, 2005). Severe defects in either mitochondrial fission or fusion result in embryonic lethality in mice (Chan, 2012).

1.2 The Human Mitochondrial Genome

1.2.1 Structure and Content of the Human Mitochondrial Genome

Each mitochondrion contains between two and ten mtDNAs (Larsson and Clayton, 1995), which results in hundreds to thousands of mtDNAs per cell. The human mtDNA is a 16, 569 base pair (bp), closed-circular, double-stranded, DNA molecule (Anderson *et al.*, 1981). The two strands are termed the heavy (H)-strand and the light (L)-strand because of their different buoyant densities in a cesium chloride gradient. The different densities are caused by biased nucleotide content, with the H-strand being guanine rich and the L-strand being cytosine rich (Falkenberg *et al*., 2007; Pagliarini *et al.*, 2008; Ryan and Hoogenraad, 2007).

The human mtDNA contains 37 genes that include 13 protein coding genes, two ribosomal ribonucleic acid (RNA) (rRNA) genes and 22 transfer RNA (tRNA) genes (Figure 1.2B). The H-strand encodes 28 of the 37 genes found in the mtDNA, with the remaining nine being encoded by the L-strand. The human mtDNA is a compact

genome that has very little non-coding DNA, most of which is found in the so called "non-coding region" (NCR) (Figure 1.2A) (Anderson *et al.*, 1981).

The NCR is found between nucleotides 16, 029 - 576 (position based on the revised Cambridge reference sequence (rCRS), GenBank NC_012920) (Andrews *et al.*, 1999) of the mtDNA. The NCR contains many of the regulatory sequences for replication and transcription of the mtDNA. As a result, the NCR is also referred to as the "control region". The origin of replication for the H-strand (O_H) is found in the NCR, whereas the origin of replication of the L-strand (O_L) is found outside the NCR, about two thirds of the way around the H-strand of mtDNA (5` to 3`) (between nucleotides 5721-5798, Figure 1.2B)(Ruiz-Pesini *et al.*, 2007). The two transcriptional promoters for the H-strand (HSP1 and HSP2) and the transcriptional promoter for the L-strand (LSP) are also located in the NCR. Other features of the NCR include three conserved sequence boxes (CSB I-III), a termination-associated sequence (TAS), and two hypervariable regions (HVR I-II). The HVRs contain many of the polymorphisms associated with the human mtDNA, including some that determine haplotypes (Anderson *et al*., 1981). The NCR also contains a unique feature called the displacement loop (D-loop), which contains a triple helix DNA structure known as the 7S mtDNA (Falkenberg *et al.*, 2007). The 7S mtDNA fragment is found between nucleotides 16, 106 - 191 (Ruiz-Pesini *et al.*, 2007). However, not all mtDNAs have the 7S fragment, with the proportion containing the 7S fragment varying by tissue (Annex and Williams, 1990). The 7S mtDNA is formed by the initiation of transcription at the LSP, which would typically transition into replication at the O_H. However, for unknown reasons, the replication is aborted, giving rise to the 7S mtDNA (Clayton, 1982). The exact function of the D-loop is not yet

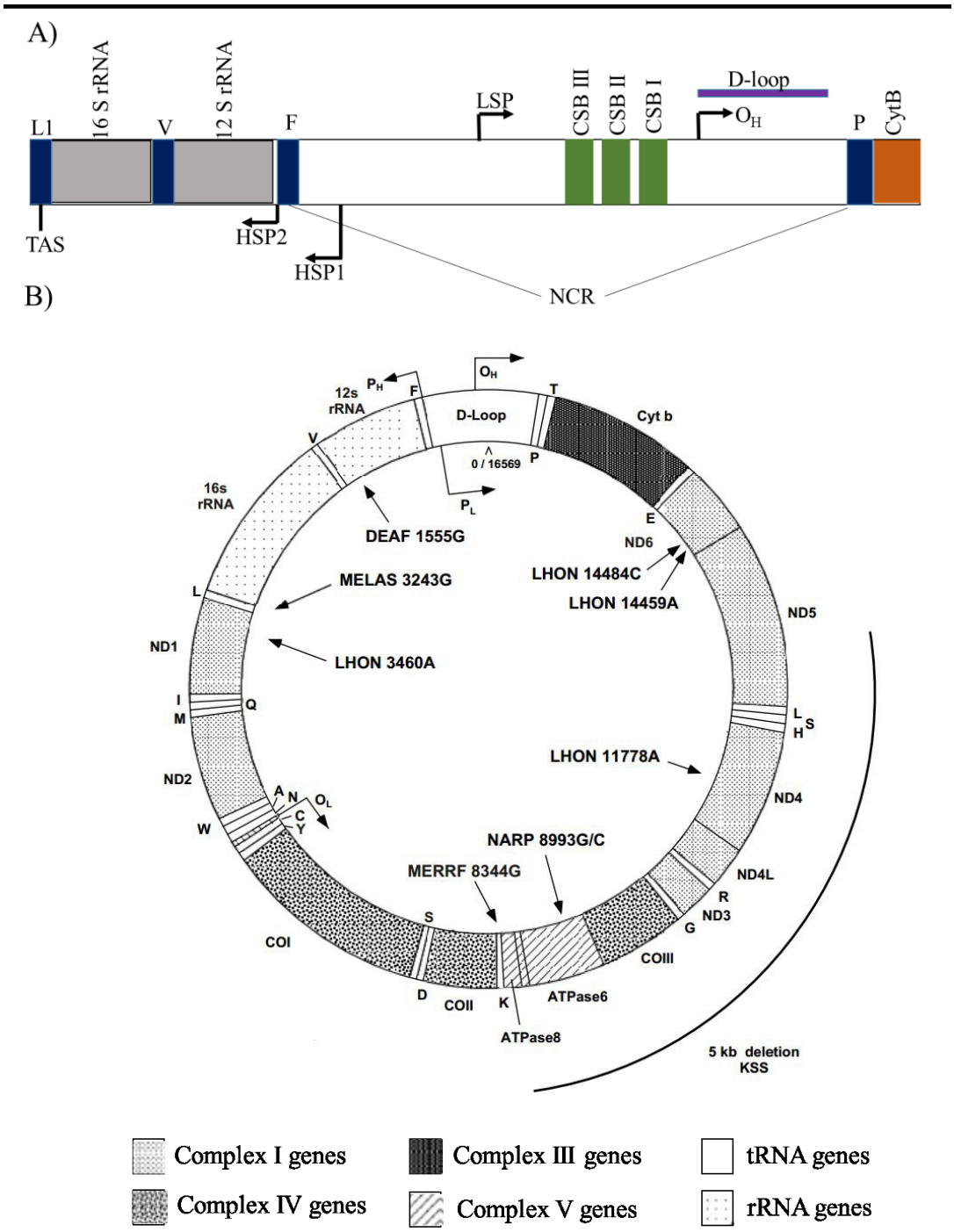

Figure 1.2. Map of the human mitochondrial genome. A) The NCR with the promoters and O_H indicating the direction of transcription or replication. The D-loop bar represents the 7S mtDNA. B) The map of the human mtDNA. The shading of the protein-coding genes indicate their respective OXPHOS complexes, the rRNAs are indicated as 16 S or 12 S and the tRNAs are indicated by the amino acid of the tRNA. The origin of replication for each strand (O_H and O_L) is indicated with an arrow for the direction of replication. Source: Mitomap (Ruiz-Pesini *et al.*, 2007).

known, but it is suspected to play a role in the organization of the nucleoid (He *et al.*, 2007).

As described above, OXPHOS is under dual genomic control, with the majority of the 89 subunits of the five complexes being encoded by the nuclear genome and only 13 subunits encoded by the mtDNA. The mtDNA genes, unlike the nuclear encoded genes, do not contain introns and are transcribed polycistronically (Anderson *et al.*, 1981). The seven subunits of Complex I that are encoded by the mtDNA are NADH dehydrogenase subunits 1-6 and 4L (ND1-6 and 4L) (Anderson *et al*., 1981; Chomyn *et al*., 1986; Chomyn *et al.*, 1985). Complex III contains cytochrome *b* (Cytb), which is mtDNA-encoded, while Complex IV contains three mtDNA encoded subunits, cytochrome *c* oxidase I-III (COI-III) (Anderson *et al*., 1981). Complex V has a total of 16 subunits of which two, ATPase 6 and 8, are mtDNA encoded (Anderson *et al.*, 1981; Chomyn *et al.*, 1985) (Figure 1.1 and 1.2). Of the 13 protein coding genes in the mtDNA, 12 are encoded on the H-strand, with ND6 being the only protein encoded on the L-strand (Suzuki *et al.*, 2011). Since some of the OXPHOS complexes are encoded by both the nuclear and mitochondrial genomes, cooperation between the two genomes is required to ensure functional OXPHOS (Ryan and Hoogenraad, 2007).

In order to translate the mtDNA's protein coding genes into polypeptides, the mtDNA also encodes 22 tRNAs. These 22 tRNAs represent all 20 amino acids, with two tRNAs for each of leucine and serine (Anderson *et al.*, 1981). The tRNAs form secondary structures with a conserved cloverleaf structure referred to as type 0 (Suzuki *et al*., 2011). Mitochondrial tRNAs can lack common tRNA characteristics when compared to the nuclear genome and prokaryotic counterparts (Suzuki *et al*., 2011). The variations

in the mitochondrial tRNAs decrease the amount of tertiary interactions, which may be why only 22 tRNAs are required for translation of the mtDNA (Anderson *et al.*, 1981).

Ribosomes are also required for the translation of the proteins encoded by the mtDNA. Although all the ribosomal proteins are encoded in the nuclear genome, the two rRNA genes for the large rRNA (16S) and the small rRNA (12S) are encoded by the mtDNA (Anderson *et al*., 1981). The two rRNAs form complex secondary structures (Glotz *et al*., 1981) that subsequently form tertiary structures with the ribosomal proteins. The mitochondrial ribosomes are the site for translation of the mitochondrial messenger RNAs (mRNAs) into polypeptides (Christian and Spremulli, 2012), and will be discussed further in Section 1.2.4.

1.2.2 Organization of the Mitochondrial Nucleoid

The mitochondrial nucleoid is a DNA-protein structure that provides organization and protection to the mtDNA (Gilkerson, 2009). The nucleoid is composed of approximately 30 proteins, some of which are involved in the packaging, replication and transcription of the mtDNA, and are encoded by the nuclear genome (Chen and Butow, 2005). The average size of the nucleoid is 70 nm in diameter, containing between two and ten mtDNAs (Gilkerson, 2009; Iborra *et al.*, 2004), though the size can vary by cell type. Typically there is one nucleoid per mitochondrion, although multiple nucleoids can also be found in a single organelle. When multiple nucleoids are present, there appears to be very little exchange of DNA between the nucleoids (Malka *et al*., 2006).

The most abundant protein in the mammalian mitochondrial nucleoid is mitochondrial transcription factor A (TFAM) (Bogenhagen, 2012). TFAM is a DNA

binding protein that is involved in the initiation of transcription, as well as the organization and maintenance of the mtDNA (Chen and Butow, 2005; Ngo *et al*., 2011; Rubio-Cosials *et al*., 2011). Knockout of *Tfam* in mice ($Tfam^{-/-}$) resulted in no detectable mtDNA in embryos at embryonic day 8.5 (E8.5) and lead to embryonic lethality between E8.5 and E10.5. Mice that were heterozygous for the *Tfam* knockout ($Tfam^{+/-}$) had a reduced copy number of the mtDNA (Larsson *et al.*, 1998). In *in vitro* studies, using both mouse and human cells, *Tfam* knock-down results in a reduction of the mtDNA copy number, whereas overexpression of *Tfam* results in increased mtDNA copy number (Kanki *et al*., 2004). Both the *in vitro* and *in vivo* studies demonstrate the importance of TFAM in the maintenance of mtDNA and mtDNA copy number.

TFAM binds to DNA in both a sequence specific and a non-sequence specific manner (Ngo *et al.*, 2011; Rubio-Cosials *et al*., 2011). The sequence specific binding is related to TFAM's role in transcription. The non-sequence specific binding allows TFAM to package the mtDNA and help to organize the nucleoid, in a manner similar to the way in which histones package the nuclear genome (Kaufman *et al.*, 2007). TFAM is predicted to bind the mtDNA in 25 bp intervals, which results in approximately 1000 molecules of TFAM per mtDNA (Kang *et al*., 2007).

Although TFAM is the most abundant protein found in the mitochondrial nucleoid, it is not the only protein. Other mitochondrial maintenance proteins have also been isolated in mitochondrial nucleoids, such as the mitochondrial helicase TWINKLE, the mitochondrial DNA polymerase gamma (POLγ), mitochondrial RNA polymerase (POLRMT), and the mitochondrial single-stranded DNA binding protein (mtSSB)

(Bogenhagen, 2012; Bogenhagen *et al.*, 2008; Bogenhagen *et al.*, 2003; Chen and Butow, 2005; Gilkerson, 2009; Malka *et al.*, 2006).

Also found in the mitochondrial nucleoid are the IMM proteins, such as ANT1 (Bogenhagen *et al.*, 2003). Although the exact roles of ANT1 in the nucleoid are unknown, they may be involved in linking the nucleoid to the IMM. Other proteins that have also been identified in nucleoid preparations include chaperones, proteins involved in lipid metabolism, cytoskeletal attachment and those required for mitochondrial ribosome biogenesis (Bogenhagen, 2012).

1.2.3 Transcription of the Mitochondrial Genome

1.2.3.1 Generation of the Mitochondrial Transcripts

The polycistronic mtDNA transcript undergoes post-transcriptional processing to yield individual transcripts for the rRNAs, tRNAs and mRNAs encoded by the mtDNA. The machinery for transcription of the mtDNA is encoded by the nuclear genome and includes TFAM, mitochondrial transcription factor B2 (TFB2M), and POLRMT (Rackham and Filipovska, 2012). These proteins facilitate transcription from three transcriptional promoters in the mtDNA, one for the L-strand and two for the H-strand. Transcription of the H-strand can start from either of two sites, HSP1 or HSP2 (Guja and Garcia-Diaz, 2012). HSP1 is located within the NCR between nucleotides 545-567 (Ruiz-Pesini *et al*., 2007), and the transcript contains the two rRNAs and two tRNAs and is terminated after the 16S rRNA (Guja and Garcia-Diaz, 2012). HSP2 is found outside the NCR at nucleotide 646 (Ruiz-Pesini *et al*., 2007; Zollo *et al.*, 2012). The transcript generated from HSP2 contains the entire H-strand, which includes 12 of the 13 proteins

and 12 of the 22 tRNAs (Guja and Garcia-Diaz, 2012). Transcription of the L-strand starts from the LSP, which is located in the NCR between nucleotides 392-445 (Ruiz-Pesini *et al*., 2007). The transcript generated from LSP encompasses the complete L-strand, which includes the single protein encoded by the L-strand, ND6, and 8 of the 22 tRNAs (Bestwick and Shadel, 2013; Guja and Garcia-Diaz, 2012).

1.2.3.2 Post-transcriptional Modifications of the Mitochondrial Transcripts

The three polycistronic transcripts generated from mtDNA require post transcriptional processing to obtain individual mRNAs, tRNAs and rRNAs, with the tRNAs serving as punctuation (Ojala *et al*., 1981). In the polycistronic transcripts, most of the mRNAs and rRNAs are flanked by tRNAs, which are excised by endonucleases (Rossmanith, 2012). Removal of the tRNAs from the transcript thus results in the mature mRNAs, tRNAs and rRNAs (Ojala *et al*., 1981; Rossmanith, 2012). The mitochondrial tRNAs tend to be smaller and have fewer modified nucleotides as compared to the nuclear tRNAs and also form unique secondary structures (Rossmanith, 2012; Suzuki *et al*., 2011). Unlike their nuclear counterparts, the mitochondrial mRNAs lack a 5` cap (Montoya *et al.*, 1981), but do have 3` poly (A) tails that add approximately 50 A's to the 3`-end of the mRNAs. Many of the mitochondrial mRNAs end with a U or a UA, and addition of the poly (A) tail completes the stop codon of "UAA" (Chang and Tong, 2012). The mitochondrial rRNAs also contain a few post-transcriptional modifications, though fewer as compared to the nuclear eukaryotic and prokaryotic counterparts (Baer and Dubin, 1981; Ofengand and Bakin, 1997).

1.2.4 Translation of the Mitochondrial Transcripts

Translation of mitochondrial transcripts occurs by the mitochondrial ribosome, which is a 55S ribosome with two subunits: the large subunit (39S) and the small subunit (28S). The 16S rRNA is located in the 39S subunit and the 12S rRNA is found in the 28S subunit. The mitochondrial ribosome is considered to be protein-heavy, since it has less rRNA and more protein when compared to its prokaryotic and nuclear eukaryotic counterparts. The 16S mitochondrial rRNA is approximately half the size of the prokaryotic 16S rRNA, while the 12S mitochondrial rRNA is approximately 40% smaller than the prokaryotic 12S rRNA (O'Brien, 2003). The rRNAs have not been shortened in random places, but tend to be missing specific structures that have been compensated for by the additional ribosomal proteins (Glotz *et al*., 1981; O'Brien, 2003; Zwieb *et al.*, 1981).

Although the rRNAs are encoded by the mtDNA, all the proteins involved with the mitochondrial ribosome are encoded by the nuclear genome. The human mitochondrial ribosome is composed of 78 identified proteins, although it is speculated that it may be composed of 85 to 100 proteins. Of the 78 identified proteins, 30 proteins are associated with the 28S ribosome subunit and 48 proteins are found in the 39S ribosome subunit (O'Brien, 2003).

Using the universal genetic code, 32 tRNAs (Crick, 1966) would be required to fully translate the mitochondrial mRNAs. However, there are only 22 tRNAs encoded by the mtDNA and no evidence of tRNA import into the mitochondrion; translation of the mitochondrial mRNAs occur via a unique genetic code, known in vertebrates as the

vertebrate mitochondrial genetic code. Although the majority of this genetic code is common with the universal genetic code, there are a few significant differences. These differences include the AUA codon, which codes for isoleucine in the universal genetic code, but codes for methionine in the vertebrate mitochondrial genetic code. The stop codon, UGA, in the universal genetic code codes for tryptophan in the vertebrate mitochondrial genetic code. The codons AGA and AGG, encoding arginine in the universal code, functions as stop codons in the mitochondria (Watanabe and Yokobori, 2011).

Once the mitochondrial mRNAs have been translated into the 13 proteins required for the OXPHOS complexes, they must be inserted into the IMM (Liu and Spremulli, 2000). The association of the mitochondrial ribosome with the IMM allows the synthesis of proteins encoded by the mtDNA to be coupled with their insertion into the IMM (Ott and Herrmann, 2010).

As mentioned earlier, all the proteins involved in the transcription and translation of the mtDNA are encoded by the nDNA and therefore defects in any of these proteins can result in mitochondrial disease. Many of these disorders result in structural defects of the mtDNA, such as the multiple mtDNA rearrangements found in mtDNA or mtDNA depletion syndromes (MDSs) (to be discussed further below).

1.2.5 Replication of the Mitochondrial Genome

Replication of the mtDNA, unlike the nDNA, is not linked to the cell cycle, but occurs throughout the cell cycle (Bogenhagen and Clayton, 1977; Holt and Reyes, 2012). As with transcription, the machinery involved in the replication of the mtDNA is encoded

by the nDNA. The replication machinery includes the mitochondrial helicase TWINKLE, POLγ, mtSSB, and POLRMT. There are three proposed mechanisms for the replication of the mtDNA: 1) asymmetric strand model, 2) strand coupled model and 3) Ribonucleotides are Incorporated ThroughOut the Lagging Strand (RITOLS) model (Holt and Reyes, 2012).

Among these mechanisms for mtDNA replication, the basic machinery and the start site for the H-strand are the same. There is only one DNA polymerase found in mitochondria, POLγ. POLγ is a 5`-deoxyribose phosphate (dRP) lyase with 3` to 5` exonuclease activity (Falkenberg *et al*., 2007; Graziewicz *et al.*, 2006). The human POLγ is composed of two subunits, a catalytic subunit (POLγA), which has the active site of POLγ, and the accessory subunit (POLγB). The functional holoenzyme is a heterotrimer with one POLγA subunit and two POLγB subunits ($POL\gamma AB_2$) (Yakubovskaya *et al*., 2006). Although POLγA contains the catalytic activities of POLγ, POLγB increases both the catalytic activity and processivity of POLγ. The reason for this is unknown, but may be due to POLγB's ability to bind DNA (Kaguni, 2004).

The mitochondrial replisome also includes the mitochondrial helicase TWINKLE, which forms either a hexamer or heptamer that catalyzes the ATP-dependent unwinding of the mtDNA (Ziebarth *et al.*, 2010). TWINKLE is capable of unwinding DNA on its own, but is more efficient when working in unison with POLγ in the replisome (Falkenberg *et al.*, 2007). In addition, mtSSB is also found in the replisome. MtSSB forms a tetramer that binds 50-70 nucleotides of ssDNA (Kaguni, 2004). During replication, the mtSSB binds to the ssDNA of the lagging strand as the replication fork proceeds, which stabilizes the ssDNA. MtSSB also has a stimulatory effect on the DNA

unwinding by TWINKLE, which may be due to a physical interaction of mtSSB with TWINKLE (Falkenberg *et al.*, 2007; Korhonen *et al.*, 2003).

The three proteins discussed above form the basic mitochondrial replisome, but it is thought that there are many other proteins involved. Since the mtDNA is supercoiled, it requires a topoisomerase to relieve the supercoiling. Mitochondrial topoisomerase (TOP1mt) is capable of relaxing negative supercoiling and is thought to be the mitochondrial topoisomerase in vertebrate cells (Zhang *et al.*, 2004). RNase H1 is also thought to have a role in mtDNA replication because knockout mice for RNase HI (*RNaseh1*$^{-/-}$) have a decreased quantity of mtDNA (Cerritelli *et al.*, 2003). The function of RNase H1 is suspected to be in the removal of short RNA primers (Falkenberg *et al.*, 2007). As with transcription, the proteins involved in the mitochondrial replication are encoded by the nuclear genome, with defects in these proteins resulting in mtDNA mutations. Mutations in genes that encode proteins involved in replication have been linked to both multiple mtDNA rearrangements and MDSs (Spelbrink *et al*., 2001; Van Goethem *et al.*, 2001; Van Goethem *et al.*, 2003). These disorders will be discussed further in Section 1.4.

1.2.6 Repair Mechanisms of the Mitochondrial Genome

Many processes involving the mtDNA, such as replication and transcription, involve distinct proteins that differ from those used for the same processes in the nucleus. In contrast, mtDNA repair shows significant overlap with nDNA repair. Much of what we know about mtDNA repair is inferred from our understanding of nDNA repair (Kazak *et al.*, 2012). In recent years, there has been evidence to suggest that base excision repair

(BER) (Kazak *et al*., 2012; Takao *et al*., 2002), DNA break repair (Bacman *et al*., 2009; Kazak *et al.*, 2012; Thyagarajan *et al*., 1996), and mismatch repair (MMR) (de Souza-Pinto *et al*., 2009) do occur in the mitochondria (Kazak *et al.*, 2012). Historically, the lack of repair thought to be associated with mtDNA has been used to explain the higher mutation rate of the mtDNA as compared to the nDNA (to be discussed further below) (Wong, 2010). If repair is more prevalent in the mitochondrion than previously thought, lack of repair is not likely to play a significant role in the higher mutation rate. However, various repair mechanisms found in mitochondria, such as homologous repair (HR) and non-homologous end joining (NHEJ), can generate deletions in the mtDNA (Bacman *et al*., 2009; Kazak *et al*., 2012; Thyagarajan *et al.*, 1996) and thereby contributing to the higher mutation rate.

1.3 Mitochondrial Genetics

1.3.1 Inheritance and Transmission of the Mitochondrial Genome

The inheritance of mtDNA does not behave according to the principles of classical Mendelian genetics. One major difference is the maternal inheritance observed in mammalian mtDNA. Two mechanisms have been proposed to explain the maternal inheritance: 1) the much larger quantity of mtDNA in the oocyte, as compared to that of the spermatozoan (John *et al.*, 2010), favors maternal inheritance, or 2) there is active elimination of the paternal mtDNA in the zygote (St John *et al.*, 2000).

The human gametes are not equal in their mitochondrial content. A mature human oocyte contains between 75 000 and 100 000 mitochondria, or approximately 200 000 copies of the mtDNA (John *et al.*, 2010). In contrast, the human spermatazoan

contains only 22 to 28 mitochondria, and thereby fewer than 100 mtDNA copies (Otani *et al.*, 1988). Since the paternal mtDNA comprises less than 0.1% of the total mtDNA in the zygote, the inheritance of the maternal mtDNA is favored. This is a passive mechanism for maternal inheritance. If it were the only mechanism for maternal inheritance, we would expect predominantly maternal inheritance, but with some reported cases of partial paternal inheritance. Thus far, there has only been one reported case of partial paternal inheritance in humans (to be discussed further below).

Interspecies crosses in murine models (Kaneda *et al.*, 1995; Shitara *et al.*, 1998) and a bovine model (Sutovsky *et al.*, 2000) have identified biparental inheritance of mtDNA. Intraspecies crosses in these same studies showed no detectable paternal mtDNA past the 4-to 8-cell stage. This is in agreement with humans, which appear to have paternal mtDNA eliminated by the 8-cell stage (St John *et al.*, 2000; Sutovsky *et al.*, 2000). Since maternal inheritance patterns are not observed in interspecies crosses, a more active species-specific mechanism that identifies and eliminates paternal mtDNA is likely.

Ubiquitination of the paternal mitochondria has been proposed as an active mechanism to eliminate the paternal mtDNA. Ubiquitin is associated with the mitochondrial sheath in the sperm of bulls, mice, rat, rhesus monkeys and humans (Cummins *et al*., 1997; Kaneda *et al*., 1995; Shalgi *et al*., 1994; Sutovsky *et al*., 1999; Sutovsky *et al*., 1996). Once the spermatozoan fertilizes the oocyte, the paternal mitochondria, which are ubiquitinated during spermatogenesis, appear to be degraded. This results in maternal inheritance of mtDNA (Sutovsky *et al.*, 2000).

As mentioned above, there has been only one documented case of paternal inheritance of mtDNA in humans. Schwartz and Vissing (Schwartz and Vissing, 2002) reported a 28-year-old male patient who had exercise intolerance and severe lactic acidosis after only minor physical exertion. Analysis of a muscle biopsy revealed 15% ragged-red fibers (RRFs) and a Complex I deficiency. Sequencing of the mtDNA from blood and muscle revealed a 2 bp deletion in the *ND2* gene in the patient's muscle, which was not detected in the mtDNA from the patient's blood. However, the more surprising finding was that the mtDNA from the blood was maternal, whereas the mtDNA found in muscle was paternal in origin. This is the only report in the literature of partial paternal mtDNA inheritance in humans, although the etiology for this observation remains unknown.

The presence of hundreds to thousands of mtDNA copies per cell, as compared to only two copies of the nDNA, is one of the factors that leads to non-Mendelian inheritance patterns. In fact, mitochondrial genetics tend to be more like population genetics than like Mendelian genetics for this reason. Random genetic drift and selection have significant roles in the inheritance of mtDNA from one generation to the next (Fan *et al.*, 2008; Jenuth *et al.*, 1997; Stewart *et al.*, 2008), as discussed further below.

1.3.2 Haplotypes and Polymorphisms Associated with the Mitochondrial Genome

The mtDNA contains numerous polymorphisms, some of which are used to classify haplotypes. A haplotype is defined as a minimum of two polymorphisms that make up a multisite haploid genotype on a single chromosome. The polymorphisms can include small insertions or deletions (indels) or single nucleotide polymorphisms (SNPs)

(Templeton, 2005), and those identified in mtDNA have been found in either the coding region or the NCR (Van Oven and Kayser, 2009). The mtDNA haplotypes have been extensively used to trace the origins and migration of humans (Cann *et al.*, 1987; Torroni *et al.*, 2006; Van Oven and Kayser, 2009) and have also been found to influence disease. Some haplotypes are over-represented in given disorders, suggesting that they may be a risk factor for that particular disorder (Wallace *et al.*, 1999). On the other hand, there are other specific haplotypes that are under-represented in some disorders, suggesting they might confer protective effect in these disorders (Poulton *et al.*, 2002). The over and under-representation of haplotypes has led to speculation that mtDNA background may modify many disorders due to subtle variations in the functional of OXPHOS.

Specific mtDNA polymorphisms, like the haplotypes, can also play a role in disease and have been found to affect the phenotypes of disorders that are either mtDNA-encoded or nDNA-encoded, likely due to small variations in mitochondrial OXPHOS(Hofmann *et al.*, 1997). Some polymorphisms in the mtDNA are more prevalent in association with specific mtDNA mutations, such as the m.16189T>C polymorphism found in association with multiple mutations in the mitochondrial gene $tRNA^{Leu(UUR)}$ (Marchington *et al.*, 1996). Therefore, any analyses of the mtDNA should include and assessment of haplotypes and SNPs.

1.3.3 Heteroplasmy and Threshold Effects

In light of the hundreds to thousands of mtDNA copies in each cell, it is not surprising that not all mtDNA copies are necessarily identical. Heteroplasmy is the term that describes the presence of multiple species of mtDNA within a single cell (DiMauro

and Schon, 2001). The level of heteroplasmy can be thought of as the "mitochondrial demographic", which can vary by tissue within an individual and even amongst cells within the same tissue. The mitochondrial demographic can also change over time, which can correlate with progression in the clinical phenotype of mitochondrial disorders (to be discussed further below) (Larsson *et al*., 1990).

The state of heteroplasmy can give rise to "threshold effects", which refers to the specific mutant load that must be present for a disease phenotype to be observed. Various disease presentations can be associated with different thresholds that can also vary by tissue. Thresholds are typically found between 60-90% mutant load (Tuppen *et al.*, 2010), although some mutations, such as the m.3233A>G mutation in mitochondrial encephalopathy, lactic acidosis, and stroke-like episodes (MELAS), can be symptomatic at a mutant load of less than 20%. Mutations with relatively high threshold, such as the m.8344A>G mutation in myoclonic epilepsy with ragged red fibers (MERRF), presents with over 80% mutant load (Wong, 2010) or are found at 100%, such as the mutations associated with Leber's hereditary optic neuropathy (LHON) (Saneto and Sedensky, 2013).

In addition to causing a disease phenotype, the mitochondrial demographic can also determine the severity of a phenotype. For example, Enns *et al.* have described individuals within a single family carrying the m.8993T>G mutation that conferred a disease phenotype above 60% (Enns *et al.*, 2006). Individuals who had between 60% and 75% mutant load had retinopathy, while individuals with a 75% to 90% mutant load had neurogenic muscle weakness, ataxia, retinitis pigmentosa (NARP). Family members with a greater than 90% mutant load presented with Leigh syndrome (Enns *et al.*, 2006; Wong,

2010). Even within the same individual, changes in the mitochondrial demographic can change the clinical phenotype. For example, a study by Larsson *et al.* described a patient who developed normally until the age of 7 years, at which point the patient came to clinical attention and was noted to have learning difficulties. The patient went on to develop vision and hearing loss by age 10, ataxia at 12 years of age, followed by muscular weakness at 14 years of age. The patient's condition continued to deteriorate until, at the age of 17 years, he could no longer walk. He died from cardiorespiratory failure at 19 years of age. This progression in phenotype correlated with an increase in the mutant loads for a 6.1 kilobase (kb) deletion, with muscle biopsies at the ages of 14, 16 and 17 revealing mutant loads of 52%, 59% and 80%, respectively (Larsson *et al.*, 1990).

The mitochondrial demographic can also change drastically from one generation to the next. In mice, the average level of heteroplasmy of all the offspring is roughly that of equal to the mother. However, each individual offspring could have a significantly different mitochondrial demographic compared to the mother (Chinnery *et al.*, 2000). Random genetic drift and the bottleneck in the female germline allows for rapid segregation of mtDNA from one generation to the next (Cree *et al.*, 2008; Jenuth *et al.*, 1996). Due to this segregation, it is not possible to accurately predict the mitochondrial demographic in offspring based solely on the mitochondrial demographic of the mother. The prediction of the mitochondrial demographic is further complicated apparent of selection against some mutations, which does not affect all mutations equally and therefore results in the inheritance of some mtDNA mutations (Fan *et al.*, 2008; Stewart *et al.*, 2008).

Although many of the examples used for heteroplasmy contrast a mutant mtDNA and a wild type (WT) mtDNA (i.e. an mtDNA without a disease causing mutation), this is not always the case. Heteroplasmy can also occur between two or more species of WT mtDNA. Homoplasmy has been considered to be the normal state of mtDNA, while heteroplasmy is considered the common state for mutations (Sharpley *et al.*, 2012). It has been suggested that heteroplasmy, even involving neutral polymorphisms, may be unstable and that homoplasmy is favored. This preference for homoplasmy has been suggested as the reason for the evolution of the maternal inheritance of mtDNA (Wallace, 2007). In support of this idea, mouse models with an admixture of two neutral mtDNA species, NZB and Balb/c, had reduced activity, reduced food intake, reduced respiratory exchange ratio, an accentuated stress response, and demonstrated cognitive impairment compared to their homoplasmic litter mates (Sharpley *et al.*, 2012). Although there seems to be a preference for homoplasmy, work performed by the Glerum lab has found that healthy individuals can be heteroplasmic for neutral mtDNA polymorphisms, with one individual having six different mtDNA species (Helmle *et al*, unpublished). This suggests that heteroplasmy may not be as detrimental as traditionally thought.

1.3.4 Mutations Found in the Mitochondrial Genome

The mtDNA has an approximately ten times higher mutation rate when compared with that of the nDNA (Brown *et al.*, 1979). This higher mutation rate may be due to the proximity of the mtDNA to reactive oxygen species (ROSs), a lack of protection for the mtDNA, crude repair mechanisms for the mtDNA and reduced proofreading by POLγ (Wong, 2010). It is likely that the higher mutation rate of mtDNA is due to a combination of these mechanisms.

The proximity of the mtDNA to the OXPHOS complexes in the IMM means the ROS generated during OXPHOS are also in close proximity to the mtDNA, leading to increased oxidative damage to the mtDNA and an increase in mutations of the mtDNA (Wong, 2010). Because the mtDNA was once thought to be "naked" and therefore less protected than the nDNA, the ROS-induced damage was viewed as a compounding factor. However, TFAM packages and protects the mtDNA, much the same as histones do for the nDNA (Bogenhagen, 2012), suggesting that oxidative damage, although it may result in a higher mutation rate, is not as significant as once thought.

In addition to ROS, the supposed lack of DNA repair in mitochondria was thought to contribute to the higher mtDNA mutation rate. As discussed above, it has recently been demonstrated that there is DNA repair in mitochondria, making it unlikely that the lack of repair underlies the higher mutation rate. However, as discussed above, some of the repair pathways may actually generate mutations, such as deletions (Bacman *et al.*, 2009). Since there is much that is still unknown about DNA repair in the mitochondria it is unknown if the repair pathways are equivalent of those found in the nucleus.

It has also been hypothesized that the proof-reading ability of POLγ is reduced compared to the polymerases found in the nucleus. The human POLγ makes approximately one error for every 500 000 nucleotides synthesized (Longley *et al.*, 2001), which is higher than the approximately one error for every 10 million to 100 million nucleotides in the nDNA (Nachman and Crowell, 2000). Therefore, the decreased proof reading of POLγ does likely contribute to the higher mutation rate seen in the mtDNA.

Mutations of the mtDNA can be divided into two categories: mtDNA rearrangements and point mutations. Rearrangements include deletions, duplications and insertions. Rearrangements are usually not inherited but arise *de novo*, whereas point mutations are typically maternally inherited (Tuppen *et al.*, 2010). Approximately 85% of mtDNA rearrangements are found between O_H and O_L and are flanked by short direct repeat regions (Samuels *et al.*, 2004). This observation led to the hypothesis that many of the large-scale deletions are generated through a slipped-strand replication mechanism. The slipped-strand model is based primarily on the asymmetric strand replication model, and suggests that the ssDNA generated through replication is broken. The two ends of the break are then ligated together to form two mtDNA with deletions, one containing the NCR and one lacking the NCR. The mtDNA lacking the NCR cannot replicate and therefore is eliminated, while the mtDNA containing the NCR results in a mtDNA with a deletion (Krishnan *et al.*, 2008). Repair of the mtDNA has also been implicated in the formation of mtDNA deletions. As discussed above, NHEJ and HR can result in deletions of DNA. In this model, a double-strand break (DSB) would occur, and exonuclease activity would generate ssDNA on either side of the DSB. The ssDNA would then bind to microhomologies, which would subsequently be repaired and ligated, creating a mtDNA strand with a deletion (Krishnan *et al*., 2008).

1.4 Mitochondrial DNA in Disease

Individual mitochondrial disorders are rare. However, the combined mitochondrial disorders are the most common inherited metabolic disease, with an estimated incidence of approximately 1 in 5000 individuals (Saneto and Sedensky, 2013; Schaefer *et al*., 2004). Given the dual genomic origins for mitochondria, disorders of this

organelle can be caused by mutations of nuclear genes encoding mitochondrial proteins or mutations in the mtDNA. Mutations of nDNA tend to be more prevalent in children and are more severe, whereas mutations in the mtDNA tend to appear in adulthood. However, there are cases of mtDNA-based disorders in the pediatric population. The mutations in the nDNA can follow multiple patterns of inheritance, whereas mutations in the mtDNA are maternally inherited or sporadic (Saneto and Sedensky, 2013). Herein, the focus will be on mtDNA-based disorders with some mention of nDNA mutations that can cause defects in the mtDNA.

Mutations in the mtDNA have been linked to a wide variety of disorders, from certain forms of cancer to common neurodegenerative disorders. These mutations can affect any tissue at any time in life, but disproportionally affect more energy demanding tissues, such as muscle and neurons (Saneto and Sedensky, 2013; Schaefer *et al*., 2004). Most mutations in the mtDNA are heteroplasmic. MtDNA-based disorders can demonstrate both phenotypic and genotypic heterogeneity, with the same mutation causing multiple phenotypes or a similar phenotype being caused by multiple mutations, respectively (Tuppen *et al.*, 2010).

Holt *et al*. (Holt *et al.*, 1988) reported the first mtDNA deletions in patients with mitochondrial myopathies in 1988. Mitochondrial myopathies are a heterogeneous groups of disorders that can affect multiple systems and are typically characterized by morphological abnormalities of muscle mitochondria (DiMauro *et al.*, 1985). Mitochondrial myopathies can present with, but are not limited to, a combination of muscle weakness, external ophthalmoplegia, pigmentary retinopathy, dementia, ataxia, seizures, movement disorders, stroke-like episodes, deafness, peripheral neuropathy and

abnormal cardiac conduction (DiMauro *et al.*, 1985; Holt *et al.*, 1988). Holt *et al*. examined the mtDNA in leukocytes from 38 patients with mitochondrial myopathies, 44 unaffected relatives and 35 healthy control subjects. Muscle biopsies were also examined from 25 patients with mitochondrial myopathies and 18 control subjects (either normal or with an unrelated neurological disorder). There were no identified mtDNA mutations in the leukocyte samples, but nine of the 25 muscle biopsies had two populations of mtDNAs: a WT mtDNA and a mtDNA with a deletion. These deletions were not found in the control subjects. Therefore, the mtDNA deletions were concluded to be the underlying cause of the mitochondrial myopathies in these nine patients. This study was also the first documented case of mtDNA heteroplasmy in humans (Holt *et al.*, 1988).

In the same year that the first mtDNA deletion was reported, the first disease causing point mutation was also identified in mtDNA. Wallace *et al.* (Wallace *et al.*, 1988) sequenced approximately 85% of the coding sequence of the mtDNA of a patient from an African American family in Georgia who had demonstrated maternal inheritance of LHON. LHON is characterized by initial unilateral acute or subacute central painless vision loss that spreads to the other eye within two months of onset. LHON typically presents between 20 and 40 years of age (Saneto and Sedensky, 2013). Wallace *et al.* found 25 base substitutions that differed from the Cambridge reference sequence (CRS), which was the mtDNA reference sequence at the time. To distinguish which of these 25 base substitutions might be the disease causing mutation, Wallace *et al.* used three criteria: the base substitution 1) must have changed an evolutionarily conserved amino acid, 2) must be commonly found in LHON patients and 3) and must not be found in control subjects. Applying these criteria, Wallace *et al.* identified the disease-causing

mutation to be m.11778G>A, as it results in a conserved arginine residue at position 340 in ND4 being replaced by a histidine residue (Wallace *et al.*, 1988).

In the ensuing 25 years there have been over 600 pathogenic mutations reported in the mtDNA. These mutations include over 130 different mtDNA deletions and a handful of mtDNA insertions, as well as more than 500 point mutations. These mutations have been found in both the coding and non-coding regions of the mtDNA and cause a wide variety of disorders (Ruiz-Pesini *et al.*, 2007). The two most prevalent mtDNA-based disorders are LHON and MELAS (Saneto and Sedensky, 2013), both of which are caused by several different point mutations.

MELAS is the most common mtDNA mutation based disorder with a prevalence of 3.65 per 100 000 individuals (Schaefer *et al.*, 2008). This is a progressive neurodegenerative disorder is associated with headaches, seizures that are resistant to treatment, short stature, exercise intolerance, muscle weakness, diabetes, progressive dementia and sensorieneural hearing loss. In neuroimaging studies, stroke-like lesions are often transient and predominantly affect the gray matter of the brain (Hirano and Pavlakis, 1994). The most common mtDNA mutation that causes MELAS, found in approximately 80% of patients, is the m.3243A>G change in the $tRNA^{Leu}$ gene (Goto *et al.*, 1990). Other mutations that have been associated with MELAS include m.3271T>C (Goto *et al.*, 1991), m.1642G>A (Taylor *et al.*, 1996), m.13513G>A (Shanske *et al.*, 2008), m.12770A>G and m.13045A>C (Liolitsa *et al.*, 2003).

LHON is only slightly less common than MELAS, with an incidence of 3.13 per 100 000 individuals (Schaefer *et al.*, 2008). Unlike the majority of mtDNA mutations,

which are heteroplasmic, most mutations associated with LHON are homoplasmic. The LHON mutations m.11778G>A, m.3460G>A and m.14484T>C make up 95% of the documented cases of LHON (Saneto and Sedensky, 2013).

Deletions that underlie mitochondrial disease can occur at almost any region of the mtDNA, but as mentioned above, approximately 85% of the known deletions occur between the O_H and O_L. The only portion of the mtDNA that has not been reported in association with a deletion is the D-loop, which is thought to be resistant to deletions as a mtDNA molecule lacking the control elements in this region would be unable to replicate. Deletions of the mtDNA can range from only a few nucleotides to a few kbs in size (Ruiz-Pesini *et al.*, 2007), with both "small deletions", which are smaller than one kb, and "large-scale deletions", which are larger than one kb. Of the large-scale deletions that have been reported, the smallest is 1.3 kb (Moraes *et al*., 1989) and the largest is 10, 987 bp (Miyabayashi *et al.*, 1991). The 1.3 kb deletion was found in a patient with progressive external ophthalmoplegia (PEO) (also known as chronic PEO (CPEO)), which is an ocular myopathy (Moraes *et al.*, 1989). The 10, 987 bp deletion was found in a patient with an encephalomyopathy who presented at 4 months with a lack of head control and abnormal eye movements. A computed tomography (CT) scan revealed diffuse mild atrophy of the brain. The patient's lactate and pyruvate levels were intermittently increased and the age of 2 years, the patient developed severe sensorineuronal hearing loss. The patient suddenly died from cardiac arrest at 3 years of age (Miyabayashi *et al.*, 1991).

In studies that examined patients with PEO and Kearns-Sayre syndrome (KSS), deletions were identified that ranged from 1.3 kb to 7 kb in size. The majority of reported

deletions occurred only in a single individual, but one specific deletion occurred in multiple unrelated individuals and is therefore referred to as the "common deletion" (Moraes *et al*., 1989; Schon *et al.*, 1989). The common deletion has been linked to KSS, CPEO and Pearson syndrome (PS), as well as general mitochondrial myopathies (Moraes *et al.*, 1989; Schon *et al.*, 1989; Tuppen *et al.*, 2010). The common deletion is 4, 977 bp and is located between nucleotides 8, 468 and 13, 446 and flanked by 13 bp repeat sequences. The common deletion has the 5` breakpoint in the *ATP 8* gene and the 3` breakpoint in the *ND5* gene. This deletion causes the *ATP 8* transcript to be truncated from 68 amino acids to 42 amino acids. In the *ND5* transcript, the common deletion causes a frame shift that results in a premature termination codon 12 nucleotides beyond the deletion breakpoint. Along with the effects on *ATP 8* and *ND5*, the common deletion also results in the complete elimination of the genes for *ATP 6, COIII, ND3, ND4L, ND4,* $tRNA^{Gly}$, $tRNA^{Arg}$, $tRNA^{His}$, $tRNA^{Ser}$, and $tRNA^{Lys}$. The common deletion is thought to arise either through the slipped-strand replication mechanism or by intramolecular homologous recombination. The 13 bp repeats on either side make this location a "hot spot" for deletions by either of these mechanisms. Although other areas of the mtDNA do have repeat sequences, deletions from these repeats would result in deletion of the D-loop region and thus these mtDNA variants would not be viable for replication (Schon *et al.*, 1989).

Mutations in nuclear genes can also cause defects in the mtDNA, which can lead to MDSs or multiple mtDNA deletions (Elpeleg *et al*., 2002). MDSs are typically inherited in an autosomal recessive manner and present with a variety of clinical phenotypes, which all show a severe reduction in the mtDNA content (El-Hattab and

Scaglia, 2013). Some of the more common clinical phenotypes associated with MDSs are severe muscle weakness, hepatic failure and renal tubulopathy. MDSs usually present in childhood, and tend to be fatal (Elpeleg *et al.*, 2002). MDSs are caused by mutations in proteins involved in either mitochondrial deoxyribonucleoside triphosphate (dNTP) synthesis or mtDNA replication (El-Hattab and Scaglia, 2013).

A single deletion in the mtDNA arises either through errors in replication or errors in repair, but does not suggest an underlying nDNA mutation. However, multiple deletions in the mtDNA suggest a mutation in a nuclear gene involved in mtDNA maintenance. For example, an autosomal dominant and autosomal recessive form of PEO have been associated with to multiple mtDNA deletions (Elpeleg *et al.*, 2002) and mutations in *POLγ* (Van Goethem *et al*., 2001; Van Goethem *et al*., 2003). Mutations in *C10orf2* (which encodes TWINKLE) (Spelbrink *et al*., 2001), *ANT1* (Kaukonen *et al*., 2000) and ribonucleotide reductase M2 B (*RRM2B*) (Tyynismaa *et al.*, 2009) have been implicated in the autosomal dominant form of PEO. Mutations in these genes result in multiple mtDNA deletions PEO, which is a disorder characterized by mtDNA deletions, is therefore seen when there are either somatic mutations in the mtDNA or in the nDNA genes encoding components of the mtDNA replication and maintenance machinery.

The disorders discussed above have all been linked to mtDNA by either the presence of a primary mtDNA mutation or a mutation in a nuclear gene that results in defects in the mtDNA. The mtDNA also plays an important role in human disease, as it can influence the presentation of many disorders (Tuppen *et al.*, 2010). Mutations in the mtDNA have also been proposed to play a role in aging (Pak *et al.*, 2005), in common neurodegenerative disorders such as Alzheimer's disease (Coskun *et al.*, 2004) and in

certain forms of cancer, although some of the reported mutations in tumors have been found to be incorrect (Baysal, 2006; Salas *et al*., 2005). In these types of diseases, it is likely that mtDNA mutations do play a role, although the primary defect lies elsewhere. The involvement of mtDNA variants in these three pathologies is still unclear and much more work is required to elucidate the mtDNA's role.

Unfortunately, there are no proven therapies for mitochondrial disorders. Treatment usually involves addressing the symptoms and using preventative measures, such as maintaining optimal health and decreasing physiological stress, to avoid stress which can worsen mitochondrial disorders. Antioxidants, such as coenzyme Q, are also used as supplements, in an effort to maximize antioxidant defenses that are typically found in mitochondria (Parikh *et al*., 2009).

1.5 Mitochondrial DNA Diagnostics

1.5.1 Clinical Diagnostics for Mitochondrial Disorders

Mitochondrial disorders can present with various symptoms, affect various tissues, and can arise at any point in life, making clinical diagnosis difficult (Munnich *et al*., 1996). At present, there are no universal diagnostic criteria for mitochondrial disorders. The diagnosis of mitochondrial disorders is based on a multidisciplinary approach that involves clinical, biochemical, histological and molecular examinations. The clinical examination can include a detailed family history, physical and neurological examinations and imaging studies (Naviaux, 2004).

1.5.2 Biochemical and Histological Diagnostics

The tissue used for these studies is important in obtaining accurate results. As discussed above, the mitochondrial demographic and mitochondrial content can vary by tissue. Histological and biochemical studies are typically carried out on skeletal muscle biopsies or cultured skin fibroblasts (Mancuso *et al.*, 2009; Siciliano *et al.*, 2007).

For histological studies, skeletal muscle biopsies are examined for either abnormal morphology of the mitochondria, or for abnormal mitochondrial proliferation. Three main tools are used to identify mitochondrial abnormalities from skeletal muscle biopsies: examination for RRFs, succinate dehydrogenase (SDH) stains and cytochrome *c* oxidase (COX) activity stains. The presence of RRFs, named so because of their appearance, is indicative of mitochondrial proliferation and can be observed by using either immunohistochemistry with anti-mitochondrial antibodies (Yuri *et al*., 2008) or modified Gomori trichrome staining (DiMauro *et al.*, 2004; Engel and Cunnigham, 1963; Mancuso *et al.*, 2009). RRFs are typically associated with mutations in the tRNAs (Mancuso *et al.*, 2009; Pillen *et al.*, 2006). However, the age of the individual should be taken into account when examining for RRFs. It is notable that older individuals tend to have some RRFs, even in the absence of a mitochondrial disorder. Generally, there should be no RRFs in healthy individuals under 30 years of age, and less than 2 % in healthy individuals over 50 years of age (Bernier *et al.*, 2002; Walker *et al.*, 1996). Higher quantities of RRFs are indicative of a mitochondrial disorder.

Staining for activity of SDH and COX is another diagnostic approach in mitochondrial disease. SDH staining cannot identify mtDNA mutations since SDH

(Complex II) is fully encoded by the nDNA, therefore SDH-staining is useful in determining mitochondrial mass. COX staining, on the other hand, can reveal an mtDNA mutation, which appears as COX-deficient fibers in a muscle specimen (DiMauro *et al.*, 2004; Mancuso *et al.*, 2009). A positive SDH stain with the appearance of COX-negative fiber indicates a defect in mtDNA protein synthesis (DiMauro *et al.*, 2004). It can also suggest a defect in either a COX subunit (which can either result from an mtDNA or nDNA mutation) or a COX accessory protein, such as SCO2 or SURF1 (DiMauro *et al.*, 2004; Sue *et al.*, 2000). Fibers that stain positive for SDH and COX suggest a defect in one of the other ten protein coding genes of the mtDNA, excluding the three mtDNA-encoded COX subunits. An exception to this is found in patients with MELAS, that are positive for both SDH and COX (DiMauro *et al.*, 2004). In this manner, the histological assays can identify a mitochondrial disorder and suggest possible underlying causes.

Biochemical assays for mitochondrial diagnostics can also be performed on skeletal muscle biopsies. Measurements of respiratory chain enzymes activity can indicate the presence of a mitochondrial disorder and identify, whether the presentation is due to a single enzyme deficiency (structural defect) or whether multiple complexes are affected (protein synthesis).

Other biochemical assays used to identify mitochondrial disorders include O_2 consumption, which is performed on isolated mitochondria (Will *et al.*, 2007), or measuring ATP production, which is typically performed on cultured fibroblasts (Shepherd *et al.*, 2006). Although the biochemical and histological studies outlined above can suggest an underlying cause, molecular studies are essential in identifying the molecular basis for a mitochondrial disorder.

1.5.3 Molecular Diagnostics for Mitochondrial DNA

As discussed above, mitochondrial disorders are typified genetic and phenotypic heterogeneity, making genotype-phenotype correlations difficult in most cases. The histological and biochemical assays described above can give insights to the possible molecular etiology of a mitochondrial disorder and can be used to direct the molecular testing needed to elucidate the underlying cause of mitochondrial disorders. As with the clinical diagnostic criteria, there are no universal molecular diagnostic criterion for mtDNA analysis (Carracedo *et al.*, 1998), with approaches determined on a lab-by-lab basis.

For molecular analysis of the mtDNA, tissue selection is very important, since the mtDNA can vary by tissue. For example, although many point mutations can be detected in blood, mtDNA rearrangements and some point mutations, such as the MELAS m.3243A>G change (McDonnell *et al*., 2004), are not typically detectable in blood (Wong *et al*., 2010). Therefore, most mtDNA diagnostics, a muscle biopsy is the preferred sample. Since a traditional muscle biopsy is very invasive (Siciliano *et al.,* 2007), some physicians prefer to attempt preliminary diagnostic approaches with other tissues (Wong *et al.*, 2010), such as oral mucosa, hair follicles, epithelial cells from urine, and cultured fibroblasts (DiMauro *et al.*, 2004; Mancuso *et al*., 2009; McDonnell *et al.*, 2004).

One of the classical methods used to detect mtDNA rearrangements is Southern blotting (DiMauro *et al.*, 2004; Mancuso *et al*., 2009; Schon *et al*., 2002; Shanske and Wong, 2004), with digestion of DNA with by restriction enzymes with *Pvu*II and *Bam*HI,

which both cut the mtDNA only once. The mtDNA is thereby linearized and can then be analyzed by a standard Southern blotting protocol and a mtDNA-specific probe. MtDNA from a healthy control sample will be visualized as a single band of ~16.6 kb. However, if a rearrangement is present there will be multiple bands, as heteroplasmy is the normal in patients. Under these circumstances the WT mtDNA will appear as a band of 16.6 kb, while another band will correspond to the mtDNA with the rearrangement (Schon *et al.*, 2002). Since agarose gel electrophoresis separates DNA by size, this method allows the size of the deletion to be determined. Furthermore, by comparing the densities of the bands, the level of heteroplasmy can be estimated for the tissue examined (DiMauro *et al.*, 2004). Through the use of various restriction enzymes the position of the rearrangement can also be determined (Bai and Wong, 2005). The Southern blotting approach can also be used to detect MDSs through the use of normalizing the quantities of DNA (DiMauro *et al.*, 2004). The problems associated with Southern blotting, for the purpose of mtDNA diagnostics, are the requirement for large amounts of DNA, and a lack of sensitivity to low levels of heteroplasmy (Bai and Wong, 2005).

MtDNA rearrangements can usually be identified using polymerase chain reaction (PCR), usually using quantitative PCR (qPCR), which allows both detection of mtDNA rearrangements and quantification of the rearrangements. MtDNA Taqman probes for *$tRNA^{Leu\ (UUR)}$, ND4, ATP 8* and the D-loop region have been used in qPCR and can be compared to the nDNA markers *AIB1, β*-2-microglobulin and β-actin to determine mtDNA content (Bai and Wong, 2005; von Wurmb-Schwark *et al.*, 2002). Long-range PCR is a more sensitive approach to detecting deletions of the mtDNA, especially those that are present at low levels of heteroplasmy. In long-range PCR, primers are used on

either side of the deletion, and the size of the product indicates whether the deletion is present (Mancuso *et al.*, 2009). PCR-based approaches are more sensitive than Southern blotting, but are more prone to "contamination" from NUMTs if precautions, such as the use of mtDNA-specific primers that have been verified using ρ^o cells or the use of purified mtDNA, are taken.

The identification of mtDNA point mutations, particularly in the absence of a family history, is challenging. To confirm a specific suspected point mutation, PCR/ restriction fragment length polymorphism (PCR/RFLP) analysis can be used (Mancuso *et al*., 2009; Shanske and Wong, 2004; Wong and Boles, 2005b). The segment of DNA to be examined can be amplified by PCR and the PCR product digested using a restriction enzyme that differentiates between the WT and the mutated sequence. Subsequent agarose gel electrophoresis allows visualization of differences in migration of the fragments that have been cleaved by the restriction enzyme (Shanske and Wong, 2004). A drawback to PCR/RFLP analysis is that, only one mutation can be examined at a time. Clearly this approach is impractical when looking for mutations at multiple loci, as would be the case in seeking to identify unknown mutations.

When investigating a patient sample for unknown point mutations, an allele-specific oligonucleotide (ASO) dot blot analysis can be useful. An ASO dot blot can examine a sample for multiple point mutations, with the more common point mutations being targeted. Typically, a multiplex PCR is used to interrogate in three mutational hotspots that cover the $tRNA^{Leu(UUR)}$, $tRNA^{Lys}/ATP$ and *ND4* regions. A small amount of the multiplex PCR is then applied to a Biodyne B+ membrane, which has an ASO probe specific for a particular mutation hybridized to the membrane. A different membrane is

prepared for each mutation, with the WT sequence ASO serving as a control (Shanske and Wong, 2004; Wong and Senadheera, 1997). An ASO dot blot is capable of detecting lower levels of heteroplasmy as compared to PCR/RFLP, and is much better suited for examining multiple mutations (Wong and Senadheera, 1997).

The assays described above can identify the common point mutations or any mutation that has been previously found in a mitochondrial disease patient. To detect unknown point mutations, single-stranded conformation polymorphism (SSCP), temperature gradient gel electrophoresis (TTGE), denaturing gradient gel electrophoresis (DGGE) or denaturing high performance liquid chromatography (dHPLC) can be used (Shanske and Wong, 2004; Wong and Boles, 2005b). All of these methods rely on amplifying a limited region of the mtDNA, followed by protocol-specific denaturation and reannealing to form heteroduplexes or homoduplexes. Subsequent chromatography or electrophoresis separates the species and allows identification of the region of mtDNA that bears the mutation, followed by sequencing to determine the mutation (Shanske and Wong, 2004; van den Bosch *et al.*, 2000; Wong and Boles, 2005a). Sequencing is considered to be the "gold" standard in identifying specific mtDNA point mutations. A drawback of Sanger sequencing, which has traditionally been used, is that it is insensitive to heteroplasmy that is below 30% (Wong and Boles, 2005b).

Next-generation sequencing (NGS) has decreased the time and cost of sequencing in recent years and has largely supplanted Sanger sequencing (Mardis, 2008). NGS uses parallel sequencing of either clonally amplified or single DNA molecules spatially separated in a flow cell (Voelkerding *et al.*, 2009). Although the general principals are the same between various NGS platforms, the exact mechanism used in NGS varies by

platform, with the Roche/454 FLX using a pyrosequencing approach, the Illumina/Solexa Genome Analyzer system using a sequencing-by-synthesis approach, and the Applied Biosystems SOLiD system working with an emulsion PCR approach (Mardis, 2008). Mardis (2008) has provided a detailed review of each of these systems, which is beyond the scope of this thesis. The advent of NGS has made mtDNA sequencing more feasible and largely replaced many of the above approaches for detecting mtDNA point mutations (Iacobazzi *et al*., 2013; Zaragoza *et al.*, 2010).

Most of the approaches to analyze mtDNA involve PCR, which is complicated by the potential amplification of NUMTs. The false positives that arise from NUMTs can be avoided if the mtDNA is pre-purified (i.e. the nDNA is eliminated from the sample), or if carefully selected mtDNA specific primers are used (Calvignac *et al.*, 2011; Yao *et al.*, 2008). The specificity of primers should always be tested using ρ^o cells, which lack mtDNA (Vergani *et al.*, 2000). A lack of amplification when on DNA from ρ^o cells is used as a template indicates that the primers are not amplifying NUMTs. Failure to verify mtDNA-specific primers has led to a proliferation of missannotation with respect to mtDNA mutations (Zhang and Hewitt, 1996).

An example of such misannotation is the study by Thangaraj *et. al*. (Thangaraj *et al.*, 2003) that claimed to have found numerous mtDNA mutations in the sperm of a patient with low sperm motility. Yao *et al*. (Yao *et al.*, 2008) demonstrated that Thangaraj *et al.* had amplified a previously identified NUMT of 5842 bp found on chromosome 1 (Herrnstadt *et al.*, 1999). Misannotation remains a considerable problem in the study of mitochondrial genetics, one that could be alleviated if purified mtDNA were available.

The assays described above are used to find variations in sequence as compared to a reference sequence, typically the rCRS. These variations are frequently referred to as "mutations", although not all sequence variants are pathogenic mutations, but rather neutral polymorphisms (Wong and Boles, 2005b). In distinguishing pathogenic mutations from neutral polymorphisms, the mtDNA sequence must be examined in the context of the haplotype and ethnicity, as this could help identify neutral polymorphisms. If a base substitution changes a conserved site, such as those involved in the structure of the RNAs or polypeptides, it is more likely to be a pathogenic mutation (Wallace *et al.*, 1988). *In vitro* studies must also be done to verify the pathogenicity, but this is done only on a research basis and cannot be done in a molecular diagnostic setting.

1.6 The Use of Microfluidic Chip Technology

Microfluidics is the science of fluid manipulation on the micrometer scale (Beebe *et al*., 2002) and has given rise to microfluidic chip (MFC), also known as "lab-on-a-chip", technologies that incorporate many aspects of chemistry and biology laboratories on small microchips (Beebe *et al.*, 2002; Fiorini and Chiu, 2005; Ramsey *et al*., 1995). In the past few decades, there have been numerous techniques that have successfully been adapted to MFCs, such as capillary electrophoresis (CE) (Barron and Blanch, 1995; Slater *et al.*, 2000; Slater *et al*., 2002), PCR (Kaigala *et al*., 2008; Lin *et al*., 2000; Liu *et al*., 2007; Wheeler *et al.*, 2011), heteroduplex analysis with single-stranded conformation polymorphisms (HA-SSCP) (Kourkine *et al.*, 2002; Taylor *et al.*, 2005), and cell sorting (Krüger *et al.*, 2002; Yao *et al.*, 2004).

MFC-based assays can offer numerous advantages over their macro-scale counterparts, enabling high-precision manipulation of samples and facilitating high-throughput analyses, as well as significantly reducing the cost and time when compared to macro-scale assays (Pan and Wang, 2011). The decrease in cost, time, and labour of MFC-based assays make them more feasible for large-scale studies. The higher precision also allows for more sensitive analysis, thus improving the limits of detection over traditional approaches. These qualities make MFCs appealing for use in numerous applications, including point-of-care (POC) diagnostics (Kuo and Chiu, 2011; Sia and Kricka, 2008).

As with any technology, there are also significant challenges associated with MFCs. The decreased scale of MFCs as compared to the traditional macro-scale assays, causes some forces to be more significant in MFCs (Beebe *et al*., 2002), and many assays therefore require novel approaches to be miniaturized and successfully incorporated on to MFCs.

1.6.1 Forces on the Micro-Scale

The physical and chemical influences that become dominant in electrophoresis at the micro-scale include such phenomena as adverse surface effects, electroosmotic flow (EOF), and laminar flow, as well as changes in diffusion and Joule heating (Beebe *et al.*, 2002; Wu *et al*., 2008). To successfully adapt electrophoresis-based assays for use on MFCs, these forces need to be taken into account.

MFCs have a higher surface area to volume ratio (SAVR) as compared to traditional assays, making the control of surface effects crucial to the success of MFC-

based assays (Beebe *et al.,* 2002; Han *et al.*, 2005; Wu *et al.*, 2008; Yates and Campbell, 2011). Non-specific adsorption of biomolecules, such as proteins and DNA, to the walls of capillaries in MFCs, a considerable challenge introduced by the significantly increased SAVR (Han *et al.*, 2005; Lucy *et al*., 2008; Situma *et al.*, 2006; Tegenfeldt *et al.*, 2004; Yates and Campbell, 2011). One approach to decreasing non-specific adsorption is through the modification of surface chemistry by the application of different surface coatings, which can include a variety of polymers and/or surfactants (Azadi and Tripathi, 2012; Doherty and Barron, 2004; Lucy *et al.*, 2008; Tegenfeldt *et al.*, 2004). These surface coatings serve to decrease interactions between the capillary surface and the biomolecules in an analyses as well as suppressing EOF (Doherty and Barron, 2004).

In addition to non-specific adsorption surface effects can also include surface tension, which is more prominent at the micrometer scale. Surface tension results from the cohesion between liquid molecules at the liquid/gas interface. The surface free energy is a measure of the surface tension of a liquid and influences the height that a liquid can travel through a capillary by capillary forces, which is inversely proportional to the radius of the capillary or MFC channel (Beebe *et al.*, 2002). Since the channels in MFCs are only micrometers in diameter, capillary action can readily be used to fill channels with liquids.

Another variable that can be significant at the micrometer scale is EOF. EOF is the counter flow of fluids under the influence of an electric field (Barron and Blanch, 1995; Fiorini and Chiu, 2005). EOF can be modulated by the zeta-potential of the surface, meaning that the chemical characteristics of the material and the surface modifications can significantly affect the EOF (Preywisch *et al.*, 2011; Sola and Chiari,

2012). The ionic strength of the buffer can also effect the EOF, with higher ionic strength resulting in a higher EOF (VanOrman *et al*., 1990), which results in decreased mobility and band broadening (i.e. reduced resolution) (Sola and Chiari, 2012; VanOrman *et al.*, 1990).

In addition to EOF, other types of flow are important to consider in MFCs. Turbulent flow is chaotic and the position of a particle cannot be predicted as a function of time, whereas laminar flow is not chaotic, meaning the velocity of a particle in a fluid stream can be predicted as a function of time. The flow of fluids can be described by the Reynolds number (Re), which is dependent on the density of the fluid, velocity of the fluid, fluid viscosity and the cross sectional area. An Re of under 2300 indicates laminar flow, while an Re of over 2300 is indicative of turbulent flow. Due to the decreased size of MFCs, laminar flow is the predominant flow-type, which allows for more control of the flow and can prevent two streams of fluids that are running parallel to each other from mixing by diffusion (Beebe *et al.*, 2002).

Diffusion is another force that is more prevalent in MFC-based assays. Diffusion describes the movement of particles from an area of higher concentration to an area of lower concentration until the overall concentration is homogenous. Diffusion over small distances occurs much more quickly than over larger distances, so in the micrometer distances used in MFCs, diffusion can rapidly affect the entire channel (Beebe *et al.*, 2002). This phenomenon can therefore be advantageous in MFCs, allowing quick and efficient mixing (Liu *et al.*, 2000). However, if mixing is not desired, it can be detrimental.

The final consideration to be discuessed here is Joule heating, which is heating caused by the passage of an electric field through a conductor. Joule heating can affect the performance of MFCs by: 1) increasing the temperature of the buffer, 2) generating radial temperature gradients within the channel and 3) creating a nonhomogeneous temperature gradient along the channel. Joule heating can decrease separation efficiency during electrophoresis, which can thus limit the electric field that can be used. The thermal conductivity of the material and the design of the MFC can play a critical role in the amount of Joule heating that occurs. Increasing the surface area to volume ratio allows for more heat dissipation thereby decreasing the effects if Joule heating. Since buffer is also important in Joule heating, as it is the conductor of the electric field (Wu *et al.*, 2008), the use of low molarity buffers decreases Joule heating in electrophoresis (Brody *et al*., 2004; Brody and Kern, 2004b; Ishido *et al*., 2010).

1.6.2 Fabrication Methods for Microfluidic Chips

The fabrication of MFCs occurs in various materials including glass, polymers and plastics. There are also numerous fabrication techniques used to generate MFCs including etching, hot embossing, injection molding and laser ablation. Each of these materials and fabrication techniques has different properties (Fiorini and Chiu, 2005). The materials properties can be either beneficial or detrimental, depending on the application, and therefore the choice of material and fabrication method is important in developing successful MFC-based assays. The material and fabrication methods used in MFCs will be discussed further in Chapter 4.

1.7 Electrophoresis

Gel electrophoresis is a common technique used in molecular biology to separate macromolecules, such as DNA and proteins, based on size, charge and conformation. Most electrophoresis is performed using either polyacrylamide or agarose as a separation medium. These polymers form a gel that, after placement in a buffer and applying an electric field, acts as a sieving matrix to separate the macromolecules (Barron and Blanch, 1995; Voet *et al*., 2008). The traditional gels that are used to perform gel electrophoresis are on the scale of centimeters, and will herein be referred to as slab gels. Our focus will be on gel electrophoresis for DNA separation.

Due to the phosphate backbone, DNA is negatively charged, and will move in the direction of the cathode during gel electrophoresis. The separation of DNA is based on size, with smaller fragments of DNA migrating more quickly than larger fragments (Barron and Blanch, 1995). Along with the size of the DNA fragments, their conformation can also affect their mobility during electrophoresis. In electrophoresis relaxed circular DNA fragments have the lowest mobility, while supercoiled circular DNA has the highest mobility, with linear DNA having an intermediate mobility (Akerman and Cole, 2002; Manage *et al*., 2008).

There are two main mechanisms that have been proposed to explain the movement of DNA during gel electrophoresis: the Ogston-Rodbard-Chrambach model and the reptation model (Figure 1.3) (Barron and Blanch, 1995). In the Ogston-Rodbard-Chrambach model (Figure 1.3A), the DNA molecule creates an “equivalent sphere”, due to a constantly changing orientation, that diffuses until it finds a large enough pore that it

can pass through. The Ogston-Rodbard-Chrambach model is thought to be more prevalent in polyacrylamide gels for small DNA fragments under 500 bp, but the model does not explain the mobility of larger DNA fragments (Barron and Blanch, 1995; Rodbard and Chrambach, 1970).

The reptation model assumes that randomly-coiled DNA molecules that are too large to go through the gel pores migrate in a "tube" using a "snake-like" movement around obstacles of the sieving matrix (Barron and Blanch, 1995; Slater *et al.*, 1988) (Figure 1.3B). The reptation model explains the movement of larger fragments of DNA more accurately than the Ogston-Rodbard-Chrambach model. The reptation model is thought to be the prevalent model for DNA mobility in agarose gels. Although the reptation model better fits the observed mobility of DNA, it does not completely explain the mobility of DNA molecules of greater than 40 kb (Barron and Blanch, 1995). To explain the mobility of larger DNA molecules, the biased reptation model, also known as reptation with stretching, was proposed. The model is based on the reptation model, but when the DNA becomes entangled on an obstacle within the sieving matrix, the DNA stretches and as it does, it is able to move off the obstacle and continue in a reptation-type mode (Barron and Blanch, 1995; Slater *et al*., 1988).

1.7.1 Trapping of Circular DNA During Electrophoresis

Large circular DNA molecules can be difficult to separate with direct current electrophoresis methods, primarily due to a phenomenon known as trapping, which occurs when circular DNA becomes ensnared on obstacles, or traps, in the sieving matrix. There are two models that have been proposed to explain trapping: 1) the

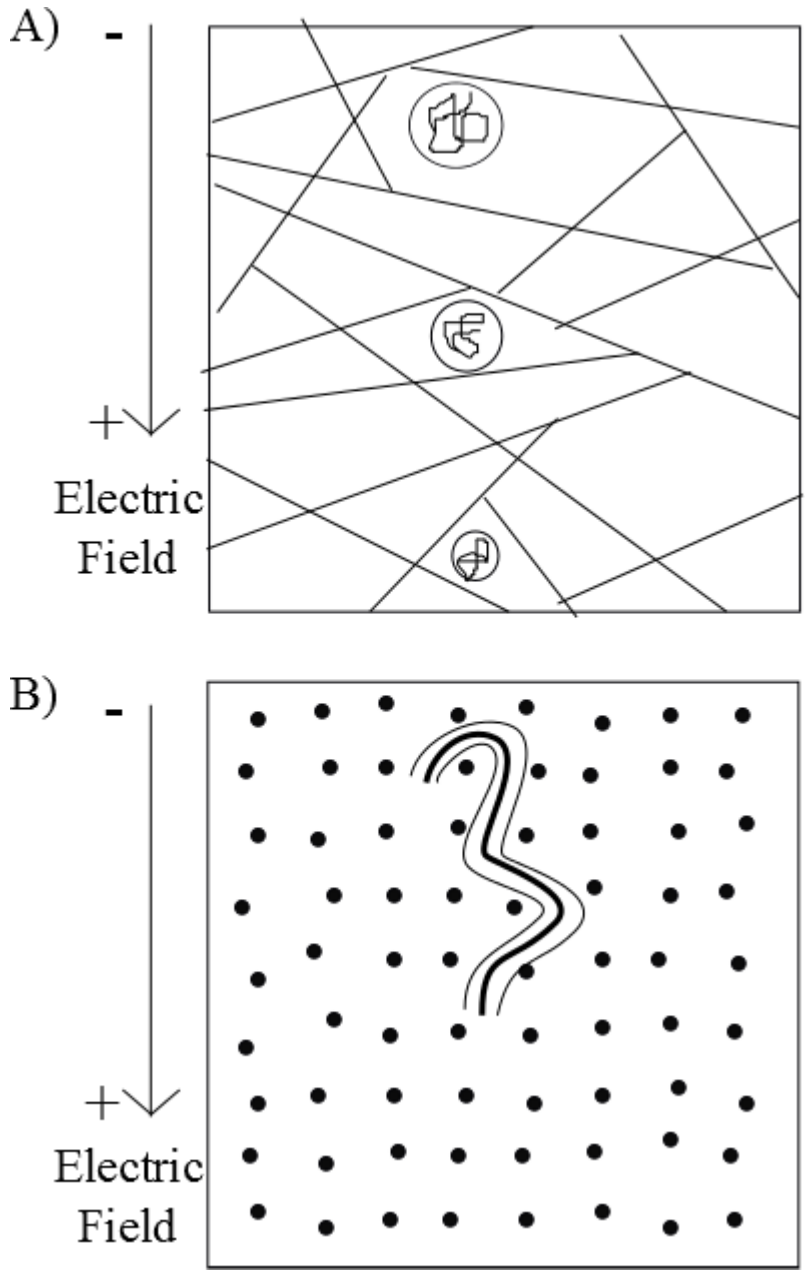

Figure 1.3. Models for DNA migration during electrophoresis. A) Ogston-Rodbard-Chrambach model. The equivalent spheres are depicted by circles filled with DNA (represented by the lines within). The fibers of the sieving matrix are represented by the straight lines. The electric field direction is indicated to the left. B) Reptation model. The obstacles of the sieving matrix are indicated by the dots and the DNA by the bolded line. The two thinner lines on either side of the DNA are the outline of the tube. The electric field is indicated to the left. Modified from (Barron and Blanch, 1995).

impalement model and 2) the lobster trap model (Figure 1.5) (Akerman and Cole, 2002; Manage *et al*., 2008).

The impalement model assumes gel fibers are anchored at only one end. As the circular DNA travels through the sieving matrix, it becomes impaled of these fibers, or traps, whereas linear DNA can move around the fibers by reptation. The circular DNA becomes permanently trapped, and therefore will no longer move, when the electric field is stronger than the upfield Brownian motion and diffusion (Figure 1.4A) (Akerman and Cole, 2002).

The lobster trap model is based on the pore size of the sieving matrix. If the sieving matrix has pores with a radius smaller than the length of the circular DNA, a lobster-type trap occurs that arrests the movement of the DNA. When the length of the circular DNA is much larger than the average pore radius in the sieving matrix, the circular DNA is unable to pass through the obstacles (Figure 1.4B). Linear DNA can pass through the pores as explained by the reptation model. The lobster trap model of trapping is thought to be more prevalent in polyacrylamide gels and less prevalent in agarose gels (Akerman and Cole, 2002) (Figure 1.4B).

1.7.2 Agarose Gel Electrophoresis

Agarose gel electrophoresis (AGE) is a commonly used technique in molecular biology. Agarose is an alternating co-polymer of β-D-galactose and 3,6-anhydro-α-L-galactose units, which is purified from seaweed (Serwer, 1983). Depending on the grade of agarose used, agarose gels typically contain more contaminants than most polyacrylamide gels. Contaminants that can be found in most commercially available

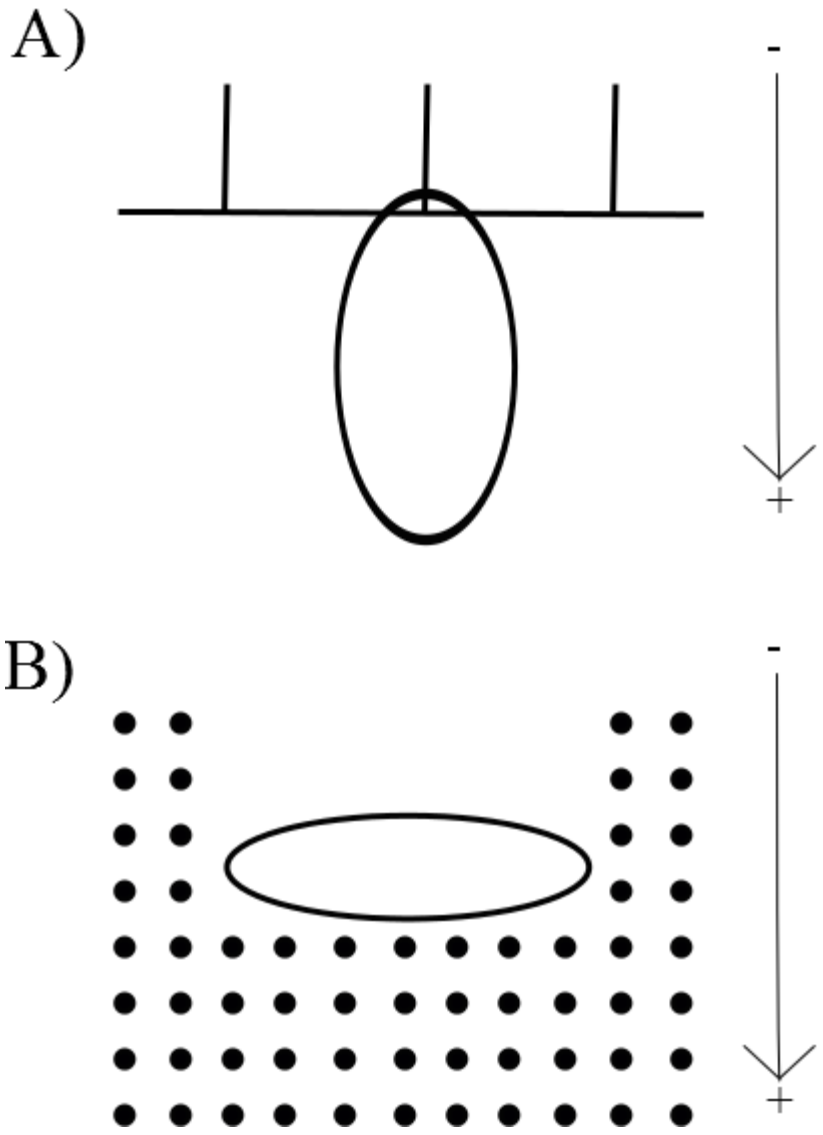

Figure 1.4. Models of circular DNA trapping in electrophoresis. The electric field direction is indicated on the right. A) The impalement model. The traps are indicated by the vertical lines and the circular DNA is indicated by the oval. B) The lobster trap model. The obstacles are represented by the dots and the circular DNA by the open oval. Based on (Barron and Blanch, 1995).

agarose include sulfates, methyls, pyruvate chains, varying polysaccharides, proteins, and salts (Barron and Blanch, 1995; Duckworth and Yaphe, 1971), which can affect the gelling temperature and the mechanical strength of the gel as well as the efficiency of the electrophoresis of the agarose gel. The amount and range of contaminants can be limited by using higher grades of agarose (Righetti, 1989).

As molten agarose solidifies, it forms networks of bundled helices that result in a more open and rigid structure than found in polyacrylamide gels. This rigid structure results in a higher mechanical strength, making the gel easier to handle and allowing for the formation of large pores ranging from hundreds of nanometers to micrometers in size (Barron and Blanch, 1995; Righetti, 1989). Agarose gels are also non-toxic, whereas the acrylamide monomer can be toxic, making agarose gels generally safer than polyacrylamide gels (Barron and Blanch, 1995).

The most commonly used agarose gel concentrations range between 0.3% and 2%, with lower concentrations producing larger pore sizes and lower mechanical strength and the higher concentrations resulting in smaller pore sizes and higher mechanical strength. Lower concentrations of agarose are typically used to separate larger DNA fragments (> 1 kb), whereas higher concentration are better suited for smaller DNA fragments (< 500 bp) (Barron and Blanch, 1995).

AGE using a steady electric field is capable of separating DNA fragments that range between 200 bp and 50 kb. This size range makes agarose the most appropriate sieving matrix for performing RFLP analysis and Southern blotting (Barron and Blanch, 1995). Larger DNA fragments of up to 10 megabases (Mb) can be separated using a

technique called pulsed field gel electrophoresis (PFGE), in which the electric field is alternated between two directions in a periodic manner (Smith and Cantor, 1987). By inverting the electric field, the larger DNA fragments are stretched, based on the stretched reptation model, which improves the size of DNA species that can be resolved.

1.7.2.1 Variations in Buffers Used in Agarose Gel Electrophoresis

AGE is typically performed by submerging a solidified agarose slab gel in a gel box containing the same type and concentration of buffer as used in preparing the agarose gel. Historically, the buffer used in AGE have been Tris-based (Brody and Kern, 2004a), as in the Tris-borate-ethylenediaminetetraacetic acid (EDTA) (TBE) and Tris-acetate-EDTA (TAE) buffers. For DNA fragments from 1 kb to 12 kb TAE is the optimal buffer, whereas smaller DNA fragments (< 1.5 kb) are better resolved in TBE (Singhal *et al.*, 2010). The compression seen for larger DNA fragments when using TBE is due to the complexes formed between borate and the DNA phosphodiester backbone (Stellwagen *et al.*, 2000a). In agarose gels made with TBE, there is thus competition between the agarose and the DNA to form complexes with the borate. When borate is limited, as would be the case in CE at low buffer concentrations, the agarose-borate complexes dominate over the DNA interactions (Stellwagen *et al.*, 2000b), and thereby improve the compression problem.

In recent years, non-Tris based buffers have been developed for use in AGE (Brody and Kern, 2004a). Many of these new buffers use alkali metals, such as lithium and sodium (Brody *et al.*, 2004; Brody and Kern, 2004b), while others feature the use of amino acids (Ishido *et al.*, 2010). It should be noted that in addition to lacking Tris, these

buffers are also low molarity. These low molarity buffers have been shown to decrease Joule heating, which in turn allows for higher electric fields to be used and improves the resolution of the separations (Brody *et al*., 2004; Ishido *et al*., 2010).

1.7.3 Capillary Electrophoresis

CE has been widely used in MFC-based separations of biomolecules (Fiorini and Chiu, 2005). CE is electrophoresis that is performed in capillaries with diameters typically under 250 micrometers (μm), such as many of the channels seen in MFCs. CE can decrease separation times compared to slab gels, given the shorter distance and higher electric fields used (Barron and Blanch, 1995). The electric field when running a typical slab gel is less than 10 volts (V) per centimeter (cm) (V/cm) (Sambrook *et al.*, 2001), whereas CE is typically performed at electric fields of hundreds of V/cm (Drossman *et al.*, 1990).

One of the variables that allows for the higher electric field is the decreased Joule heating seen in capillaries. As discussed above, Joule heating can be detrimental to electrophoresis, but smaller channel diameters increase the surface area to volume ratio and thus improve the heat dissipation (Grushka *et al.*, 1989). The decrease in Joule heating allows for CE to be performed at higher electric fields, thus decreasing the separation times from hours to minutes (Barron and Blanch, 1995). It was the application of this technology that allowed the Human Genome Project to be completed early and under budget (Collins *et al.*, 2003; Dovichi and Zhang, 2000).

1.7.3.1 Agarose Capillary Electrophoresis

Agarose capillary electrophoresis (ACE) has seen only limited use in MFCs and CE. Many ACE applications use agarose concentrations of between 1% and 2 % in capillaries that ranged from 13 mm to 720 mm in length (Bocek and Chrambach, 1991; Bocek and Chrambach, 1992; Chen *et al.*, 1996; Hjertén *et al.*, 1994; Li *et al.*, 2006; Manage *et al.*, 2008; Motsch *et al.*, 1991). EOF is present in AGE, but not as prevalent in ACE, since agarose forms a solid gel and therefore should not be surrounded by liquid buffer within the channel. As it solidifies in the channel it prevents liquids from traversing the channel (Swedberg, 1992), thus potentially eliminating EOF. EOF can be further reduced by using low EOF agarose, such as that used for PFGE (Barron and Blanch, 1995).

1.8 Mitochondrial DNA Analysis and Microfluidic chips

As described in Section 1.5.3, the analysis of mtDNA is complicated by numerous factors, making accurate analysis difficult and large population studies impractical. Importantly, there are no universal standards for mtDNA diagnostics, leading to variability and misannotations. The power of MFC t0echnologies could be used to greatly decrease the time and cost of analysis and greatly improved accuracy in analysis as compared to traditional laboratory assays. Although there is a lot of potential for mtDNA analysis using MFCs, there are very few published reports. There have been some mtDNA analysis applied to microarrays such as the Agilent 2100 bioanalyzer (Agilent Technologies, Palo Alto, CA) (Lu *et al.*, 2002) or the human MitoChip (Maitra *et al.*, 2004; Zhou *et al.*, 2006), which examine point mutations of the mtDNA in a total

genomic DNA (gDNA) sample. These large-scale screening approaches do not feature controls to ensure there is no NUMT contamination and an examination of the results from such studies (Palanichamy and Zhang, 2010) found inconsistencies in the samples analyzed, suggesting issues with sample purity.

Aside from the microarrays, there have been relatively few studies examining the use of MFCs for mtDNA analysis. The Lee group from the National Cheng Kung University claim to be able to use a MFC to purify mtDNA (Chang *et al*., 2010; Chang *et al*., 2011; Chang *et al.*, 2013). The Lee group's MFC-based mtDNA extraction is based on magnetic beads that bind the mtDNA to extract it from cells. Unfortunately, real-time PCR analysis generated multiple bands, suggesting that the primers are non-specific and have led to amplification of different DNA fragments. When these primers were tested *in silico* using Primer BLAST (Ye *et al.*, 2012) there were 55 potential unintended templates within the human genome, with seven corresponding to the size of the additional PCR products seen by Chang *et al.*. It is plausible that the primary band is mtDNA, but the additional bands suggests nDNA contamination in the extraction. This extraction approach therefore does not result in a purified mtDNA sample and is therefore susceptible to false positives from NUMTs. Therefore, at this time there are no MFC-based approaches that are able to purify mtDNA.

Previous work from our group had begun to examine the use of MFCs for analyzing mtDNA. In a study by Taylor *et al*. (Taylor *et al.*, 2005), a fragment of the mtDNAwas amplified from a healthy individual and cloned into a plasmid vector, and the plasmid then isolated using standard DNA preparation approaches. Clonal analysis allowed identification of individual mtDNA sequence, thereby ensuring "homoplasmy"

of each plasmid preparation. This study demonstrated that for isolated mtDNA fragments, we could analyze mutations using an HA-SSCP method on MFCs. In order to, apply this approach to human cells, the mtDNA needs to be isolated and purified.

1.9 Focus of This Study

In this study we explore the use of MFC technologies for analyzing mtDNA isolated from only a few thousand human cells. Using plasmids as a model for the mtDNA, we explore the requirements for manipulating picogram quantities of DNA, amounts relevant for the expected quantities of mtDNA found in several thousand leukocytes. We will discuss attempts to purify mtDNA on MFCs, from both cultured skin fibroblasts and leukocytes isolated from blood.

Studies using plasmids as models for mtDNA are also used to develop a separation with a resolution relevant to mtDNA molecules. We describe a CE-based method that allows resolution of mtDNA-sized plasmids that differ by 1.5 kb, which is close to the size of the smallest reported large-scale mtDNA deletion. The work presented in this thesis provides an important foundation for future development of MFC-based mtDNA purification approaches.

CHAPTER 2- MATERIAL AND METHODS

2.1 Buffers and Common Solutions

2.1.1 Preparation of the Agarose Used for Capillary Electrophoresis

As discussed in Chapter 1, the use of a higher grade agarose can decrease EOF and contaminants (Barron and Blanch, 1995) and for this reason, we have used PFGE-grade Agarose III (Amresco Inc. CAS-No-9012-36-6, Solon, OH, USA) for all agarose-based CE.

2.1.1.1 Preparation of the Running Agarose

The running agarose, used as the sieving matrix in CE, unless otherwise stated, was 0.6% (w/v) agarose in the appropriate buffer. Since various buffers and concentrations were used throughout this study, the buffer type and concentration will be indicated for each experiment. The running agarose was made in either a 15 millilitre (mL) or 50 mL polypropylene conical tube. The conical tube containing the running agarose is placed in a 600 mL beaker with a 5% (w/v) glucose solution, which is heated on a hot plate with stirring to 102^{o}C (temperature is verified using a thermometer). The solution is kept at 102^{o}C until the agarose has completely dissolved and the solution is clear. Once the running agarose has completely dissolved, the beaker with the glucose solution and the running agarose is removed from heat but the stirring is maintained. The heating of the agarose described above applies to all running agarose solutions within this study. However, the exact method for cooling does vary depending on the MFC and application.

The running agarose used with glass MFCs was centrifuged at 3000 x g for 5 minutes immediately after being removed from the heat to remove air bubbles. After

centrifugation, the running agarose was placed back in the beaker with the glucose solution and cooled to 70ºC. At this point, the running agarose is ready to be used and can be kept at 70ºC for up to six hours.

The running agarose used in poly (methylmeracrylate) (PMMA) MFCs was first cooled to 95ºC and divided into 1 mL aliquots in 1.5 mL Eppendorf tubes. The 1.5 mL Eppendorf tubes were then centrifuged at 14 000 rotations per minute (rpm) in a microcentrifuge for 2 minutes to remove air bubbles. The aliquots could be stored at 4ºC for up to three weeks or, if for immediate use, the aliquots could be kept at 70ºC for up to six hours. Aliquots previously stored at 4ºC could be prepared for use by placing in the glucose solution and heating to 102ºC in the same manner described above. Upon cooling to 95ºC, the tubes are centrifuge at 14 000 rpm for 2 minutes and then placed back in the glucose solution to cool to 70ºC. We did not observe any differences in electrophoretic behaviours between freshly made agarose and agarose stored at 4ºC.

2.1.1.2 Preparation of the Agarose Coating

To improve the adherence of the running agarose to the channel walls of the PMMA MFCs we used a 0.1 % (w/v) agarose coating, modified from (Swedberg, 1992). The 0.1 % (w/v) coating agarose solution was made in the same buffer type and concentration as used in the running agarose. The coating agarose solution was heated to 102ºC in the same manner as for the running agarose, except that the coating agarose was not centrifuged as air bubbles do not adversely affect the coating. The 0.1 % agarose cooled to 40ºC and then placed in a 30ºC incubator for a minimum of one hour. The temperature of the agarose coating was verified to be 30ºC using a thermometer prior to

coating the MFCs. If the solution was too warm, the coating was not effective; if it was too cool, it solidified within the channel.

2.1.2 Preparation of Buffers and Media

2.1.2.1 Preparation of Buffers Used in Capillary Electrophoresis

Various buffer have been used in CE for this study including TBE, TAE (Maniatis *et al*., 1982), Tris-TAPS-EDTA (TTE) (Manage *et al*., 2008), lithium boric acid (LBa), sodium boric acid (SBa) (Brody *et al*., 2004), sodium threonine (ST) (Ishido *et al*., 2010), and sodium threonine EDTA (STE). All CE buffers were made to a 10 X concentration and subsequently diluted to the required concentrations. The recipe for the 10 X stock solutions of the buffers used for CE are given in Table 2.1. The pH of each solution, given in Table 2.1, was verified using a pH meter, except for LBa and SBa. LBa and SBa were made by starting with 10 mM lithium hydroxide and 100 mM sodium hydroxide, respectively, and boric acid was subsequently added to decrease the pH to 8.5 (Brody *et al*., 2004). The concentrations of boric acid for LBa and SBa in Table 2.1 are the amount used to decrease the pH to 8.5. All buffers were filtered prior to use.

2.1.2.2 Preparation of Mammalian Cell Culture Media

Eagle's Alpha minimal essential medium (α-MEM) was used to culture human fibroblast cell line GM5565. The α-MEM medium was prepared for use by adding 50 mL of fetal calf serum (FCS), 25 mg of uridine and 50 mg of sodium pyruvate to 450 mL of α-MEM. Herein, α-MEM medium will refer to the prepared media described above and α-MEM will refer to manufacturer's α-MEM (Sigma). Leukocytes and fibroblasts

Table 2.1. CE buffer recipes.

Buffer	Recipe for 10 X solution	pH
TBE	980 mM Tris, 980 mM Boric acid, 20 mM EDTA	8.3
TAE	400mM Tris, 200 mM acetic acid, 10 mM EDTA	7.6
TTE	500 mM Tris, 500 mM TAPS, 10 mM EDTA	8.3
LBa	10 mM Lithium hydroxide, 29 mM boric acid	8.5
SBa	100 mM sodium hydroxide, 347 mM boric acid	8.5
ST	170 mM sodium hydroxide, 390 mM threonine	9.0
STE	170 mM sodium hydroxide, 390 mM threonine, 10 mM EDTA	9.0

were frozen at -80ºC for up to a week. The freezing media consisted of 70% α-MEM, 20% FCS and 10% dimethyl sulfoxide (DMSO).

2.2 Fabrication of MFCs

2.2.1 Fabrication of Glass MFCs Using Glass Etching

Glass MFCs were fabricated using standard glass etching techniques and fusion bonding processes (Kaigala *et al*., 2006; Northrup *et al*., 2010). The glass 4-port minis (4-PMs) were 2.4 cm x 1.6 cm with channels that were 100 μm wide and 45 μm deep (Figure 2.1). The injection channel, located between the sample reservoir (SR) and sample waste (SW), was 1.63 cm and the separation channel, located between the buffer reservoir (BR) and the buffer waste (BW), was 2.77 cm. The wells have a 1 millimeter (mm) radius and hold 3 μL of liquid (Figure 2.1). The glass mtDNA isolation MFC is 2.2 cm x 1.9 cm. The channel is 2.4 mm in length, 150 μm wide and 130 μm deep. The wells have a radius of 1 mm and a depth of 1.5 mm and hold 4 μL of fluid (Figure 2.2).

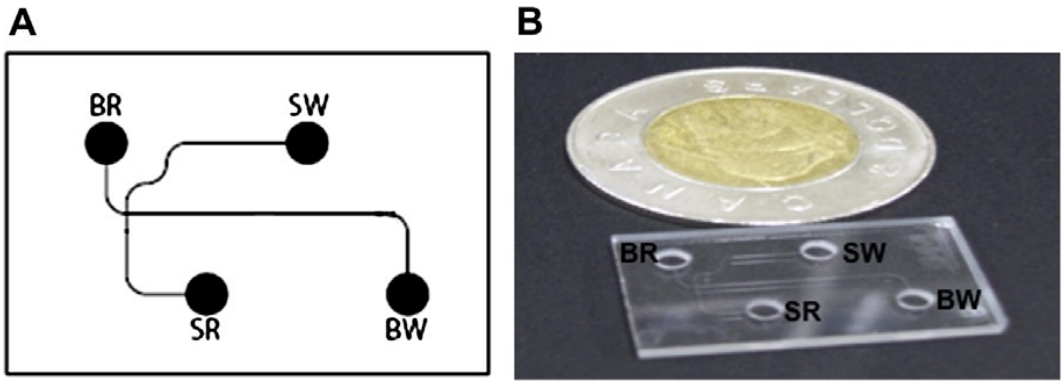

Figure 2.1. Glass 4-PM MFCs. A) Schematic of the glass 4-PM with the circles representing the wells and lines representing the channels. BR is the buffer reservoir, BW is the buffer waste, SR is the sample reservoir and SW is the sample waste. B) Picture of glass 4-PM next to a toonie for size comparison. Taken from (Northrup *et al*., 2010).

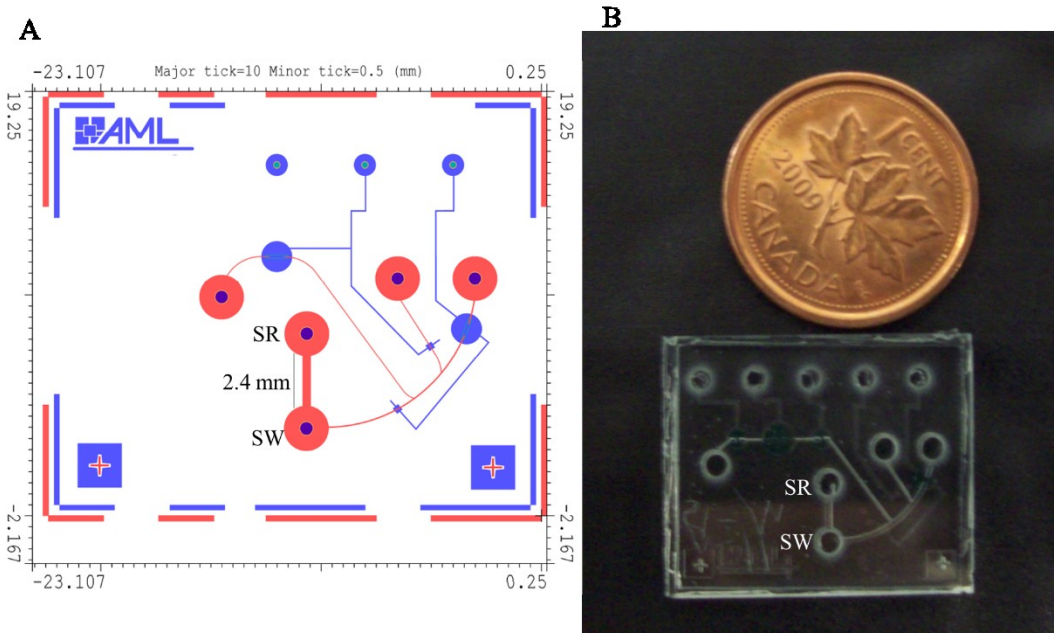

Figure 2.2. Glass mtDNA isolation MFC. A) Schematic of the glass mtDNA isolation MFC. The red circles represent the wells and lines represent channels. Blue circles represent pumps. In this study only the SR and SW, and the channel between them were used. B) Picture of the glass mtDNA isolation MFC next to a penny for size comparison.

2.2.2 Fabrication of PMMA MFCs using Laser ablation

PMMA 4-PMs were fabricated by laser ablation using a 30 W 10.6 μm CO_2 laser system (VLS 2.30) from Universal Laser Systems (Ma *et al*., 2012). The MFC designs were imported into CorelDraw X5 (Corel Corp., version 15.0.0.486), which was used to print the MFCs using the laser. The settings of the laser are outlined in Table 2.2. Two sections of approximately 10 cm long were cut from 1.5 mm thick sheets of extruded Arcylite-FF PMMA. The two sections are used to form the top and bottom of the MFC. The top sheet has the channels engraved on one side and the wells on the other. The bottom plate contains features that are used to complete the channels. Once the features have been ablated, the two sheets of PMMA are annealed by placing them between glass plates. The PMMA sheets between the glass plates are placed in an oven at 130^{o}C for 10 minutes. The oven was then decreased to 80^{o}C for 1 hour. The PMMA sheets are then removed from the oven and from between the glass plates.

To bond the PMMA MFCs, the two sheets are soaked in ethanol for 30 seconds then dried with filtered air. The two sides (top and bottom) are aligned using the alignment posts (Figure 2.3A) and placed in an oven at 110^{o}C for two hours, followed by an additional hour at 80^{o}C. The strip of three PMMA MFCs are then removed from the oven and cooled to room temperature. The strip is placed in the laser to make the final cut (detachment of chips in Table 2.2). This results in a strip of three PMMA 4-PMs (Figure 2.3A).

To obtain the individual PMMA 4-PMs (Figure 2.3B-C), the PMMA 4-PMs are cracked out of the strip using pliers and the edge of a bench. This results in three PMMA

Table 2.2. Settings of the CO_2 laser for the fabrication of PMMA MFCs.

Mode	Power (%)	Speed (%)	PPI	# of passes
Rastering of text	36	100	500	1
Vector cut of frame	20	5	1000	1
Vector cut of wells	20	5	1000	1
Engraving of channels	0.8	3	1000	2
Detachment of chips	100	8.6	1000	1

4-PMs that have a separation channel that is 19.6 mm long and an injection channel of 16.7 mm in length. The channels have a width of 150 µm and a depth of 130 µm, with the wells having a radius of 1 mm and holding 5 µL of fluid (Ma *et al*., 2012).

The PMMA mtDNA isolation MFCs (Figure 2.4) were fabricated using a similar protocol as the PMMA 4-PMs. The PMMA mtDNA isolation MFCs were 2.4 cm by 1.6 cm with a single channel that was 2.4 mm in length, 150 µm in width and 130 µm deep. The two wells had a radius of 1 mm and could hold 5 µL (Figure 2.4).

2.3 Pretreatments of the channels in the MFCs

2.3.1 Poly-N, N-dimethylacrylamide and poly-N-hydroxyethylacrylamide

A 5 % (w/w) poly-N,N-dimethylacrylamide (PDMA) was made using free radical polymerization of N,N-dimethylacrylamide (DMA), modified from Albarghouthi *et al*.(Albarghouthi *et al*., 2002) and Hestekin *et al*. (Hestekin *et al*., 2006). Briefly, DMA was added to Milli Q water and nitrogen was bubbled through the solution for approximately two hours to remove oxygen. 0.02% (w/v) 2, 2'-azobis(2-methylpropionamide) dihydrochloride was added to the solution to catalyze the polymerization and placed at 47^{o}C overnight. The solution was then covered in tinfoil to

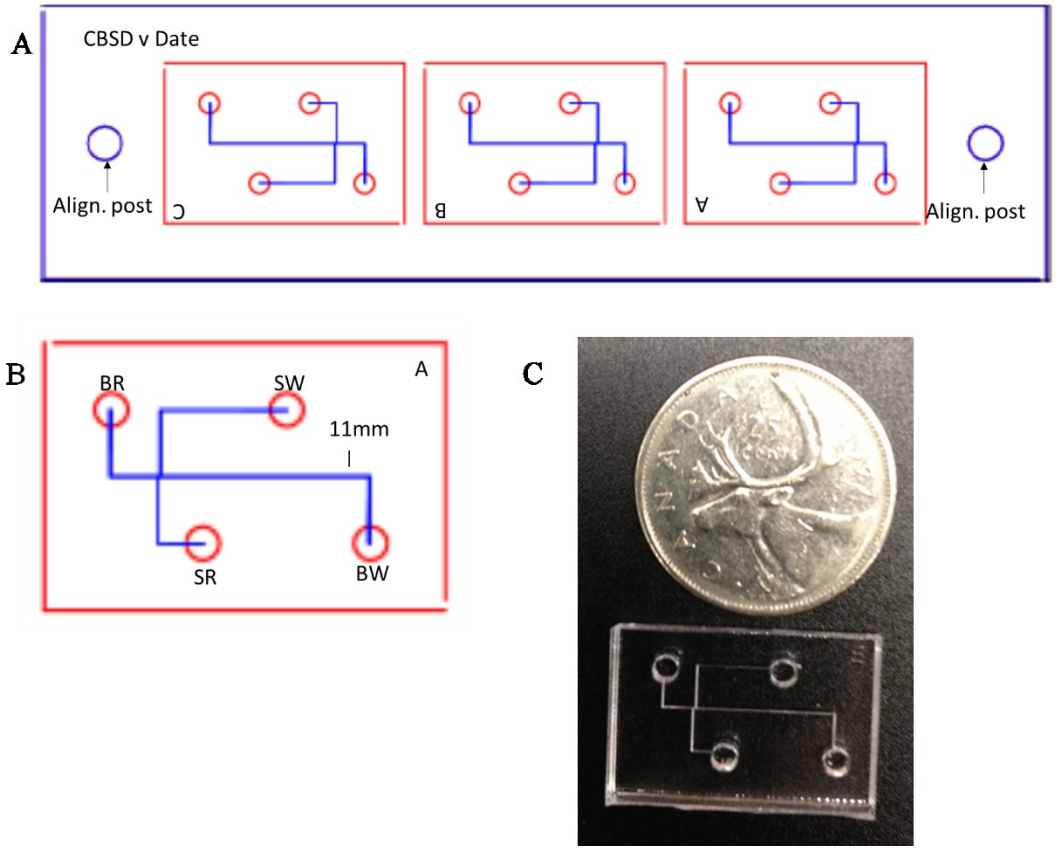

Figure 2.3. PMMA 4-PM. A) Schematic of a strip of three PMMA 4-PMs. The version and the date are indicated on the strip and each individual 4-PM is marked as either A, B or C. The alignment post are indicated by Align. Post. B) Schematic of individual PMMA 4-PM. The channels are represented by blue lines and the reservoirs are indicated by red circles. The names of the reservoirs are the same as Figure 2.1. The 11 mm alignment mark is indicated by 11 mm and the letter of the chip from the strip is in the top right corner. C) Picture of the PMMA 4-PM next to a quarter for size comparison. Modified from (Ma *et al.*, 2012).

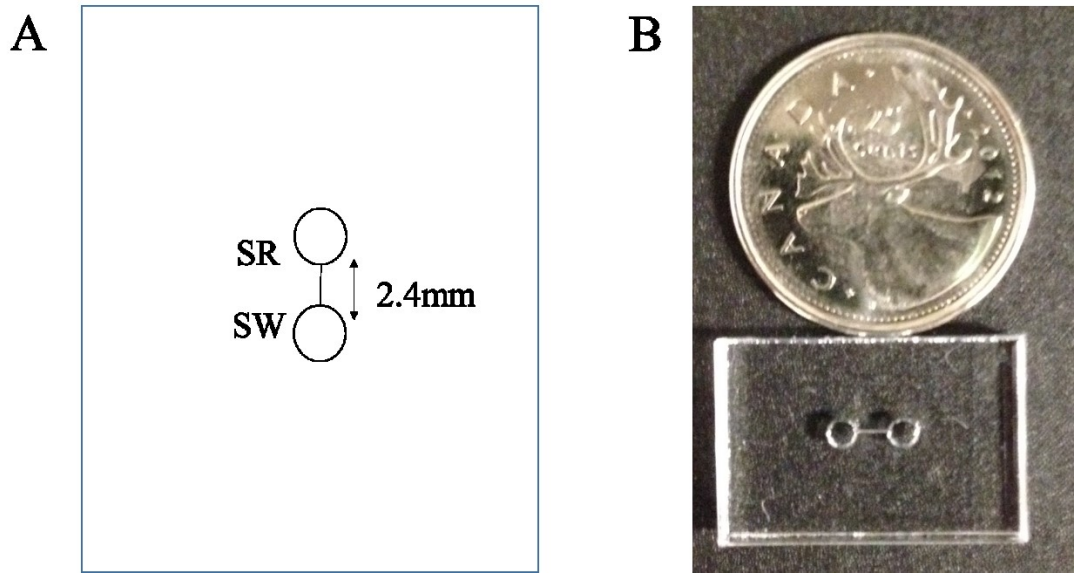

Figure 2.4. The PMMA mtDNA MFC. A) Schematic of the PMMA mtDNA MFC (not drawn to scale) with circles representing wells and the line between the circles representing the channel, which is 2.4 mm in length. The PMMA mtDNA isolation MFCs were 1.6 cm by 2.4 cm. B) Image of a PMMA mtDNA MFC next to a quarter for size comparison.

protect from light and stored at 4ºC for up to three weeks. A 5% (w/w) poly-N-hydroxyethylacrylamide (PHEA) was made in the same manner by polymerizing N-hydroxyethylacrylamide (HEA) (Albarghouthi *et al*., 2002).

The 5% (w/w) PDMA was used in glass MFCs to decrease the non-specific surface adsorption of DNA to the channel walls (discussed in Chapter 3). To condition the surface of the channels prior to the PDMA coating, 5 µL of 0.1 M HCl was added to the BW well and the channels were filled by capillary action. An additional 3 µL of 0.1 M HCl was added to the other three wells (SR, SW, and BR). The 0.1 M HCl was incubated in the channels for 15 minutes then rinsed with Milli Q water and dried with pressurized air. To coat the channels with PDMA, 4 µL of 5 % (w/w) PDMA was added to the BW and allowed to fill the channels by capillary action. An additional 3 µL of 5 % (w/w) PDMA was added to the other three wells and the MFC incubated for 15 minutes, after which the PDMA was aspirated and the channels were rinsed with Milli Q water and dried with pressurized air (Northrup *et al*., 2010). The 5% (w/w) PHEA coating was applied in the same manner as the 5% (w/w) PDMA.

2.3.2 Linear Polyacrylamide Coating

The generation and coating procedure for linear polyacrylamide (LPA) was modified from Han and Singh (Han and Singh, 2004) and Hjerten (Hjerten, 1985). The LPA coating was a 4% (w/v) acrylamide solution, containing 0.1% (w/v) potassium persulfate and 0.1% (v/v) N,N,N,N-Tetramethylethylenediamine (TEMED). The acrylamide and potassium persulfate solution was sonicated for 10 minutes to remove air

bubbles, prior to the addition of TEMED. Once the TEMED was added, the solution was mixed gently to prevent the generation of air bubbles.

Glass MFCs that were coated with LPA were treated with H_2SO_4 and heated to 350^oC for 15 minutes. Once the MFC was cooled, it was rinsed with distilled water and then filled with 1 M NaOH for 10 minutes, after which it was rinsed again with distilled water and dried with pressurized nitrogen. To prepare the channel for permanent LPA, a silane functionalization layer solution (5.75 mM acetic acid (pH 3.0) with 0.4 % (v/v) 3-(Trimethoxysilyl)propyl acrylate) was added to the channel and incubated for one hour. The channels were rinsed again with distilled water and dried with pressurized nitrogen. 3 μL of the LPA solution was added to the BW well and the channels filled by capillary action, with an additional 3 μL of LPA was added to the SR, SW, and BR. The LPA solution was incubated for 30 minutes, while the MFC was protected from light. After 30 minutes, the LPA was removed and the channels were rinsed with distilled water, dried with nitrogen, and submerged in buffer.

2.3.3 Cross-Linked Poylacrylamide Coating

The cross linked polyacrylamide (CPA) coating was modified from Huang *et al*. (Huang *et al*., 1992). The CPA coating consisted of 5% (w/v) acrylamide solution that contained 1% (w/v) azobisisobutyronitrile (AIBN), and 1% (w/v) methylene bisacrylamide in methylene chloride. The CPA coatings also required a silane functionalization layer to improve the covalent bonding to the MFCs.

MFCs to be coated with CPA were treated with 1M NaOH for 1 hour, then rinsed with Milli Q water and dried with pressurized air. The channels were treated with

methanol for two hours and then rinsed with Milli Q water and dried with air. To prepare the channel for the CPA coating, the silane functionalization layer solution was applied and incubated for one hour. The channel was rinsed with Milli Q water and dried with air. The CPA solution was then added to the channels for 30 minutes. Finally, the channel was rinsed with Milli Q water, dried with air and submerged in buffer.

2.3.4 Agarose Coating

To improve the adherence of the running agarose in PMMA MFCs, an agarose coating was applied directly to the channels. The 0.1% (w/v) agarose solution was placed in a 10 mL syringe that was fitted with a 1 mL pipette tip cut to adapt the syringe to the well of the PMMA MFC. The syringe was then applied to the BW well and the agarose solution was pushed through the channels slowly at a rate of 1 mL to 1.5 mL per minute for 5 minutes. The agarose solution in the syringe should provide enough resistance to keep the flow rate between 1 mL to 1.5 mL per minute. If the agarose solution does not provide enough resistance to control the flow, it is too warm and will not properly adhere to the wall. After 5 minutes, the agarose solution was pushed out of the channels using filtered air. The MFC was examined under a microscope to verify the channels were cleared. Any debris left in the channel was removed using more of the agarose coating solution. This is done by filling a 1 mL syringe fitted with a 1 mL pipette tip as described above. The channel was then dried with clean dry air. Once the MFC was cleared and dried it is placed in a clean dry environment for 10 minutes, after which the MFC was ready to be filled with the running agarose. Swedberg allowed the 0.1% agarose coating to set overnight, although we found no detectable differences in electropherograms from

MFCs with a 10 minute incubation as compared to MFCs for which 0.1% agarose coat allowed to set overnight.

2.4 Capillary Electrophoresis

2.4.1 MFC-based Plasmid Segregation

For the "low picogram" plasmid segregations, glass 4-PMs (Figure 2.1) coated with 5% (w/w) PDMA and loaded with 0.6 % agarose in 1 X TBE (unless otherwise stated), were used. To load the agarose, the MFC was placed on a steel block that had been heated to 40^{o}C to warm the MFC for 20 seconds. 5µL of agarose was placed in the BW and the channels filled by capillary action, followed by 5µL of agarose being added to each of the SR, SW and BR. The 4-PM was examined under a light microscope for air bubbles, with the presence of bubbles excluding the load from analysis. After 20 minutes, the agarose was removed from the wells using a scalpel and replaced with buffer. The SR and BR wells were loaded with 0.5 X TBE, 3 µg of bovine serum albumin (BSA) and 1 pg pCOX15/ST8 plasmid, while the SW and BW wells were loaded with only 0.5 X TBE and 3 µg of BSA, unless otherwise stated. Loaded glass 4-PMs were placed into the microfluidic tool kit (µTK), a microchip-based electrophoresis system (Micralyne, Edmonton, AB, Canada) and the voltage program (Table 2.3), direction and magnitude of the electric field was loaded into Labview to control the µTK and perform CE. The current, as measured in the SR, must be within the range indicated in Table 2.3 or the load was eliminated from analysis since variation in current is indicative of a problem in the CE.

After CE, the glass 4-PM was removed from the μTK. The contents of each well were extracted and placed in 0.2 mL PCR tubes. 10 μL of Milli Q water was added to each tube, which was then placed at -20°C until analysis by PCR. A successful plasmid segregation is defined by the presence of pCOX15/ST8 plasmid in the SW, as indicated by a positive PCR.

Table 2.3. Voltage program used for plasmid segregation and plasmid miniprep.

Step	Duration (s)	Electric field (V/cm)	Current (μA)
1	50	193.3	-14 to -15
2	20	-32*	2 to 2.5
3	600	32	-2 to -2.5

* The negative electric field indicates a reverse in direction of the electric field.

2.4.2 MFC-based Plasmid Minipreps

The MFC-based plasmid miniprep was performed using the same protocol as the plasmid segregation in Section 2.4.1 with the following modifications: The SR and BR contained 1 X TBE, 3 μg of BSA and 10^5 *Escherichia coli* cells in 10 mM Tris-Cl, pH 8.0 and 1 μL of lysis buffer (5% (v/v) Triton X-100 in 10 mM EDTA). The SW and BW each contained 1 X TBE and 3 μg of BSA. After the samples were loaded in the glass 4-PM, it was allowed to sit at room temperature for 5 minutes to allow for lysis prior to CE, which was run as described in Section 2.4.1. A successful plasmid miniprep is defined as the presence of pCOX15/ST8 in the SW, as indicated by a positive PCR.

2.4.3 MFC-based Plasmid Separations

The plasmid separations were, unless otherwise stated, performed on PMMA 4-PMs (Figure 2.2) coated with 0.1 % agarose in 1 X STE (unless otherwise stated) and loaded with 0.6% agarose in 1X STE, unless otherwise stated. The PMMA 4-PM was placed on a heated steal block (50ºC) for at least 20 seconds prior to agarose loading and remained on the heated steal block until completion of the loading. The agarose was allowed to solidify in a humidified environment at room temperature for 10 minutes, followed by immersion in buffer for an additional 5 minutes. The agarose was removed from the wells, using a scalpel, while the PMMA 4-PM was still submerged in the buffer. The PMMA 4-PM was then removed from the buffer and excess buffer removed using a Kimwipe. The buffer in the wells must be retained there until such time as the buffer is ready to be replaced with the CE buffers.

Once the surface was dried, the contents of the wells were replaced with the reagents as described in Table 2.4. The loaded PMMA 4-PM was placed in the µTK and the electrodes were lowered into the wells. The laser was positioned in the separation channel, 11 mm from the intersection, using the 11 mm alignment mark as a reference point (Figure 2.3B). Once the laser was focused, the photo multiplier tube (PMT) was placed in position, the voltage program loaded into Labview (Table 2.5), and CE performed. Laser-induced fluorescence (LIF) was used to detect Sytox orange (SO)-labeled DNA, with an excitation of 532 nanometers (nm) and detection at 570 nm.

Each load consists of four runs and each run consists of an injection, in which the electric field is applied along the injection channel, and a separation, in which the electric

field is applied along the separation channel. The first run will have a longer injection time than all subsequent runs, since the DNA must travel from the SR to the intersection (Figure 2.5A-B). The injection phase does not lead to separation based on size due to the constant influx of DNA from the SR. During the separation phase, there is no electric field being applied along the injection channel and therefore the DNA remains static within the injection channel, and only the DNA that is in the intersection will be moved along the separation channel (Figure 2.5C). After the first run is complete, the second run will have a shortened injection time since there is already DNA in the injection channel below the intersection (towards the SR). This second, and all subsequent injections, move the DNA that is already in the injection channel into the intersection (Figure 2.5D) for examination during subsequent separation steps. The separation phase is necessarily the same for each run, to allow detection of DNA fragments at 11 mm along the separation channel (Figure 2.5E).

Table 2.4. Contents of the wells of the PMMA 4-PMs in plasmid separations.

Well	**Sample type**	**[STE]**	**[Sample] (ng)**	**[SO] (μM)**
SR	***SC ladder	0.1 X	75	0.04
	Single Plasmids	0.1 X	10*	0.004**
	Double plasmids	0.1 X	20 (10 of each)*	0.008**
B, SW, BW	All	1 X	n/a	n/a

* Concentrations are subject to change as required.
** If the concentrations of the plasmid is changed the concentration of SO will also change to maintain the ratio of SO to bp of DNA of ~1:600.
***Supercoiled DNA ladder from Invitrogen (Carlsbad, CA, USA).

Table 2.5. Voltage program for plasmid separations.

Sample	Injection			Separation	
	Time (s)		Electric field (V/cm)	Time (s)	Electric field (V/cm)
	1st	Subsequent			
100 bp ladder	250	20	42	350	25
SC ladder	300	50	42	600	20
Plasmids	250	50	29.4	500	20

2.4.3.1 Exclusion Criteria for Plasmid Separations

The PMMA 4-PMs need to be examined under a microscope for any deformities that might adversely impact the CE. The channels should be examined from both the top and bottom, with the bottom (i.e. wells facing down) usually being the most informative. A deformity can be a disruption in the channel, such as in Figure 2.6A-B, or a fiber embedded in the MFC channel and such deformities or embedded fibers, rendering such a MFC unusable.

After each load the PMMA 4-PM is examined for air bubbles and/or fibers in the channels, although the current and character of the electropherogram can already be suggestive of specific problems. Air bubbles that occlude over 50 % of the channel will result in reduced or absent current and any subsequent CE would not be representative; hence, such a load would be excluded from analysis (Figure 2.6D). Smaller air bubbles that occlude less than 50% (Figure 2.6E) of the channel but are found in the separation channel (black box in Figure 2.6C), will result in an excluded load (Figure 2.6G-H). If the smaller air bubble is outside of the black box delineated in Figure 2.6C, it does not generally affect the load and the load can be included in data analysis. A fiber in the

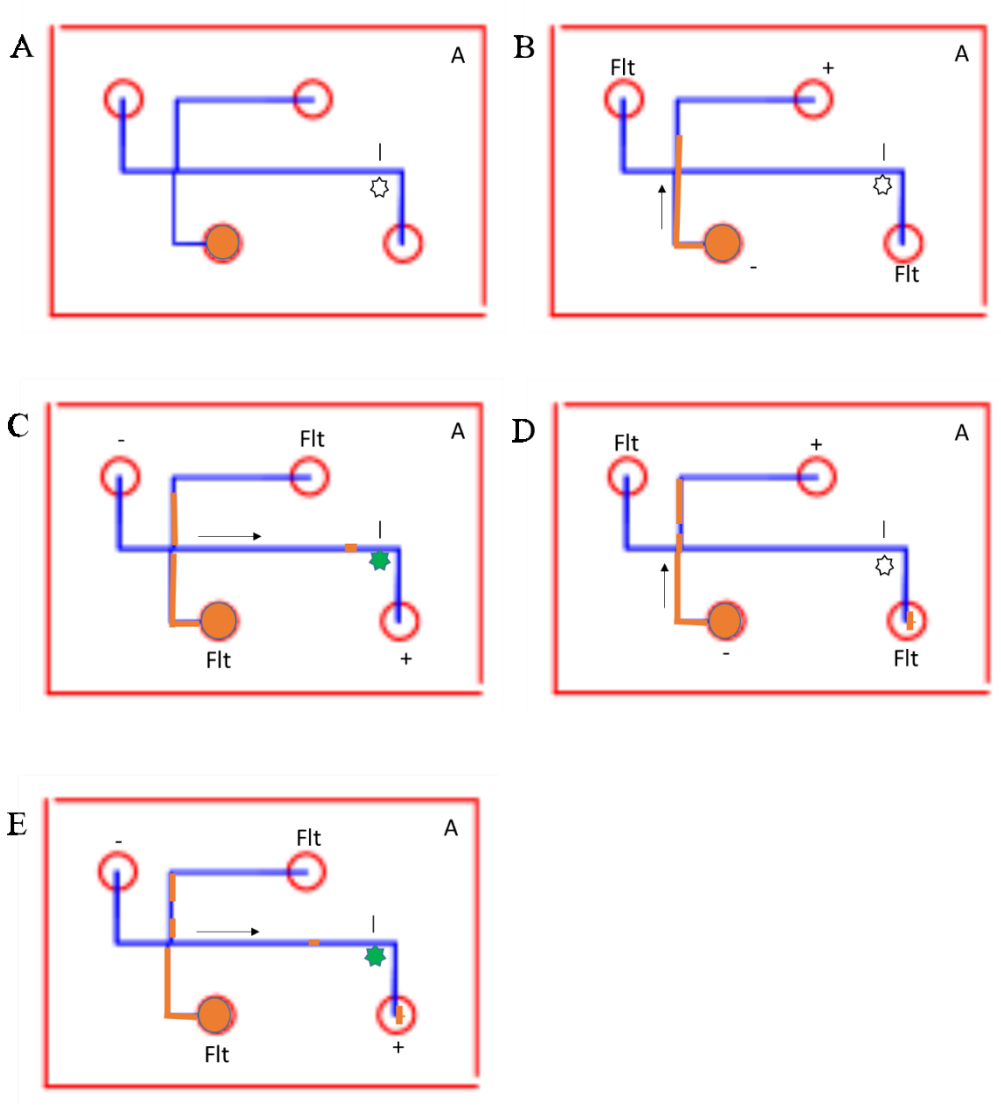

Figure 2.5. Schematic of steps involved in a plasmid separation. A) Loaded PMMA 4-PM prior to plasmid separation. The DNA is orange and is found only in the SR. The PMT, indicated by a white ☼, is switched off. B) The injection of the first run of a load moves the DNA from the SR past the intersection. During the injection the electric field is applied to the injection channel as indicated by the arrow, with the SR being the anode and the SW being the cathode (indicated by – and + respectively). The electrodes in the BR and BW are not active, indicated by Flt. C) During the first separation, the DNA is moved along the separation channel towards the BW, as indicated by the arrow. The DNA is detected at the 11 mm alignment mark by the PMT, which is on as indicated by a green ☼. There is no electric field along the injection channel. D) During the second injection, and all subsequent injections, the DNA that remained below the intersection during the previous run is moved into the intersection. E) The second separation, and all subsequent separations, are performed in the same manner as the first.

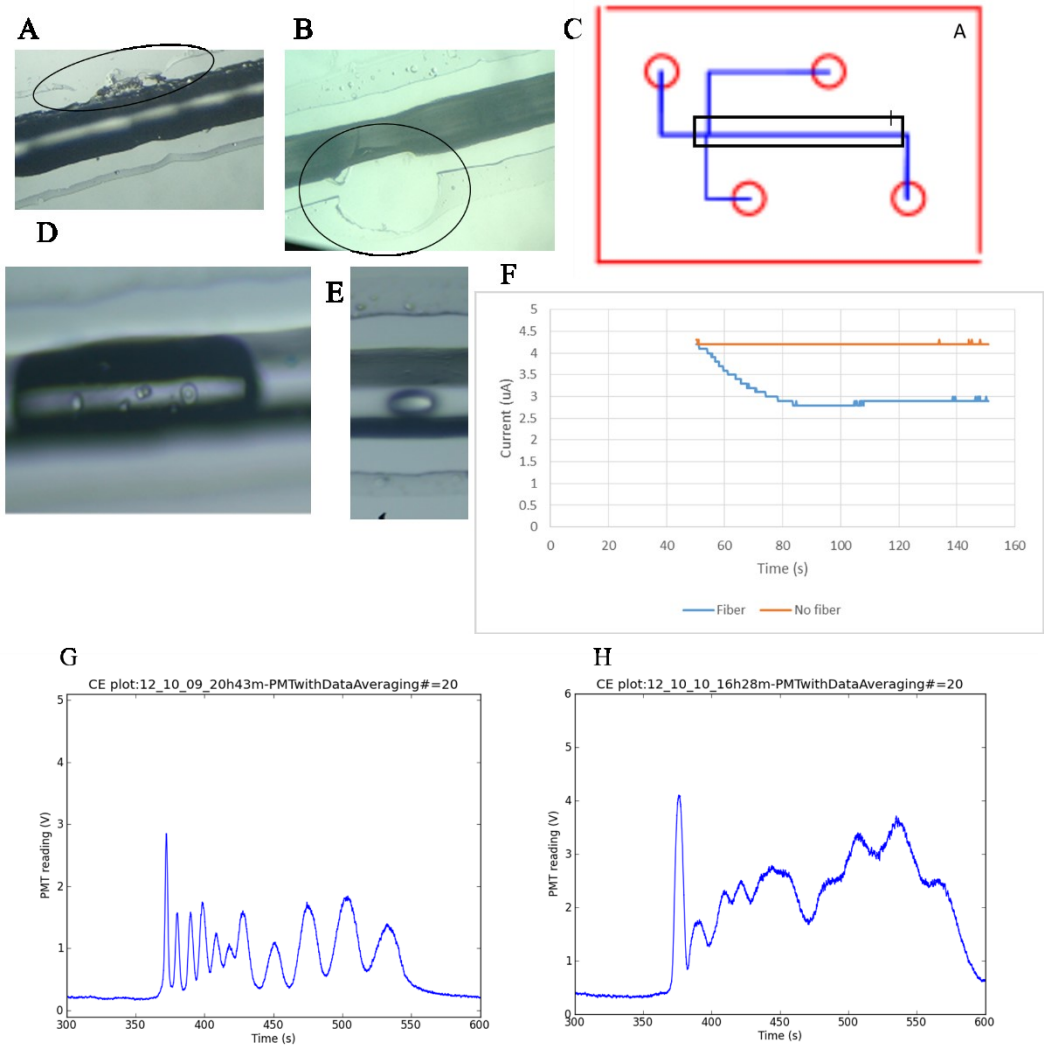

Figure 2.6. Conditions associated with the exclusion of plasmid separations. A and B are examples of deformities along the channel that would result in a PMMA 4-PM being excluded. C) Area of the PMMA 4-PM in which the presence of an air bubbles would exclude the load (indicated by the black rectangle). D) is an example of an air bubble that occludes over 50% of the channel width and would cause exclusion of the load. E) is an example of an air bubble that occludes less than 50% of the channel. This load would not be excluded if the bubble were found outside the rectangle in C. F) shows the current during a normal CE (no fiber) or during CE with a fiber in the running agarose (fiber). G) shows an electropherogram from a CE with no problems and H) is a sample electropherograms from CE with a small air bubble in the intersection, but occluding less than 50% of the channel.

running agarose in any of the channels will also result in an excluded load. When a fiber is present anywhere in the running agarose, the current will begin at the expected level but drop by more than 1 μA during the run (Figure 2.6F), adversely affecting the separation. Lastly, if the current for a given run is outside of the acceptable range, the load is also excluded from analysis. For CE run at 25 V/cm in PMMA 4-PMs, the expected current through 0.5 X TBE is -1.6 μA to -2.4 μA and through 1X STE is between -3.5 μA and -4.5 μA.

2.4.4 MFC-based Mitochondrial DNA Isolations

A glass mtDNA isolation MFC (Figure 2.2) was coated with 5 % (w/w) PDMA, as described in Section 2.3.1, with the exception that reagents were introduced to the SW using a syringe. The MFC was placed on a steel block at 40^{o}C for 20 seconds prior to loading the agarose. A 0.6% agarose solution was added to the channels using a 1 mL syringe with a fitted pipette tip to push the agarose through the channels via the SW. Once the channel was filled, agarose was added to the SR and allowed to solidify for 20 minutes at room temperature, which the agarose was removed from the wells using a scalpel and replaced by buffers. The SR contained, unless otherwise stated, 0.1 X TBE, 3 μg of BSA, and 3000 cells (cell type specified for each experiment) and 5 % Triton X-100. The SW was filled with 0.1 X TBE and 3 μg of BSA. The loaded mtDNA isolation MFC was placed in a home-made jig that contained electrodes connected to a low voltage power supply. CE was performed by applying 6 V (25 V/cm) for 300 seconds. Following CE, the contents of each well were extracted and placed in 0.2 mL PCR tubes and 5 μL of Milli Q water was added to each tube. The contents of the wells were held at -20^{o}C until analysis by PCR. A successful mtDNA purification would contain mtDNA in

the SW with no nDNA, which is indicated by a positive PCR for mtDNA and a negative PCR for nDNA using the SW contents as template.

The mtDNA isolation on PMMA MFCs (Figure 2.4) is performed in a similar manner as that with glass MFCs except that the MFCs are coated with 0.1% (w/v) agarose instead of PDMA. In addition the 0.6% agarose is loaded and allowed to sit for 10 minutes in a humidified environment, after which it is submerged in buffer for 5 additional minutes as described in Section 2.4.3. For mtDNA isolation experiments the SR was loaded with 1X STE, 3 µg BSA and 3000 leukocytes, while the SW lacked cells, unless otherwise stated. The CE conditions and analysis with PCR is the same as above with the glass MFCs.

2.5 MFC Cleaning Procedures

2.5.1 Glass MFC Cleaning

In order to allow reuse of existing MFCs the agarose was removed from previously used MFCs by immersion in boiling water for 10 seconds followed by flushing the channel with 0.5 mL of boiling water. The channels were dried with pressurized air and DNAway was applied to the channel and incubated for 10 minutes. The DNAway was rinsed out of the channel using Milli Q water and the channels again dried with pressurized air, upon which the MFC was ready for re-coating and further work. This allowed for MFCs to be used multiple times.

2.5.2 PMMA MFC Cleaning

Two different approaches were developed for removing agarose from previously used PMMA MFCs. After preliminary agarose removal as described for glass MFCs (i.e. 10 seconds boil and flushing with 0.5 mL boiling water, a vacuum was attached to the BW well and the MFC was submerged (under vacuum) into boiling water for 5 minutes. However, this method does damage the MFC and limits its reuse to only three loads.

We developed a less intense method of agarose removal, which incorporated the "10 second boil" and then the MFC was filled with 70^{o}C Milli Q water and submerged in a conical tube also containing Milli Q water at 70^{o}C. The submerged MFC was incubated for 30 minutes, after which 2 mL of 70^{o}C Milli Q water (0.5 mL per well) was pushed through the channels using a 1 mL syringe. The MFC was then dried with pressurized air. This method allowed up to 15 loads without noticeably affecting the CE results, as indicated by consistent results between loads (data not shown).

2.6 Sample preparations

2.6.1 *E. coli*

E. coli were thawed and spread on Luria broth (LB)-agar plates with ampicillin (LB-Amp) and placed in a 37^{o}C incubator overnight. For *E. coli* used in the MFC-based minipreps, a colony was picked from the plate using a sterile toothpick and suspended in a 10 mM Tris-Cl, pH 8.0 solution. The concentration of the suspended *E. coli* was determined using optical density (OD_{600}). The *E. coli* for Qiagen minipreps were grown on the LB-Amp plates overnight. A colony was transferred to 2 mL of liquid LB medium and placed in a 37^{o}C rotating incubator at 225 rpm overnight.

2.6.1.2 Off-chip Plasmid Minipreps

Since the alkaline miniprep is arguably one of the most common DNA purification approaches used (Birnboim and Doly, 1979), it was used as a point of comparison for the MFC-based plasmid miniprep. In the alkaline miniprep, a colony of *E. coli* containing the plasmid of interest was picked from a plate using a sterile toothpick and transferred to a 1.5 mL Eppendorf tube containing 100 µL of lysis buffer (50 mM glucose, 25 mM Tris-Cl, pH 8.0, 10 mM EDTA, 5 mg/mL lysozyme and 0.02 mg/mL ribonuclease A) and placed on ice for 1 minute. 200 µL of 0.2 M NaOH with 1% sodium dodecyl sulfate (SDS) was added to the cell lysate and the tube inverted. The cell suspension was neutralized by adding 150 µL of 7.5 M ammonium acetate and the solution was mixed by shaking. The cellular debris was pelleted by microcentrifugation at 14000 rpm for 8 minutes. The supernatant was transferred to a fresh Eppendorf tube containing 300 µL isopropanol and 0.2% Triton X-100, and centrifuged at 14000 rpm for 8 minutes to pellet the plasmid DNA (pDNA). The pellet was rinsed with 1 mL of 80% ethanol containing 0.2 mM EDTA and again centrifuged at 14000 rpm for 8 minutes and the supernatant discarded. Following a second rinse with 80% ethanol, the pellet was dried and resuspended in MilliQ water.

The QIAprep spin miniprep kit (Qiagen) was used to isolate plasmid from *E. coli* using the instructions provided by the manufacturer.

2.6.2 Fibroblasts

The fibroblast cell line GM5565 was cultured in T-75 cell culture flasks. Frozen cells were thawed and suspended in 12 mL of α-MEM media and incubated at 37ºC with

5% CO_2. The fibroblasts were passaged every three to four days when they reached 70-90% confluence. Passaging involved aspirating the old medium and washing the fibroblasts three times with 1 X phosphate buffered saline (PBS). To detach the cells from the flask, 2 mL of 0.25% trypsin in 1 X PBS was added and the cells were incubated at 37°C for 2-3 minutes, until the cells had visibly detached. After trypsinizing, 10 mL of α-MEM medium was added the cells were mixed by pipetting and split in to two or three separate flasks, followed by additional α-MEM medium to bring the total volume to 12 mL.

Fibroblasts were allowed to grow to 90-100 % confluency prior to harvesting for experiments. The medium was aspirated and the cells were rinsed three times with 1X PBS and then detached from the flask by trypsinization as described for passaging. Once the cells were detached, 7 mL of 1X PBS was added to the flask and cells were transferred to a 15 mL conical tube and centrifuged at 1600 rpm for 3 minutes. The cell pellet was resuspended in 10 mL 1 X PBS and centrifuged at 1600 rpm for 3 minutes to wash out remnants of trypsin. The supernatant was discarded and the cells were resuspended in 0.5 mL of 1 X PBS and transferred to a 1.5 mL Eppendorf tube. The cells were centrifuged again at 3500 rpm for 3 minutes in a microcentrifuge and the resultant pellet resuspended in 100 µL of 1X PBS. The cells were kept on ice until use.

If the cells were to be frozen for use within 48 hours after the final wash they were resuspended in 1.5 mL freezing medium (70% α-MEM, 20% FCS and 10% DMSO) and transferred to a 2 mL cryovial. The cryovial was slowly cooled to -80°C using isopropanol. For use in the MFC-based mtDNA isolations, the cells were removed from -80°C and thawed on ice for 30-45 minutes. The cell suspension was transferred to a 1.5

mL Eppendorf tube and centrifuged at 3500 rpm for 3 minutes in a microcentrifuge. The pellet was then washed three times with 1 X PBS and then resuspended in 100 µL of 1X PBS and kept on ice until use.

2.6.3 Leuckocytes

Leukocytes were isolated from heparinized blood, using the protocol from the Hereditary Diseases Laboratory at the University of Alberta Hospital. This protocol is derived from that of Fotino *et al*.(Fotino *et al.*, 1971). Heparinized blood (6 mL) was obtain by venipuncture (in BD Vacutainer tubes) by a trained phlembotomist. The blood was centrifuged at 1200 x g for 5 minutes at room temperature to separate the different blood components. The plasma (top) layer was discarded, leaving approximately 2 mm of the plasma layer above the buffy coat layer, which is a thin white layer between the plasma layer and erythrocyte layer. The remaining 2 mm of the plasma layer, the buffer layer and 5 mm of the erythrocyte layer were transferred to a 15 mL conical tube containing 5 mL of 1 X PBS. Transferring a small portion of both layers above and below the buffy coat layer ensures complete transfer of the buffy coat layer. The blood cells were mixed with the PBS by pipetting the mixture using a Pasteur pipette, which caused foam to form on top of the mixture. The blood and PBS mixture was slowly transferred to a 15 mL conical tubes containing 4 mLFicoll-Paque Plus by transferring the foam first. The rest of the mixture is carefully layered on top of the Ficoll-Paque to avoid mixing. The Ficoll-Paque with the blood mixture was centrifuged at 600 x g for 20 minutes at room temperature, following which the top clear layer was discarded and the leukocyte layer (Figure 2.7) transferred to a clean 15 mL conical tube. The conical tube was filled with 1 X PBS up to 15 mL and centrifuged at 1200 x g for 5 minutes at 4^{o}C.

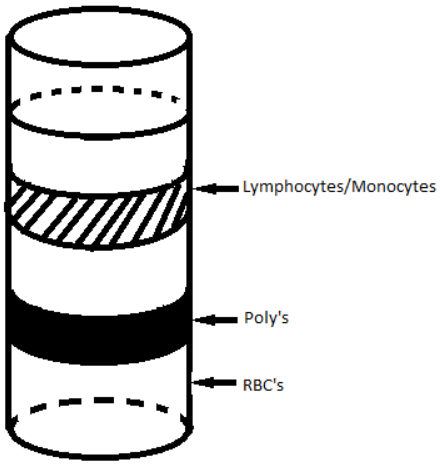

Figure 2.7. The layering of the sample after centrifugation with Ficoll-Paque Plus. The lymphocyte/monocyte layer corresponds to the leukocyte layer.

Following centrifugation the supernatant was discarded and the pellet resuspended in the residual supernatant. A Pasteur pipette was used to scratch the pellet to help with the resuspension. 2 mL of cold sterile MilliQ water was added to the cell suspension and mixed well for 50 seconds. 2 mL of hypertonic solution (0.33 M NaCl) was added and the tubes were inverted to gently mix the solution. The cells were centrifuged at 1200 x g for 5 minutes at 4^{o}C and the supernatant was discarded. The pellet was resuspended in the residual supernatant and 1 mL of cold MilliQ water was added and mixed well for 50 seconds and then washed with 1 mL of hypertonic solution. The final cell suspension was transferred to a clean 2 mL cryovial, which was placed in a clean 15 mL conical tube. The cells were centrifuged at 1200 x g for 5 minutes at 4^{o}C. The supernatant was discarded and the cryovial was placed inverted on Kimwipes to allow the pellet to dry. Once the pellet was dried, if the cell were to be used that day, 100 µL of 1 X PBS was added. If the cells were to be frozen, 1.5 mL of freezing media was added to resuspend the cells, after which they were placed at -80^{o}C in isopropanol to slowly decrease the temperature. If the leukocytes were to be used that day, they were placed on ice until use.

To thaw frozen cells for use, they were placed on ice for 40-50 minutes to thaw. Thawed cells were transferred to a 1.5 mL Eppendorf tube and centrifuged at 1200 x g for 3 minutes. The supernatant is discarded and the pellet is resuspended in 1 mL of 1 X PBS. The cells were centrifuged at 1200 x g for 3 minutes to form a pellet. The cells were rinsed in PBS twice more and then resuspended in 100 µL of 1 X PBS and placed on ice until use.

2.6.4 Other samples

2.6.4.1 Genomic DNA

Genomic DNA was prepared from heparinized blood using either Qiagen's QIAamp DNA blood mini kit or Gentra Puregene blood kit, both according to the manufacturers instructions.

Lower concentrations of gDNA were isolated from blood using a rapid extraction protocol based on Ali *et al*.(Ali *et al*., 2008). The blood was divided into 500 µL aliquots in 1.5 mL Eppendorf tubes. To each tube, 1 mL of red cell lysis buffer (0.01M Tris-Cl, pH 7.6, 320 mM sucrose, 5 mM $MgCl_2$ and 1% Triton X-100) was added, mixed and centrifuged at 7000 rpm for 2 minutes. The supernatant was discarded and the lysis repeated until all the haemoglobin was removed (the solution will become clear). On the final lysis, the tube was inverted to completely remove the supernatant. 400 µL of the nucleic lysis buffer (0.01M Tris-Cl, 11.4 mM sodium citrate, 1 mM EDTA and 1 % SDS) was added to the pellet followed by 100 µL of saturated (~5 M) NaCl and 600 µL of chloroform. The tubes were placed on a rotating mixer at room temperature for 5 minutes, followed by microcentrifugation at 7000 rpm for 2 minutes. The top layer of the supernatant was transferred to a new Eppendorf tube and the DNA precipitated by the addition of 800 µL of cold (-20^{o}C) ethanol. After vortexing, the solution was microcentrifuged at 12000 rpm for 1 minute to pellet the gDNA. The supernatant was discarded and the pellet dried and resuspended in 50 µL MilliQ water.

2.7 Standard Molecular Biology Techniques

2.7.1 Polymerase Chain Reaction

PCR was used for the detection of the MFC-based plasmid segregations, plasmid minipreps, and mtDNA isolations. The primers used in this study are found in Table 2.6. The PCR recipes and corresponding PCR programs are found in Table 2.7 and Table 2.8, respectively. PCRs products were run on agarose slab gels for analysis.

Table 2.6. Primers used for CE analysis.

Primer	**Sequence (5`→3`)**
COX15-F	TATGGATCCTTCCTTTATCG
COX15-R	ATTTAAAGCTTCTCGTAGGG
***CyoE*-F**	GTATGCGAGTCCGGTACCAT
***CyoE*-R**	ATTGCTGGCTTTATGCTGCT
HVI-F	GTACCACCCAAGTATTGA
HVI-R	CGGAGGATGGTGGTCAA
Sco2-cDNA-F3	GGTGCTGATGTACTTTGGCTTC
Sco2-cDNA-R	GCCGCTGGTACAGATCAC
hCOX11-2F	AAACTTGGGTCCAAATGGATTA
hCOX11-2R	TCCTCTGACAGTTTAAGTGATG

2.7.2 Restriction Enzyme Digestion

Restriction enzyme digestion was performed to verify successful isolation of the plasmids after Qiagen plasmid minipreps and alkaline plasmid minipreps. The restriction digest of the pCOX15/ST8 plasmid was performed using *Hind*III and *Bam*HI. The restriction enzyme digestion contained 1 X New England Biolabs (NEB) restriction digest buffer 2, 2 µg BSA, 5 U of each restriction enzyme and 20 ng of pDNA. The

Table 2.7. PCR recipes by primer set.

Reagent	COX15	CyoE	HVI	Sco2	hCOX11
Milli Q H_2O	To fill				
PCR buffer	1X	1X	1X	1X	1 X
$MgCl_2$	1 mM	1 mM	1 mM	1 mM	1mM
dNTP's	200 µM	200 µM	200 µM	200 µM	200 µM
BSA	4 µg	4 µg	4 µg	4µg	4 µg
DMSO	n/a	n/a	n/a	0.04%	n/a
Primer F	800 nM	800 nM	800 nM	800 nM	800 nM
Primer R	800 nM	800 nM	800 nM	800 nM	800 nM
Taq	2.5 U	2.5 U	1 U	1 U	2 U
DNA	1 pg*	10^5 *E. coli**	1-50 ng	1-50 ng	1-50ng

* The DNA/*E. coli* concentration varied to correspond with the amount of DNA/ *E. coli* used on the MFC.

Table 2.8. PCR programs by primer sets.

Step	COX15	CyoE	HVI	Sco2	hCOX11
Initial Denaturation	1 min 20 s @ 94ºC	1 min 20 s @ 94ºC	n/a	2 min @ 94ºC	2 min @ 94ºC
Denaturation	15 s @ 94ºC	15 s @ 94ºC	30 s @ 92ºC	30 s @ 94ºC	30 s @ 94ºC
Annealing	20 s @ 57ºC	20 s @ 57ºC	40 s @ 55ºC	30 s @ 54ºC	40 s @ 54ºC
Extension	1 min @ 68ºC	1 min @ 68ºC	50 s @ 72ºC	30 s @ 72ºC	50 s @ 72ºC
Cycles	36	36	36	36	36
Final extension	5 min @ 72ºC	5 min @ 72ºC	5 min @ 72ºC	5 min @ 72ºC	5 min @ 72ºC
Hold	4ºC	4ºC	4ºC	4ºC	4ºC

plasmids were incubated at 37ºC for one hour then separated on an agarose slab gel for analysis.

2.7.3 Bacterial Transformations

E. coli transformations were performed with plasmids prepared both on-chip and by conventional off-chip approaches to verify the purity of the pDNA. The concentration

of competent DH5α *E. coli* was measured spectrophotometrically at 600 nm (OD_{600}). The *E. coli* were diluted to approximately 10^6 bacterial cells in 20 µL, to correspond to the amount of *E. coli* used for the MFC-based plasmid minipreps. The *E. coli* were transformed using either 2 µL of pDNA from the MFC-based minipreps or 1 µL of pDNA from a traditional miniprep in an attempt to normalize the amount of DNA being used for transformation. The *E. coli* were incubated with pDNA on ice for 30 minutes on ice and then exposed to heat shock (42ºC for 30 seconds), after which they were placed back on ice. 80 µL of LB was added to each transformation reaction and the mixture transferred to 15 mL conical tubes, with subsequent incubation at 37ºC in a rotating incubator at 225 rpm for 1 hour. The transformation reactions were spread on LB-AMP plates and incubated at 37ºC overnight (Northrup *et al*., 2010).

2.7.4 Agarose Gel Electrophoresis

Unless otherwise stated, agarose slab gels consisted of 1 % agarose in either 1 X TAE or 0.5 X TBE. The gel was prepared by heating the agarose/buffer mixture in a microwave until the agarose was dissolved. The molten agarose was cooled prior to the addition of 1 µg/mL ethidium bromide and casting, which required approximately 20 minutes for completed gelling. Once solidified, the agarose gel was loaded into the electrophoresis apparatus and submerged in buffer. Samples were mixed with 10 X bromophenol blue/ xylene cyanol and loaded into the wells. The agarose gels were typically run at 120 V for approximately 1 hour or until the dye front had travelled ¾ of the way down the gel. Agarose slab gels were visualized on an imaging apparatus under UV light.

2.8 Analysis of CE Electropherograms

2.8.1 Generation of Electropherograms Using Geany Plot

The electropherograms from CE were generated using Geany, a python-based program, with the script written by Tianchi Ma (Ma, 2012). Each run was exported as a .txt file from Labview into the Geany program. Unless otherwise stated, the plots were generated using a 20 point running average, which allows for smoother electropherograms without changing the shapes of the curves. The full width at half max (FWHM), arrival times and resolution can all be calculated (to be described below) by zooming in on the appropriate peaks in Geany.

2.8.2 Calculations

The arrival time for each peak is the time (x-value in seconds) at which peak maximum is found (c and i in Figure 2.8). The FWHM is defined as the width of the peak (in seconds) at half the maximum peak height (in Volts). To calculate the FWHM, you must first determine the FWHM PMT value (Volts). Equation 2.1 is used to calculate the FWHM PMT:

$$\text{FWHM PMT} = \frac{(\text{Max PMT} - \text{Baseline PMT})}{2} + \text{Baseline PMT} \qquad \text{Eq.2.1}$$

where the max PMT is the PMT value at the top of the peak (d and j in Figure 2.8) and baseline PMT is the PMT value of the baseline (a in Figure 2.8), which is found prior to the arrival of the peaks. Once the FWHM PMT has been determined, the time corresponding to the FWHM PMT is found on the left and right side of the peak (e and k in Figure 2.8). The FWHM, in seconds, is calculated using Equation 2.2:

$$FWHM=(FWHM\ right-FWHM\ left) \qquad \text{Eq 2.2}$$

where FWHM right is the time corresponding the FWHM PMT value to the right of the peak (g and m in Figure 2.8) and FWHM left corresponds to the left side of the peak (f and l in Figure 2.8).

The arrival time and the FWHM were calculated for each individual peak and were used to determine the resolution of two peaks. The resolution (R_{bp}) is defined as the size difference (in bp) required between two DNA species to be capable of resolving the resultant peaks to their FWHM. The resolution is calculated using Equation 2.3:

$$R_{bp}= 0.5\ (bp(\frac{FWHM_1+FWHM_2}{t_2-t_1})) \qquad \text{Eq 2.3}$$

where bp is the difference in size between the two DNA species, $FWHM_1$ and $FWHM_2$ are the FWHMs of the smaller DNA fragment (first peak in the electropherogram) and the larger DNA fragment (second peak in the electropherogram), respectively, and t_1 and t_2 are the arrival times of the smaller and larger DNA species, respectively.

The data from the electropherograms were imported to a Microsoft Excel spreadsheet, where the averages and standard deviations (STD) were calculated. The percent variation for each criterion was calculated by dividing the STD by the average for that criterion.

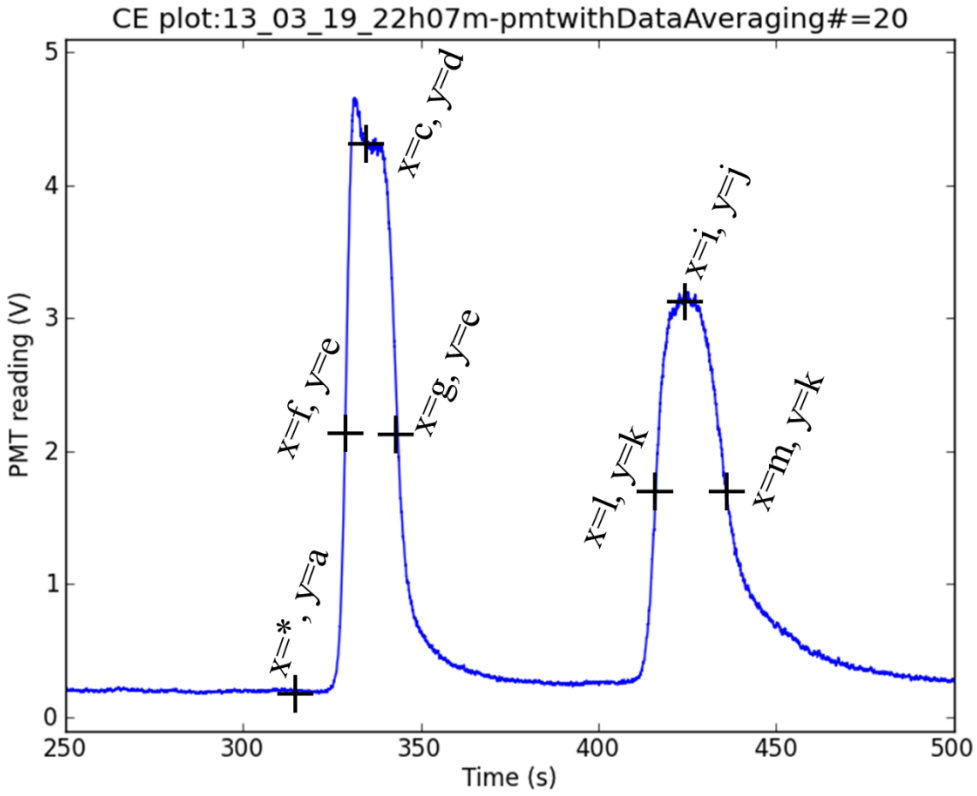

Figure 2.8. Sample electropherogram produced using Geany, illustrating the separation of the two distinct plasmid species. The data points that are to be recorded for analysis are marked with + signs (these are approximate position). At each + there is an x and y value, representing the time and the PMT value respectively, which correspond to the required criteria for analysis outlined in Section 2.8.2. For the baseline, x-value is not important so as long as it is examined prior to the DNA arrival where the line is flat.

CHAPTER 3- THE MANIPULATION OF SMALL QUANTITIES OF PLASMID DNA USING MICROFLUIDIC CHIPS

Some material from this chapter has been previously published

Northrup, V.A., C.J. Backhouse, and D.M. Glerum. 2010. Development of a microfluidic chip-based plasmid miniprep. *Anal. Biochem.* **402**: 185-190.

3.1 Introduction

3.1.1 The Use of Plasmids as a Model for the Mitochondrial DNA

Plasmids are valuable vectors in molecular biology that can be used to in cloning, gene segregation and introducing recombinant DNA into cells (Sambrook *et al*., 1989). Plasmids, like mtDNA, are extrachromosomal, closed-circular, double-stranded, DNA molecules that are typically a few kilobases in size, thus making plasmids a good model for mtDNA in CE. The size difference between plasmids and the gDNA of bacterial cells is similar to the size disparity between the mtDNA and the nDNA of mammalian cells, with plasmids and mtDNA being kilobases in size and the gDNA of bacteria or nDNA of mammalian cells being megabases in size. Therefore, bacteria containing a plasmid should be a suitable *in vivo* model for mtDNA in mammalian cells in CE.

3.1.2 Techniques for Extraction of Extrachromsomal DNA

The plasmid miniprep is a common molecular biology technique used to rapidly isolate pDNA from cells. The pDNA that is isolated by minipreps can be used for numerous downstream molecular biology techniques including cloning, restriction enzyme digestion and cell transformation. However, the pDNA from minipreps is not usually sufficiently pure for more sensitive methodologies, such as many enzymatic assays, PCR, and sequencing. In addition, contaminating gDNA can interfere with accurate spectrometric pDNA quantification (Paul *et al*., 2008). Impurities can be removed by further purification, using techniques such as affinity capture (Marko *et al.*, 1982), phenol and chloroform extraction (Mukhopadhyay and Mandal, 1983), or caesium chloride (CsCl) gradients (Radloff *et al*., 1967), but these are time consuming and not feasible for rapid plasmid screening.

There are a variety of miniprep protocols that vary in the chemicals used and the specific procedures, but they all follow the same basic principles. One of the most common miniprep protocols is the alkaline plasmid miniprep (Birnboim and Doly, 1979; Paul *et al*., 2008), with boiling and lithium minipreps also in common use (Paul *et al.*, 2008). Standard protocols start with growth of the bacterial cells, typically for 16-40 hours, to obtain on the order of 10^{10} to 10^{11} bacterial cells, which are then lysed with detergents under alkaline condition (in the alkaline miniprep). Detergents and bases are then used to denature the chromosomal DNA by disrupting base-pairing. When the solution is neutralized the pDNA renatures since it is small and supercoiled, while the larger gDNA is unable to renature. A further centrifugation step is used to pellet the denatured genomic DNA and the pDNA can be recovered from the supernatant. There are MFCs that have been developed to manipulate plasmids (Kim *et al.*, 2007; Nagamine *et al*., 2005) and analyze plasmids (Ding *et al*., 2003), but in all cases the plasmids are isolated off-chip. There have also been MFC-based assays that lyse bacterial cells on-chip to examine the bacterial gDNA (Wang *et al*., 2007; Yeung and Hsing, 2006), but these studies do not describe the separation of pDNA from gDNA. To develop a "micro total analysis system" (μTAS) to manipulate and analyze plasmids, a critical missing step has been the ability to isolate pDNA from bacterial cells on a MFC.

3.1.3 Surface Modification in Capillary Electrophoresis

As discussed in Chapter 1, the larger surface area to volume ratio in MFCs make surface effects more prevalent, thereby making control of the surface chemistry a critical factor in developing reliable MFC-based assays (Doherty *et al*., 2002; Horvath and Dolnik, 2001; Yates and Campbell, 2011). The surface chemistry can affect the EOF and

adsorption of analytes, such as proteins and DNA, to the channel walls. Adsorption is thought to be largely governed by van der Waals interactions, hydrophobic attraction and hydrogen bonding (Azadi and Tripathi, 2012; Fa *et al*., 2005). One method that is used to modify the surface of MFCs is the use of surface coatings, which are usually polymers or surfactants (Doherty *et al*., 2002; Lucy *et al*., 2008). Surface coatings can shift the hydrodynamic plane of shear away from the underlying surface charge, thereby decreasing the EOF and adsorption (Barron and Blanch, 1995; Doherty *et al*., 2002). For DNA separations, an ideal coating is charge-neutral, hydrolytically stable, can adhere to the channel wall, and has a minimal thickness equal to the electrical double layer (Doherty *et al*., 2002).

One of the most commonly used surface coatings is covalently bound LPA (Doherty *et al*., 2002; Hjerten, 1985). LPA coating decreases adsorption and EOF, but has a limited lifetime and stability, as well as being time-consuming, and generates an uneven layer with an unknown thickness. Dynamic coatings are typically produced by a low-viscosity aqueous solution of an adsorbing polymer. Dynamic coatings can interact with a silica surface, such as the channel walls in glass MFCs, by either hydrophobic attraction (Chiari *et al*., 2000), electrostatic forces (Katayama *et al*., 1998; Rodriguez and Li, 1999), or hydrogen bonding (Mathur and Moudgil, 1997). These dynamic coatings eliminate the need for organic solvents, high temperatures and viscous solutions that are required for covalent coatings, such as LPA. PDMA (Albarghouthi and Barron, 2000; Albarghouthi *et al*., 2002) and polyvinylpyrrolidone (PVP) are two of the most common dynamic coatings (Doherty *et al.*, 2002). PHEA is another dynamic coating that has been used to modify surfaces in CE (Albarghouthi and Barron, 2000; Lucy *et al.*, 2008).

3.1.4 Analysis of Circular DNA in Capillary Electrophoresis

Since both plasmids and mtDNA are closed-circular DNA molecules, they are prone to the phenomenon trapping in CE-based assays. One of the first studies to demonstrate the phenomenon of trapping was by Levene and Zimm (Levene and Zimm, 1987) who found that under direct current, larger plasmids would arrest in AGE, but smaller plasmids could migrate normally. When they applied PFGE they could abolish the trapping effect, and the larger plasmids could also migrate during AGE. This demonstrated that circular DNA was getting trapped and that trapping could be reversed with a PFGE approach.

As discussed in Chapter 1, the critical field for CE separation of a plasmid is inversely proportional to the size of the plasmid (Akerman and Cole, 2002; Manage *et al*., 2008). Manage *et al*. (Manage *et al.*, 2008) studied the effects of electric field on trapping of a supercoiled DNA (SC) ladder, with 11 plasmid species that ranged from 2 kb to 16.2 kb. At the lowest electric field tested (32 V/cm) the 14.2 kb plasmid was not trapped while the 16.2 kb plasmid was trapped. This result suggest that the critical field for mtDNA, which is 16.6 kb, would be less than 32 V/cm. Since Manage *et al.* did not examine electric fields below 32 V/cm, they were unable to determine the critical field for the 16.2 kb plasmid.

3.1.5 Objective

In this chapter, we have used a 7.8 kb plasmid (pCOX15/ST8) (Glerum *et al.*, 1997) as a model for mtDNA in CE. Using the plasmid we examine the factors required to decrease the threshold, the lowest quantity of pDNA that could be successfully moved

during CE, to mere picograms of pDNA. Using a CE-based approach we demonstrate the ability to move only 1 pg of pDNA, which is the lowest quantity of pDNA to be successfully manipulated as found in the current literature. We take this a step further by applying the segregation to a MFC-based plasmid miniprep using only 10^5 *E. coli*, orders of magnitude fewer cells than needed for existing minipreps. The picogram plasmid segregation and plasmid miniprep will form the basis for an MFC-based mtDNA segregation for only a few thousand human cells.

3.2 Results

3.2.1 The Determination of Critical Fields for Plasmids in Capillary Electrophoresis

Previous work has demonstrated the critical field of a 16.2 kb plasmid was less than 32 V/cm (Manage *et al*., 2008). To more accurately determine the critical field for the 16.2 kb plasmid required to prevent trapping, we performed CE using the SC ladder at 27 V/cm and 32 V/cm (Figure 3.1). In this plasmid separation we used glass 4-PMs that were coated with 5% (w/w) PDMA and used 1 X TBE as the buffer. The separation distance, the distance between the intersection and the detection point, was 13 mm. The critical field for a 16.2 kb plasmid was determined to be 27 V/cm, indicated by the presence of the 16.2 kb plasmid at an electric field of 27 V/cm but its absence at an electric field of 32 V/cm. Therefore, we concluded that the critical field for the 16.2 kb plasmid is 27 V/cm. Since the mtDNA is 16.6 kb we can assume the critical field of the mtDNA would also 27 V/cm.

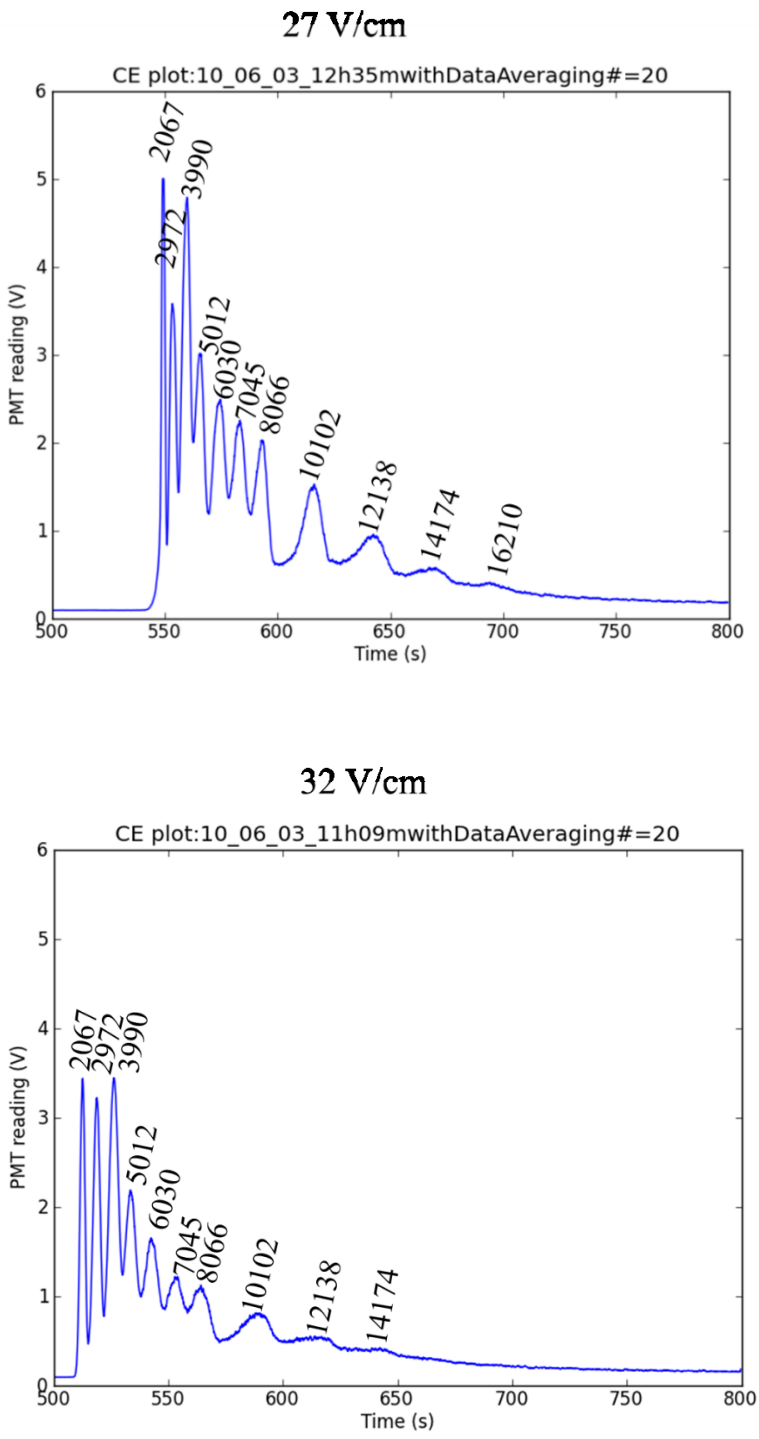

Figure 3.1. Examination of trapping in CE using the SC ladder. Each separation was run in PDMA coated glass 4-PMs in 0.6% agarose and 1 X TBE. The top electropherogram is from CE run at 27 V/cm and all 11 species of the SC ladder are present. The bottom electropherogram is from CE run at 32 V/cm, in which only 10 of the 11 species of the SC ladder are present (the 16 210 bp plasmid is absent).

3.2.2 Manipulation of Picogram Quantities of Plasmids DNA Using Capillary Electrophoresis

Fibroblasts contain approximately 600 mtDNA copies per cell (Dimmock *et al.*, 2010), which amounts to less than 10 pg of mtDNA in 1500 fibroblasts. Therefore, a threshold, the lowest concentration of pDNA that could be successfully segregated, of 1 pg would be sufficient to be adapted to isolating the mtDNA from only 1500 fibroblasts. Using the plasmid pCOX15/ST8 as a model for mtDNA, we endeavored to develop a plasmid segregation that could move only 1 pg of pCOX15/ST8 from the SR to the SW using CE.

With the larger surface area to volume ratio found in MFC-based assays, we hypothesized that surface chemistry was an important variable that affected the threshold due to non-specific adsorption of DNA. Non-specific adsorption of DNA increases the threshold because DNA is lost to the channel walls during CE and can therefore not successfully migrate to the SW. To investigate the issue of surface chemistry on glass 4-PMs, we applied four different surface coatings, two covalent coatings and two dynamic coatings. For the covalent coatings, we chose LPA (Hjerten, 1985) because of LPA's broad usage and CPA (Huang *et al*., 1992), since Huang and colleagues found CPA had almost twice the efficiency of LPA in protein separations. For the dynamic coatings, we chose PDMA and PHEA (also known as polyDuramide) based on studies from the Barron group, which suggest these dynamic coatings gave more robust results for our plasmid segregation compared to an LPA coating (Albarghouthi *et al*., 2002; Hestekin *et al*., 2006). We hypothesized that PHEA would result in the lowest threshold based on the improved resolution seen in the studies from the Barron group.

Each coating was tested by performing the plasmid segregation with pCOX15/ST8 at 10 pg and 25 pg. All of these plasmid segregations were run using 1 X TTE in the 0.6% agarose and 0.1 X TTE in the running buffer. The threshold for LPA and CPA was determined to be 25 pg as indicated by the presence of pCOX15/ST8 in the SW for the 25 pg plasmid segregation (Figure 3.2) and the unsuccessful plasmid segregations using 10 pg (data not shown). The threshold for PHEA was not determined, but was higher than 25 pg indicated by the absence of pCOX15/ST8 in the SW well in the 25 pg plasmid segregation (Figure 3.2). The final surface coating tested, PDMA, resulted in a threshold of 10 pg (Figure 3.2), which was the lowest threshold obtained at the time. Since PDMA demonstrated the lowest threshold of the coatings tested, it was chosen as the surface coating in developing our picogram plasmid separation.

Once we had decreased the threshold to 10 pg using the PDMA coating, we continued to examine other variables that contributed to the threshold, such as the voltage program. The voltage program determines the direction and strength of the electric field used during CE. Since we were performing CE on plasmids, we must consider trapping when developing a useful voltage program. The critical field of pCOX15/ST8, which is a 7.8 kb plasmid, is approximately 55 V/cm (based on the critical field of the 8 kb plasmid in the study by Manage *et al.* 2008). Since we intend to apply the plasmid segregation to mtDNA in future experiments we chose 32 V/cm for our voltage programs, as it is

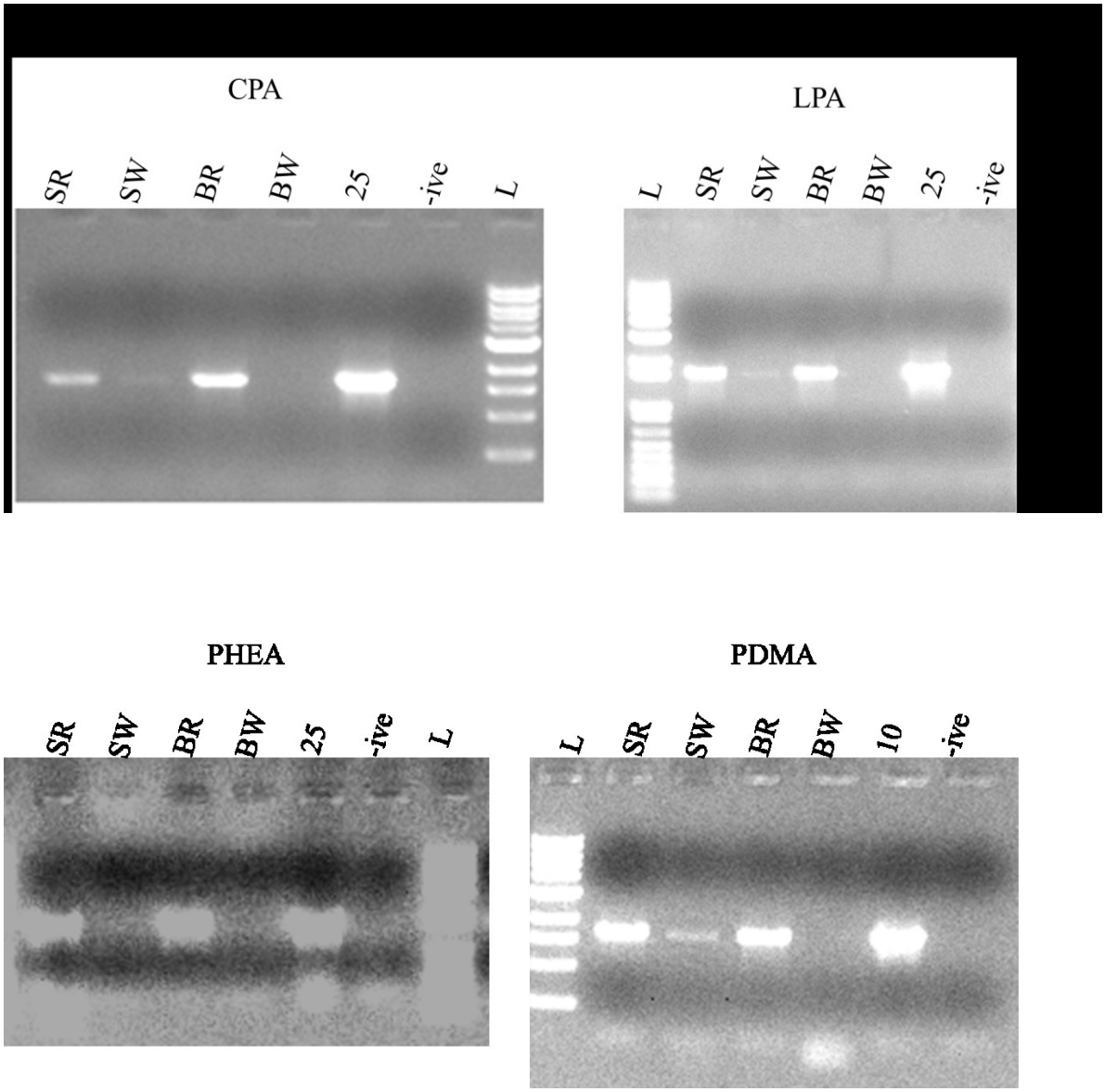

Figure 3.2. The thresholds of various surface coatings in CE. PCR results from plasmid segregations of pCOX15/ST8. CPA is cross-linked polyacrylamide, LPA is linear polyacrylamide, PHEA is poly-N-hydroxyethylacrylamide and PDMA is poly-N,N-dimethylacrylamide, SR, SW, BR and BW correspond to the PCR reactions using the contents of their respective wells after the CE, 25 and 10 are positive controls of either 25 pg and 10 pg pDNA respectively, which corresponds to the concentration of pDNA used in the plasmid segregation and –ive is the off-chip negative control. The SR and BR are on-chip positive controls and BW is the on-chip negative control.

below the critical field of pCOX15/ST8 and close to that of the critical field of the mtDNA (27 V/cm) making it easier to adapt the plasmid segregation for mtDNA. One of the voltage programs examined used a constant electric field of 32 V/cm for 600 seconds (the 600 s voltage program). We found that, while the 600 second voltage program could successfully segregate 10 pg of pDNA (data not shown), we could not obtain a successful plasmid segregation at 1 pg (Figure 3.3). We attempted longer single step injections at 32 V/cm and found the results were not reproducible (data not shown). The 3-step injection uses a combination of PFGE and low electric fields, which have both been demonstrated to counteract trapping (Levene and Zimm, 1987; Manage *et al*., 2008). The first step uses a high electric field (167.3 V/cm) to promote the entrance of pDNA into the channel, but since 167.3 V/cm is well above the 55 V/cm critical field, it causes trapping. To counteract the trapping caused in the first step, the second step reverses the direction of the electric field (the cathode is in the SR and anode in the SW), effectively untraping the plasmid. The third and final step is applying an electric field of 32 V/cm for 600 seconds, which should move the pDNA but also prevent further trapping. The 3-step injection resulted in a threshold of 1pg and was therefore chosen as the voltage program for the plasmid segregation. It should be noted that the 32 V/cm used for step two and three of the 3-step injection would need to be reduced to 27 V/cm for an approximately 16 kb plasmid or the mtDNA to become trapped at 32 V/cm.

Since buffers have been found to have a large effect on electrophoresis, we hypothesized that the buffer used affected the threshold. Tris-based buffers have commonly been used for AGE in many molecular biology laboratories. Two of the most

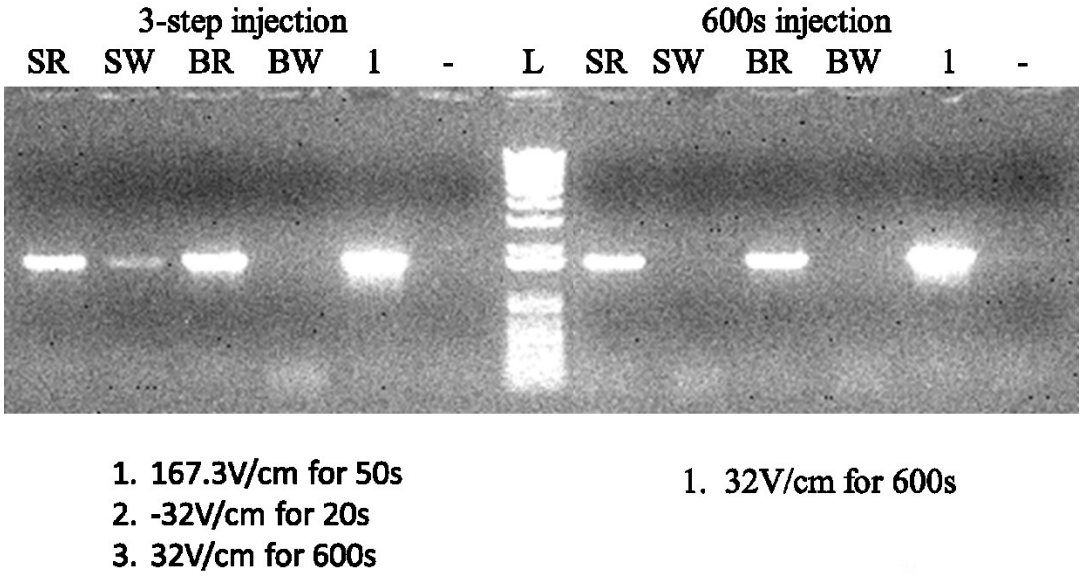

Figure 3.3. The effects of the voltage program on the threshold in CE. Both plasmid segregations were performed using 0.1 X TTE. SR, SW, BR and BW correspond PCR reactions using the contents of their respective wells after CE, 1 is the off-chip positive control that uses 1 pg of pDNA, which corresponds to the concentration of pDNA used in the plasmid segregation and –ive is the off-chip negative control. The SR and BR are on-chip positive controls and BW is the on-chip negative control. The steps of each voltage program are indicated below their respective gel images.

commonly used buffers are TBE and TAE (Brody and Kern, 2004a; Singhal *et al*., 2010; Stellwagen *et al*., 2000a). TTE is another Tris-based buffer that has also been used in CE (Albarghouthi and Barron, 2000; Manage *et al*., 2008). We tested these three Tris-based buffers to determine their effects on the threshold of the plasmid segregation. The presence of pDNA is indicated by the PCR product that can only occur in the presence of template (i.e. pDNA). The threshold of TAE was above 10 pg, indicated by the unsuccessful plasmid segregation using 10 pg of pCOX15/ST8 (Figure 3.4). TTE had a threshold of 10 pg, indicated by a successful plasmid segregation at 10 pg and an unsuccessful plasmid segregation at 1 pg. TBE had a threshold of 1 pg, indicated by a successful plasmid segregation at both 10 pg and 1 pg (Figure 3.4). Therefore, TBE was chosen as the buffer for the MFC-based plasmid segregation.

Once TBE was chosen as the buffer, the optimal concentration needed to be determined as the concentration was found to be important in obtaining a reproducible plasmid segregation. We were initially using 0.1 X TBE and found the CE to be unreliable at this concentration, which led us to hypothesize that 0.1 X TBE might not have sufficient buffer capacity. By increasing the concentration of buffer we could ensure sufficient buffering capacity on all plasmid segregations and obtain a reliable 1 pg MFC-based plasmid segregation. To test this hypothesis we used the concentrations 0.1 X TBE, 0.5 X TBE and 1 X TBE in the plasmid segregation. Figure 3.5 shows a representative plasmid segregation run using each of the TBE concentrations. The results for 0.1X TBE were not reproducible, and at the higher end, 1 X TBE did not result in a successful 1 pg plasmid segregation. At 0.5 X TBE we were able to obtain a reproducible 1 pg plasmid segregation (Figure 3.5). We therefore proceeded to verify the

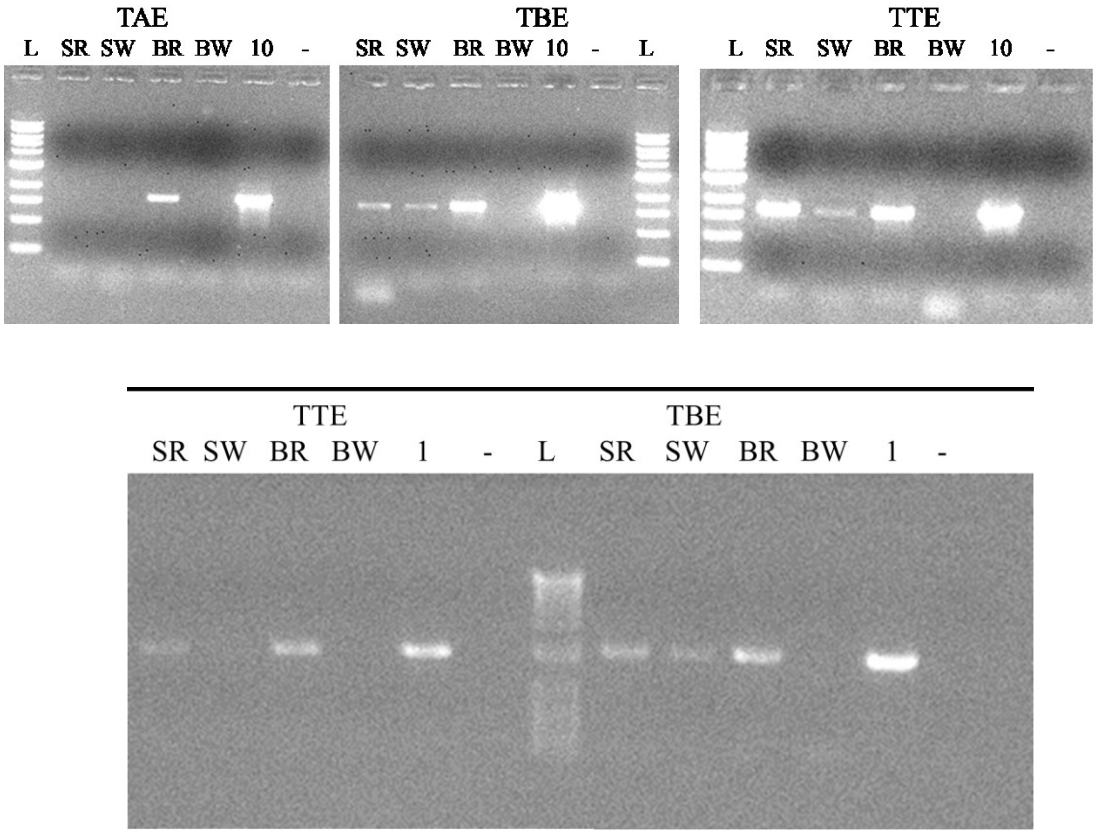

Figure 3.4. Tris-based buffers affects the plasmid segregation. The top row of gel images show the results from CEs of 10 pg of pCOX15/ST8 using 0.1 X TAE, 0.1 X TBE and 0.1X TTE. The bottom row of gel images show the CE results of 1 pg of pCOX15/ST8 using 0.1 X TTE and 0.1X TBE. SR, SW, BR and BW correspond to be PCR reactions using the contents of their respective wells after CE, 1 and 10 are the off-chip positive controls that use 1 pg and 10 pg pDNA respectively, which corresponds to the concentration of pDNA used in the plasmid segregation and –ive is the off-chip negative control. The SR and BR are on-chip positive controls and BW is the on-chip negative control.

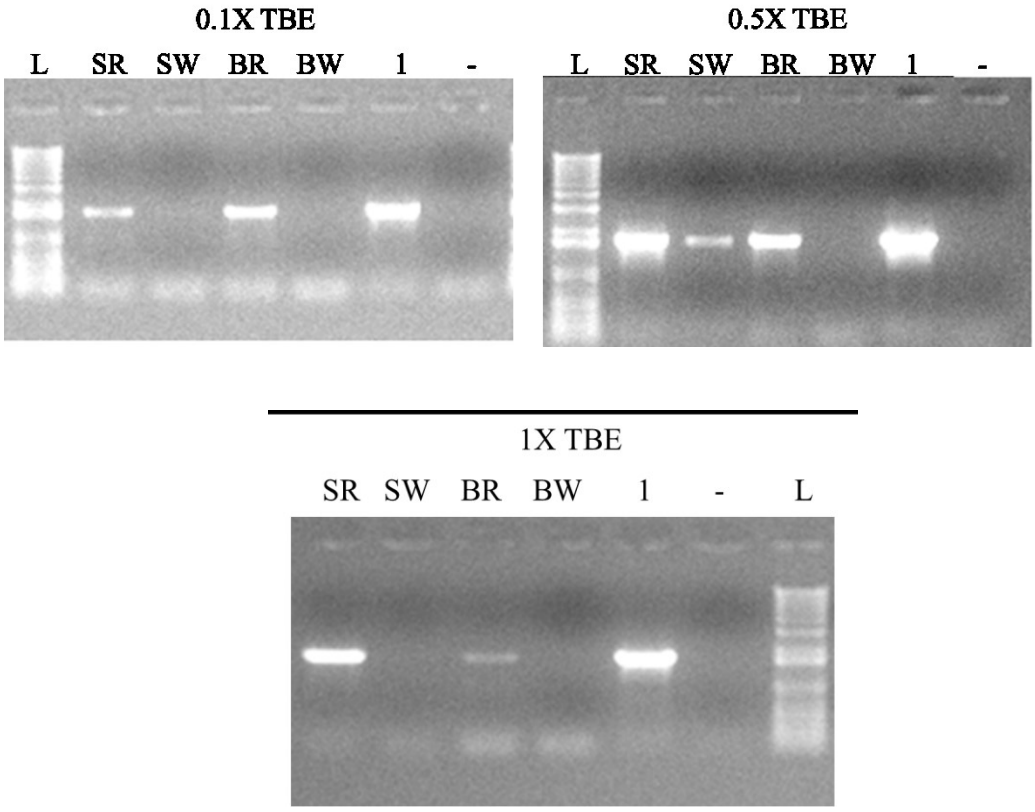

Figure 3.5. TBE concentrations affect the plasmid segregation. The concentration of TBE used is indicated above each of the gel images. SR, SW, BR and BW correspond PCR reactions using the contents of their respective wells after CE, 1 is the off-chip positive control that uses 1 pg of pDNA, which corresponds to the concentration of pDNA used in the plasmid segregation and –ive is the off-chip negative control. The SR and BR are on-chip positive controls and BW is the on-chip negative control.

reliability of the 1pg plasmid segregation using 0.5X TBE.

As shown above, we could obtain a successful 1 pg plasmid segregation on glass 4-PMs using a 5% (w/w) PDMA coating, 0.5 X TBE running buffer and the 3-step injection voltage program. This resulted in a reproducible 1 pg plasmid segregation using the plasmid pCOX15/ST8. Figure 3.6 shows the results of three separate plasmid segregations, which are representative of the plasmid segregations using this protocol. Many other MFC-based assays have been described using at least an order of magnitude more DNA as compared to the MFC-based plasmid segregation reported here. To the best of our knowledge, this is the lowest concentration of pDNA that has successfully been manipulated in a CE-based assay. The ability to manipulate 1 pg of pDNA could potentially be used to manipulate the picogram quantities of mtDNA found in only a few thousand cells.

3.2.3 Isolating Plasmids From Bacterial Cells Using Capillary Electrophoresis

A key element for the development of a μTAS system to analyze and manipulate plasmids is the ability to purify plasmids on-chip. We have adapted the 1 pg plasmid segregation described above to develop the first MFC-based plasmid miniprep, using only 10^5 (approximately 100 ng) *E. coli* containing the plasmid pCOX15/ST8 (Figure 3.7). One main difference between the MFC-based plasmid segregations described above and the MFC-based plasmid miniprep is that initial bacterial cell lysis step in any plasmid miniprep.

In traditional alkaline minipreps approximately 10^{10} to 10^{11} bacterial cells are lysed using detergents in an alkaline buffer, which also contains lysozyme to digest the

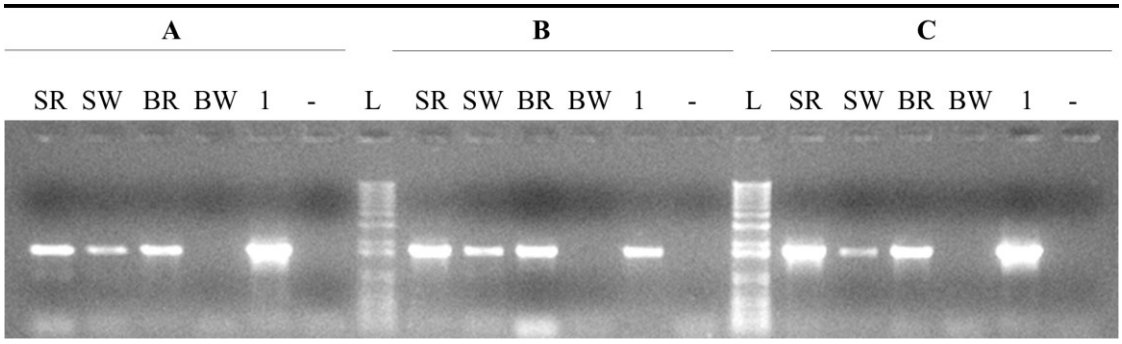

Figure 3.6. Reproducibility of the 1 pg MFC-based plasmid segregation. Three plasmid segregations, represented by A, B and C, performed using a 5% (w/w) PDMA coating, 0.5 X TBE and a 3-step injection voltage program. SR, SW, BR and BW correspond to PCR reactions using the contents of their respective wells after CE, 1 is the off-chip positive control that uses 1 pg of pDNA, which corresponds to the concentration of pDNA used in the plasmid segregation and –ive is the off-chip negative control. The SR and BR are on-chip positive controls and BW is the on-chip negative control.

peptidoglycan layer of the bacterial cell wall (Birnboim and Doly, 1979). One of the requirements for achieving a MFC-based plasmid miniprep was the use of a non-ionic detergent for the lysis step, to avoid having the detergent migrate during the CE step. Triton X-100 is a non-ionic detergent that has been widely used to lyse bacteria (Cornett and Shockman, 1978) and was therefore a good detergent choice for the MFC-based miniprep. Although Triton X-100 has been documented to contain contaminants (Ashani and Catravas, 1980), we did not observe these in our experiments. In the MFC-based miniprep, *E. coli* containing pCOX15/ST8 were lysed on glass 4-PMs that had been coated with 5% (w/w) PDMA and loaded with 0.6% agarose in 1 X TBE. Lysis of the *E. coli* took place in the SR well, which contained 1.67 % Triton X-100 in 0.33 mM EDTA, 1 X TBE, 3 µg of BSA and 10^5 *E. coli* and was incubated at room temperature for 5 minutes to allow for lysis followed by CE along the injection channel to move the pCOX15/ST8 from the SR to the SW. We speculate the alkaline environment generated by the TBE promotes the lysis of the *E. coli* by Triton X-100, similar to an alkaline miniprep. Therefore the increase in TBE to 1 X, instead of the 0.5 X TBE used in the MFC-based plasmid segregation, is to accommodate the role of TBE in lysis and as the CE buffer. Most minipreps use denaturation and renaturation to separate the pDNA from the bacterial gDNA, followed by a centrifugation step to isolate the pDNA. In the MFC-based miniprep, we use CE to isolate the pDNA since the larger gDNA is too large to enter the 0.6 % agarose sieving matrix, unless it has been fragmented (Gao *et al*., 2007), and therefore gDNA and cellular debris should remain in the SR while the pDNA migrates to the SW.

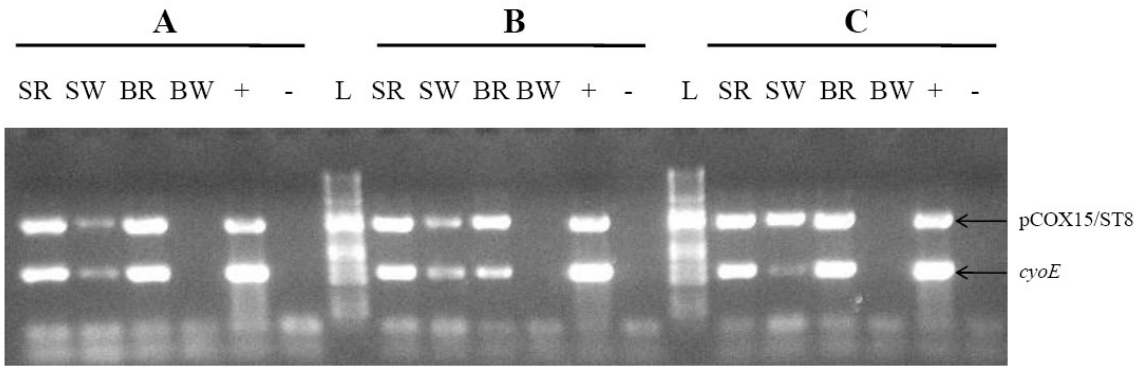

Figure 3.7. Reproducibility of the MFC-based plasmid miniprep. The results of a multiplexed PCR from three MFC-based plasmid minipreps, indicated by A, B and C. The top PCR band represents pCOX15/ST8 and the bottom band represents the gDNA from the *E. coli* (*cyoE*). SR, SW, BR and BW correspond to PCR reactions using the contents of their respective wells after CE, + is the off-chip positive control that uses 10^5 *E. coli*, which corresponds to the concentration of *E. coli* used in the plasmid miniprep and –ive is the off-chip negative control. The SR and BR are on-chip positive controls and BW is the on-chip negative control. Taken from (Northrup *et al.*, 2010).

A successful MFC-based miniprep is indicated by the presence of pCOX15/ST8 in the SW well at the end of the CE. A multiplex PCR was carried out to detect both pCOX15/ST8 and *cyoE*, which encodes the *E. coli's* heme O synthase and serves as a marker for the presence of *E. coli* gDNA. We expected that the MFC-based plasmid minipreps would result in pCOX15/ST8 being electrophoresed to the SW, while the *E. coli* gDNA would remain in the SR. As expected, both the plasmid and gDNA were found in both the SR and BR and neither was found in the BW. We were able to successfully isolate the plasmid in the SW (top band in Figure 3.7), but there was also some gDNA from the *E. coli* (bottom band in Figure 3.7). The electrophoresis of the gDNA is probably due to sheared gDNA arising from dead cells present in the cell suspension (Paul *et al*., 2008), or from shearing of the DNA caused by the pipetting used in preparing the sample for CE (Gao *et al*., 2007). This indicates that we have successfully segregated the plasmid, although the MFC-based miniprep also contains some gDNA contamination. We hypothesize the gDNA observed in the MFC-based plasmid miniprep was also present in conventional minipreps, and was therefore not a concern for the MFC-based miniprep.

To confirm the gDNA seen in the MFC-based plasmid miniprep was not problematic, we conducted experiments on products from the MFC-based miniprep compared to products from conventional minipreps. Plasmid minipreps are typically verified using restriction enzyme digestion of the isolated plasmid. However, due to the low concentration of pDNA used in the MFC-based plasmid miniprep, we used PCR, which is much more sensitive than restriction enzyme digest to small quantities of DNA, to detect the plasmid and the bacterial gDNA. The use of PCR allows for detection of the

small concentration of pDNA used in the MFC-based miniprep, but PCR is also more sensitive to gDNA contamination. We therefore asked whether there is gDNA contamination in miniprep DNA obtained from commercially available plasmid purification kits would also be positive for gDNA when analyzed using PCR. We examined the products of an alkaline lysis miniprep protocol and a Qiagen kit miniprep using PCR and found that they also contain gDNA contamination (Figure 3.8). Our data demonstrate that the purity of the MFC-based plasmid miniprep is comparable to that of the commercially available off-chip minipreps.

To verify that the gDNA contamination found in the off-chip minipreps in Figure 3.8 would not be detected by restriction enzyme digestion, we performed a restriction enzyme digest of the pCOX15/ST8 isolated from the off-chip minipreps (Figure 3.9). The gDNA, which was verified to be present in Figure 3.8, was not seen in the restriction enzyme digestion (Figure 3.9). This also verifies that the gDNA does not affect the restriction enzyme digestion that is typically used to verify plasmid minipreps. The MFC-based plasmid minipreps were not used in the restriction enzyme digestion since the concentration of the pDNA is too low and would therefore not be visualized in an agarose slab gel with ethidium bromide.

One of the most often used end points for purified plasmids is for transformation into bacterial or eukaryotic cells. To demonstrate that the plasmid isolated using our MFC-based plasmid miniprep was suitable for *E. coli* transformation, we carried out an off-chip transformation of *E. coli* (Figure 3.10). The MFC-based plasmid minipreps used

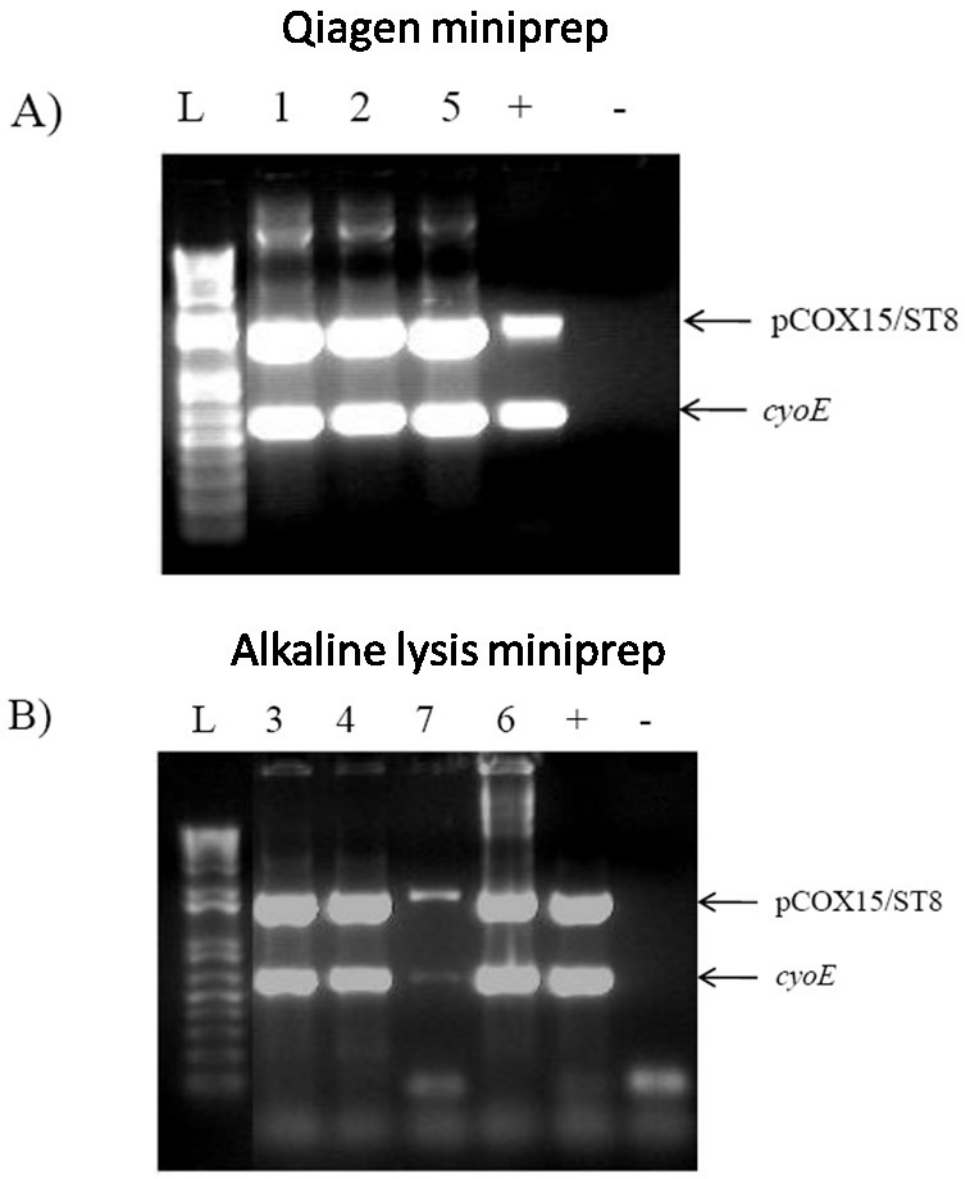

Figure 3.8. Examination of off-chip plasmid miniprep products using PCR. A) PCR results of plasmid minipreps using the Qiagen miniprep kit. B) PCR results of alkaline plasmid miniprep. L is the 1 kb plus ladder, the numbers 1-7 correspond to different miniprep preparations with 1-4 corresponding to 1-4 in Figure 3.9. + is the positive control of a colony PCR using *E. coli* and – is negative water control. The top band is the pCOX15/ST8 and the bottom band in the *E. coli* gDNA (represented by *cyoE*). Taken from (Northrup *et al*., 2010).

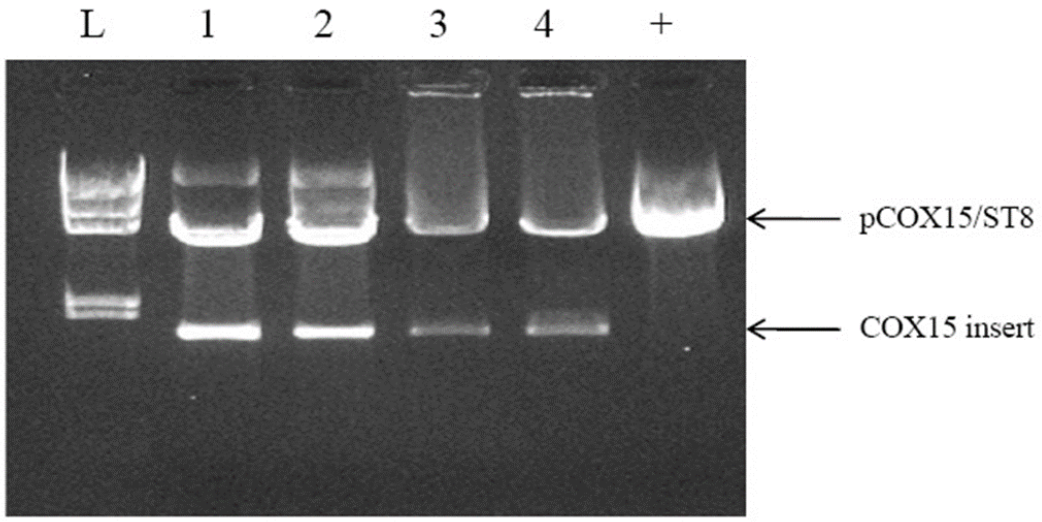

Figure 3.9. Restriction enzyme digestion of off-chip plasmid minipreps. The restriction enzyme digestion was performed using *Hind*III and *Bam*HI. The L is the *Hind*III ladder, the numbers 1-4 correspond to the minipreps in Figure 3.8 and + is the uncut pCOX15/ST8 plasmid. The higher band is the pCOX15/ST8 plasmid and smaller band is the COX15 insert. Taken from (Northrup *et al*., 2010).

for the bacterial transformation used 10^6 *E. coli,* which is still significantly less than used in other minipreps. Since the MFC-based plasmid miniprep uses orders of magnitude less *E. coli*, it results in almost 100 times less plasmid compared to the off-chip plasmid minipreps. To account for the lower plasmid concentration, we down-scaled the transformation to use 10^6 *E. coli.* Figure 3.10 shows a restriction enzyme digestion of plasmids isolated using a Qiagen miniprep kit from *E. coli* that were transformed using either the products of the MFC-based plasmid miniprep or the products of an off-chip plasmid miniprep. This further confirms the quality of the MFC-based plasmid miniprep is similar to the off-chip plasmid minipreps, but it uses over 100 times fewer bacterial cells, which decreases the time required for bacterial growth.

3.3 Discussion

One of the largest challenges to developing a MFC-based mtDNA analysis tool is the ability to manipulate picogram quantities of DNA. Although many MFCs use small quantities of sample compared to most traditional assays, they still typically use nanogram quantities. We are aiming to be able to use approximately 1500 fibroblasts, which based on fibroblast containing 600 mtDNA copies per cell (Dimmock *et al*., 2010), are estimated to contain a total of approximately 1 pg of mtDNA. We have chosen fibroblasts as a starting point because they are easily cultured and are used in mtDNA analysis (Mancuso *et al*., 2009). Once we are able to manipulate mtDNA from fibroblasts, the methodologies could be adapted for leukocytes or myocytes, from blood or muscle respectively. To be able to manipulate small quantities of DNA, we needed to determine the various factors that contributed to the threshold in the MFC-based plasmid segregation.

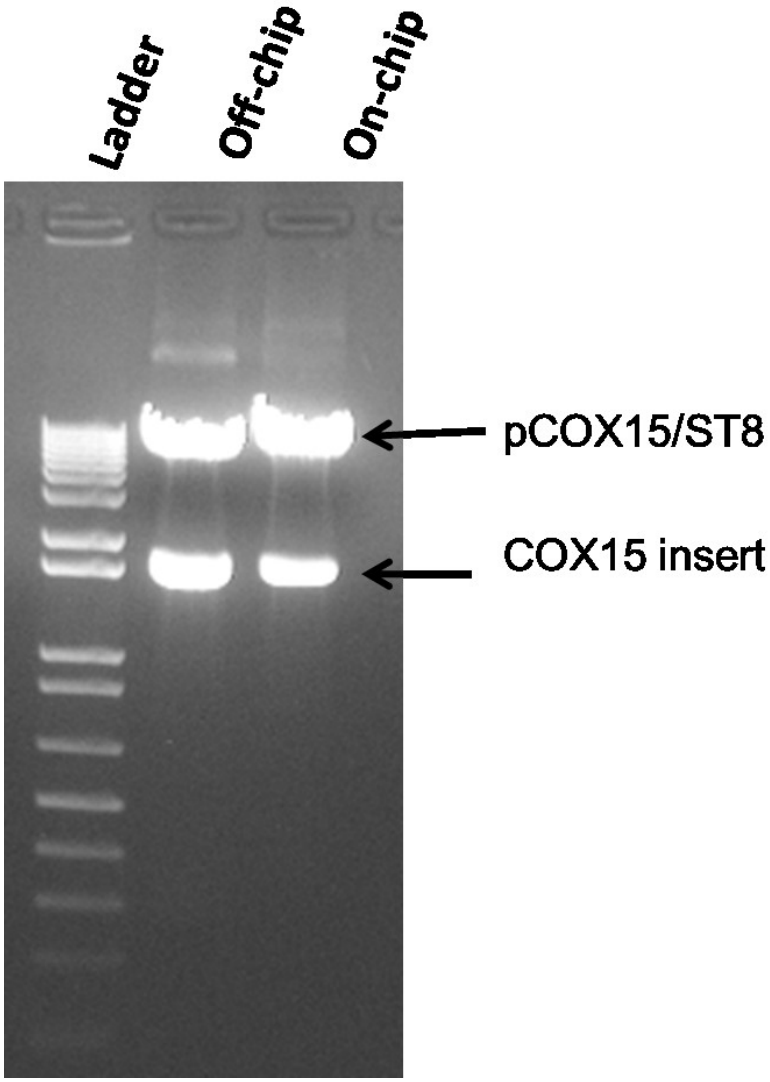

Figure 3.10. Comparing plasmids isolated from *E. coli* using either the MFC-based or off-chip plasmid minipreps. The L is the 1 kb plus ladder, off-chip used pDNA isolated using from a Qiagen miniprep kit (off-chip) and the on-chip plasmid miniprep used pDNA from a MFC-based plasmid miniprep using 10^6 *E. coli*. The top band is the pCOX15/ST8 plasmid and the bottom band is the COX15 insert. The agarose slab gel shows the restriction enzyme digestion with *Hind*III and *Bam*HI of plasmids that was isolated from transformed *E. coli.*

3.3.1 The Effects of Surface Chemistry on the Threshold

One of the factors that we found affected the threshold was surface chemistry. We tested various surface coatings, both covalent and dynamic, to decrease non-specific adsorption in the MFC-based plasmid segregations and minipreps. The coatings tested herein are all acrylamides. Although we had also initially examined the non-acrylamide coating parylene C, the agarose was unable to adhere to the parylene C coating. It was not tested in CE, as agarose adherence is a requirement for agarose based CE (agarose adherence will be discussed further in Chapter 4). Doherty *et al.* (Doherty *et al*., 2002) found that DMA, the monomer for PDMA, interacts with silica surfaces by carbonyl-silanol hydrogen bonding. Since all acrylamides contain a carbonyl group (indicated by the rectangles in Figure 3.11), it seems probable that carbonyl-silanol hydrogen bonding is the mechanism by which all the coatings tested in our glass MFCs interact with the capillary walls and may have also contributed to the agarose adherence.

The Barron group reported that PHEA resulted in a better resolution with less EOF compared to PDMA (Hestekin *et al*., 2006; Kourkine *et al.*, 1999). We found that PDMA resulted in the lowest threshold, whereas PHEA resulted in the highest threshold. This difference is probably due to the differences in the application. Herein, we are using the surface coatings to decrease a threshold to mere picograms of DNA, whereas Barron's group used nanograms of DNA and examined the separation efficiency, which was determined by resolution of HA-SSCP fragments. This suggests that the appropriate surface coating may be application dependent. For our purposes, the threshold is more important than the resolution in the MFC-based plasmid segregation. Therefore, PDMA was the chosen surface coating for developing a MFC-based plasmid segregation.

We hypothesize that one of the reasons for non-specific adsorption of DNA is hydrogen bonding. Hydrogen bonding is an attractive force between the hydrogen of an X-H group, where X is more electronegative than H (O, N or F), and another electronegative atom (Arunan *et al*., 2011; Voet *et al*., 2008). The difference in the chemical structure of the coatings tested resides in the amine group. LPA and CPA contain a primary amine group, PHEA contains a secondary amine with an hydroxyethyl group and PDMA bears a tertiary amine with two methyl groups (Figure 3.11) (Lucy *et al*., 2008). Based on the amine functional groups, PDMA is the only one that cannot hydrogen bond because it contains two methyl groups, which are not capable of hydrogen bonding. Therefore, the variation in the amine groups could explain why PDMA resulted in the lower threshold observed in the MFC-based plasmid segregation.

3.3.2 Consideration of Trapping during Capillary Electrophoresis

Since plasmids, like the mtDNA, are closed-circular DNA molecules they are susceptible to trapping on agarose fibers when in an electric field, making trapping an important factor in the development of a suitable voltage program. Our 3-step injection voltage program combines elements of PFGE and used low electric fields to counteract trapping. The first two steps of the 3-step injection uses a PFGE-like approach, a technique demonstrated by Levene and Zimm (Levene and Zimm, 1987) to reverse trapping. The first step is 167.3 V/cm, which is higher than the critical field of pCOX15/ST8 and therefore does cause trapping. However, the higher electric field drives pCOX15/ST8 to enter the agarose from the SR by a sample stacking effect. Sample stacking is a technique that promotes movement of a sample from a large volume, such as in the SR, to a smaller a volume, such as the channel, and is commonly used to

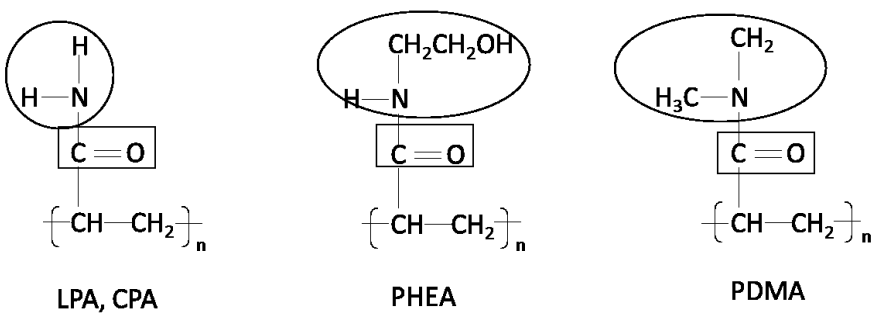

Figure 3.11. Chemical structure of the surface coatings. The carbonyl groups responsible for interaction will silica surfaces are indicated by rectangles and the functional groups thought to be responsible for interaction with DNA are indicated by circles/ovals.

improve sample injection (Mikkers *et al*., 1979). The sample stacking is why the 3-step injection performed better than the single step injection programs. Based on the mobility of the 8 kb plasmid of the SC ladder (49.3 μm/s), pCOX15/ST8 would take approximately 325 seconds to migrate from the SR to the SW. However, this does not take into account the plasmid entering the agarose, which would explain the variability of the one step injection voltage programs. The sample stacking in the first step helps to improve the reliability of the plasmid entering the agarose and therefore making the MFC-based plasmid segregation reproducible. This is followed by a short reversal in the electric field to release the trapped plasmid.

The third step uses a low electric field to move the pDNA while preventing further trapping during CE. We have found that the critical field for a 16.2 kb plasmid, which is similar in size to the mtDNA, is 27 V/cm. The critical field for an 8 kb plasmid, similar to the size of pCOX15/ST8, is 55 V/cm (Manage *et al*., 2008). Since our goal is to apply the plasmid segregation to an mtDNA segregation we chose 32 V/cm, which is close to the critical field for mtDNA and significantly lower than the actual critical field of pCOX15/ST8. The combination of the PFGE-like approach in steps one and two and the low electric field in step three resulted in a reliable voltage program.

3.3.3 The Role of Buffer in Capillary Electrophoresis

The buffer composition was found to be important for a reproducible MFC-based plasmid segregation of only 1 pg of pDNA, with TBE resulting in the lowest threshold compared to TAE and TTE. One possible explanation for the improved threshold with TBE is the formation of the borate-agarose complexes. In slab gels, TBE is the preferred

buffer for separating small DNA species under 1.5 kb, while causing compression of larger DNA fragments (Singhal *et al*., 2010). The compression observed in TBE is caused by the borate forming complexes with DNA. While the improved resolution of smaller species arises from the complexes formed by borate with agarose (Stellwagen *et al*., 2000a). Since our work uses larger DNA species the compression of DNA could be detrimental. However, in CE the agarose-borate complexes are typically dominant over the DNA-borate complexes (Stellwagen *et al.*, 2000b), and therefore we do not observe as much compression in CE compared to slab gel electrophoresis.

Using 0.1 X TBE we were able to obtain some successful 1 pg MFC-based plasmid segregations, but they were not reproducible. This suggests that 0.1 X TBE is on the edge of adequate buffering capacity for the MFC-based plasmid segregation, and by increasing the buffer concentration to 0.5 X TBE we obtained a reproducible 1 pg MFC-based plasmid segregation. The concentration of the buffer appears to be a greater factor at lower concentrations of DNA. The DNA is negatively charged, which is what causes it to migrate towards the cathode (or SW in our MFCs) during electrophoresis (Barron and Blanch, 1995). The buffer in electrophoresis provides ions that carry the current and maintain a consistent pH (Brody and Kern, 2004a). If there is not a sufficient buffering capacity it results in buffer depletion, which causes swings in pH that can cause erratic behaviour in electrophoresis and damages DNA. Therefore, DNA damage by buffer depletion increases the threshold required for a successful MFC-based plasmid segregation. By using a sufficient buffer concentration, which in the MFC-based plasmid segregation is 0.5 X TBE, we obtained a reliable 1 pg MFC-based plasmid segregation.

3.3.4 MFC-based Plasmid Segregation

As more molecular biology techniques are adapted to MFCs, the ability to manipulate smaller quantities of DNA is required thereby decreasing the amount of sample needed. In a diagnostic setting, this can result in a smaller tissue sample being required from a patient. For example, instead of requiring a full muscle biopsy for mtDNA diagnostics, which is very invasive (Siciliano *et al*., 2007), a thin needle muscle biopsy could be used. We have been able to reproducibly segregate as little as 1 pg of pDNA using a CE-based approach. To the best of our knowledge, this is the lowest amount of pDNA that has been successfully manipulated on a MFC. By decreasing our threshold to only one picogram, we are in the range of the amount of mtDNA in only 1500 fibroblasts or the contents of a thin needle muscle biopsy. A MFC-based method for the segregation of mtDNA would also help to decrease the time, cost and labour involved in mtDNA diagnostics. Thus a MFC-based mtDNA analysis tool could decrease the strain on patients and improve the time required for and feasibility of mtDNA diagnostics.

3.3.5 MFC-based Plasmid Miniprep

Once we could reproducibly segregate a plasmid, we went on to develop a MFC-based plasmid miniprep using 10^5 *E. coli,* over 10 000 fewer *E. coli* than used in most minipreps, as an example of an *in vivo* system. As with the MFC-based plasmid segregation, to the best of our knowledge this is the smallest quantity of *E. coli* to be used in a plasmid miniprep. Typically minipreps require 16-40 hours to allow the bacteria to grow to sufficient quantities. By decreasing the amount of *E. coli* used, it decreases the

time that would be required for growth. The MFC-based plasmid miniprep is also quicker than other plasmid minipreps, with most plasmid minipreps requiring at least an hour, whereas our MFC-based plasmid miniprep can be done in under 20 minutes. Therefore, our MFC-based plasmid miniprep significantly decreases the time and amount of sample required for a plasmid miniprep.

The MFC-based plasmid miniprep is the first MFC assay that is capable of isolating plasmids from bacteria. Although other studies have reported MFCs that are capable of analyzing plasmids (Ding *et al*., 2003; Manage *et al*., 2008) and manipulating plasmids (Kim *et al*., 2007; Nagamine *et al*., 2005), these MFCs require off-chip plasmid preparation. One of the areas that was missing towards a μTAS for plasmid analysis was the ability to purify plasmids using MFCs. Our MFC-based plasmid miniprep provides a method to isolate plasmids from bacteria that can be used for down-stream applications, such as transformation. Due to the simplicity of the MFC-based miniprep it could be adapted for other MFCs to allow integration of plasmid segregation and analysis on a single MFC. A platform that is capable of both rapidly isolating and subsequently analyzing plasmids would allow for rapid identification in such application as screening for antibacterial resistance plasmids (Boerlin and Reid-Smith, 2008) or screening for plasmids in bacterial culture, such as those that are found in the gut (Bjerketorp *et al*., 2008). It could also be integrated onto MFCs (Kim *et al*., 2007; Nagamine *et al.*, 2005) to enable rapid segregation and transfection on a single MFC. This would allow isolation, identification and transfection of new plasmid constructs within a single day. The integration of these molecular biology techniques could drastically improve current recombinant engineering technologies.

CHAPTER 4- THE USE OF PMMA MICROFLUIDIC CHIPS IN ANALYSING PLASMIDS BY CAPILLARY ELECTROPHORESIS

Some material from this chapter has been previously published

Ma, T.*, V. Northrup*, A.O. Fung, D.M. Glerum, and C.J. Backhouse. 2012. Polymeric rapid prototyping for inexpensive and portable medical diagnostics. *In* Photonics North 2012. International Society for Optics and Photonics. 84140B-84120B-84128.

*These authors contributed equally.

4.1 Introduction

4.1.1 Materials Used in the Fabrication of MFCs

Glass has been extensively used in the development of MFCs, especially in the early work on MFCs. Glass has the advantage of being generally solvent compatible, and having surface stability and beneficial optical properties (i.e. is transparent). Due to the common use of glass, the fabrication techniques for glass MFCs are well understood and include various etching and lithography methods. Many of the fabrication techniques used for glass MFCs requires clean room facilities and large amounts of equipment, which increases the cost and time for production, thus decreasing the feasibility for rapid-prototyping, disposability, and POC use (Fiorini and Chiu, 2005).

Due to the increased cost and time associated with glass MFCs, many recent studies have examined the use of thermoplastic materials to fabricate MFCs, which can decrease the cost of the MFCs by 10 to 100 fold compared to glass (Kuo and Chiu, 2011; Zhang *et al*., 2009). The decrease in cost does make thermoplastic materials more applicable to disposable, POC diagnostics. Some commonly used thermoplastic materials include cyclic olefin copolymers (COC) (Kameoka *et al*., 2001), polyethylene terephthalate (PET) (Reymond *et al*., 2002), thermoset polyester (TPE) (Fiorini *et al*., 2004), polycarbonate (PC) (Tsao and DeVoe, 2009), and PMMA (Kuo and Chiu, 2011; Zhang *et al*., 2009). PMMA is the least hydrophobic of the common thermoplastics and has rigid mechanical properties, good optical transparency and is compatible with electrophoresis. These qualities, along with the low cost, makes PMMA a useful material in developing affordable MFCs (Zhang *et al*., 2009).

4.1.2 Fabrication Techniques Used to Develop MFCs

Along with the various materials used to fabricate MFCs, there is also various fabrication methods. The fabrication methods can include wet and dry etching, reactive ion etching, conventional machining, photolithography, soft lithography, hot embossing, injection molding, *in situ* construction, plasma etching and laser ablation (Fiorini and Chiu, 2005). Herein, we will focus on etching techniques and laser ablation.

Etching techniques use molds to generate the design onto the MFC (Fiorini and Chiu, 2005). These methods are typically performed in a cleanroom facility, which increases the cost and time, while decreasing their accessibility. Although etching fabrication techniques allow for high-throughput fabrication, they are not reasonable for rapid prototyping since it can take weeks to months to make changes to a design (Pan and Wang, 2011).

Laser ablation uses a high-powered pulse laser, usually a UV or a CO_2 laser, to carve out, or ablate, the features of the MFC from a sheet of thermoplastic, such as PMMA. The depth of the ablation is dependent on the pulse rate of the laser and the characteristics of the material being ablated and the width of the channel is determined by the focus of the laser. In laser ablation, a direct-write process using a computer program is used to pattern the MFCs. This allows for easy changes to the program design, making laser ablation a useful fabrication method for rapid-prototyping. However, the serial nature of many of these direct-write processes limits the throughput as they can only produce small quantities at one time, making laser ablation less optimal for high-throughput. One disadvantage of laser ablation is the tendency for the laser to cause

uneven surface properties, which can increase EOF (Fiorini and Chiu, 2005) and restrict the application of laser ablation for the fabrication of MFCs.

4.1.3 The Use of Agarose as a Sieving Matrix in Capillary Electrophoresis

Studies that use agarose as the sieving matrix for CE vary in the percentage of agarose and the length of the capillary, which makes direct comparisons difficult. Also, since many of the studies do not explicitly calculate the resolution, only qualitative comparisons can be made. One conclusion that has been made by multiple studies is that the temperature affect the CE (Bocek and Chrambach, 1991; Bocek and Chrambach, 1992; Motsch *et al*., 1991).

Multiple studies have examined agarose CE at various temperatures. Motsch *et al.* (Motsch *et al*., 1991) examined the separation of ΦX-174-RF DNA, digested with *Hae*III, in a 2% agarose in an unspecified buffer. The DNA was analyzed at 72 cm at 10^{o}C, 15^{o}C and 25^{o}C. Motsch *et al*. found the resolution was similar between the different temperatures but the peaks arrived earlier at higher temperatures. Two studies by Boček and Chrambach (Bocek and Chrambach, 1991; Bocek and Chrambach, 1992) found that the separation was more efficient at 40^{o}C compared to 25^{o}C. These studies examined a 1 kb ladder in 1.7% agarose in 1X TBE with capillaries that were 20 cm and 27 cm. Although they were able to resolve all the DNA species in the ladder, their separation seems to be more efficient with the smaller species and less so for the species of over 10 kb (Bocek and Chrambach, 1992), and would likely not work well for any size above 12 kb.

The study by Boček and Chrambach (1992) suggested that higher temperatures have a beneficial effect on separation, which contradicts the previously reported detrimental effects of Joule heating, as discussed in Chapter 1. This deviation could be due to the difference in DNA fragments examined. The majority of studies examining CE have used smaller fragments of under 1 kb. Some studies have suggested that although higher temperatures are detrimental to the resolution for smaller DNA fragments (Guttman and Cooke, 1991), higher temperatures result in a better resolution for the larger DNA fragments. The activation energy in non-crossed linked polymers decreases with increasing fragment lengths, which is associated with distortion of the polymer fibers. The distortion of the polymer fibers allows the passage of larger DNA species, resulting in an improved resolution for larger DNA fragments (Fang *et al*., 1996). This would explain the improvement observed at higher temperatures in agarose using larger DNA fragments.

In the above studies the largest DNA species examined was 12 kb, but a study by Chen *et al*. (Chen *et al*., 1996) showed the ability to separate DNA sizes from 125 bp to 23 kb using PFGE. Chen *et al*. used an 86 mm capillary with 1 % agarose in 0.5 X TBE. By employing PFGE, which can be used to separate larger DNA species in slab gels, they were able to separate DNA fragments of 125 bp, 564 bp, 2028/2322 bp, 4371 bp, 6557 bp, 9419 bp and 23130 bp. The use of PFGE improved the resolution of CE compared to the direct current approach.

The above studies have used linear DNA in relatively long capillaries. The study by Manage *et al.*(Manage *et al*., 2008) examined the SC ladder in glass MFCs in 0.6 % agarose using 1 X TTE. In this study they were able to separate the different supercoiled

DNA species within the ladder, but as the electric field was increased the larger species could no longer be examined at 13 mm. This is due to trapping and suggested that to separate supercoiled DNA species of 16.2 kb the electric field must be below 32 V/cm or the circular DNA would be trapped. As discussed in Chapter 3, when we used a similar approach as Manage *et al.* we determined the critical field for the 16.2 kb plasmid to be 27 V/cm.

4.1.4 Objectives

The use of PMMA MFCs fabricated using laser ablation allows for rapid prototyping, which is beneficial in developing new technologies (Fiorini *et al*., 2004; Preywisch *et al*., 2011). By switching from glass MFCs to PMMA MFCs we are able to make modifications to the MFC design in a reasonable time frame, facilitating the development of novel methods for mtDNA analysis using MFCs. However, the change to PMMA does require examination of the features of the MFC that affect CE. In this Chapter we will examine the development of a CE-based plasmid separation on PMMA MFCs. We will attempt to resolve plasmids that range from 8.1 kb to 17.2 kb in order to mimic a patient who has multiple mtDNA species present.

4.2 Results

4.2.1 The Fabrication Criteria for PMMA Microfluidic Chips

Our previous work, described in Chapter 3, has been on glass MFCs fabricated using standard glass etching techniques (Kaigala *et al.*, 2006; Northrup *et al.*, 2010). Due to the advantages of PMMA MFCs fabricated using laser ablation, which have been outlined above, we have transitioned to using PMMA MFCs. To successfully make the

transition to the PMMA MFCs we needed to ascertain the features of the MFCs that affect CE. We define a successful CE as having a resolution of under 2 kb in 0.6 % agarose and consistent arrival times to within 5% STD. The criteria were chosen since a 2 kb resolution would be sufficient to resolve the majority of large-scale mtDNA rearrangements, which range from 1.3 kb (Moraes *et al*., 1989) to almost 11 kb (Miyabayashi *et al*., 1991) and the 5% STD is considered an acceptable degree of variation in CE (Barron and Blanch, 1995).

One feature of the PMMA MFCs that was found to affect the cut-off for CE (i.e. the largest DNA species that could be reliably resolved) is the smoothness of the channel (Ma *et al*., 2012). There is an inverse correlation between the number of constrictions, a reduction in the channel width of greater than 20%, and the cut-off (Figure 4.1 and Table 4.1). Images of the separation channels of five PMMA 4-PM MFCs are shown in Figure 4.1 with corresponding electropherograms of the 100 bp ladder in 2% agarose in 1X TBE

Table 4.1. Channel smoothness affects cut-off.

Chip	# Constrictions	Cut-off (bp)
12-05-10-5A	2	1500
12-06-27-3A	9	800
12-06-27-7B	13	400
12-07-04-5A	16	300
12-06-27-4C	17	300

The name of the MFC corresponds to the MFC in Figure 4.1. The "# Constrictions" column shows the amount of constrictions found in the separation channel and the cut-off refers to the largest species in the 100 bp ladder that is reliably resolved. Based on Table 3 in Ma *et al*. 2012.

(Note: these sets of CE were performed on PMMA 4-PM MFCs that had been pretreated with 100 % ethanol and 1 M HCl prior to loading the agarose and running the 100 bp ladder). The constrictions cause changes in the diameter of the channel, which can cause localized variations in the electric field. The more constrictions found within the channel, the more likely there would be variation in the electric fields within the channel. Since the constrictions result in a smaller volume in the channel, the electric field would be stronger, resulting in a lower cut-off. For each of these electropherograms the resolution between the 200 bp and 300 bp DNA species was similar.

4.2.2 Variation in Arrival Times due to Incomplete Adherence

Incomplete adherence is a situation in which the agarose sieving matrix does not completely adhere to the channel wall. Incomplete adherence can allow for fluids, such as buffer and its contents, to circumvent the agarose sieving matrix during CE. In untreated channels in the PMMA 4-PMs we observed variable delays in arrival times between run 3 and run 4 for all plasmids, though we have focused on those plasmids between 8066 bp and 16210 bp (Table 4.2). Delays were inconsistent and ranged from 6 seconds to almost 20 seconds, and we hypothesized that the delays were due to incomplete adherence of the agarose. Swedberg (Swedberg, 1992) used a dilute (0.1%) agarose solution to coat the channels prior to loading the running agarose to improve adherence. To test if the observed delays were due to incomplete adherence we decided to test a dilute agarose coating prior to loading the running agarose. When we applied 0.1 % agarose as a coating, we observed consistent delays in arrival times of approximately 10 seconds (±2 seconds) from run 3 to run 4 (Table 4.2). The consistency seen with the

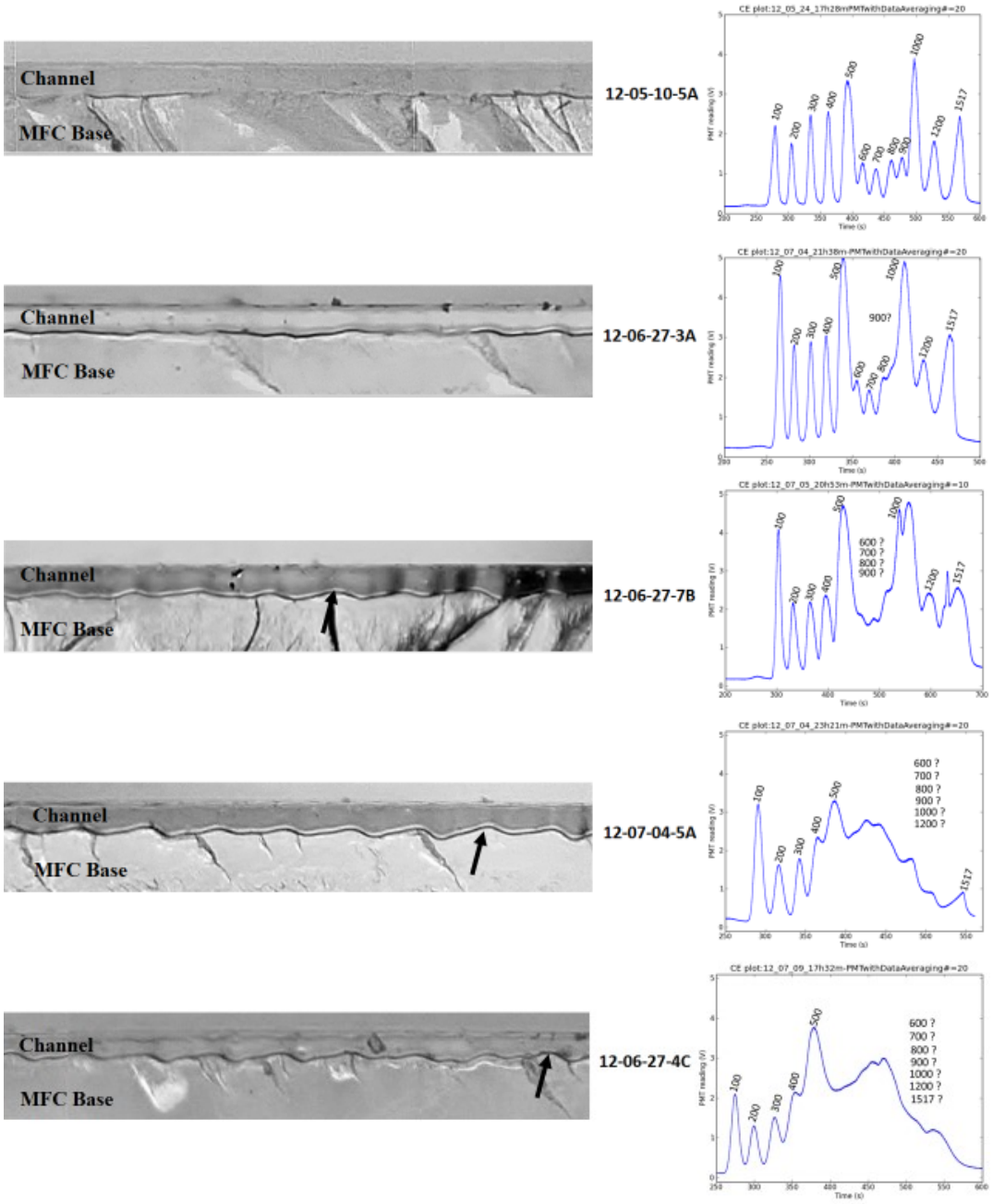

Figure 4.1. Channel smoothness affects the "cut-off" in CE. The images to the left are of at least 3 mm of the separation channel, which is representative of the entire separation channel, for the respective PMMA 4-PM MFCs. The name of the PMMA 4-PM MFCs are in the middle and an electropherogram obtained with the specific MFC is to the right. Each represents a CE run of the 100 bp ladder in 2% agarose and 1X TBE. The different sized fragments of the 100 bp ladder are indicated on the electropherograms with those that are not resolved indicated by a ?. The time (s) is on the x-axis of the electropherograms, with the PMT readings (V) given on the y-axis (Modified from Figures 2-7 in Ma *et al*. 2012).

agarose coating indicates a more controlled adherence and therefore we have used it to develop a reliable CE protocol.

Table 4.2. Difference in arrival times between the 3rd and 4th runs.

Chip	Condition	Load	Δ arrival times (s)				
			8066 bp	10102 bp	12138 bp	14174bp	16210 bp
CBSD 12-08-28 TC 2C	no pretreatment	1	12.3	12.8	13.3	12.4	14.0
CBSD 12-08-28 TC 2C	no pretreatment	2	8.28	7.9	7.4	7.0	6.6
CBSD 12-08-28 TC 2C	no pretreatment	3	16.6	16.7	16.0	17.4	17.8
CBSD 12-08-20 TC 2C	Pretreatment	1	11.6	11.0	10.2	9.6	10.6
CBSD 12-10-01 TC 3A	Pretreatment	1	10.2	10.3	10.7	10.3	10.2
CBSD 12-10-31 TC 1C	Pretreatment	3	10.5	9.7	9.7	10.0	10.9

MFCs with no pretreatment were not treated with 0.1% agarose prior to loading the running agarose and MFCs with pretreatment were first treated with 0.1% agarose to coat the channels prior to loading the running agarose.

4.2.3 A Reliable Capillary Electrophoresis-based Plasmid Separation

Reproducibility is an essential quality for any assay. To test the reproducibility of our PMMA 4-PM MFCs and the CE protocol outlined in Chapter 2 (Section 2.4.3), we examined the plasmid species of the SC ladder (Invitrogen), which contains 11 plasmids species that range from 2066 bp to 16210 bp, in CE. SO was used as the intercalator at a ratio of one molecule of SO per 600 bp to limit the effects of the intercalator on mobility (Manage *et al*., 2008). We analyzed the separation of the five largest plasmids (8066 bp, 10102 bp, 12138 bp, 14174 bp and 16210 bp), because they are the closest in size to the mtDNA (16 569 bp) and its associated deletions that range from 1.3 kb (Moraes *et al.*, 1989) to almost 11 kb (Miyabayashi *et al.*, 1991; Ruiz-Pesini *et al.*, 2007) (resulting in mtDNAs that range from 15.3 kb and 5.6 kb, respectively). We examined the resolution,

arrival times and the difference in arrival times between plasmids as outlined Chapter 2 (Section 2.8.2).

Using the SC ladder, CE was run on five different PMMA 4-PM MFCs, for a total of ten loads between the MFCs, as shown in Table 4.3 and electropherograms for three of the ten loads are shown in Figure 4.2. For each of these electropherograms, the larger species that we focused on can be successfully resolved with a resolution of under 2 kb. It should be noted that the arrival times in the fourth runs are approximately ten seconds later than the third runs, as discussed above. There is also variation in the heights of the peaks due to small variations in the gain used during CE and due to the nature of the CE. The CE consists of two steps, an injection followed by a separation. During the injection step, DNA is constantly entering the agarose, and therefore does not separate by size. During the separation step, a small plug of DNA that is in the intersection is moved along the separation channel, allowing the species to separate based on size. Given the nature of the injection, there can be varying amounts of DNA in the intersection that are analyzed during the separation, which results in small variations in peak intensities.

Table 4.3. The PMMA 4-PM MFCs used to test the stability of the CE protocol.

PMMA 4-PM MFCs	# of Loads
CBSD 12-08-20 TC 2C	2
CBSD 12-10-01 TC 2C	1
CBSD 12-10-01 TC 3A	3
CBSD 12-10-01 TC 2C	1
CBSD 12-10-31 TC 1C	3

The name of the MFC is given on the left and the amount of loads performed on the particular MFC to test the stability of the CE protocol are shown on the right.

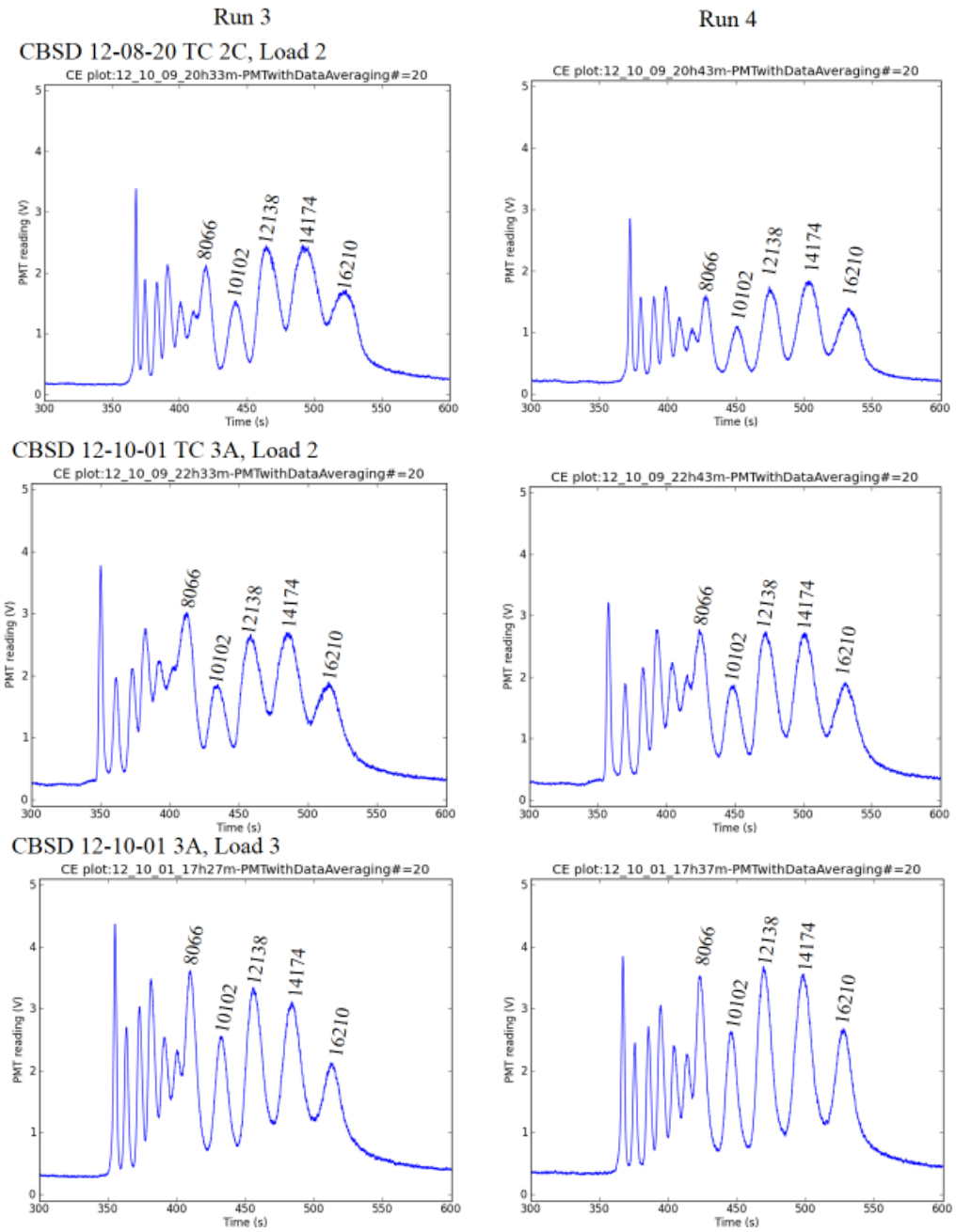

Figure 4.2. Stability of CE in PMMA 4-PM MFCs. All of these CEs runs were performed in 0.6% agarose in 0.5 X TBE on PMMA 4-PMs that were coated with 0.1 % agarose. For each electropherogram the name of the 4-PM and the load number is indicated just above the electropherogram for run 3. The run number is indicated at the top with run 3 to the left and run 4 to the right. The peaks corresponding to the plasmid species between 8066 bp -16210 bp are indicated. For each electropherogram the time (total run time), from 300 to 600 seconds, is on the x-axis and the PMT reading (V), from 0 to 5 V, is on the y-axis. The file name across the top of the electropherogram is generated by the control program.

The arrival times for the 8066 bp -16210 bp plasmids are shown in Table 4.4. The 16210 bp plasmid has an arrival time of 475.0 s ± 10.4 s (a mobility of 23.2 μm/s), which is a variation of under 5% (max 2.2%), which demonstrates the required level of reproducibility in the arrival times. Figure 4.3A plots the arrival times versus the plasmid size, which shows a linear relationship with an R^2 value of 0.9966. Using the equation of the linear trendline generated by Excel in Figure 4.3A we obtain Equation 4.1:

$$bp = \frac{t - 263.14}{0.0129} \qquad \text{Equation 4.1}$$

where bp is the size of the plasmid (bp) and t is the arrival time (s). Equation 4.1 can be used to determine the approximate size of a closed-circular, double-stranded DNA molecules to within 1 kb based on the arrival time, or determine the arrival time of a known-sized plasmid to within 10.4 seconds.

Table 4.4. Arrival times for the plasmids in the SC ladder in 0.5 X TBE.

Plasmid	**8066 bp**	**10102 bp**	**12138 bp**	**14174 bp**	**16210 bp**
Average	369.67	392.74	416.75	444.96	474.95
STD	6.45	7.15	7.96	9.14	10.39
% variation	1.7	1.8	1.9	2.1	2.2

For each plasmid species the average and STD are given in seconds.

The difference in arrival times between plasmids are shown in Table 4.5. We chose to examine the difference in arrival time between the plasmid species because we had observed it to be more consistent than the absolute arrival times. As discussed above, the arrival times can vary by run (third or fourth), but the difference in the arrival times between the plasmids species showed very little difference between runs. Therefore, we

A)

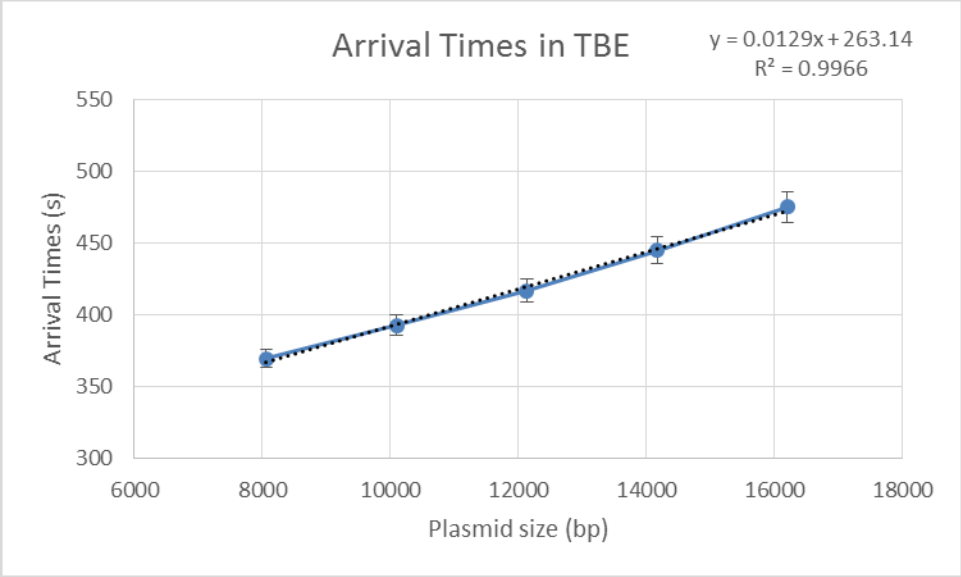

B)

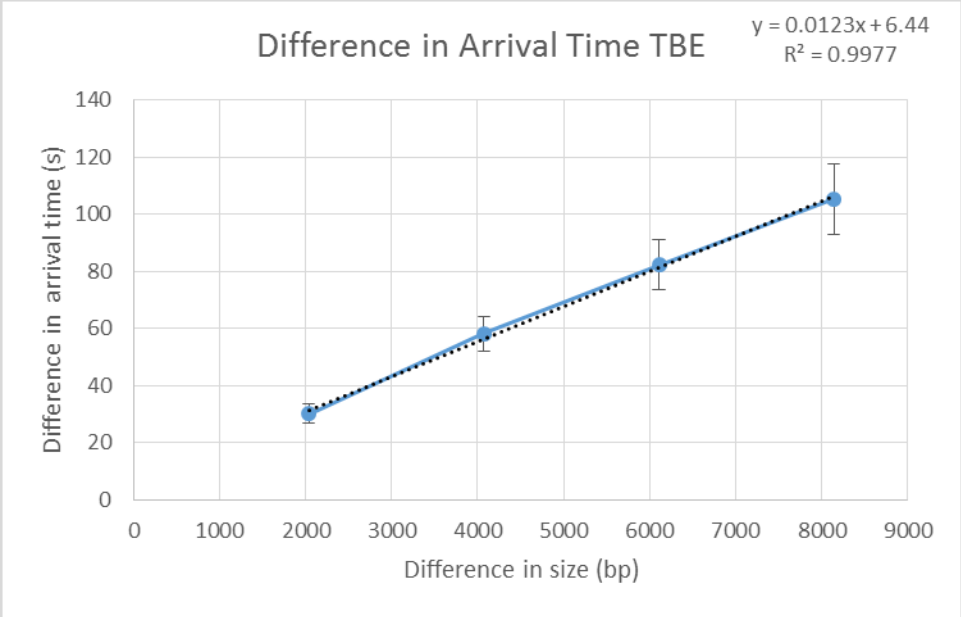

Figure 4.3. Arrival times in CE using 0.5 X TBE. A) Arrival times of the plasmid species of the SC ladder. The size of the plasmid is on the x-axis (bp) and the arrival times are on the y-axis (s). The linear trendline equation and the R^2 value are shown in the top right corner. The error bars represent STD. B) The difference in arrival times of the plasmid species of the SC ladder. The difference in size of the plasmids (bp) is given along the x-axis and the difference in arrival times (s) is shown in the y-axis. The linear trendline equation and R^2 value are shown in the top right corner. The STD is shown by the error bars.

hypothesized that the difference between the DNA species could be used to determine size differences, such as the size of a deletion of a mtDNA with a deletions compared to a WT mtDNA. The difference in arrival times between the 14174 bp and 16210 bp plasmids was 30.0s ±1.7 s. The difference in arrival times versus the difference in the size between plasmids are shown in Figure 4.3B. Based on the linear trendline equation generated by Excel we obtained Equation 4.2 to predict the difference between arrival times:

$$\Delta bp = \frac{(6.4408 - \Delta t)}{(0.0123)} \qquad \text{Eq.4.2}$$

where Δbp is the difference in size between the plasmid species (bp) and Δt is the difference in arrival times (s).

Table 4.5. Differences in arrival times of the SC ladder plasmids in 0.5 X TBE.

Plasmid pair	**8066-16210**	**10102-16210**	**12138-16210**	**14174-16210**
Average	105.3	82.2	58.2	30.0
STD	6.1	4.5	3.0	1.7
% variation	5.8	5.5	5.2	5.7

For each species the average and STD are given in seconds. The plasmid pairs are in bp.

Table 4.6. Resolution of the plasmids of the SC ladder in 0.5 X TBE.

Plasmid pair	**8066-10102**	**10102-12138**	**12138-14174**	**14174-16210**
Average	1234.1	1355.8	1391.8	1508.1
STD	210.1	225.3	216.8	201.3
% variation	17.0	16.6	15.6	13.3

For each species the average, STD and plasmid pairs are given in bp.

The resolutions for the plasmid pairs are shown in Table 4.6. The resolution was calculated using Equation 2.3, which calculates the minimum size difference between two plasmids to resolve the peaks to the FWHM:

$$R_{bp} = 0.5\ (bp(\frac{FWHM_1+FWHM_2}{t_2-t_1})) \qquad \text{Eq 2.3}$$

where bp is the difference in size between the two DNA species, $FWHM_1$ and $FWHM_2$ is the FWHM of the smaller DNA species (first peak in the electropherogram) and the larger DNA species (second peak in the electropherogram) respectively, and t_1 and t_2 is the arrival time of the smaller and larger DNA species, respectively. The resolution of the 14174 bp and 16210 bp plasmids is 1508.1 bp ± 201.4 bp. Therefore, we can distinguish two plasmids to FWHM that have an approximately 1.5 kb difference in size using this CE-based method. This resolution would allow us to distinguish most, if not all, reported large-scale mtDNA deletions. Based on these analysis we can conclude we have a reproducible CE protocol that results in a resolution of 1508 bp ± 402 bp with a variation in arrival times of under 5%.

4.2.4 Influence of Non Tris-based Buffers on Capillary Electrophoresis

Buffers have been shown to influence electrophoresis (Brody *et al.*, 2004; Brody and Kern, 2004b; Ishido *et al*., 2010), so once we were able to demonstrate a stable protocol for CE in the PMMA 4-PM MFCs, we tested different types of buffers in an attempt to improve the CE. Based on the literature we chose to test three non-Tris based buffers; 1 mM lithium boric acid (LBa), 10 mM sodium boric acid (SBa) (Brody *et al*., 2004), and 39 mM sodium threonine (ST) (Ishido *et al*., 2010). Figure 4.4A-D shows a representative electropherogram obtained from the separations of the SC ladder in each of the three buffers and from a separation in TBE as a reference point.

The use of LBa did not result in a useable CE since even after a 1000 seconds separation, compared to the 600 seconds separation in TBE, we only observe two peaks that are likely the 2067 bp and 2972 bp plasmids species (Figure 4.4B). Subsequent separations did not result in any additional peaks (data not shown). Since we could not observe the larger species of plasmids, especially the 16210 bp plasmid, LBa would not be a suitable buffer for a mtDNA analysis and was therefore eliminated.

Although CE using SBa did result in observable peaks for all the plasmids of the SC ladder, the resolution was significantly worse when compared to TBE (Figure 4.4C and E). For the 14174 bp and 16210 bp plasmids, the resolution for SBa was 2972 bp ± 433 bp compared to the 1508 bp ± 201 bp obtained with TBE. The resolution of 2972 bp did not meet our criteria of a successful CE, a resolution under 2 kb, and therefore SBa would not be a suitable buffer for mtDNA analysis and was also eliminated.

ST also resulted in a worse resolution, 1958.99 bp ± 423.84 bp for the 14174 bp and 16210 bp plasmids, compared to TBE (Figure 4.4D and E). However, the arrival times of the plasmids in ST were more consistent from run to run. As mentioned above, the arrival times in TBE would shift by approximately 10 seconds each run. The consistent arrival times of ST suggest that it might improve the adherence of the agarose, thereby improving the reproducibility of the arrival times (Table 4.7). We hypothesize this may be due to a decrease in the EOF since the ionic strength is lower in 1 X ST than 0.5 X TBE. Although the resolution is reduced, it is still under the 2 kb that defines a successful CE and is therefore acceptable. We hypothesized that some of the nDNA contamination seen in the MFC-based mtDNA isolation was due to incomplete adherence, and therefore improving agarose adherence may decrease the nDNA

contamination (discussed in Chapter 6). Therefore, even though the resolution was worse, we decided to examine ST further in attempts to improve the reliability of the arrival times in CE.

Table 4.7. Influence of buffers on plasmid separations in CE.

Buffer	**Stat**	**8066 bp**	**10102 bp**	**12138 bp**	**14174 bp**	**16210 bp**
TBE	Average	369.66	392.74	416.75	444.96	474.95
TBE	STD	6.45	7.15	7.97	9.14	10.39
TBE	% variation	1.7	1.8	1.9	2.1	2.2
SBa	Average	411.75	432.35	457.12	483.24	513.96
SBa	STD	11.62	14.32	13.67	15.08	13.72
SBa	%variation	2.8	3.3	3.0	3.1	2.7
ST	Average	292.42	314.92	338.84	364.76	394.32
ST	STD	5.59	4.46	4.21	4.48	6.24
ST	% variation	1.9	1.4	1.2	1.2	1.6
STE	Average	26910	292.06	314.62	339.08	364.99
STE	STD	9.9	12.09	14.48	16.5	18.2
STE	% variation	3.7	4.1	4.6	4.9	5.0

The average and STD are given in seconds.

EDTA is a chelating agent (Dominguez and Ward, 2009) that is commonly found in electrophoresis buffers to chelate many of the proteases and DNases found in cell suspensions. In more recent years, EDTA has been removed from some of the electrophoresis buffers since many of the samples being used are purified DNA in which the proteases and DNases have been removed (Brody and Kern, 2004b). Since our goal is to find a buffer that could be used in CE of cells lysed on a MFC, EDTA will be required in our buffer as proteases and DNases will still be present. Since CE using ST

had consistent arrival times, we decided to add 1 mM EDTA to the ST buffer to generate 39 mM sodium threonine EDTA (1X STE). The buffer STE originally demonstrated a slightly improved resolution when compared to ST (Figure 4.4D-F), 1740.8 bp ± 73.97 bp and 1958.99 bp ± 423.84 bp respectively, and the consistent arrival times were maintained. However, further experiments on other PMMA 4-PMs resulted in a worse resolution (1943.38 bp ± 228.36 bp) and variations in the arrival times, which is outlined in Appendix I. Although the resolution in STE is still slightly worse than in TBE, it is still sufficient to distinguish many of the large-scale rearrangements reported for mtDNA. We thought the consistency originally observed in STE would improve our ability to predict arrival times based on the size of the plasmid, or mtDNA, as well as eliminate nDNA from the MFC-based mtDNA isolation. Therefore, we decided to proceed with using 1X STE as the buffer in our CE.

The arrival times in STE were plotted versus the plasmid size in Figure 4.5A. The arrival times show a linear relationship with an R^2 value of 0.9986. Using the equation from the linear trendline generated by Excel we obtain Equation 4.3:

$$bp = \frac{t - 173.4}{0.0118} \qquad \text{Eq. 4.3}$$

where bp is the size of the plasmid (bp) and t is the arrival time (s). For the 16 210 bp

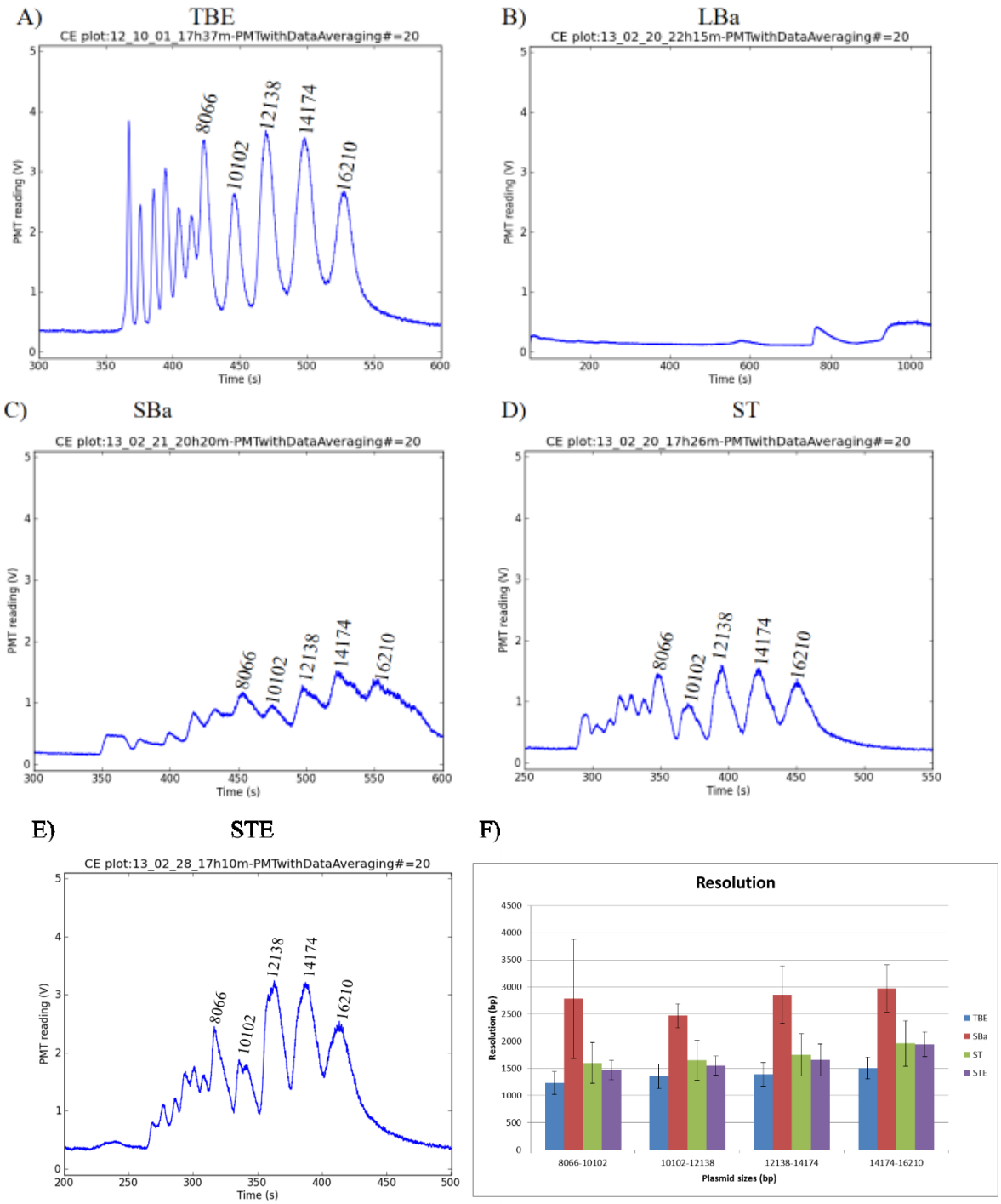

Figure 4.4. Effects of non Tris-based buffers on CE. Electrophergrams of CE using A) 0.5 X TBE, B) 1 mM LBa, C) 10 mM SBa, D) 39 mM ST and E) 39 mM STE. For all except LBa, the species from 8066bp -16210 bp are indicated. For each electropherogram the time (s) is on the x-axis and the PMT reading (V) is on the y-axis. F) Resolution of plasmids in CE using various buffers, except LBA since the resolutions could not be calculated. The error bars represent the STD.

plasmid the arrival time is 365 sv±18.2 s (a mobility of 30.1 μm/s). As with TBE, we also examined the difference in arrival times between the plasmids, which is shown in Figure 4.5B. Using the equation for the linear trendline generated by Excel we obtain Equation 4.4:

$$\Delta bp = \frac{(\Delta t - 3.5632)}{(0.0114)} \qquad \text{Eq. 4.4}$$

where Δbp is the difference in size between the two plasmids (bp) and Δt is the difference in arrival times (s). Our next step was to apply the CE protocol to purified plasmids to determine how accurately Equations 4.3 and 4.4 can predict arrival times and differences in arrival times, respectively.

4.2.5 Plasmid Separations Using STE

Above we have used the SC ladder to develop a CE protocol to separate closed-circular, double-stranded DNA molecules, such as plasmids or mtDNA. We next wanted to apply the CE protocol to isolated plasmids of known size as a model for mtDNA. We chose the plasmids pPET309/ST1 (9.2 kb) and pG93/T1 (15.7 kb) due to their similarity in size to the mtDNA, and pG19/T4 (17.2kb) was chosen to model a mtDNA molecule with a deletion. The first step was to run each individual plasmid using CE to verify the arrival times, shape and number of peaks (Figure 4.6). The peaks for pG93/T1 and pG19/T4 are the bell shaped peaks, as seen with the SC ladder, but the peak for pPET309/ST1 is a doublet. This is probably due to two conformations within the sample, which causes very small variations in the mobility of the plasmid (Akerman and Cole, 2002).

A)

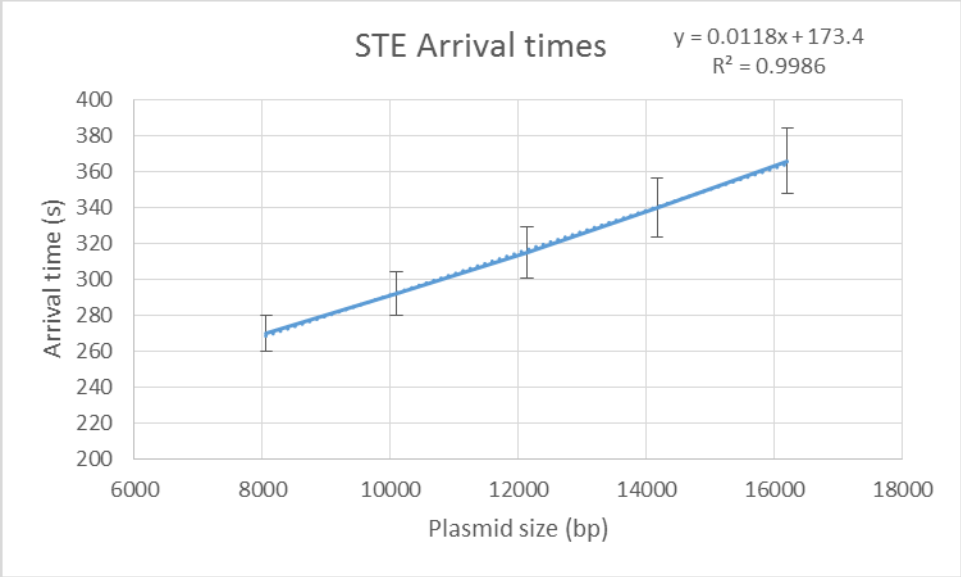

B)

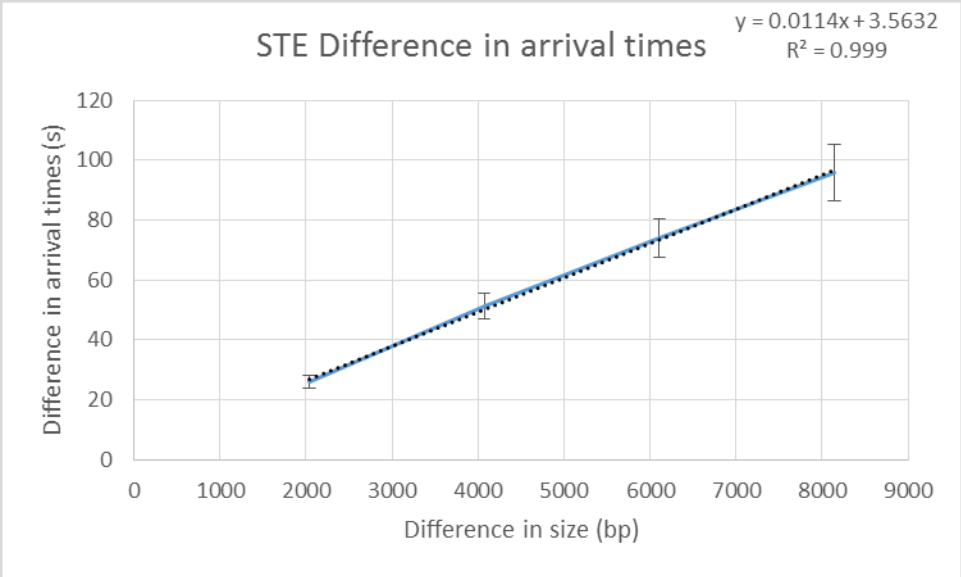

Figure 4.5. Analysis of the A) arrival times and B) difference in arrival times in 1 X STE. A) The arrival times for plasmids in STE with the size of the plasmid (bp) on the x-axis and the arrival times (s) is on the y-axis. The linear trendline is represented by the dashed line. The equation for the linear trendline and the R^2 value are in the top right corner. Error bars represent the STD. B) The difference in arrival times of the plasmids in 1 X STE with the difference in size (bp) on the x-axis and the difference in arrival times (s) is on the y-axis. The linear trendline is represented by a dashed line. The equation for the linear trendline and R^2 value are in the top right corner. The error bars represent the STD.

Once we established the appearance of each individual plasmid, we combined two plasmids in the CE. The plasmid pairing and the difference in size between the plasmids are shown in Table 4.8. For the three plasmid pairs, we were able to successfully resolve both peaks (Figure 4.7). For the combinations of pPET309/ST1 and pG93/T1 (Figure 4.7A) and pPET309/ST1 and pG19/T4 (Figure 4.7C), with size differences of 6.5 kb and 8 kb respectively, we can resolve both peaks to the baseline. For the combination of pG93/T1 and pG19/T4 (Figure 4.7B) that only has a size difference of 1.5 kb we can only see the tips of each peak. This demonstrates that even for smaller size differences, such as 1.5 kb, we can discern two peaks. These results suggest that for deletions as small as 1.5 kb, this CE protocol could be used to discern two species of mtDNA.

The above plasmid CEs were run with the plasmids in a 1:1 ratio, which would represent a heteroplasmy of 50% (50% deleted and 50% WT mtDNA). To verify that CE could be used to detect varying levels of heteroplasmy we used the plasmids in different ratios (Figure 4.7). For each CE, the smaller plasmid made up 10 % of the total pDNA content and the larger plasmid made up 90%, reflecting a heteroplasmy of 10% for an mtDNA with a deletion, represented by the smaller plasmid, with the larger plasmid representing a 90% level of WT mtDNA. Therefore, we can conclude that the CE protocol we have developed could be used to detect mtDNA deletions with as low as 10 % heteroplasmy.

Equations 4.3 and 4.4 developed above can be used to calculate the arrival times and difference in arrival time between plasmids, respectively. Table 4.9 shows the predicted arrival times and difference in arrival times for the plasmids along with the

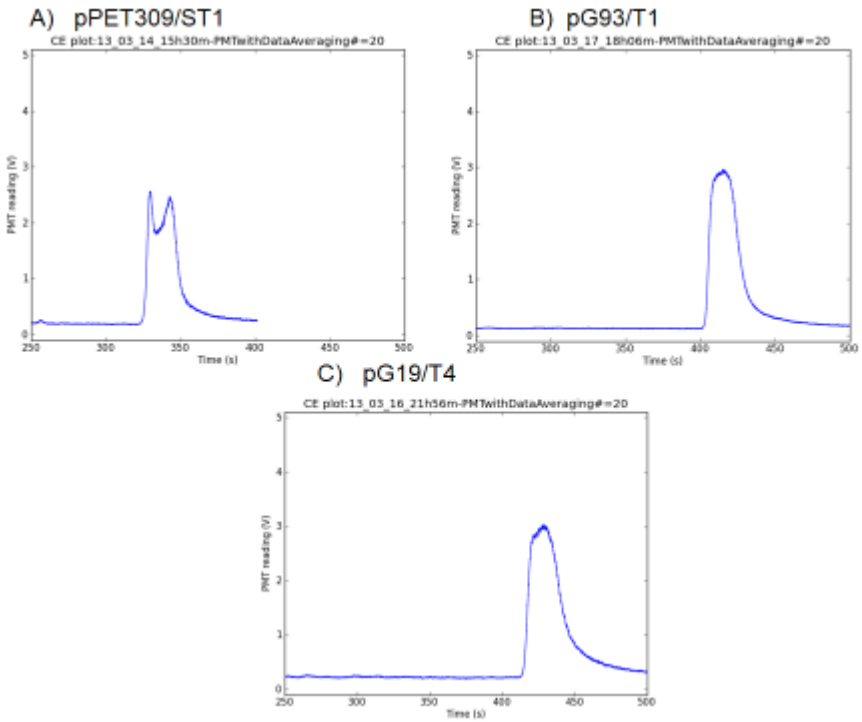

Figure 4.6. Electropherograms produced from CE of single plasmids. A) pPET309/ST1 that is 9.2 kb, B) pG93/T1 that is 15.7 kb and C) pG19/T4 that is 17.2 kb. For each of the CE loads, 7.5 ng of pDNA was loaded into the PMMA 4-PM MFC. The time is on the x-axis (s) and the PMT reading (V) is on the y-axis.

Table 4.8. Plasmid combinations run in CE using 1 X STE.

Plasmid 1	Plasmid 2	Δ size (kb)
pPET309/ST1	pG93/T1	6.5
pPET309/ST1	pG19/T4	8
pG93/T1	pG19/T4	1.5

Plasmid 1 is the smallest plasmid in the pairing and plasmid 2 is the larger plasmid in the pairing. The difference in size (kb) between the two plasmids is shown in the Δ size column.

the observed arrival times and difference in arrival times. The observed arrival times correspond to the average of the arrival times for similar runs. The observed arrival times agree with the predicted arrival time to within 11 seconds, representing an approximately 3% variation, and thereby demonstrating the validity of Equation 4.3 in determining the size of a closed-circular DNA molecules using these conditions. It should be noted that larger variation are observed (mainly being later than predicted by Equation 4.3) in PMMA 4-PMs fabricated in 2013.

The predicted difference in arrival times did not seem to agree as well with the observed difference in arrival times. The observed difference in arrival times were between 3 and 5 seconds faster than predicted, which is significant considering the much shorter time frames. Therefore, we conclude that Equation 4.3 can be used to predict the arrival times of a closed-circular, double-stranded DNA molecules to within 18 seconds.

4.3 Discussion

4.3.1 Fabrication of PMMA MFCs Capable of Plasmid Analysis

One feature of the MFCs that we found affected the cut-off of the CE is the channel smoothness. With increased constrictions in the channel we observed a decrease in the cut-off, which we suspect is due to the localized changes in electric fields through

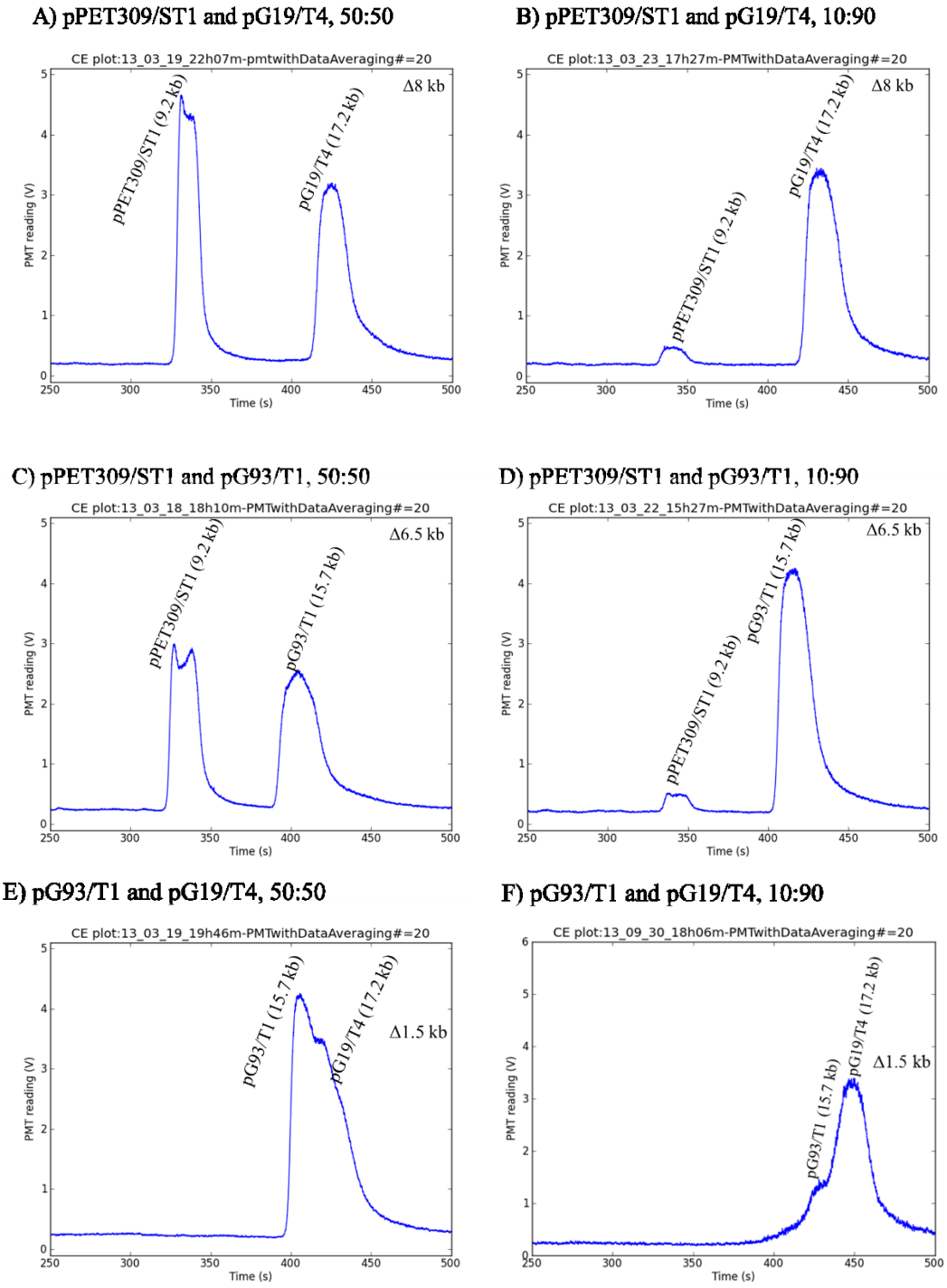

Figure 4.7. Electropherograms produced from CE using multiple plasmids. A) 7.5 ng pPET309/ST1 and 7.5 ng pG19/T4. B) 1 ng of pPET309/ST1 and 9 ng of pG19/T4. C) 7.5 ng of pPET309/ST1 and 7.5 ng of pG93/T1. D) 1ng of pPET309/ST1 and 9 ng of pG93/T4. E) 7.5 ng of pG93/T1 and 7.5 ng pG19/T4. F) 1 ng of pG93/T1 and 9 ng of pG19/T4. For each electropherogram the time (s) is on the x-axis and the PMT reading (V) is on the y-axis. The plasmids are labeled and the size differences are indicated.

Table 4.9. Predicted and observed arrival times and difference in arrival times for the plasmids in CE.

Plasmid 1	Plasmid 2	Δbp	Arrival time 1			Arrival time 2			Δ time		
			Predicted	Actual	Difference	Predicted	Actual	Difference	Predicted	Actual	Difference
pPET309/ST1	n/a	9200	282.0	277.4	-4.6	n/a	n/a	n/a	n/a	n/a	n/a
pG93/T1	n/a	15700	358.7	359.3	+0.6	n/a	n/a	n/a	n/a	n/a	n/a
pG19/T4	n/a	17200	376.4	386.6	+10.2	n/a	n/a	n/a	n/a	n/a	n/a
pG93/T1	pG19/T4	1500	358.7	362.0	+3.2	376.4	379.3	+2.9	20.7	15.0	-5.7
pPET309/ST1	pG93/T1	6500	282.0	285.4	+3.4	358.7	357.6	-1.1	77.7	72.2	-5.5
pPET309/ST1	pG19/T4	8000	282.0	289.2	+7.2	376.4	380.4	+4.0	94.8	91.2	-3.6

For the single plasmids the column for Δ bp gives the size of the plasmid and for the double plasmids the size difference between the two plasmids. For each arrival time and difference in arrival times the predicted time is compared to the actual to obtain the difference. The difference column shows the amount the actual deviated from the predicted. All times are given in seconds.

the constrictions, as they change the diameter of the channel. More constrictions within the channel would result in more localized variations in electric fields, which resulted in a higher average electric field that decreased the efficiency of the separation of the larger species of DNA.

The variations in the surfaces also plays a large role in CE (Albarghouthi *et al.*, 2002; Doherty *et al.*, 2002; Lucy *et al.*, 2008; Swedberg, 1992). We found that the PMMA 4-PM MFCs required a dilute agarose coating to improve the adherence of the running agarose to obtain more reliable arrival times during CE.

We suspect the coating improves the adherence of the running agarose, thereby blocking buffer from entering the channel and decreasing the EOF, thereby decreasing the delays (EOF has been shown to cause delays in CE (Sola and Chiari, 2012)). The increased consistency in the arrival times suggest the agarose coating makes the agarose adherence more uniform within the channel allowing better control over the surface.

The delays due to incomplete adherence were not observed with the use of STE. EOF does correlate with the ionic strength of a buffer (VanOrman *et al*., 1990), and the ionic strength of 0.5 X TBE is higher than that of 1 X STE, and therefore TBE would be predicted to have a higher EOF that STE. We suspect that one of the possible causes of the nDNA contamination in the glass MFC-based mtDNA isolation is caused by incomplete adherence. If the incomplete adherence is responsible for the nDNA contamination, the use of the agarose coating and STE could improve the MFC-based mtDNA isolation, and it was for this reason we chose to proceed with STE even with the reduced resolution.

4.3.2 Reproducibility of the Plasmid Separations with TBE

Reproducibility is a key requirement of any protocol. Therefore, once we were able to develop MFCs and the accompanying protocols for CE we needed to verify they produced reproducible results. We examined the reproducibility using three metrics based on the CE of the SC ladder: 1) resolution of the 14174 bp and 16210 bp of under 2 kb, 2) consistent arrival times within 5% STD and 3) consistent difference in arrival times between peaks. We were able to demonstrate reproducibility using five PMMA 4-PM MFCs used in a total of ten loads. The plasmid separation resulted in a resolution that is sufficient to distinguish many of the mtDNA deletions, ranging from 1.3 kb (Moraes *et al*., 1989) up to almost 11 kb (Miyabayashi *et al.*, 1991; Ruiz-Pesini *et al*., 2007), which makes the CE applicable to mtDNA analysis.

Based on the above CE, we have developed an equation to predict the arrival times of plasmids in 0.5 X TBE. Using Equation 4.1 we can predict the arrival time of a given species to within 11 seconds, which allows for the determination of the size of a closed-circular, double-stranded DNA molecule based on an arrival time. Using Equation 4.2 we can determine the difference in arrival times between two closed-circular, double-stranded DNA molecules, or predict the difference in size based on the difference in arrival times. This could be useful in determining the size of a deletion in an mtDNA analysis by determining the difference in arrival time between the WT mtDNA and the mtDNA with a deletion. Since most mtDNA rearrangements are heteroplasmic, we hypothesized the WT mtDNA can be identified by arrival time and additional peaks analyzed using the difference in arrival times.

Many previous studies that have examined CE with agarose as a sieving matrix, have used various concentrations of agarose, typically higher than 0.6%, and various capillary lengths. Many of these studies also used linear DNA, such as Chen *et al.* (Chen *et al*., 1996), who used 1% agarose with an effective separation distance of 86 mm, to separate linear DNA fragments of up to 23130 bp in 130 minutes. We have demonstrated the ability to separate plasmid up to 17.2 kb at a much shorter distance of only 11 mm. To the best of our knowledge, this is the shortest reported distance used for CE with agarose in the literature. The shorter distance decreases the CE time to under an hour for four runs (a single load). The shorter distance also decreases the size of the MFC, which can decrease the size of the equipment needed to run the MFC. The decreased size is beneficial for versatility and possible POC applications. Therefore, our CE-based plasmid separation could be adapted for a relatively quick and versatile POC mtDNA analysis.

As mentioned above, the agarose concentrations of many of the previous studies have were higher than the 0.6 % used in this study. The higher agarose concentrations results in better resolution for the smaller DNA fragments compared to that seen in this study (Bocek and Chrambach, 1992; Motsch *et al*., 1991). However, the resolution is poor for larger species of DNA in many of the other studies. For our purposes we are examining larger DNA fragments and therefore the 0.6 % agarose that we have used appears to improve the resolution for the species above 10 kb. Therefore, compared to previous CEs using agarose, our CE has improved resolution for larger DNA species at a shorter distance.

4.3.3 The Buffer Affects Resolution and Arrival Times

Once we had a reproducible CE, we decided to test three non-Tris based buffers in attempts to improve the CE. The buffers LBa and SBa were chosen due to the low Joule heating, which allow running at higher electric fields, found by Brody *et al.* (Brody *et al*., 2004). ST was chosen due to the improved stability it demonstrated compared to SBa for supercoiled DNA (Ishido *et al.*, 2010). We found that ST had similar resolution compared to TBE, but did not have delays in the arrival times from one run to the next. This suggest that ST improves adherence (which has been discussed above), or decreases EOF. Since we suspect that incomplete adherence may have played a role in the nDNA contamination of the mtDNA isolation using glass MFCs (to be discussed further in Chapter 6), the improved adherence was considered more relevant for our purposes than the small decrease in the resolution. Therefore, we decided to examine the ST buffer further.

Since we are developing a CE protocol that could be adapted to our MFC-based mtDNA isolation from leukocytes, we decided to add 1mM EDTA to the ST buffer, resulting in STE buffer. For the MFC-based mtDNA isolation we lyse the cells on-chip and therefore the proteases and DNases are still present and EDTA as a chelating agent (Dominguez and Ward, 2009) will be required. We observed a similar resolution between the 14 174 bp and 16210 bp with STE, 1943.38 bp ± 228.36 bp, and the consistency in arrival times was maintained. Although there is a slightly worse resolution compared to TBE, we hypothesized that the consistency in the arrival times indicated a better agarose adherence, which we determined to be more important for our purposes.

4.3.4 Separating Plasmids using Capillary Electrophoresis

In developing the CE protocol we have used the SC ladder since it contains plasmids that ranged from 2066 bp to 16210 bp. The larger species were examined, from 8066 bp to 16210 bp, due to the similarity in size to the mtDNA and its associated rearrangements. Using the SC ladder we were able to develop a stable CE protocol, which allows for the prediction of the arrival times and difference in arrival times, for closed-circular, double-stranded DNA molecules, such as plasmids or mtDNA. To validate the accuracy of these equations and verify our CE protocol can be applied to more than just the SC ladder, we decided to run CE using plasmids of 9.2 kb, 15.7 kb and 17.2 kb. We used Equation 4.3 and 4.4 to calculate the predicted arrival times and difference in arrival times (Table 4.10). We then compared the actual arrival times to our predicted arrival times. The largest variance from the predicted arrival times was 10.2 s. However, it should be noted that those run on PMMA 4-PMs fabricated in 2013 had more significant delays from the predicted arrival times. Since the majority of the plasmid separations were performed using PMMA 4-PMs fabricated in 2012 the averages of the predicted arrival times agree with Equation 4.3 and 4.4. Given the general agreement of the observed arrival times we can conclude that Equation 4.3 can predict an arrival time of a closed-circular, double-stranded DNA molecule to within 35 seconds (this is to account for the variation seen in the various PMMA 4-PMs). However, we did not find the difference in arrival times to be as accurate. Therefore, we propose the use of Equation 4.3 for predictions of arrival times, but not Equation 4.4 for difference in arrival times.

These plasmids have been used as a model for mtDNA. Using the plasmids we have demonstrated ability to separate two closed-circular, double-stranded DNA molecules that have a difference in size of as little as 1.5 kb. Given the smallest recorded large-scaled mtDNA deletion is 1.3 kb (Moraes *et al*., 1989), although most are over 2 kb (Ruiz-Pesini *et al*., 2007), we could detect most, if not all, large-scale mtDNA deletions using this CE method and using Equation 4.3 we could determine the size of the species seen in CE. Therefore, we can conclude that this CE method would be applicable for detecting large-scale mtDNA rearrangements.

We also examined different ratios of pDNA in the CE to reflect heteroplasmy. Many of the methods used to determine large-scale mtDNA deletions are only able to determine levels of heteroplasmy to approximately 20 % (Wong and Boles, 2005b). We tested our CE by having the smaller plasmid, which represents the deleted mtDNA species, to be only 10% of the sample. This is representative of 10% heteroplasmy, and we found we could still distinguish the two plasmid species. Therefore, our CE-based plasmid separation would be acceptable for detecting heteroplasmy as low as 10% for large-scaled mtDNA rearrangements.

CHAPTER 5- MFC-BASED ELECTROPHORETIC SEPARATION OF MITOCHONDRIAL DNA FROM WHOLE CELL LYSATES

5.1 Introduction

5.1.1 Variation in the Mitochondrial DNA Copy Number

There are hundreds to thousands of copies of the mtDNA per cell, with exact number of copies varying by cell type (Tuppen *et al.*, 2010). For example, muscle, which is a high "energy-demanding" tissue, contains 2700 ± 1600 mtDNAs per cell. Blood, which is a less "energy-demanding" tissue, contains only 330 ± 160 mtDNAs per cell (Dimmock *et al*., 2010). However, there can be a large amount variation in mtDNA copy number even within the same tissue. Some variables that affect the mtDNA copy number include age, activity level and the degree of cellular stress (Dimmock *et al*., 2010; Miller *et al*., 2003; Shen *et al*., 2008; Xu *et al.*, 2013).

5.1.2 Isolating Mitochondrial DNA

Mutations in the mtDNA have been linked to a wide variety of disorders, ranging from common neurodegenerative disorders to certain forms of cancer (Saneto and Sedensky, 2013; Schaefer *et al*., 2004). Although mtDNA mutations can play a significant role in disease, analysis of the mtDNA is complicated by numerous factors including the presence of NUMTs (Gaziev and Shaikhaev, 2010; Selosse *et al*., 2001), which can lead to false positives in PCR-based assays (Bensasson *et al*., 2001; Calvignac *et al.*, 2011; Yao *et al*., 2008; Zhang and Hewitt, 1996). To prevent false positives from NUMTs, either mtDNA-specific primers must be carefully designed or the mtDNA must be purified (Calvignac *et al*., 2011; Yao *et al*., 2008). Unfortunately, since these approaches are difficult and impractical for large-scale studies, they are not always used. This has lead controversial results pertaining to some reported mtDNA mutations (Palanichamy and Zhang, 2010).

5.1.3 Objective

Although there have been MFCs developed to examine specific aspects of mtDNA, such as DNA damage in the mtDNA (Wirtz *et al*., 2005), quantification of nucleoids (Navratil *et al*., 2007), or examination of amplified regions of the mtDNA (Alonso *et al.*, 2006; Backhouse *et al*., 2002), all of these MFC approaches require off-chip sample preparation. Although there have been attempts made in developing a MFC-based mtDNA isolations (Chang *et al*., 2010), as discussed in Chapter 1 there are concerns with the purity of the isolated mtDNA. The ability to purify mtDNA with no nDNA contamination on a MFC is therefore a critical step that is still missing in the development of a μTAS for mtDNA. In this chapter, we will describe several approaches taken in an attempt to purify mtDNA from fibroblasts and leukocytes using MFCs.

5.2 Results

5.2.1 Mitochondrial DNA Isolation in Glass MFCs

5.2.1.1 Modification the Plasmid Segregation

In our previous work using pCOX15/ST8 in glass 4-PMs, we decreased the threshold for the plasmid segregation to 1 pg (Chapter 3). The plasmid segregation required just over ten minutes for pCOX15/ST8, which is a 7.8 kb plasmid (Glerum *et al*., 1997), to migrate the length of the injection channel (16.3 mm). Since the mtDNA is larger than pCOX15/ST8 the mtDNA will take longer to migrate to the SW. One of the factors that can limit the length of time of the CE is the buffer capacity, as a prolonged CE can cause buffer depletion that can lead to erratic behaviour (Brask *et al*., 2005). However, we cannot decrease the time by increasing the electric field in our MFC assays since this will lead to trapping. Trapping limits the electric field since the mtDNA will

become trapped above its critical field (Akerman and Cole, 2002; Manage *et al*., 2008) of 27 V/cm. Therefore, to decrease the CE time while maintaining the critical field, we decreased the length of the channel to 2.4 mm for the mtDNA MFCs.

Since we have changed the MFC design, we first needed to verify that the 1 pg pCOX15/ST8 plasmid segregation, which was reliable on glass 4-PMs, was successful on the new glass mtDNA MFCs. Using the same protocol as the 1 pg plasmid segregation, with the exception that the voltage program was 25 V/cm for 150 seconds, we successfully segregated 1 pg of pCOX15/ST8 on the glass mtDNA isolation MFCs (Figure 6.1). This demonstrates that the glass mtDNA isolation MFCs behaves similar to the glass 4-PMs that were used to decrease our threshold to 1 pg in Chapter 3. However, the smaller channel allows a faster mtDNA isolation that helps to avoid buffer depletion.

5.2.1.2 Using Fibroblasts to Isolate Mitochondrial DNA Using MFCs

One picogram is the approximate amount of mtDNA in 1500 fibroblasts, since fibroblasts contain 600 ± 300 mtDNAs per cell (Dimmock *et al*., 2010). Upon establishing that the new design for mtDNA isolation MFCs was suitable for segregating as little as 1 pg of pCOX15/ST8, we attempted to isolate mtDNA from cultured fibroblasts. We used the GM5565 cell line, a WT fibroblast line (Coates *et al*., 1985). As described in Chapter 2, the SR well contained approximately 3000 fibroblasts, 5 % Triton X-100, 3 µg BSA, and 0.1 X TBE. Since we had successfully lysed bacterial cells in the plasmid miniprep with Triton X-100, it was used as a detergent for lysis of the cells in the SR for the mtDNA isolation. For the mtDNA isolation, the contents of each well were examined using a PCR to verify the presence (or absence) of mtDNA (*HVI*) and the nDNA (either *hCOX11* or *SCO2*). A successful mtDNA isolation is defined as

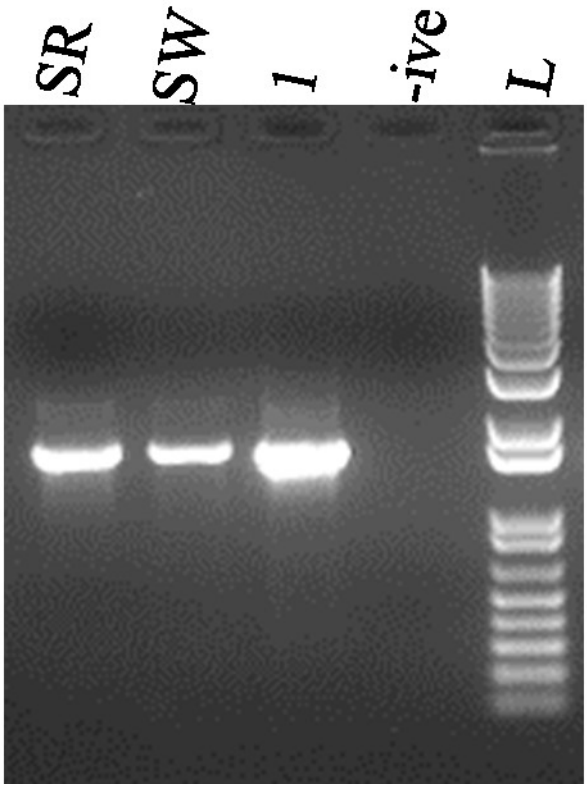

Figure 5.1. Segregation of 1 pg pCOX15/ST8 on glass mtDNA isolation MFCs. An agarose gel image of the PCR products from the 1pg plasmid segregation. SR is the sample reservoir, the SW is sample waste, 1 is the off-chip positive control with 1 pg of pCOX15/ST8, -ive is the off-chip negative control and L is the 1 kb plus ladder.

containing mtDNA in the SW with no nDNA. The SR will contain both mtDNA and nDNA since the cells are lysed in the SR.

We decided to first attempt the MFC-based mtDNA isolation with 3000 fibroblasts since it is above our threshold. Using approximately 3000 GM5565 cells we were able to isolate the mtDNA, as shown by the presence of the mtDNA in the SW (Figure 6.2). However, there was also a small amount of nDNA indicated by a positive PCR in the SW for nDNA (Figure 6.2). Therefore, we do not consider this a successful mtDNA isolation.

Since the signal for nDNA is very faint it does demonstrate the majority of the nDNA did not migrate during CE. The fibroblasts cells used in the isolation in Figure 6.2 had a viability of 85% and therefore the sample would have contained approximately 500 dead fibroblasts. We have found that cell samples with lower viabilities tend to have more nDNA contamination (as indicated by a stronger PCR product from the SW). Therefore, we suspect at least some of nDNA found in the SW is due to sheared nDNA from dead cells. For freshly isolated fibroblasts our viabilities usually ranged between 85-90%, which dropped to 75-80% for fibroblasts frozen as described in Chapter 2 for one day. Fibroblasts that have been frozen for more than a day usually had viabilities of less than 50%. Therefore, freshly isolated fibroblasts are more likely to result in a successful MFC-based mtDNA isolation.

6.2.1.3 Using Leukocytes to Isolate Mitochondrial DNA Using MFCs

After being able to isolate mtDNA from fibroblasts, albeit with small amounts of nDNA contamination, we decided to attempt a MFC-based mtDNA isolation using leukocytes obtained from blood. Leukocytes contain about half the number of copies of

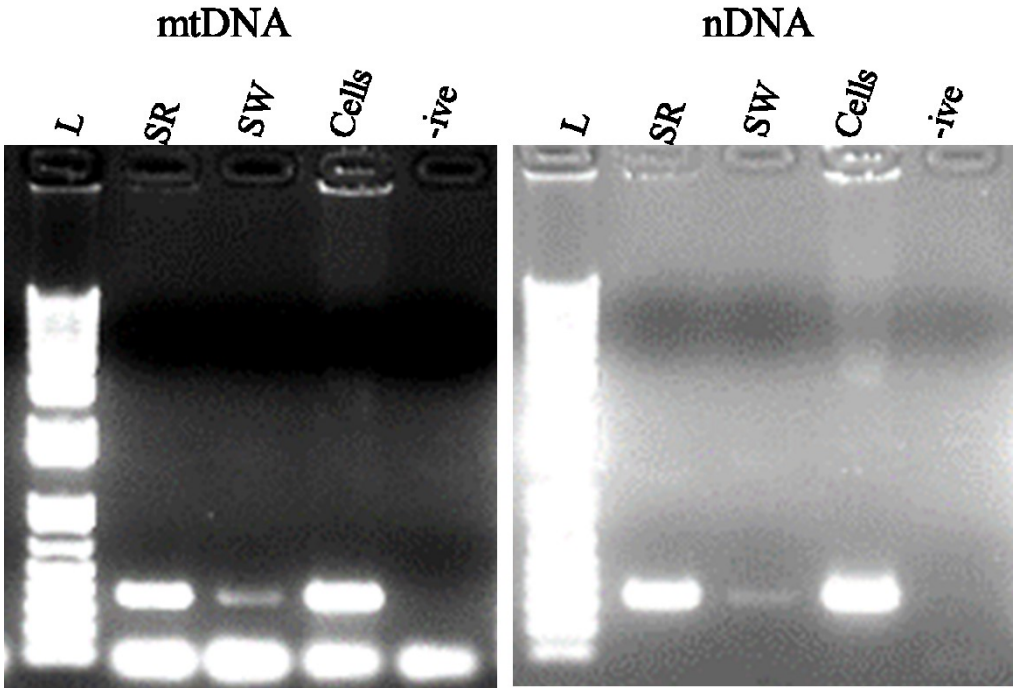

Figure 5.2. MFC-based mtDNA isolation from GM5565 fibroblasts using glass mtDNA isolation MFCs. The SR and SW represent amplification of the contents of the SR and SW wells recovered after CE, cells is an off-chip positive control with ~3000 GM5565 fibroblasts, and –ive is the off-chip negative control, and L is the 1 kb plus ladder. The image to the left represents mtDNA (HVI) and the right represents nDNA (hCOX11). The mtDNA isolation was performed using approximately 3000 GM5565 fibroblasts with an 85% viability, 0.1 X TBE, 5% Triton X-100 and 3 µg BSA in the SR and 0.1X TBE and 3 µg BSA in the SW. CE was run at 25 V/cm for 200 seconds.

mtDNA when compared to fibroblasts (300 and 600 respectively (Dimmock *et al*., 2010)). Due to the difference between the two cell types, we attempted the mtDNA isolation with both 5000 and 3000 leukocytes. We were able to isolate mtDNA from both 5000 and 3000 leukocytes (3000 leukocyte isolation shown in Figure 6.3). Although the number of cells is the same as the fibroblasts, it represents the ability to isolate even lower amounts of mtDNA than we have in the MFC-based mtDNA isolation using fibroblasts (only 1 pg of mtDNA in 3000 leukocytes). To isolate mtDNA from leukocytes, the buffer concentration was lowered from 0.1X TBE to 0.01X TBE. However, as with the fibroblasts there is still a small amount of nDNA contamination.

5.2.1.4 Effects of Varying Buffer Concentrations

In all experiments described above, and in Chapter 3, the 0.6 % agarose sieving matrix was prepared in 1 X TBE, and the running buffer in the wells has varied as indicated. When we examined the effect of various buffer conditions on AGE in slab gels, we found that agarose gels made with 1 X TBE, but run with a 0.1 X TBE buffer, showed significant compression of DNA species compared to using the same concentration of buffer in both the agarose and the running buffer (Figure 6.4). This resulted in slower migrations than seen when both gel and running buffer were at the same concentration. It should be noted that 0.1 X TBE already had slower migrations compared to other TBE concentrations, but these were still not as slow as when the buffer concentrations were different. The slower migrations of 0.1 X TBE could be due to buffer depletion since each run was 80 minutes.

Based on the observations seen in the slab gels, we decided to examine what effect different buffer concentration had on our MFC-based mtDNA isolation. We

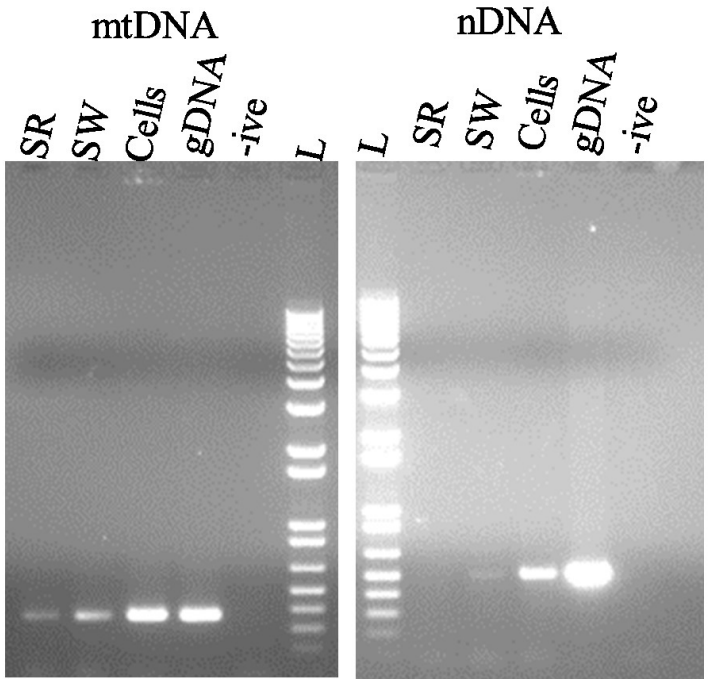

Figure 5.3. MFC-based mtDNA isolation from leukocytes using glass mtDNA isolation MFCs. The SR and SW represents amplification of the contents of the SR and SW wells recovered after CE, cells is an off-chip positive control with ~3000 leukocytes with 15 % Triton X-100, gDNA is an off-chip positive control with gDNA, –ive is the off-chip negative control and L is the 1 kb plus ladder. The image to the left represents mtDNA (HVI) and the right represents nDNA (SCO2). The mtDNA isolation was performed using approximately 3000 leukocytes with a 93% viability, 0.01 X TBE, 5% Triton X-100 and 3 µg BSA in the SR and 0.01X TBE and 3 µg BSA in the SW. CE was run at 25 V/cm for 200 seconds.

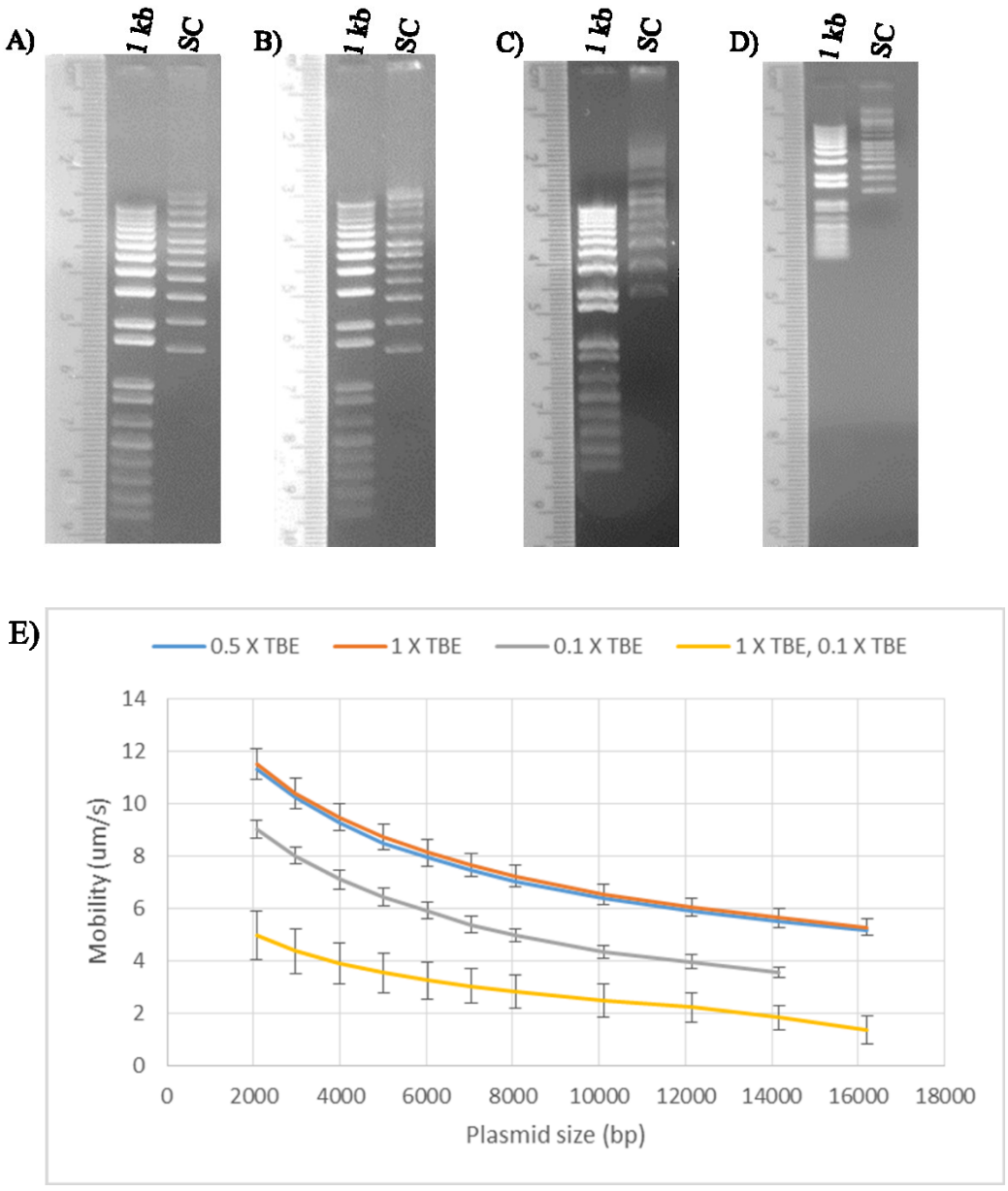

Figure 5.4. DNA ladders separated in 0.6 % agarose slab gels in A) 0.5 X TBE, B) 1X TBE, C) 0.1 X TBE and D) with the agarose made with 1 X TBE and run in 0.1 X TBE. Each agarose slab gel used Amresco III (PFGE grade) agarose in the appropriate buffer and were run at 5.3 V/cm for 80 minutes. 1 kB is the 1 kb plus ladder and SC is the Supercoiled DNA ladder. Each image includes a ruler to the left to allow for scaling. E) The mobility (μm/s) of the species in the SC ladder for the various buffer concentrations. The average mobility of three gels is shown with error bars representing the STD.

originally hypothesized that keeping the agarose buffer and the running buffer the same concentration would decrease the time of the isolation. However, we also observed that the amount of nDNA contamination, when both the running and agarose buffers were the same, was decreased compared to when the agarose and running buffer concentrations were different (Figure 6.5). Figure 6.5 A shows the results for mtDNA (left) and nDNA (right) for a CE with 1 X TBE in the agarose and 0.01X TBE in the running buffer. Figure 6.5 B shows the results for mtDNA (left) and nDNA (right) for CE with 0.01X TBE in both the agarose and running buffer. These two CEs were performed using the same cells, which had a viability of 60%, and therefore should have similar amounts of nDNA contamination. However, we observed a decrease in the nDNA contamination when the buffer in the agarose and running buffer were the same concentration compared to when they differed. This suggest that the buffer could be contributing to the nDNA contamination seen in the mtDNA isolations in glass MFC-based mtDNA MFCs.

5.2.2 Isolating mtDNA using PMMA MFCs

Our previous attempts to purify mtDNA in glass MFCs resulted in isolated mtDNA with a small amount of nDNA contamination. One mechanism that we hypothesize is contributing to the nDNA contamination is that the nDNA is bypassing the agarose sieving matrix. As discussed in Chapter 4, there was incomplete adherence of the agarose sieving matrix that caused delays in the arrival times of the plasmid species of the SC ladder during the plasmid separations. Since we suspect the agarose is not completely adhering to the channel wall, it can allow fluids, such as the contents in the wells, to move between the wells without having to go through the agarose. Although it was not studied in glass MFC, there are some observations that suggest that incomplete

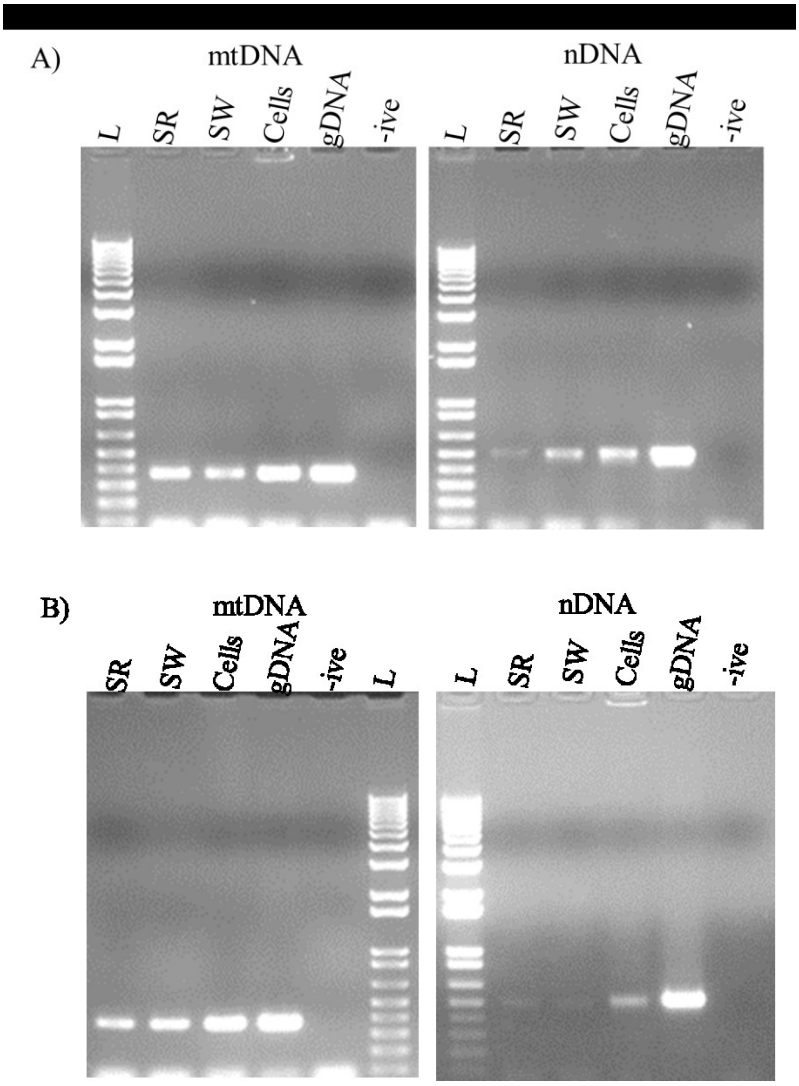

Figure 5.5. Influence of buffer concentration on the MFC-based mtDNA isolation. A) Run with the running buffer of 0.01X TBE and the agarose buffer of 1 X TBE. B) Run with the running buffer and agarose buffer of 0.01 X TBE. The SR and SW represent amplification of the contents of the SR and SW wells recovered after CE, cells is an off-chip positive control with ~3000 leukocytes and 15 % Triton X-100, gDNA is an off-chip positive control with gDNA, –ive is the off-chip negative control and L is the 1 kb plus ladder. The image to the left represents mtDNA (HVI) and the right represents nDNA (SCO2). The mtDNA isolation was performed using approximately 3000 leukocytes with a 60% viability, 0.01 X TBE, 5% Triton X-100 and 3 µg BSA in the SR and 0.01X TBE and 3 µg BSA in the SW. CE was run at 25 V/cm for 200 seconds.

adherence may have also occurred in glass MFCs. In glass mtDNA MFCs, the contents of the wells were extracted after each run. In some MFC-based mtDNA isolations, there was less fluid, and in some cases very little to none, extracted from one well compared to the other. This suggest movement of the fluids between the wells since they have the same starting volume. This could be due to the increased EOF caused by incomplete adherence. Therefore, we hypothesized that the 0.1% agarose coating would help to decrease, or even eliminate, the nDNA contamination associated with the MFC-based mtDNA isolation in PMMA mtDNA MFCs.

Based on the hypothesis that some of the nDNA contamination may be caused by incomplete adherence of the sieving matrix to the channel walls, we chose to use the 0.1 % agarose coating and 0.5 X and 0.1 X STE as the buffer. We chose these STE concentrations because the glass MFC-based mtDNA isolations used lower concentrations of buffer compared to the plasmid segregations and plasmid separations. Since we used 1 X STE in the plasmid separations in PMMA, we attempted the mtDNA isolation at half (0.5 X) and one tenth (0.1 X) the buffer concentration for the PMMA MFC-based mtDNA isolations. Unfortunately, neither of these MFC-based mtDNA isolations were successful (Figure 6.6). There was no mtDNA or nDNA found in the SW, indicating that neither were capable of migrating from the SR to the SW. Therefore, we have not been able to successfully purify mtDNA using MFCs.

5.3 Discussion

5.3.1 Adaptation of Plasmid Segregation to Mitochondrial DNA Isolation

In our previous work (described in Chapter 3), we have used the pCOX15/ST8 plasmid as a model for mtDNA in CE. Using the pCOX15/ST8 plasmid, we were able to

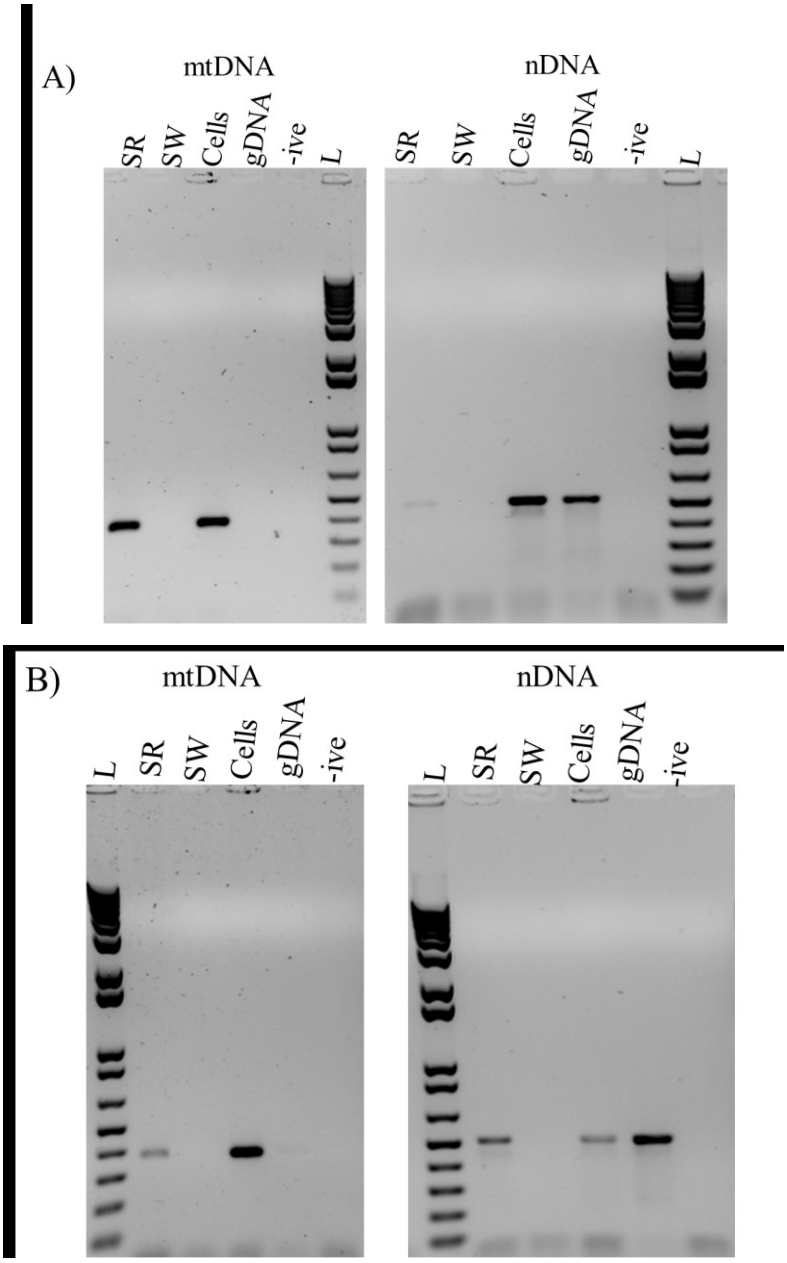

Figure 5.6. MFC-based mtDNA isolation from 3000 leukocytes with an 86% viability on PMMA mtDNA isolation MFCs in A) 0.1 X STE and B) 0.5X STE. The SR and SW represent the amplification of the contents of the SR and SW after CE, cells is an off-chip positive control with ~3000 leukocytes with 15 % Triton X-100, gDNA is an off-chip positive control with gDNA, –ive is the off-chip negative control and L is the 1 kb plus ladder. The image to the left represents mtDNA (HVI) and the right represents nDNA (SCO2). The mtDNA isolation was performed using approximately 3000 leukocytes with a 86% viability, STE, 5% Triton X-100 and 3 µg BSA in the SR and STE and 3 µg BSA in the SW. CE was run at 25 V/cm for 200 seconds.

decrease the threshold for the plasmid segregation down to 1 pg, the approximate amount of mtDNA found in 1500 fibroblasts or 3000 leukocytes. The plasmid segregation experiments were run on glass 4-PMs with a channel (the injection channel) that is 16.3 mm long (Manage *et al*., 2008; Northrup *et al.*, 2010). Since the mtDNA is about twice the size of pCOX15/ST8, the run length for CE would be considerably longer for mtDNA. A potential problem arising from increasing the time needed for CE is buffer depletion, which can lead to erratic behaviour (Brask *et al.*, 2005). With 0.1 X TBE we would expect the buffer to be depleted in approximately 850 seconds. Based on the velocity observed during the plasmid separations for a 16.2 kb plasmid (0.03mm/s), we would expect the mtDNA to take approximately 543.3 seconds to migrate the 16.3 mm of the injection channel. However, this time does not take into account sample injection. Initial attempts to simply prolong the injection (up to 1000 seconds) were unsuccessful (data not shown). Since mtDNA is circular, we cannot decrease the CE time by increasing the electric field past the critical field of 27 V/cm. To better facilitate the mtDNA isolation, we developed new MFCs that had a shorter channel of only 2.4 mm. By decreasing the length of the channel it allows us to decrease the time required for the isolation, while maintaining the appropriate electric field and avoiding buffer depletion. Based on the velocity of the 16.2 kb plasmid we would predict the mtDNA to migrate the 2.4 mm long channel in approximately 75 seconds, which is well below the predicted buffer depletion time.

Once we had developed the glass mtDNA isolation MFCs, we adapted the protocols used for the pCOX15/ST8 plasmid segregation for the MFC-based mtDNA isolation. The isolations on the glass mtDNA MFC did not require the 3-step injection

voltage program used for the plasmid segregation in the glass 4-PMs, but instead used one low electric field step. Due to the decreased channel length and the use of a power supply instead of the μTK for CE, the use of the 3-step injection was logistically problematic for the mtDNA isolations. On the glass mtDNA MFCs, the plasmid segregation took only 150 seconds at 25 V/cm and the mtDNA isolation took 200 seconds at 25 V/cm. Based on the arrival times calculated from the 27 V/cm CE in Figure 3.1, we would expect pCOX15/ST8 (7.8 kb) to migrate 2.4 mm in approximately 55 seconds and the mtDNA (16.6 kb) would take approximately 75 seconds. These estimated times are about a third of the actual times required for the respective isolations, probably due to the time required for the mtDNA to enter the agarose sieving matrix. Therefore, to accommodate sample injection the injection time was approximately three times longer than the predicted time for just mtDNA migration.

For the plasmid segregation, we used 0.5 X TBE as the running buffer, and for the plasmid miniprep, we used 1 X TBE. In adapting the plasmid segregation to the mtDNA isolation, we found that lower buffer concentrations were required to move the mtDNA during CE. Therefore, we used 0.1 X TBE for fibroblasts and 0.01X TBE for leukocytes. The decrease in buffer concentrations is thought to reflect the decreased time required, as well as the contribution of the cell lysate to the buffer. As with the plasmid miniprep, we lysed the cells in the SR with Triton X-100, as it is a non-ionic detergent (Cornett and Shockman, 1978), and therefore should not migrate during CE. In our MFC-based mtDNA isolation Triton X-100 also facilitates the removal of proteins from the DNA, such as the histones and TFAM. Since we use PCR to detect the mtDNA and nDNA for the MFC-based mtDNA isolations, we require a reliable PCR to analyze the MFC-based

mtDNA isolations. We had found that using lower levels of Triton X-100 would lyse the cells, but we obtained irregular PCR results when using cells (data not shown). Therefore, we use 5% Triton X-100 to both lyse the cells and to dissociate the proteins to improve the PCR. Al-Soud and Rådström examined PCR using leukocytes and determined that the lactoferrin in leukocytes inhibited PCR. However, the inhibition of lactoferrin could be overcome by the use of BSA (Al-Soud and Rådström, 2001), and therefore our PCR for leukocytes also required BSA. We also found BSA to be required for reliable PCR results when using leukocytes as a template.

5.3.2. Mitochondrial DNA Isolations Using MFCs

To ensure reliable results for mtDNA analysis either the mtDNA must be purified or mtDNA-specific primers must be used to avoid amplification of NUMTs (Calvignac *et al*., 2011; Yao *et al.*, 2008). Extensive validation is required to generate mtDNA-specific primers and the purification of mtDNA is time consuming and laborious. Since there are no universal standards for mtDNA diagnostics (Carracedo *et al*., 1998), it can lead to variability in mtDNA diagnostics. Although there have been some studies that have examined aspects of mtDNA analysis using MFCs, there have been no successful mtDNA purifications using MFCs reported in the literature. The ability to purify mtDNA in MFCs could facilitate a μTAS that could improve the reliability of mtDNA analysis, while decreasing the time and cost associated with mtDNA analysis.

We attempted to purify mtDNA first from cultured fibroblasts (GM5565) and then from leukocytes isolated from blood. Although we were able to successfully isolate mtDNA, there was nDNA contamination. We suspect that the viability of the cell sample is a factor in the nDNA contamination, as we observed that cell samples with lower

viabilities had more nDNA contamination (indicated by a stronger band for the nDNA in the PCR for the SW). This is likely due to fragmentation of the nDNA caused by the endogenous endonucleases during apoptosis (Wyllie, 1987). Since the hypothesized mechanism by which the MFC-based mtDNA isolation is based on the nDNA chromosome being megabases, and therefore much larger than the mtDNA, smaller nDNA fragments are problematic.

We also found that buffer concentration had an effect on the amount of nDNA contamination. The compression observed when using different buffer concentrations in slab gels lead us to suspect the buffer concentration could play a role in the time required for the MFC-based mtDNA isolation. However, when we examined this in CE, we found that isolations that had the same buffer concentration in the agarose sieving matrix and the running buffer had less nDNA contamination compared to the isolations that had 1 X TBE in the agarose sieving matrix and 0.01X TBE in the running buffer. In some of the isolations using the same buffer concentration in the agarose and running buffer resulted in a purified mtDNA isolation (i.e. mtDNA present in SW with no nDNA). However, there was still some nDNA contamination is other MFC-based mtDNA isolations using the same buffer in the agarose and running buffer, and therefore we do not consider the MFC-based mtDNA purification reproducible. Nevertheless, this does indicate that the buffer concentrations do play a role in the nDNA contamination, although the exact mechanism is not known.

One possible mechanism for the decreased nDNA contamination observed when the buffer concentrations are the same in the agarose and running buffer is due to the variation causing a buffer gradient. A variation in buffer gradient is a technique that can

improve sample stacking, thereby improving the sample injection (Mikkers *et al*., 1979). In 0.6 % agarose the larger sized nDNA should not enter the agarose sieving matrix (Gao *et al*., 2007), which should allow for the separation of the mtDNA from the nDNA. However, sample stacking may assist some of the larger species in entering the agarose, resulting in more nDNA contamination. This mechanism is more likely to occur in samples that already have fragmented nDNA, such as samples with cells undergoing apoptosis. Although we do not know the exact size limitation for sample stacking, the megabase sizes of the chromosomes would probably still be too large to enter the agarose.

Another possible contribution to the nDNA contamination may have been due to the incomplete adherence of the agarose sieving matrix increasing the EOF. In the plasmid separations in PMMA 4-PMs, we hypothesized that incomplete adherence caused delays in arrival times between runs. We were able to control adherence with an agarose coating (Swedberg, 1992) and the use of STE buffer (Ishido *et al*., 2010). Since we did observe some variability in the quantity of the fluid in the wells at the end of CE in our glass MFC-based mtDNA isolations, we suspected that incomplete adherence may have also occurred in the glass MFC-based mtDNA isolations. If the agarose was not adhering to the channels, it could allow for movement between the wells that bypassed the agarose sieving matrix, and would therefore not be limited by size. Especially given the very short channel length of the mtDNA MFCs, this could allow some nDNA to migrate to the SW, regardless of size, and therefore account for some of the nDNA contamination. It should be noted that we did not observe any variation in the amount of fluid in each well after CE in the PMMA MFC-based mtDNA isolations that used the

agarose coating and STE. This indicates there is no fluid bypassing the agarose in the channel and therefore we have better agarose adherence. As we suspect the incomplete adherence was a factor in the nDNA contamination seen in the glass MFC-based mtDNA isolations, if we can isolate mtDNA using the new mtDNA PMMA MFC that accounts for incomplete adherence, we may obtain a successful MFC-based mtDNA isolation.

CHAPTER 6- DISCUSSION

6.1 Towards Using MFCs to Analyze Mitochondrial DNA

Analysis of mtDNA is complicated by numerous factors, which have been discussed in previous chapters, thereby making many large scale studies unfeasible for mtDNA. A method that could decrease the time, cost and amount of sample required would help improve mtDNA analysis for numerous applications. Therefore, we have attempted to use MFCs to isolate and analyze mtDNA.

In this study, we have used plasmids as a model for mtDNA due to their shared physical similarities. Using plasmid we were able to reduce the threshold for manipulating circular DNA to picogram quantities, orders of magnitude lower than previous reports. We were able to apply the 1 pg pCOX15/ST8 segregation to develop a MFC-based plasmid miniprep that used only 10^5 *E. coli*. Based on the approach developed for the plasmid segregation and plasmid miniprep, and by decreasing the separation channel length, we were able to partially purify mtDNA from fibroblasts and leukocytes.

In attempts to develop a MFC-based method to rapidly screen for mtDNA rearrangements we have also developed a CE-based plasmid separation that is capable of resolving two plasmids with as little as 1.5 kb size difference between them. This CE-based plasmid separation allows for a resolution of 2 kb, which is sufficient to distinguish most large-scale mtDNA rearrangements, at separation length of only 11 mm. This is shorter than any other electrophoretic separation distance reported in the literature.

6.2 The Importance of Thresholds for the Plasmid Segregations

The mtDNA comprises approximately 0.1 % of the total cellular DNA (Lander *et al*., 2001), which is why mtDNA analysis requires a large quantity of tissue. The amount

of tissue needed, as well as the time and equipment required, makes many large-scale studies of mtDNA impractical. MFCs allow anticipation of assays typically performed at the laboratory bench onto a small microchip (Beebe *et al.*, 2002; Fiorini and Chiu, 2005; Ramsey *et al*., 1995). Due to the decreased size of MFCs they can typically be used to analyze smaller samples compared to their traditional counterparts. With most MFC-based assays using nanogram quantities. Since there are only picogram quantities of mtDNA in a few thousands cells, to facilitate the manipulation and analysis of mtDNA we required a threshold orders of magnitude lower than other MFC-based approaches reported in the literature.

In the CE-based plasmid segregation our threshold is defined as the lowest concentration of plasmid that can be successfully segregated. We used the plasmid pCOX15/ST8, which is 7.8 kb (Glerum *et al*., 1997), to allow us to study the various factors that affected the threshold. One factor that was important in decreasing our threshold was the surface chemistry. Since MFCs have a larger surface area to volume ratio compared to traditional assays, the surface effects are more prevailent in MFC-based assays compared to traditional laboratory assays (Doherty *et al*., 2002; Horvath and Dolnik, 2001; Yates and Campbell, 2011). We hypothesized that non-specific adsorption was causing pDNA to adsorb to the wall of the MFC channels, thereby increasing our threshold. To address the non-specific adsorption we used a 5 % (w/w) PDMA coating, which decreased our threshold to 10 pg. Adsorption has been linked to van der Waals forces, hydrophobic attraction, and hydrogen bonding (Azadi and Tripathi, 2012; Doherty *et al*., 2002; Fa *et al*., 2005). We had compared PDMA to three other acrylamides, PHEA, LPA and CPA, which vary in structure primarily by virtue of their amine group,

and we suspect the two methyl groups of the tertiary amine in PDMA prevent hydrogen bonding with the DNA and therefore result in less non-specific adsorption and thus a lower threshold.

To continue to decrease our threshold from 10 pg to only 1 pg we examined other factors that might be contributing to the threshold. Plasmids and mtDNA are closed-circular DNA molecules, and therefore trapping is an important variable to consider in the voltage program (Akerman and Cole, 2002; Manage *et al.*, 2008). We found a combination of PFGE-like approach and low electric fields, in a voltage program called the 3-step injection, was suitable for the plasmid segregation. The first step uses a high electric field that promotes the entrance of the plasmid into the agarose sieving matrix (sample injection), that is likely to cause trapping of the plasmid. The second step reverses the electric field to reverse the trapping and is followed by the final low electric field that allows separation on the basis of size without trapping the plasmid of interest of the CE. To ensure we did not trap the plasmid we used 32 V/cm, since it was previously shown to be lower than the critical field for an 8 kb plasmid (Manage *et al*., 2008), which is similar in size to pCOX15/ST8. The combination of these two approaches improves the sample injection and accounts for trapping, resulting in the lower threshold.

The final variable in obtaining a reproducible 1 pg plasmid segregation was related to the buffer, with respect to both type and concentration. We found that 0.5 X TBE resulted in a reproducible 1 pg plasmid segregation, which demonstrates the lowest concentration of DNA to be successfully manipulated on a MFC. The ability to manipulate picogram quantities of pDNA can facilitate the manipulation of mtDNA from only a few thousand cells.

Using the 1 pg plasmid segregation, we developed a MFC-based plasmid miniprep that used only 10^5 *E. coli* cells, which is significantly lower than the 10^{10} to 10^{11} *E. coli* used in conventional minipreps (Birnboim and Doly, 1979). This demonstrates we could isolate a plasmid from an *in vivo* source, which is important since we would go on to attempt to isolate mtDNA from cells. The 1pg threshold would permit us to manipulate the mtDNA found in just a few thousand cells. The MFC-based plasmid miniprep is an example of the plasmid segregation in which lysis in carried out on-chip, as would be required for a MFC-based mtDNA isolation. This is, to the best of our knowledge, the first MFC-based plasmid preparation method. We then used the plasmid segregation and plasmid miniprep as the basis for a MFC-based mtDNA isolation using only a few thousand human cells.

6.3 Developing a MFC-based Mitochondrial DNA Isolation

By adapting the approach needed to manipulate plasmids on a MFC to a MFC with a small 2.4 mm long channel, we were able to partially purify mtDNA from fibroblasts and leukocytes. The nDNA contamination is problematic since it can cause false-positives for PCR-based analysis down-stream (Bensasson *et al*., 2001; Calvignac *et al*., 2011; Yao *et al*., 2008; Zhang and Hewitt, 1996). We did observe that the buffer concentration and the viability in the cell sample affected the amount of nDNA contamination. Based on the observation that the higher viability of the sample correlated with less nDNA contamination, we hypothesized that a portion of the nDNA contamination was generated due to DNA fragmentation caused by endogenous endonucleases in dead cells (Wyllie, 1987). Although using freshly isolated cells does increase the overall viability of the sample, there are still usually a few hundred dead

cells in a sample of a few thousand cells, which could be problematic in developing a successful MFC-based mtDNA isolation. Therefore, we hypothesize that a sample with 100% viability would not suffer from nDNA contamination in the MFC-based mtDNA isolation. Fluorescence activated cell sorting (FACS) is a technique used to sort two cell populations (Sasaki *et al*., 1987), such as live or dead cells. However, the manipulation of the cells after the sorting during FACS harms the cell viability, and therefore traditional FACS would not be useful for sample preparation for our MFCs. However, there have been MFC-based FACS assays reported (Krüger *et al.*, 2002; Yao *et al.*, 2004), which may be less harmful to the cell viability than the traditional FACS because there is minimal manipulation of the cells after they are sorted. By using a MFC-based FACS, we could ensure our starting sample had a 100 % viability, thereby eliminating the fragmented nDNA arising from the dead cells. This could help to facilitate a successful MFC-based mtDNA isolation.

Along with cell viability, buffer concentration was also found to affect the amount of nDNA in our MFC-based mtDNA isolation. The different concentrations of buffer can produce a buffer gradient, which has been shown to enhance sample stacking (Mikkers *et al*., 1979). Sample stacking is a technique used to concentrate DNA from a large volume into a smaller volume (Gebauer and Boček, 2009), such as from the wells into the channel of MFCs. This could allow larger fragments than predicted to enter the agarose, such as sheared fragments of the nDNA, thereby contaminating the mtDNA isolation. The buffer gradient is absent when the buffer concentrations are the same between the agarose and the running buffer, allowing only mtDNA or small fragments of nDNA to enter the agarose. Since both increased cell viability and equal buffer concentrations in

the agarose and running buffer result in a very small amount of nDNA contamination, it is possible that combining these two conditions could result in a MFC-based mtDNA purification. However, due to limited sample and MFC availability we were unable to test freshly isolated leukocytes on the glass mtDNA MFCs with the same concentration of buffer in both the agarose and running buffer.

Another variable that we hypothesize may have also contributed to the nDNA contamination is the incomplete adherence of the agarose to the channel wall of the MFC. Swedberg (Swedberg, 1992) found that the use of a dilute agarose solution to coat the walls of the capillary channel, improved the adherence of the agarose sieving matrix to the channel wall. We found that the use of the agarose coating in STE buffer using PMMA MFCs improved the reliability of the arrival times during CE, suggesting better adherence of the agarose to the channel wall. Although we did not examine incomplete adherence originally in glass MFCs, we suspect it may have played a role in the nDNA contamination. If the agarose did not completely adhere to the channel wall, it could allow for flow of DNA that bypassed the agarose and therefore would not be restricted by size. Based on the improvement seen in CE of plasmids in MFCs with the agarose coating, we decided to attempt the mtDNA isolation on PMMA mtDNA MFCs using the agarose coating instead of PDMA. Unfortunately, this approach was not successful. We hypothesize that the different surface chemistry may have increased the threshold for successful DNA electrophoresis in the PMMA mtDNA MFC-based isolation. We had eliminated PDMA for use with PMMA MFCs due to poor resolution in CE when the PMMA MFCs were coated with PDMA (data not shown), which agrees with results from the Barron group (Albarghouthi *et al*., 2002). As discussed in Chapter 3, PDMA may not

be as well suited for CE-based DNA separations but we have found that it can decrease non-specific adsorption and aide in isolations of small quantities of DNA.

Another significant variable that has changed from the glass mtDNA isolation to the PMMA mtDNA isolation is the buffer. We chose to attempt the MFC-based mtDNA isolation on PMMA MFCs with STE based on the consistency of the arrival times of a supercoiled plasmid DNA ladder in CE run with 1 X STE. Since we hypothesized that incomplete adherence was contributing to the nDNA contamination in the mtDNA isolation, we hypothesized that STE would help in preventing nDNA contamination. Our inability to isolate mtDNA could indicate that STE is not an appropriate buffer for the mtDNA isolation, or that the buffer concentration was not appropriate for the mtDNA isolation. We have found that the buffer concentration is an important variable in mtDNA isolations on glass MFCs, and are therefore likely to be important in mtDNA isolations on PMMA MFCs. We based the buffer concentration used on the mtDNA isolations in glass MFCs, which used lower concentrations of TBE than those used for the plasmid separations. However, we were limited by the availability of PMMA mtDNA isolation MFCs could and therefore not test a larger range of STE concentrations. In conclusion, the surface chemistry and the buffer conditions need to be examined for manipulating picogram concentrations of DNA, to determine the optimal conditions for PMMA MFCs.

6.4 Separating Plasmids Using Capillary Electrophoresis

Plasmids share physical similarities with mtDNA, making them a good models for mtDNA in CE. We have used plasmids to develop an electrophoretic protocol that is

capable of separating plasmids, which have as little as a 1.5 kb size difference. We used the SC ladder that contains 11 plasmid species ranging from 2 kb to 16.2 kb, and we examined the larger species of 8.1 kb to 16.2 kb plasmids in the ladder as they encompass the range of sizes associated with WT and deleted mtDNA. We were able to obtain a resolution of approximately 2 kb, which is sufficient to detect the majority of the over 130 deletions reported on MITOMAP (Ruiz-Pesini *et al*., 2007). To improve the consistency of arrival times we used a dilute agarose coating and STE buffer. In addition to the SC ladder separations, we were able to successfully separate individual plasmids that had 8 kb, 6 kb and 1.5 kb size differences.

6.5 Future Directions

6.5.1 Future Directions for MFC-based Mitochondrial DNA Isolation

We have developed techniques using MFCs that could be applied to the analysis of mtDNA. Some modification will be required to successfully analyze mtDNA using MFCs. As previously discussed, the sample viability, the buffer concentration and incomplete adherence are thought to contribute to the nDNA contamination seen in the MFC-based mtDNA isolation. Further study is needed to elucidate the extent to which each of these variable affects the nDNA contamination and to examine if they can be adjusted to prevent nDNA contamination and result in a successful MFC-based mtDNA isolation. Some possible directions that could be followed include the use of a MFC-based FACS to eliminate dead cells from the sample, further modifying the surface chemistry, adjusting the buffer.

The experiments carried out using the same buffer concentration in the agarose and the running buffer were all run with leukocyte samples with lower viabilities (40-60% viability), and these runs all contained do contain more nDNA contamination than samples with higher viabilities. As discussed above, we suspect that the viability of the sample does contribute to the nDNA contamination seen in the MFC-based mtDNA isolation. It is likely that some combination of equal the same buffer concentrations and the use of a freshly isolated leukocyte sample (higher viability sample) may result in a successful MFC-based mtDNA isolation.

One thing that should be noted is that, regardless of approach, any isolation will result in some dead cells. With freshly isolated leukocytes, we typically observed a viability of 90-95%, which still leaves 150 to 300 dead cells in a 3000 leukocyte cell sample. FACS with propidium iodide (PI) is a method that can distinguish between viable and non-viable cells (Sasaki *et al*., 1987), although the manipulation during the FACS can harm the cell viability. Therefore, it is impractical to use conventional FACS to obtain a sample with 100% viability in a sample of a few thousand cells. There have been MFC-based FACS systems developed, which decrease the amount of manipulation after the cell sorting (Krüger *et al*., 2002; Yao *et al*., 2004), and could precede a MFC-based mtDNA isolation, to eliminate the dead cells.

In our PMMA mtDNA MFCs, using the 0.1% agarose coating instead of a PDMA coating, we were unable to isolate mtDNA from leukocytes. As discussed in Chapter 3, we suspect that hydrogen bonding contributed to the non-specific adsorption of DNA during the plasmid segregations. The carbonyl group of the PDMA was responsible for the binding to the glass MFCs (Doherty *et al*., 2002) and we suspect the methyl groups of

the tertiary amine group prevented H-bonding to DNA. PMMA contains an ester group (Dang *et al.*, 2009), of which the carbonyl group may cause hydrogen bonding to DNA (Azadi and Tripathi, 2012; Dang *et al*., 2009; Fa *et al*., 2005). We had thought the agarose coating might prevent adsorption, since it places a layer between the PMMA and the sieving matrix. However, the agarose does not appear to be suitable for preventing non-specific adsorption as shown by our inability to detect (partially) purified mtDNA. A PDMA coating may also decrease the threshold in PMMA MFCs, and this could be verified by performing the 1 pg plasmid segregation on PMMA MFCs that have been coated with 5% (w/w) PDMA.

The other variable that has changed from the glass MFC-based mtDNA isolations is the buffer. In glass mtDNA MFCs, we used TBE and in the PMMA mtDNA MFCs we used STE. STE has been found to improve the resolution in AGE for supercoiled DNA (Ishido *et al*., 2010). We had chosen to proceed with STE since we thought the improved reliability of the arrival times may improve the mtDNA isolation. Due to a limited amount of PMMA mtDNA MFCs, we were only able to test two concentrations of STE. We chose 0.5 X and 0.1 X, as the mtDNA isolations performed on glass MFCs tended to use lower concentrations of buffer than the plasmid separations. Unfortunately, neither of these concentrations yielded any isolated mtDNA. This could indicate that either we did not use the appropriate concentration of STE, or that STE is not a suitable buffer for a MFC-based mtDNA isolation. To distinguish between these two options, the MFC-based mtDNA isolation should be conducted with a broader range of concentrations of STE, such as 0.05 X and 0.01 X STE, and compared to MFC-based mtDNA isolation conducted using TBE. If a different concentration of STE yields similar or improved

results compared to the TBE it will indicate we did not have the appropriate buffer concentration. However, if the MFC-based plasmid segregation does not work with a lower concentration of STE, then TBE may be a more suitable buffer.

6.5.2 Future Directions for the MFC-based Plasmid Separation

We have developed a CE-based method to analyze plasmids based on size which is meant to form the basis for using a similar approach to analyze mtDNA rearrangements. To verify that the mobility of mtDNA is similar to that of the plasmids, a sample of purified mtDNA should be run in CE and the arrival time compared to the Equations developed for plasmids in Chapter 4. The use of purified mtDNA will allow us to confirm any peaks observed result from mtDNA and thus confirm the arrival time of the mtDNA.

Although purified mtDNA would eliminate possible background noise from other DNA in a sample, such as nDNA, it is difficult to obtain. Therefore, it would beneficial to use a sample that is readily available, such as gDNA. We attempted preliminary experiments to use gDNA isolated using Invitrogen's Gentra Puregene blood kit, a kit that uses DNA stabilizers during the lysis to increase the size of the fragmented DNA. In our preliminary experiments peaks did not correspond to what was expected for mtDNA likely due to fragmented nDNA overlapping the mtDNA. To eliminate the issue of fragmented DNA either a protocol to eliminate the fragmentation of the nDNA must be introduced or a mtDNA specific probe will be required to visualize mtDNA.

CHAPTER 7- REFERENCES

Abramson, J., M. Svensson-Ek, B. Byrne, and S. Iwata. 2001. Structure of cytochrome *c* oxidase: a comparison of the bacterial and mitochondrial enzymes. *Biochimica et Biophysica Acta (BBA)-Protein Structure and Molecular Enzymology*. 1544:1-9.

Akerman, B., and K.D. Cole. 2002. Electrophoretic capture of circular DNA in gels. *Electrophoresis*. 23:2549-2561.

Al-Soud, W.A., and P. Rådström. 2001. Purification and characterization of PCR-inhibitory components in blood cells. *Journal of Clinical Microbiology*. 39:485-493.

Albarghouthi, M.N., and A.E. Barron. 2000. Polymeric matrices for DNA sequencing by capillary electrophoresis. *Electrophoresis*. 21:4096-4111.

Albarghouthi, M.N., B.A. Bucholz, P.J. Huiberts, T.M. Stein, and A.E. Barron. 2002. Poly-N-hydroxyethylacrylamide (polyDuramide): a novel, hydrophilic, self-coating polymer matrix for DNA sequencing by capillary electrophoresis. *Electrophoresis*. 23:1429-1440.

Ali, S.M., S. Mahnaz, and T. Mahmood. 2008. Rapid genomic DNA extraction (RGDE). *Forensic Science International: Genetics Supplement Series*. 1:63-65.

Alonso, A., C. Albarran, P. Martín, P. García, J. Capilla, O. García, C. de la Rua, N. Izaguirre, F. Pereira, and L. Pereira. 2006. Usefulness of microchip electrophoresis for the analysis of mitochondrial DNA in forensic and ancient DNA studies. *Electrophoresis*. 27:5101-5109.

Anderson, S., A.T. Bankier, B.G. Barrell, M.H. de Bruijn, A.R. Coulson, J. Drouin, I.C. Eperon, D.P. Nierlich, B.A. Roe, F. Sanger, P.H. Schreier, A.J. Smith, R. Staden, and I.G. Young. 1981. Sequence and organization of the human mitochondrial genome. *Nature*. 290:457-465.

Andersson, G., O. Karlberg, B. Canbäck, and C.G. Kurland. 2003. On the origin of mitochondria: a genomics perspective. *Philosophical Transactions of the Royal Society of London. Series B: Biological Sciences*. 358:165-179.

Andrews, R.M., I. Kubacka, P.F. Chinnery, R.N. Lightowlers, D.M. Turnbull, and N. Howell. 1999. Reanalysis and revision of the Cambridge reference sequence for human mitochondrial DNA. *Nature genetics*. 23:147-147.

Annex, B.H., and R.S. Williams. 1990. Mitochondrial DNA structure and expression in specialized subtypes of mammalian striated muscle. *Mol Cell Biol*. 10:5671-5678.

Arunan, E., G.R. Desiraju, R.A. Klein, J. Sadlej, S. Scheiner, I. Alkorta, D.C. Clary, R.H. Crabtree, J.J. Dannenberg, and P. Hobza. 2011. Defining the hydrogen bond: An account (IUPAC Technical Report). *Pure & Applied Chemistry*. 83:1619-1636.

Ashani, Y., and G.N. Catravas. 1980. Highly reactive impurities in Triton X-100 and Brij 35: partial characterization and removal. *Analytical biochemistry*. 109:55-62.

Azadi, G., and A. Tripathi. 2012. Surfactant-induced electroosmotic flow in microfluidic capillaries. *Electrophoresis*. 33:2094-2101.

Backhouse, C.J., H.J. Crabtree, and D.M. Glerum. 2002. Frontal analysis on a microchip. *The Analyst*. 127:1169-1175.

Bacman, S.R., S.L. Williams, and C.T. Moraes. 2009. Intra-and inter-molecular recombination of mitochondrial DNA after in vivo induction of multiple double-strand breaks. *Nucleic acids research*. 37:4218-4226.

Baer, R.J., and D.T. Dubin. 1981. Methylated regions of hamster mitochondrial ribosomal RNA: structural and functional correlates. *Nucleic acids research*. 9:323-337.

Bai, R.-K., and L.-J.C. Wong. 2005. Simultaneous detection and quantification of mitochondrial DNA deletion (s), depletion, and over-replication in patients with mitochondrial disease. *The Journal of Molecular Diagnostics*. 7:613-622.

Barron, A.E., and H.W. Blanch. 1995. DNA Separations by Slab Gel, and Capillary Electrophoresis: Theory and Practice. *Separation & Purification Reviews*. 24:1-118.

Baysal, B. 2006. Mitochondria: More than mitochondrial DNA in cancer. *PLoS medicine*. 3:413.

Beebe, D.J., G.A. Mensing, and G.M. Walker. 2002. Physics and applications of microfluidics in biology. *Annual review of biomedical engineering*. 4:261-286.

Bensasson, D., D. Zhang, D.L. Hartl, and G.M. Hewitt. 2001. Mitochondrial pseudogenes: evolution's misplaced witnesses. *Trends Ecol Evol*. 16:314-321.

Bernier, F., A. Boneh, X. Dennett, C. Chow, M. Cleary, and D. Thorburn. 2002. Diagnostic criteria for respiratory chain disorders in adults and children. *Neurology*. 59:1406-1411.

Bestwick, M.L., and G.S. Shadel. 2013. Accessorizing the human mitochondrial transcription machinery. *Trends in Biochemical Sciences*. 38:283-291.

Birnboim, H.C., and J. Doly. 1979. A rapid alkaline extraction procedure for screening recombinant plasmid DNA. *Nucleic acids research*. 7:1513-1523.

Bjerketorp, J., A. Ng Tze Chiang, K. Hjort, M. Rosenquist, W.T. Liu, and J.K. Jansson. 2008. Rapid lab-on-a-chip profiling of human gut bacteria. *J Microbiol Methods*. 72:82-90.

Bocek, P., and A. Chrambach. 1991. Capillary electrophoresis of DNA in agarose solutions at 40 degrees C. *Electrophoresis*. 12:1059-1061.

Bocek, P., and A. Chrambach. 1992. Capillary electrophoresis in agarose solutions: extension of size separations to DNA of 12 kb in length. *Electrophoresis*. 13:31-34.

Boerlin, P., and R.J. Reid-Smith. 2008. Antimicrobial resistance: its emergence and transmission. *Animal Health Research Reviews*. 9:115-126.

Bogenhagen, D., and D.A. Clayton. 1977. Mouse L cell mitochondrial DNA molecules are selected randomly for replication throughout the cell cycle. *Cell*. 11:719-727.

Bogenhagen, D.F. 2012. Mitochondrial DNA nucleoid structure. *Biochimica et Biophysica Acta (BBA)-Gene Regulatory Mechanisms*. 1819:914-920.

Bogenhagen, D.F., D. Rousseau, and S. Burke. 2008. The Layered Structure of Human Mitochondrial DNA Nucleoids. *Journal of Biological Chemistry*. 283:3665-3675.

Bogenhagen, D.F., Y. Wang, E.L. Shen, and R. Kobayashi. 2003. Protein components of mitochondrial DNA nucleoids in higher eukaryotes. *Molecular & Cellular Proteomics*. 2:1205-1216.

Brandt, U. 2006. Energy converting NADH: quinone oxidoreductase (complex I). *Annu. Rev. Biochem.* 75:69-92.

Brask, A., J.P. Kutter, and H. Bruus. 2005. Long-term stable electroosmotic pump with ion exchange membranes. *Lab on a Chip*. 5:730-738.

Brody, J.R., E.S. Calhoun, E. Gallmeier, T.D. Creavalle, and S.E. Kern. 2004. Ultra-fast high-resolution agarose electrophoresis of DNA and RNA using low-molarity conductive media. *BioTechniques*. 37:598-600.

Brody, J.R., and S.E. Kern. 2004a. History and principles of conductive media for standard DNA electrophoresis. *Analytical biochemistry*. 333:1-13.

Brody, J.R., and S.E. Kern. 2004b. Sodium boric acid: a Tris-free, cooler conductive medium for DNA electrophoresis. *BioTechniques*. 36:214-217.

Brown, W.M., M. George, and A.C. Wilson. 1979. Rapid evolution of animal mitochondrial DNA. *Proceedings of the National Academy of Sciences*. 76:1967-1971.

Calvignac, S., L. Konecny, F. Malard, and C.J. Douady. 2011. Preventing the pollution of mitochondrial datasets with nuclear mitochondrial paralogs (*numts*). *Mitochondrion*. 11:246-254.

Cann, R., M. Stoneking, and A. Wilson. 1987. Mitochondrial DNA and human evolution. *Nature*. 325:1-5.

Carracedo, A., E. D'Aloja, B. Dupuy, A. Jangblad, M. Karjalainen, C. Lambert, W. Parson, H. Pfeiffer, H. Pfitzinger, M. Sabatier, D. Syndercombe Court, and C. Vide. 1998. Reproducibility of mtDNA analysis between laboratories: a report of the European DNA Profiling Group (EDNAP). *Forensic Sci Int*. 97:165-170.

Cecchini, G. 2003. Function and structure of complex II of the respiratory chain. *Annual Review of Biochemistry*. 72:77-109.

Cerritelli, S.M., E.G. Frolova, C. Feng, A. Grinberg, P.E. Love, and R.J. Crouch. 2003. Failure to Produce Mitochondrial DNA Results in Embryonic Lethality in *Rnaseh1* Null Mice. *Molecular cell*. 11:807-815.

Chan, C.X., and D. Bhattacharya. 2010. The origin of plastids. *Nature Edu*. 3:84.

Chan, D.C. 2012. Fusion and fission: interlinked processes critical for mitochondrial health. *Annual review of genetics*. 46:265-287.

Chang, C.-M., L.-F. Chiou, C.-C. Lin, D.-B. Shieh, and G.-B. Lee. 2010. Three-dimensional microfluidic chip for the extraction of mitochondrial DNA. *Microfluidics and Nanofluidics*. 9:489-498.

Chang, C.-M., L.-F. Chiu, P.-W. Wang, D.-B. Shieh, and G.-B. Lee. 2011. A microfluidic system for fast detection of mitochondrial DNA deletion. *Lab on a Chip*. 11:2693-2700.

Chang, C.-M., L.-F. Chiu, Y.-H. Wei, D.-B. Shieh, and G.-B. Lee. 2013. Integrated three-dimensional system-on-chip for direct quantitative detection of mitochondrial DNA mutation in affected cells. *Biosensors and Bioelectronics*. 48:6-11.

Chang, J.H., and L. Tong. 2012. Mitochondrial poly (A) polymerase and polyadenylation. *Biochimica et Biophysica Acta (BBA)-Gene Regulatory Mechanisms*. 1819:992-997.

Chen, H., and D.C. Chan. 2005. Emerging functions of mammalian mitochondrial fusion and fission. *Human molecular genetics*. 14:R283-R289.

Chen, N., L. Wu, A. Palm, T. Srichaiyo, and S. Hjerten. 1996. High-performance field inversion capillary electrophoresis of 0.1-23 kbp DNA fragments with low-gelling, replaceable agarose gels. *Electrophoresis*. 17:1443-1450.

Chen, X.J., and R.A. Butow. 2005. The organization and inheritance of the mitochondrial genome. *Nature Reviews Genetics*. 6:815-825.

Chiari, M., M. Cretich, F. Damin, L. Ceriotti, and R. Consonni. 2000. New adsorbed coatings for capillary electrophoresis. *Electrophoresis*. 21:909-916.

Chinnery, P.F., D.R. Thorburn, D.C. Samuels, S.L. White, H.H.M. Dahl, D.M. Turnbull, R.N. Lightowlers, and N. Howell. 2000. The inheritance of mitochondrial DNA heteroplasmy: random drift, selection or both? *Trends in Genetics*. 16:500-505.

Chomyn, A., M. Cleeter, C.I. Ragan, M. Riley, R.F. Doolittle, and G. Attardi. 1986. URF6, last unidentified reading frame of human mtDNA, codes for an NADH dehydrogenase subunit. *Science*. 234:614-618.

Chomyn, A., P. Mariottini, M. Cleeter, C.I. Ragan, A. Matsuno-Yagi, Y. Hatefi, R.F. Doolittle, and G. Attardi. 1985. Six unidentified reading frames of human mitochondrial DNA encode components of the respiratory-chain NADH dehydrogenase. *Nature*. 314:592-597.

Christian, B.E., and L.L. Spremulli. 2012. Mechanism of protein biosynthesis in mammalian mitochondria. *Biochimica et Biophysica Acta (BBA)-Gene Regulatory Mechanisms*. 1819:1035-1054.

Clayton, D.A. 1982. Replication of animal mitochondrial DNA. *Cell*. 28:693-705.

Coates, P.M., D.E. Hale, C.A. Stanley, B.E. Corkey, and J.A. Cortner. 1985. Genetic deficiency of medium-chain acyl coenzyme A dehydrogenase: studies in cultured skin fibroblasts and peripheral mononuclear leukocytes. *Pediatric research*. 19:671-676.

Collins, F.S., M. Morgan, and A. Patrinos. 2003. The Human Genome Project: lessons from large-scale biology. *Science*. 300:286-290.

Cornett, J.B., and G.D. Shockman. 1978. Cellular lysis of Streptococcus faecalis induced with triton X-100. *Journal of Bacteriology*. 135:153-160.

Coskun, P.E., M.F. Beal, and D.C. Wallace. 2004. Alzheimer's brains harbor somatic mtDNA control-region mutations that suppress mitochondrial transcription and replication. *Proceedings of the National Academy of Sciences*. 101:10726-10731.

Cree, L.M., D.C. Samuels, S.C. de Sousa Lopes, H.K. Rajasimha, P. Wonnapinij, J.R. Mann, H.H. Dahl, and P.F. Chinnery. 2008. A reduction of mitochondrial DNA molecules during embryogenesis explains the rapid segregation of genotypes. *Nature genetics*. 40:249-254.

Crick, F. 1966. Codon—anticodon pairing: the wobble hypothesis. *Journal of molecular biology*. 19:548-555.

Cummins, J.M., T. Wakayama, and R. Yanagimachi. 1997. Fate of microinjected sperm components in the mouse oocyte and embryo. *Zygote*. 5:301-308.

Dang, F., T. Hasegawa, V. Biju, M. Ishikawa, N. Kaji, T. Yasui, and Y. Baba. 2009. Spontaneous Adsorption on a Hydrophobic Surface Governed by Hydrogen Bonding. *Langmuir*. 25:9296-9301.

de Souza-Pinto, N.C., P.A. Mason, K. Hashiguchi, L. Weissman, J. Tian, D. Guay, M. Lebel, T.V. Stevnsner, L.J. Rasmussen, and V.A. Bohr. 2009. Novel DNA mismatch-repair activity involving YB-1 in human mitochondria. *DNA repair*. 8:704-719.

DiMauro, S., E. Bonilla, M. Zeviani, M. Nakagawa, and D.C. DeVivo. 1985. Mitochondrial myopathies. *Annals of neurology*. 17:521-538.

DiMauro, S., and E.A. Schon. 2001. Mitochondrial DNA mutations in human disease. *Am J Med Genet*. 106:18-26.

DiMauro, S., S. Tay, and M. Mancuso. 2004. Mitochondrial encephalomyopathies: diagnostic approach. *Annals of the New York Academy of Sciences*. 1011:217-231.
Dimmock, D., L.-Y. Tang, E.S. Schmitt, and L.-J.C. Wong. 2010. Quantitative evaluation of the mitochondrial DNA depletion syndrome. *Clinical chemistry*. 56:1119-1127.
Ding, L., K. Williams, W. Ausserer, L. Bousse, and R. Dubrow. 2003. Analysis of plasmid samples on a microchip. *Analytical Biochemistry*. 316:92-102.
Doherty, E.A., K.D. Berglund, B.A. Buchholz, I.V. Kourkine, T.M. Przybycien, R.D. Tilton, and A.E. Barron. 2002. Critical factors for high-performance physically adsorbed (dynamic) polymeric wall coatings for capillary electrophoresis of DNA. *Electrophoresis*. 23:2766-2776.
Doherty, E.A.S., and A.E. Barron. 2004. DNA sequencing and genotyping in miniaturized electrophoresis systems. *Electrophoresis*. 25:3564-3588.
Dominguez, K., and W.S. Ward. 2009. A novel nuclease activity that is activated by Ca2+ chelated to EGTA. *Systems biology in reproductive medicine*. 55:193-199.
Dovichi, N.J., and J. Zhang. 2000. How capillary electrophoresis sequenced the human genome. *Angewandte Chemie International Edition*. 39:4463-4468.
Drossman, H., J.A. Luckey, A.J. Kostichka, J. D'Cunha, and L.M. Smith. 1990. High-speed separations of DNA sequencing reactions by capillary electrophoresis. *Analytical chemistry*. 62:900-903.
Duckworth, M., and W. Yaphe. 1971. The structure of agar: Part I. Fractionation of a complex mixture of polysaccharides. *Carbohydrate Research*. 16:189-197.
El-Hattab, A.W., and F. Scaglia. 2013. Mitochondrial DNA Depletion Syndromes: Review and Updates of Genetic Basis, Manifestations, and Therapeutic Options. *Neurotherapeutics*. 10:186-198.
Elpeleg, O., H. Mandel, and A. Saada. 2002. Depletion of the other genome-mitochondrial DNA depletion syndromes in humans. *Journal of Molecular Medicine*. 80:389-396.
Emelyanov, V.V. 2001. Rickettsiaceae, rickettsia-like endosymbionts, and the origin of mitochondria. *Bioscience reports*. 21:1-17.
Engel, W., and G. Cunnigham. 1963. Rapid examination of muscle tissue. An improved trichrome method for fresh-frozen biopsy sections. *Neurology*. 13:919-923.
Enns, G.M., R.-K. Bai, A.E. Beck, and L.-J. Wong. 2006. Molecular–clinical correlations in a family with variable tissue mitochondrial DNA T8993G mutant load. *Molecular genetics and metabolism*. 88:364-371.
Ernster, L., and G. Schatz. 1981. Mitochondria: a historical review. *The Journal of cell biology*. 91:227s-255s.
Fa, K., V.K. Paruchuri, S.C. Brown, B.M. Moudgil, and J.D. Miller. 2005. The significance of electrokinetic characterization for interpreting interfacial phenomena at planar, macroscopic interfaces. *Physical Chemistry Chemical Physics*. 7:678-684.
Falkenberg, M., N.-G. Larsson, and C.M. Gustafsson. 2007. DNA replication and transcription in mammalian mitochondria. *Annu. Rev. Biochem.* 76:679-699.
Fan, W., K.G. Waymire, N. Narula, P. Li, C. Rocher, P.E. Coskun, M.A. Vannan, J. Narula, G.R. MacGregor, and D.C. Wallace. 2008. A mouse model of mitochondrial disease reveals germline selection against severe mtDNA mutations. *Science*. 319:958-962.

Fang, Y., J.Z. Zhang, J.Y. Hou, H. Lu, and N.J. Dovichi. 1996. Activation energy of the separation of DNA sequencing fragments in denaturing noncross-linked polyacrylamide by capillary electrophoresis. *Electrophoresis*. 17:1436-1442.

Fiorini, G.S., and D.T. Chiu. 2005. Disposable microfluidic devices: fabrication, function, and application. *BioTechniques*. 38:429-446.

Fiorini, G.S., R.M. Lorenz, J.S. Kuo, and D.T. Chiu. 2004. Rapid prototyping of thermoset polyester microfluidic devices. *Analytical chemistry*. 76:4697-4704.

Flannery, D., and M. Walter. 2012. Archean tufted microbial mats and the Great Oxidation Event: new insights into an ancient problem. *Australian Journal of Earth Sciences*. 59:1-11.

Fotino, M., E. Merson, and F. Allen Jr. 1971. Micromethod for rapid separation of lymphocytes from peripheral blood. *Annals of clinical laboratory science*. 1:131-133.

Gao, L., J. Wu, D. Gao, and J. Wu. 2007. Separation of long DNA molecules through cleavage of hydrogen bonds under a stretching force. *Applied Physics Letters*. 91:113902.

Gaziev, A., and G. Shaikhaev. 2010. Nuclear mitochondrial pseudogenes. *Molecular Biology*. 44:358-368.

Gebauer, P., and P. Boček. 2009. Electrophoretic sample stacking. *Electrophoresis*. 30:S27-S33.

Gilkerson, R.W. 2009. Mitochondrial DNA nucleoids determine mitochondrial genetics and dysfunction. *International Journal of Biochemistry and Cell Biology*. 41:1899-1906.

Glerum, D.M., I. Muroff, C. Jin, and A. Tzagoloff. 1997. COX15 codes for a mitochondrial protein essential for the assembly of yeast cytochrome oxidase. *Journal of Biological Chemistry*. 272:19088-19094.

Glotz, C., C. Zwieb, R. Brimacombe, K. Edwards, and H. Kössel. 1981. Secondary structure of the large subunit ribosomal RNA from *Escherichia coli, Zea mays chloroplast*, and human and mouse mitochondrial ribosomes. *Nucleic Acids Research*. 9:3287-3306.

Goto, Y.-i., I. Nonaka, and S. Horai. 1990. A mutation in the tRNALeu (UUR) gene associated with the MELAS subgroup of mitochondrial encephalomyopathies. *Nature*. 348:651-653.

Goto, Y.-i., I. Nonaka, and S. Horai. 1991. A new mtDNA mutation associated with mitochondrial myopathy, encephalopathy, lactic acidosis and stroke-like episodes (MELAS). *Biochimica et Biophysica Acta (BBA)-Molecular Basis of Disease*. 1097:238-240.

Gray, M.W., G. Burger, and B.F. Lang. 2001. The origin and early evolution of mitochondria. *Genome Biol*. 2:1018.1011-1018.1015.

Graziewicz, M.A., M.J. Longley, and W.C. Copeland. 2006. DNA polymerase gamma in mitochondrial DNA replication and repair. *Chemical reviews*. 106:383-405.

Grushka, E., R. McCormick, and J. Kirkland. 1989. Effect of temperature gradients on the efficiency of capillary zone electrophoresis separations. *Analytical Chemistry*. 61:241-246.

Guja, K.E., and M. Garcia-Diaz. 2012. Hitting the brakes: termination of mitochondrial transcription. *Biochimica et Biophysica Acta (BBA)-Gene Regulatory Mechanisms*. 1819:939-947.

Guttman, A., and N. Cooke. 1991. Effect of temperature on the separation of DNA restriction fragments in capillary gel electrophoresis. *Journal of Chromatography A*. 559:285-294.

Han, J., and A.K. Singh. 2004. Rapid protein separations in ultra-short microchannels: microchip sodium dodecyl sulfate–polyacrylamide gel electrophoresis and isoelectric focusing. *Journal of Chromatography A*. 1049:205-209.

Han, S.P., S. Yoda, K.J. Kwak, K. Suga, and M. Fujihira. 2005. Interpretation of DNA adsorption on silanized surfaces by measuring interaction forces at various pHs using atomic force microscopy. *Ultramicroscopy*. 105:148-154.

Hatefi, Y. 1985. The mitochondrial electron transport and oxidative phosphorylation system. *Annual review of biochemistry*. 54:1015-1069.

He, J., C.-C. Mao, A. Reyes, H. Sembongi, M. Di Re, C. Granycome, A.B. Clippingdale, I.M. Fearnley, M. Harbour, and A.J. Robinson. 2007. The AAA+ protein ATAD3 has displacement loop binding properties and is involved in mitochondrial nucleoid organization. *The Journal of cell biology*. 176:141-146.

Herrnstadt, C., W. Clevenger, S.S. Ghosh, C. Anderson, E. Fahy, S. Miller, N. Howell, and R.E. Davis. 1999. A novel mitochondrial DNA-like sequence in the human nuclear genome. *Genomics*. 60:67-77.

Hestekin, C.N., J.P. Jakupciak, T.N. Chiesl, C.W. Kan, C.D. O'Connell, and A.E. Barron. 2006. An optimized microchip electrophoresis system for mutation detection by tandem SSCP and heteroduplex analysis for p53 gene exons 5-9. *Electrophoresis*. 27:3823-3835.

Hirano, M., and S.G. Pavlakis. 1994. Topical review: mitochondrial myopathy, encephalopathy, lactic acidosis, and strokelike episodes (MELAS): current concepts. *Journal of child neurology*. 9:4-13.

Hjerten, S. 1985. High-performance electrophoresis: elimination of electroendosmosis and solute adsorption. *Journal of chromatography*. 347:191-198.

Hjertén, S., T. Srichaiyo, and A. Palm. 1994. UV-transparent, replaceable agarose gels for molecular-sieve (capillary) electrophoresis of proteins and nucleic acids. *Biomedical Chromatography*. 8:73-76.

Hofmann, S., R. Bezold, M. Jaksch, B. Obermaier-Kusser, S. Mertens, P. Kaufhold, W. Rabl, W. Hecker, and K.-D. Gerbitz. 1997. Wolfram (DIDMOAD) syndrome and Leber hereditary optic neuropathy (LHON) are associated with distinct mitochondrial DNA haplotypes. *Genomics*. 39:8-18.

Holt, I.J., A.E. Harding, and J.A. Morgan-Hughes. 1988. Deletions of muscle mitochondrial DNA in patients with mitochondrial myopathies. *Nature*. 331:717-719.

Holt, I.J., and A. Reyes. 2012. Human Mitochondrial DNA Replication. *Cold Spring Harbor perspectives in biology*. 4:a012971.

Horvath, J., and V. Dolnik. 2001. Polymer wall coatings for capillary electrophoresis. *Electrophoresis*. 22:644-655.

Huang, M., W.P. Vorkink, and M.L. Lee. 1992. High efficiency cross-linked polyacrylamide coating for capillary electrophoresis of proteins. *Journal of Microcolumn Separations*. 4:233-238.

Iacobazzi, V., A. Castegna, V. Infantino, and G. Andria. 2013. Mitochondrial DNA methylation as a next-generation biomarker and diagnostic tool. *Molecular genetics and metabolism*. 110:25-34.

Iborra, F., H. Kimura, and P. Cook. 2004. The functional organization of mitochondrial genomes in human cells. *BMC biology*. 2:9.

Ishido, T., M. Ishikawa, and K. Hirano. 2010. Analysis of supercoiled DNA by agarose gel electrophoresis using low-conducting sodium threonine medium. *Analytical Biochemistry*. 400:148-150.

Jenuth, J., A. Peterson, K. Fu, and E.A. Shoubridge. 1996. Random genetic drift in the female germline explains the rapid segregation of mammalian mitochondrial DNA. *Nature genetics*. 14:146-151.

Jenuth, J.P., A.C. Peterson, and E.A. Shoubridge. 1997. Tissue-specific selection for different mtDNA genotypes in heteroplasmic mice. *Nature genetics*. 16:93-95.

John, J.C.S., J. Facucho-Oliveira, Y. Jiang, R. Kelly, and R. Salah. 2010. Mitochondrial DNA transmission, replication and inheritance: a journey from the gamete through the embryo and into offspring and embryonic stem cells. *Human reproduction update*. 16:488-509.

Kaguni, L.S. 2004. DNA polymerase γ, the mitochondrial replicase 1. *Annual review of biochemistry*. 73:293-320.

Kaigala, G.V., V.N. Hoang, A. Stickel, J. Lauzon, D. Manage, L.M. Pilarski, and C.J. Backhouse. 2008. An inexpensive and portable microchip-based platform for integrated RT-PCR and capillary electrophoresis. *Analyst*. 133:331-338.

Kaigala, G.V., R.J. Huskins, J. Preiksaitis, X.L. Pang, L.M. Pilarski, and C.J. Backhouse. 2006. Automated screening using microfluidic chip-based PCR and product detection to assess risk of BK virus-associated nephropathy in renal transplant recipients. *Electrophoresis*. 27:3753-3763.

Kameoka, J., H.G. Craighead, H. Zhang, and J. Henion. 2001. A polymeric microfluidic chip for CE/MS determination of small molecules. *Analytical Chemistry*. 73:1935-1941.

Kaneda, H., J. Hayashi, S. Takahama, C. Taya, K.F. Lindahl, and H. Yonekawa. 1995. Elimination of paternal mitochondrial DNA in intraspecific crosses during early mouse embryogenesis. *Proceedings of the National Academy of Sciences*. 92:4542-4546.

Kang, D., S.H. Kim, and N. Hamasaki. 2007. Mitochondrial transcription factor A (TFAM): roles in maintenance of mtDNA and cellular functions. *Mitochondrion*. 7:39-44.

Kanki, T., K. Ohgaki, M. Gaspari, C.M. Gustafsson, A. Fukuoh, N. Sasaki, N. Hamasaki, and D. Kang. 2004. Architectural role of mitochondrial transcription factor A in maintenance of human mitochondrial DNA. *Molecular and cellular biology*. 24:9823-9834.

Karp, G. 1999. Cell and Molecular Biology: concepts and experiments. John Wiley & Sons, Ltd, United States. 816 pp.

Katayama, H., Y. Ishihama, and N. Asakawa. 1998. Stable cationic capillary coating with successive multiple ionic polymer layers for capillary electrophoresis. *Analytical chemistry*. 70:5272-5277.

Kaufman, B.A., N. Durisic, J.M. Mativetsky, S. Costantino, M.A. Hancock, P. Grutter, and E.A. Shoubridge. 2007. The mitochondrial transcription factor TFAM coordinates the assembly of multiple DNA molecules into nucleoid-like structures. *Molecular biology of the cell*. 18:3225-3236.

Kaukonen, J., J.K. Juselius, V. Tiranti, A. Kyttälä, M. Zeviani, G.P. Comi, S. Keränen, L. Peltonen, and A. Suomalainen. 2000. Role of adenine nucleotide translocator 1 in mtDNA maintenance. *Science*. 289:782-785.

Kazak, L., A. Reyes, and I.J. Holt. 2012. Minimizing the damage: repair pathways keep mitochondrial DNA intact. *Nature Reviews Molecular Cell Biology*. 13:659-671.

Kim, S.K., J.H. Kim, K.P. Kim, and T.D. Chung. 2007. Continuous low-voltage dc electroporation on a microfluidic chip with polyelectrolytic salt bridges. *Anal.Chem*. 79:7761-7766.

Korhonen, J.A., M. Gaspari, and M. Falkenberg. 2003. TWINKLE has 5′→ 3′ DNA helicase activity and is specifically stimulated by mitochondrial single-stranded DNA-binding protein. *Journal of Biological Chemistry*. 278:48627-48632.

Kourkine, I.V., C.N. Hestekin, and A.E. Barron. 2002. Technical challenges in applying capillary electrophoresis-single strand conformation polymorphism for routine genetic analysis. *Electrophoresis*. 23:1375.

Kourkine, I.V., C.N. Hestekin, B.A. Buchholz, and A.E. Barron. 1999. High-Throughput, High-Sensitivity Genetic Mutation Detection by Tandem Single-Strand Conformation Polymorphism/Heteroduplex Analysis Capillary Array Electrophoresis. *Electrophoresis*. 20:1177-1185.

Krishnan, K.J., A.K. Reeve, D.C. Samuels, P.F. Chinnery, J.K. Blackwood, R.W. Taylor, S. Wanrooij, J.N. Spelbrink, R.N. Lightowlers, and D.M. Turnbull. 2008. What causes mitochondrial DNA deletions in human cells? *Nature genetics*. 40:275-279.

Krüger, J., K. Singh, A. O'Neill, C. Jackson, A. Morrison, and P. O'Brien. 2002. Development of a microfluidic device for fluorescence activated cell sorting. *Journal of Micromechanics and Microengineering*. 12:486.

Kuo, J.S., and D.T. Chiu. 2011. Disposable microfluidic substrates: transitioning from the research laboratory into the clinic. *Lab on a Chip*. 11:2656-2665.

Lancaster, C.R.D., and A. Kröger. 2000. Succinate: quinone oxidoreductases: new insights from X-ray crystal structures. *Biochimica et Biophysica Acta (BBA)-Bioenergetics*. 1459:422-431.

Lander, E.S., L.M. Linton, B. Birren, C. Nusbaum, M.C. Zody, J. Baldwin, K. Devon, K. Dewar, M. Doyle, and W. FitzHugh. 2001. Initial sequencing and analysis of the human genome. *Nature*. 409:860-921.

Lang, B.F., M.W. Gray, and G. Burger. 1999. Mitochondrial genome evolution and the origin of eukaryotes. *Annual review of genetics*. 33:351-397.

Larsson, N., and D.A. Clayton. 1995. Molecular genetic aspects of human mitochondrial disorders. *Annual review of genetics*. 29:151-178.

Larsson, N.G., E. Holme, B. Kristiansson, A. Oldfors, and M. Tulinius. 1990. Progressive increase of the mutated mitochondrial DNA fraction in Kearns-Sayre syndrome. *Pediatr Res*. 28:131-136.

Larsson, N.G., J. Wang, H. Wilhelmsson, A. Oldfors, P. Rustin, M. Lewandoski, G.S. Barsh, and D.A. Clayton. 1998. Mitochondrial transcription factor A is necessary for mtDNA maintenance and embryogenesis in mice. *Nat Genet*. 18:231-236.

Levene, S.D., and B.H. Zimm. 1987. Separations of open-circular DNA using pulsed-field electrophoresis. *Proceedings of the National Academy of Sciences*. 84:4054-4057.

Li, G., R. Ran, H. Zhao, K. Liu, and J. Zhao. 2006. Design of a PMMA chip for selective extraction of size-fractioned DNA. *In* Nano/Micro Engineered and Molecular Systems, 2006. NEMS'06. 1st IEEE International Conference on. IEEE. 105-109.

Lin, Y.C., M.Y. Huang, K.C. Young, T.T. Chang, and C.Y. Wu. 2000. A rapid micro-polymerase chain reaction system for hepatitis C virus amplification. *Sensors & Actuators: B.Chemical*. 71:2-8.

Liolitsa, D., S. Rahman, S. Benton, L.J. Carr, and M.G. Hanna. 2003. Is the mitochondrial complex I ND5 gene a hot-spot for MELAS causing mutations? *Annals of neurology*. 53:128-132.

Liu, M., and L. Spremulli. 2000. Interaction of mammalian mitochondrial ribosomes with the inner membrane. *Journal of Biological Chemistry*. 275:29400-29406.

Liu, P., T.S. Seo, N. Beyor, K.J. Shin, J.R. Scherer, and R.A. Mathies. 2007. Integrated portable polymerase chain reaction-capillary electrophoresis microsystem for rapid forensic short tandem repeat typing. *Anal.Chem*. 79:1881-1889.

Liu, R.H., M.A. Stremler, K.V. Sharp, M.G. Olsen, J.G. Santiago, R.J. Adrian, H. Aref, and D.J. Beebe. 2000. Passive mixing in a three-dimensional serpentine microchannel. *Microelectromechanical Systems, Journal of*. 9:190-197.

Longley, M.J., D. Nguyen, T.A. Kunkel, and W.C. Copeland. 2001. The fidelity of human DNA polymerase gamma with and without exonucleolytic proofreading and the p55 accessory subunit. *The Journal of biological chemistry*. 276:38555-38562.

Lu, C.-Y., D.-J. Tso, T. Yang, Y.-J. Jong, and Y.-H. Wei. 2002. Detection of DNA mutations associated with mitochondrial diseases by Agilent 2100 bioanalyzer. *Clinica chimica acta*. 318:97-105.

Lucy, C.A., A.M. MacDonald, and M.D. Gulcev. 2008. Non-covalent capillary coatings for protein separations in capillary electrophoresis. *J Chromatogr A*. 1184:81-105.

Ma, T. 2012. Geany CE data Plot Single File. Vol. v2.6. Ma, Tianchi, University of Waterloo.

Ma, T., V. Northrup, A.O. Fung, D.M. Glerum, and C.J. Backhouse. 2012. Polymeric rapid prototyping for inexpensive and portable medical diagnostics. *In* Photonics North 2012. *International Society for Optics and Photonics.* 84120B-84120B-84128.

Maitra, A., Y. Cohen, S.E. Gillespie, E. Mambo, N. Fukushima, M.O. Hoque, N. Shah, M. Goggins, J. Califano, D. Sidransky, and A. Chakravarti. 2004. The Human MitoChip: a high-throughput sequencing microarray for mitochondrial mutation detection. *Genome Res*. 14:812-819.

Malka, F., A. Lombès, and M. Rojo. 2006. Organization, dynamics and transmission of mitochondrial DNA: focus on vertebrate nucleoids. *Biochimica et Biophysica Acta (BBA)-Molecular Cell Research*. 1763:463-472.

Manage, D.P., I. Imriskova-Sosova, D.M. Glerum, and C.J. Backhouse. 2008. A microfluidic study of mechanisms in the electrophoresis of supercoiled DNA. *Electrophoresis*. 29:2466-2476.

Mancuso, M., D. Orsucci, G. Ali, A. Lo Gerfo, G. Fontanini, and G. Siciliano. 2009. Advances in molecular diagnostics for mitochondrial diseases. *Expert Opin Med Diagn.* 3:557-569.

Maniatis, T., E.F. Fritsch, and J. Sambrook. 1982. Molecular cloning: a laboratory manual. Cold Spring Harbor Laboratory Cold Spring Harbor, NY.

Marchington, D.R., J. Poulton, A. Sellar, and I.J. Holt. 1996. Do sequence variants in the major non-coding region of the mitochondrial genome influence mitochondrial mutations associated with disease? *Human molecular genetics*. 5:473-479.

Mardis, E.R. 2008. Next-generation DNA sequencing methods. *Annu. Rev. Genomics Hum. Genet.* 9:387-402.

Margulis, L. 1970. Origin of eukaryotic cells: Evidence and research implications for a theory of the origin and evolution of microbial, plant, and animal cells on the Precambrian earth. Yale University Press New Haven.

Marko, M., R. Chipperfield, and H. Birnboim. 1982. A procedure for the large-scale isolation of highly purified plasmid DNA using alkaline extraction and binding to glass powder. *Analytical biochemistry*. 121:382-387.

Martin, W., and K. Kowallik. 1999. Annotated English translation of Mereschkowsky's 1905 paper 'Über Natur und Ursprung der Chromatophoren imPflanzenreiche'. *European Journal of Phycology*. 34:287-295.

Mathur, S., and B.M. Moudgil. 1997. Adsorption mechanism (s) of poly (ethylene oxide) on oxide surfaces. *Journal of colloid and interface science*. 196:92-98.

McDonnell, M.T., A.M. Schaefer, E.L. Blakely, R. McFarland, P.F. Chinnery, D.M. Turnbull, and R.W. Taylor. 2004. Noninvasive diagnosis of the 3243A> G mitochondrial DNA mutation using urinary epithelial cells. *European journal of human genetics*. 12:778-781.

McFarland, R., and D.M. Turnbull. 2009. Batteries not included: diagnosis and management of mitochondrial disease. *J Intern Med*. 265:210-228.

Mewies, M., W.S. McIntire, and N.S. Scrutton. 1998. Covalent attachment of flavin adenine dinucleotide (FAD) and flavin mononucleotide (FMN) to enzymes: the current state of affairs. *Protein Science*. 7:7-21.

Mikkers, F., F. Everaerts, and T.P. Verheggen. 1979. Concentration distributions in free zone electrophoresis. *Journal of Chromatography A*. 169:1-10.

Miller, F.J., F.L. Rosenfeldt, C. Zhang, A.W. Linnane, and P. Nagley. 2003. Precise determination of mitochondrial DNA copy number in human skeletal and cardiac muscle by a PCR-based assay: lack of change of copy number with age. *Nucleic acids research*. 31:e61-e61.

Miyabayashi, S., H. Hanamizu, H. Endo, K. Tada, and S. Horai. 1991. A new type of mitochondrial DNA deletion in patients with encephalomyopathy. *Journal of inherited metabolic disease*. 14:805-812.

Montoya, J., D. Ojala, and G. Attardi. 1981. Distinctive features of the 5′-terminal sequences of the human mitochondrial mRNAs. *Nature* 290:465-470.

Moraes, C.T., S. DiMauro, M. Zeviani, A. Lombes, S. Shanske, A.F. Miranda, H. Nakase, E. Bonilla, L.C. Werneck, and S. Servidei. 1989. Mitochondrial DNA deletions in progressive external ophthalmoplegia and Kearns-Sayre syndrome. *New England Journal of Medicine*. 320:1293-1299.

Motsch, S.R., M.H. Kleemiß, and G. Schomburg. 1991. Production and application of capillaries filled with agarose gel for electrophoresis. *Journal of High Resolution Chromatography*. 14:629-632.

Mukhopadhyay, M., and N. Mandal. 1983. A simple procedure for large-scale preparation of pure plasmid DNA free from chromosomal DNA from bacteria. *Analytical biochemistry*. 133:265-270.

Munnich, A., A. Rötig, D. Chretien, V. Cormier, T. Bourgeron, J.-P. Bonnefont, J.-M. Saudubray, and P. Rustin. 1996. Clinical presentation of mitochondrial disorders in childhood. *Journal of inherited metabolic disease*. 19:521-527.

Nachman, M.W., and S.L. Crowell. 2000. Estimate of the mutation rate per nucleotide in humans. *Genetics*. 156:297-304.

Nagamine, K., S. Onodera, Y. Torisawa, T. Yasukawa, H. Shiku, and T. Matsue. 2005. On-chip transformation of bacteria. *Anal.Chem*. 77:4278-4281.

Nass, S., and M.M. Nass. 1963. Intramitochondrial fibers with DNA characteristics II. Enzymatic and other hydrolytic treatments. *The Journal of cell biology*. 19:613-629.

Naviaux, R.K. 2004. Developing a systematic approach to the diagnosis and classification of mitochondrial disease. *Mitochondrion*. 4:351-361.

Navratil, M., B.G. Poe, and E.A. Arriaga. 2007. Quantitation of DNA copy number in individual mitochondrial particles by capillary electrophoresis. *Analytical chemistry*. 79:7691-7699.

Ngo, H.B., J.T. Kaiser, and D.C. Chan. 2011. The mitochondrial transcription and packaging factor Tfam imposes a U-turn on mitochondrial DNA. *Nature structural & molecular biology*. 18:1290-1296.

Northrup, V.A., C.J. Backhouse, and D.M. Glerum. 2010. Development of a microfluidic chip-based plasmid miniprep. *Analytical Biochemistry*. 402:185-190.

O'Brien, T.W. 2003. Properties of human mitochondrial ribosomes. *IUBMB life*. 55:505-513.

Ofengand, J., and A. Bakin. 1997. Mapping to nucleotide resolution of pseudouridine residues in large subunit ribosomal RNAs from representative eukaryotes, prokaryotes, archaebacteria, mitochondria and chloroplasts. *Journal of molecular biology*. 266:246-268.

Ojala, D., J. Montoya, and G. Attardi. 1981. tRNA punctuation model of RNA processing in human mitochondria. *Nature*. 290:470-474.

Otani, H., O. Tanaka, K.I. Kasai, and T. Yoshioka. 1988. Development of mitochondrial helical sheath in the middle piece of the mouse spermatid tail: regular dispositions and synchronized changes. *The Anatomical Record*. 222:26-33.

Ott, M., and J.M. Herrmann. 2010. Co-translational membrane insertion of mitochondrially encoded proteins. *Biochimica et Biophysica Acta (BBA)-Molecular Cell Research*. 1803:767-775.

Pagliarini, D.J., S.E. Calvo, B. Chang, S.A. Sheth, S.B. Vafai, S.-E. Ong, G.A. Walford, C. Sugiana, A. Boneh, and W.K. Chen. 2008. A mitochondrial protein compendium elucidates complex I disease biology. *Cell*. 134:112-123.

Pagniez-Mammeri, H., S. Loublier, A. Legrand, P. Bénit, P. Rustin, and A. Slama. 2012. Mitochondrial complex I deficiency of nuclear origin: I. Structural genes. *Molecular genetics and metabolism*. 105:163-172.

Pak, J.W., F. Vang, C. Johnson, D. McKenzie, and J.M. Aiken. 2005. MtDNA point mutations are associated with deletion mutations in aged rat. *Experimental gerontology*. 40:209-218.

Palanichamy, M., and Y.-P. Zhang. 2010. Potential pitfalls in MitoChip detected tumor-specific somatic mutations: a call for caution when interpreting patient data. *BMC cancer*. 10:597.

Pan, T., and W. Wang. 2011. From cleanroom to desktop: emerging micro-nanofabrication technology for biomedical applications. *Annals of biomedical engineering*. 39:600-620.

Parikh, S., R. Saneto, M.J. Falk, I. Anselm, B.H. Cohen, and R. Haas. 2009. A modern approach to the treatment of mitochondrial disease. *Current treatment options in neurology*. 11:414-430.

Paul, B., C. Cloninger, M. Felton, R. Khachatoorian, and S. Metzenberg. 2008. A nonalkaline method for isolating sequencing-ready plasmids. *Analytical Biochemistry*. 377:218-222.

Pillen, S., E. Morava, M. Van Keimpema, H. Ter Laak, M. De Vries, R. Rodenburg, and M. Zwarts. 2006. Skeletal muscle ultrasonography in children with a dysfunction in the oxidative phosphorylation system. *Neuropediatrics*. 37:142-147.

Poulton, J., J.a. Luan, V. Macaulay, S. Hennings, J. Mitchell, and N.J. Wareham. 2002. Type 2 diabetes is associated with a common mitochondrial variant: evidence from a population-based case–control study. *Human molecular genetics*. 11:1581-1583.

Preywisch, R., M. Ritzi-Lehnert, K.S. Drese, and T. Röser. 2011. Justification of rapid prototyping in the development cycle of thermoplastic-based lab-on-a-chip. *Electrophoresis*. 32:3115-3120.

Punter, F.A. 2003. Delineating the role of *COX17* in the mitochondrial copper transport pathway. *In* Medical Genetics. Vol. Ph.D. University of Alberta, Edmonton, AB. 209.

Rackham, O., and A. Filipovska. 2012. The role of mammalian PPR domain proteins in the regulation of mitochondrial gene expression. *Biochimica et Biophysica Acta (BBA)-Gene Regulatory Mechanisms*. 1819:1008-1016.

Radloff, R., W. Bauer, and J. Vinograd. 1967. A dye-buoyant-density method for the detection and isolation of closed circular duplex DNA: the closed circular DNA in HeLa cells. *Proceedings of the National Academy of Sciences of the United States of America*. 57:1514.

Ramsey, J.M., S.C. Jacobson, and M.R. Knapp. 1995. Microfabricated chemical measurement systems. *Nature Medicine*. 1:1093-1095.

Reymond, F., J.S. Rossier, and H.H. Girault. 2002. Polymer microchips bonded by O_2-plasma activation. *Electrophoresis*. 23:782-790.

Righetti, P.G. 1989. Of matrices and men. *Journal of biochemical and biophysical methods*. 19:1-20.
Rodbard, D., and A. Chrambach. 1970. Unified theory for gel electrophoresis and gel filtration. *Proceedings of the National Academy of Sciences*. 65:970-977.
Rodriguez, I., and S. Li. 1999. Surface deactivation in protein and peptide analysis by capillary electrophoresis. *Analytica Chimica Acta*. 383:1-26.
Rossmanith, W. 2012. Of P and Z: mitochondrial tRNA processing enzymes. *Biochimica et Biophysica Acta (BBA)-Gene Regulatory Mechanisms*. 1819:1017-1026.
Rubio-Cosials, A., J.F. Sydow, N. Jiménez-Menéndez, P. Fernández-Millán, J. Montoya, H.T. Jacobs, M. Coll, P. Bernadó, and M. Solà. 2011. Human mitochondrial transcription factor A induces a U-turn structure in the light strand promoter. *Nature structural & molecular biology*. 18:1281-1289.
Ruiz-Pesini, E., M.T. Lott, V. Procaccio, J.C. Poole, M.C. Brandon, D. Mishmar, C. Yi, J. Kreuziger, P. Baldi, and D.C. Wallace. 2007. An enhanced MITOMAP with a global mtDNA mutational phylogeny. *Nucleic acids research*. 35:D823-D828.
Ryan, M.T., and N.J. Hoogenraad. 2007. Mitochondrial-nuclear communications. *Annu. Rev. Biochem.* 76:701-722.
Sagan, L. 1967. On the origin of mitosing cells. *Journal of theoretical biology*. 14:225-IN226.
Salas, A., Y. Yao, V. Macaulay, A. Vega, A. Carracedo, and H. Bandelt. 2005. A critical reassessment of the role of mitochondria in tumorigenesis. *PLoS medicine*. 2:1158.
Sambrook, J., E. Fritsch, and T. Maniatis. 1989. Molecular cloning: a laboratory manual.
Sambrook, J., D.W. Russell, and D.W. Russell. 2001. Molecular cloning: a laboratory manual (3-volume set).
Samuels, D.C., E.A. Schon, and P.F. Chinnery. 2004. Two direct repeats cause most human mtDNA deletions. *Trends in Genetics*. 20:393-398.
Saneto, R.P., and M.M. Sedensky. 2013. Mitochondrial Disease in Childhood: mtDNA Encoded. *Neurotherapeutics*. 10:1-13.
Sasaki, D.T., S.E. Dumas, and E.G. Engleman. 1987. Discrimination of viable and non-viable cells using propidium iodide in two color immunofluorescence. *Cytometry*. 8:413-420.
Schaefer, A.M., R. McFarland, E.L. Blakely, L. He, R.G. Whittaker, R.W. Taylor, P.F. Chinnery, and D.M. Turnbull. 2008. Prevalence of mitochondrial DNA disease in adults. *Annals of neurology*. 63:35-39.
Schaefer, A.M., R.W. Taylor, D.M. Turnbull, and P.F. Chinnery. 2004. The epidemiology of mitochondrial disorders—past, present and future. *BBA-Bioenergetics*. 1659:115-120.
Schatz, G., E. Haslbrunner, and H. Tuppy. 1964. Deoxyribonucleic acid associated with yeast mitochondria. *Biochemical and Biophysical Research Communications*. 15:127-132.
Scheffler, I.E. 2007. Mitochondria. Wiley-Liss.
Schon, E.A., A. Naini, and S. Shanske. 2002. Identification of mutations in mtDNA from patients suffering mitochondrial diseases. *Methods in molecular biology (Clifton, N.J.)*. 197:55-74.

Schon, E.A., R. Rizzuto, C.T. Moraes, H. Nakase, M. Zeviani, and S. DiMauro. 1989. A direct repeat is a hotspot for large-scale deletion of human mitochondrial DNA. *Science*. 244:346-349.

Schwartz, M., and J. Vissing. 2002. Paternal Inheritance of Mitochondrial DNA. *New England Journal of Medicine*. 347:576-580.

Selosse, M.-A., B. Albert, and B. Godelle. 2001. Reducing the genome size of organelles favours gene transfer to the nucleus. *Trends in ecology & evolution*. 16:135-141.

Serwer, P. 1983. Agarose gels: Properties and use for electrophoresis. *Electrophoresis*. 4:375-382.

Shalgi, R., A. Magnus, R. Jones, and D.M. Phillips. 1994. Fate of sperm organelles during early embryogenesis in the rat. *Molecular reproduction and development*. 37:264-271.

Shanske, S., J. Coku, J. Lu, J. Ganesh, S. Krishna, K. Tanji, E. Bonilla, A.B. Naini, M. Hirano, and S. DiMauro. 2008. The G13513A mutation in the ND5 gene of mitochondrial DNA as a common cause of MELAS or Leigh syndrome: evidence from 12 cases. *Archives of neurology*. 65:368.

Shanske, S., and L.-J.C. Wong. 2004. Molecular analysis for mitochondrial DNA disorders. *Mitochondrion*. 4:403-415.

Sharpley, M.S., C. Marciniak, K. Eckel-Mahan, M. McManus, M. Crimi, K. Waymire, C.S. Lin, S. Masubuchi, N. Friend, and M. Koike. 2012. Heteroplasmy of Mouse mtDNA Is Genetically Unstable and Results in Altered Behavior and Cognition. *Cell*. 151:333-343.

Shen, M., L. Zhang, M.R. Bonner, C.S. Liu, G. Li, R. Vermeulen, M. Dosemeci, S. Yin, and Q. Lan. 2008. Association between mitochondrial DNA copy number, blood cell counts, and occupational benzene exposure. *Environmental and molecular mutagenesis*. 49:453-457.

Shepherd, R., N. Checcarelli, A. Naini, D. De Vivo, S. DiMauro, and C. Sue. 2006. Measurement of ATP production in mitochondrial disorders. *Journal of inherited metabolic disease*. 29:86-91.

Shitara, H., J.-I. Hayashi, S. Takahama, H. Kaneda, and H. Yonekawa. 1998. Maternal inheritance of mouse mtDNA in interspecific hybrids: segregation of the leaked paternal mtDNA followed by the prevention of subsequent paternal leakage. *Genetics*. 148:851-857.

Sia, S.K., and L.J. Kricka. 2008. Microfluidics and point-of-care testing. *Lab Chip*. 8:1982-1983.

Siciliano, G., L. Volpi, S. Piazza, G. Ricci, M. Mancuso, and L. Murri. 2007. Functional diagnostics in mitochondrial diseases. *Bioscience reports*. 27:53-67.

Singhal, H., Y.R. Ren, and S.E. Kern. 2010. Improved DNA Electrophoresis in Conditions Favoring Polyborates and Lewis Acid Complexation. *PloS one*. 5:e11318.

Situma, C., M. Hashimoto, and S.A. Soper. 2006. Merging microfluidics with microarray-based bioassays. *Biomolecular engineering*. 23:213-231.

Slater, G.W., C. Desruisseaux, S.J. Hubert, J.F. Mercier, J. Labrie, J. Boileau, F. Tessier, and M.P. Pepin. 2000. Theory of DNA electrophoresis: A look at some current challenges. *Electrophoresis*. 21:3873-3887.

Slater, G.W., S. Guillouzic, M.G. Gauthier, J.F. Mercier, M. Kenward, L.C. McCormick, and F. Tessier. 2002. Theory of DNA electrophoresis(~ 1999-2002 ½). *Electrophoresis(Weinheim.Print)*. 23:3791-3816.

Slater, G.W., J. Rousseau, J. Noolandi, C. Turmel, and M. Lalande. 1988. Quantitative analysis of the three regimes of DNA electrophoresis in agarose gels. *Biopolymers*. 27:509-524.

Smeitink, J., L. van den Heuvel, and S. DiMauro. 2001. The genetics and pathology of oxidative phosphorylation. *Nature Reviews Genetics*. 2:342-352.

Smith, C.L., and C.R. Cantor. 1987. Preparation and manipulation of large DNA molecules: advances and applications. *Trends in Biochemical Sciences*. 12:284-287.

Sola, L., and M. Chiari. 2012. Modulation of electroosmotic flow in capillary electrophoresis using functional polymer coatings. *Journal of Chromatography A*. 1270:324-329.

Spelbrink, J.N., F.-Y. Li, V. Tiranti, K. Nikali, Q.-P. Yuan, M. Tariq, S. Wanrooij, N. Garrido, G. Comi, and L. Morandi. 2001. Human mitochondrial DNA deletions associated with mutations in the gene encoding Twinkle, a phage T7 gene 4-like protein localized in mitochondria. *Nature genetics*. 28:223-231.

St John, J., D. Sakkas, K. Dimitriadi, A. Barnes, V. Maclin, J. Ramey, C. Barratt, and C.D. Jonge. 2000. Failure of elimination of paternal mitochondrial DNA in abnormal embryos. *The Lancet*. 355:200.

Stellwagen, N.C., A. Bossi, C. Gelfi, and P.G. Righetti. 2000a. DNA and Buffers: Are There Any Noninteracting, Neutral pH Buffers? *Analytical Biochemistry*. 287:167-175.

Stellwagen, N.C., C. Gelfi, and P.G. Righetti. 2000b. DNA and buffers: the hidden danger of complex formation. *Biopolymers*. 54:137-142.

Stewart, J.B., C. Freyer, J.L. Elson, A. Wredenberg, Z. Cansu, A. Trifunovic, and N.G. Larsson. 2008. Strong purifying selection in transmission of mammalian mitochondrial DNA. *PLoS Biol*. 6:e10.

Sue, C., C. Karadimas, N. Checcarelli, K. Tanji, L. Papadopoulou, F. Pallotti, F. Guo, S. Shanske, M. Hirano, and D. De Vivo. 2000. Differential features of patients with mutations in two COX assembly genes, SURF-1 and SCO2. *Annals of neurology*. 47:589-595.

Sutovsky, P., R.D. Moreno, J. Ramalho-Santos, T. Dominko, C. Simerly, and G. Schatten. 1999. Development: Ubiquitin tag for sperm mitochondria. *Nature*. 402:371-372.

Sutovsky, P., R.D. Moreno, J. Ramalho-Santos, T. Dominko, C. Simerly, and G. Schatten. 2000. Ubiquitinated sperm mitochondria, selective proteolysis, and the regulation of mitochondrial inheritance in mammalian embryos. *Biology of Reproduction*. 63:582-590.

Sutovsky, P., C.S. Navara, and G. Schatten. 1996. Fate of the sperm mitochondria, and the incorporation, conversion, and disassembly of the sperm tail structures during bovine fertilization. *Biology of reproduction*. 55:1195-1205.

Suzuki, T., A. Nagao, and T. Suzuki. 2011. Human mitochondrial tRNAs: biogenesis, function, structural aspects, and diseases. *Annual review of genetics*. 45:299-329.

Swedberg, S.A. 1992. Electrophoresis capillary with agarose. Vol. 5089103. Hewlett-Packard Company, USA.

Takao, M., S.-i. Kanno, T. Shiromoto, R. Hasegawa, H. Ide, S. Ikeda, A.H. Sarker, S. Seki, J.Z. Xing, and X.C. Le. 2002. Novel nuclear and mitochondrial glycosylases revealed by disruption of the mouse *Nth1* gene encoding an endonuclease III homolog for repair of thymine glycols. *The EMBO journal*. 21:3486-3493.

Taylor, P., D.P. Manage, K.E. Helmle, Y. Zheng, D.M. Glerum, and C.J. Backhouse. 2005. Analysis of mitochondrial DNA in microfluidic systems. *J Chromatogr B Analyt Technol Biomed Life Sci*. 822:78-84.

Taylor, R., P. Chinnery, F. Haldane, A. Morris, L. Bindoff, D. Turnbull, and J. Wilson. 1996. MELAS associated with a mutation in the valine transfer RNA gene of mitochondrial DNA. *Annals of neurology*. 40:459-462.

Tegenfeldt, J.O., C. Prinz, H. Cao, R.L. Huang, R.H. Austin, S.Y. Chou, E.C. Cox, and J.C. Sturm. 2004. Micro-and nanofluidics for DNA analysis. *Analytical and bioanalytical chemistry*. 378:1678-1692.

Templeton, A.R. 2005. Haplotype trees and modern human origins. *American journal of physical anthropology*. 128:33-59.

Thangaraj, K., M.B. Joshi, A.G. Reddy, A.A. Rasalkar, and L. Singh. 2003. Sperm mitochondrial mutations as a cause of low sperm motility. *Journal of andrology*. 24:388-392.

Thyagarajan, B., R.A. Padua, and C. Campbell. 1996. Mammalian mitochondria possess homologous DNA recombination activity. *Journal of Biological Chemistry*. 271:27536-27543.

Torroni, A., A. Achilli, V. Macaulay, M. Richards, and H.-J. Bandelt. 2006. Harvesting the fruit of the human mtDNA tree. *TRENDS in Genetics*. 22:339-345.

Tsao, C.-W., and D.L. DeVoe. 2009. Bonding of thermoplastic polymer microfluidics. *Microfluidics and Nanofluidics*. 6:1-16.

Tuppen, H.A., E.L. Blakely, D.M. Turnbull, and R.W. Taylor. 2010. Mitochondrial DNA mutations and human disease. *Biochim Biophys Acta*. 1797:113-128.

Tyynismaa, H., E. Ylikallio, M. Patel, M.J. Molnar, R.G. Haller, and A. Suomalainen. 2009. A Heterozygous Truncating Mutation in *RRM2B* Causes Autosomal-Dominant Progressive External Ophthalmoplegia with Multiple mtDNA Deletions. *The American Journal of Human Genetics*. 85:290-295.

van den Bosch, B.J., R.F. de Coo, H.R. Scholte, J.G. Nijland, R. van den Bogaard, M. de Visser, C.E. de Die-Smulders, and H.J. Smeets. 2000. Mutation analysis of the entire mitochondrial genome using denaturing high performance liquid chromatography. *Nucleic acids research*. 28:e89-e89.

van den Heuvel, L., and J. Smeitink. 2001. The oxidative phosphorylation (OXPHOS) system: nuclear genes and human genetic diseases. *Bioessays*. 23:518-525.

Van Goethem, G., B. Dermaut, A. Löfgren, J.-J. Martin, and C. Van Broeckhoven. 2001. Mutation of POLG is associated with progressive external ophthalmoplegia characterized by mtDNA deletions. *Nature genetics*. 28:211-212.

Van Goethem, G., J. Martin, B. Dermaut, A. Löfgren, A. Wibail, D. Ververken, P. Tack, I. Dehaene, M. Van Zandijcke, and M. Moonen. 2003. Recessive *POLG* mutations presenting with sensory and ataxic neuropathy in compound

heterozygote patients with progressive external ophthalmoplegia. *Neuromuscular disorders*. 13:133-142.

Van Oven, M., and M. Kayser. 2009. Updated comprehensive phylogenetic tree of global human mitochondrial DNA variation. *Human mutation*. 30:E386-E394.

VanOrman, B.B., G.G. Liversidge, G.L. McIntire, T.M. Olefirowicz, and A.G. Ewing. 1990. Effects of buffer composition on electroosmotic flow in capillary electrophoresis. *Journal of Microcolumn Separations*. 2:176-180.

Vergani, L., A.R. Prescott, and I.J. Holt. 2000. Rhabdomyosarcoma ρ^0 cells: isolation and characterization of a mitochondrial DNA depleted cell line with 'muscle-like'properties. *Neuromuscular Disorders*. 10:454-459.

Voelkerding, K.V., S.A. Dames, and J.D. Durtschi. 2009. Next-generation sequencing: from basic research to diagnostics. *Clinical chemistry*. 55:641-658.

Voet, D., J.G. Voet, and C.W. Pratt. 2008. Fundamentals of biochemistry: Life at the molecular level. Hoboken. NJ: Wiley.

von Wurmb-Schwark, N., R. Higuchi, A. Fenech, C. Elfstroem, C. Meissner, M. Oehmichen, and G. Cortopassi. 2002. Quantification of human mitochondrial DNA in a real time PCR. *Forensic science international*. 126:34-39.

Walker, U., S. Collins, and E. Byrne. 1996. Respiratory chain encephalomyopathies: a diagnostic classification. *European neurology*. 36:260-267.

Wallace, D.C. 2007. Why do we still have a maternally inherited mitochondrial DNA? Insights from evolutionary medicine. *Annu. Rev. Biochem.* 76:781-821.

Wallace, D.C., M.D. Brown, and M.T. Lott. 1999. Mitochondrial DNA variation in human evolution and disease. *Gene*. 238:211-230.

Wallace, D.C., G. Singh, M.T. Lott, J.A. Hodge, T.G. Schurr, A.M. Lezza, L.J. Elsas 2nd, and E.K. Nikoskelainen. 1988. Mitochondrial DNA mutation associated with Leber's hereditary optic neuropathy. *Science*. 242:1427.

Wallin, I.E. 1923. The mitochondria problem. *American Naturalist*:255-261.

Wang, Y., Q. Jin, and J. Zhao. 2007. A Single PDMS Based Chip for E. Coli Bacteria Lysis, DNA Extraction and Amplification. *In* 2nd IEEE International Conference on Nano/Micro Engineered and Molecular Systems, 2007. NEMS'07. 458-461.

Watanabe, K., and S.-i. Yokobori. 2011. tRNA Modification and genetic code variations in animal mitochondria. *Journal of nucleic acids*. 2011.

Wheeler, E., C. Hara, J. Frank, J. Deotte, S. Hall, W. Benett, C. Spadaccini, and N. Beer. 2011. Under-three minute PCR: probing the limits of fast amplification. *Analyst*. 136:3707-3712.

Will, Y., J. Hynes, V.I. Ogurtsov, and D.B. Papkovsky. 2007. Analysis of mitochondrial function using phosphorescent oxygen-sensitive probes. *Nature Protocols*. 1:2563-2572.

Wirtz, M., C.A. Schumann, M. Schellenträger, S. Gäb, J. vom Brocke, M.A. Podeschwa, H.J. Altenbach, D. Oscier, and O.J. Schmitz. 2005. Capillary electrophoresis-laser induced fluorescence analysis of endogenous damage in mitochondrial and genomic DNA. *Electrophoresis*. 26:2599-2607.

Wong, L.-J.C., F. Scaglia, B.H. Graham, and W.J. Craigen. 2010. Current molecular diagnostic algorithm for mitochondrial disorders. *Molecular genetics and metabolism*. 100:111-117.

Wong, L.-J.C., and D. Senadheera. 1997. Direct detection of multiple point mutations in mitochondrial DNA. *Clinical chemistry*. 43:1857-1861.

Wong, L.J., and R.G. Boles. 2005a. Mitochondrial DNA analysis in clinical laboratory diagnostics. *Clin Chim Acta*. 354:1-20.

Wong, L.J.C. 2010. Molecular genetics of mitochondrial disorders. *Developmental disabilities research reviews*. 16:154-162.

Wong, L.J.C., and R.G. Boles. 2005b. Mitochondrial DNA analysis in clinical laboratory diagnostics. *Clinica Chimica Acta*. 354:1-20.

Wu, D., J. Qin, and B. Lin. 2008. Electrophoretic separations on microfluidic chips. *Journal of Chromatography A*. 1184:542-559.

Wyllie, A. 1987. Apoptosis: cell death in tissue regulation. *The Journal of pathology*. 153:313-316.

Xu, E., W. Sun, J. Gu, W.-H. Chow, J.A. Ajani, and X. Wu. 2013. Association of mitochondrial DNA copy number in peripheral blood leukocytes with risk of esophageal adenocarcinoma. *Carcinogenesis*:bgt230.

Yakubovskaya, E., Z. Chen, J.A. Carrodeguas, C. Kisker, and D.F. Bogenhagen. 2006. Functional human mitochondrial DNA polymerase γ forms a heterotrimer. *Journal of Biological Chemistry*. 281:374-382.

Yao, B., G.-a. Luo, X. Feng, W. Wang, L.-x. Chen, and Y.-m. Wang. 2004. A microfluidic device based on gravity and electric force driving for flow cytometry and fluorescence activated cell sorting. *Lab Chip*. 4:603-607.

Yao, Y.-G., Q.-P. Kong, A. Salas, and H.-J. Bandelt. 2008. Pseudomitochondrial genome haunts disease studies. *Journal of medical genetics*. 45:769-772.

Yates, J.T., and C.T. Campbell. 2011. Surface chemistry: Key to control and advance myriad technologies. *Proceedings of the National Academy of Sciences*. 108:911-916.

Ye, J., G. Coulouris, I. Zaretskaya, I. Cutcutache, S. Rozen, and T.L. Madden. 2012. Primer-BLAST: a tool to design target-specific primers for polymerase chain reaction. *BMC bioinformatics*. 13:134.

Yeung, S.W., and I.M. Hsing. 2006. Manipulation and extraction of genomic DNA from cell lysate by functionalized magnetic particles for lab on a chip applications. *Biosens Bioelectron*. 21:989-997.

Youle, R.J., and A.M. van der Bliek. 2012. Mitochondrial fission, fusion, and stress. *Science*. 337:1062-1065.

Yu, C.-A., H. Tian, L. Zhang, K.-P. Deng, S.K. Shenoy, L. Yu, D. Xia, H. Kim, and J. Deisenhofer. 1999. Structural basis of multifunctional bovine mitochondrial cytochrome bc 1 complex. *Journal of bioenergetics and biomembranes*. 31:191-200.

Yuri, T., Y. Kondo, K. Kohno, Y.-C. Lei, S. Kanematsu, M. Kuwata, T. Iwasaka, and A. Tsubura. 2008. An autopsy case of chronic progressive external ophthalmoplegia with renal insufficiency. *Medical molecular morphology*. 41:233-237.

Zaragoza, M.V., J. Fass, M. Diegoli, D. Lin, and E. Arbustini. 2010. Mitochondrial DNA variant discovery and evaluation in human Cardiomyopathies through next-generation sequencing. *PloS one*. 5:e12295.

Zhang, D.-X., and G.M. Hewitt. 1996. Nuclear integrations: challenges for mitochondrial DNA markers. *Trends in Ecology & Evolution*. 11:247-251.

Zhang, H., L.H. Meng, D.B. Zimonjic, N.C. Popescu, and Y. Pommier. 2004. Thirteen-exon-motif signature for vertebrate nuclear and mitochondrial type IB topoisomerases. *Nucleic acids research*. 32:2087-2092.

Zhang, W., S. Lin, C. Wang, J. Hu, C. Li, Z. Zhuang, Y. Zhou, R.A. Mathies, and C.J. Yang. 2009. PMMA/PDMS valves and pumps for disposable microfluidics. *Lab on a Chip*. 9:3088-3094.

Zhou, S., K. Kassauei, D.J. Cutler, G.C. Kennedy, D. Sidransky, A. Maitra, and J. Califano. 2006. An oligonucleotide microarray for high-throughput sequencing of the mitochondrial genome. *The Journal of Molecular Diagnostics*. 8:476-482.

Ziebarth, T.D., R. Gonzalez-Soltero, M.M. Makowska-Grzyska, R. Núñez-Ramírez, J.-M. Carazo, L.S. Kaguni, T.D. Ziebarth, R. Gonzalez-Soltero, M.M. Makowska-Grzyska, and R. Núñez-Ramírez. 2010. Dynamic effects of cofactors and DNA on the oligomeric state of human mitochondrial DNA helicase. *Journal of Biological Chemistry*. 285:14639-14647.

Zollo, O., V. Tiranti, and N. Sondheimer. 2012. Transcriptional requirements of the distal heavy-strand promoter of mtDNA. *Proceedings of the National Academy of Sciences*. 109:6508-6512.

Zwieb, C., C. Glotz, and R. Brimacombe. 1981. Secondary structure comparisons between small subunit ribosomal RNA molecules from six different species. *Nucleic Acids Research*. 9:3621-3640.